A Numerical Model for Self-Compacting Concrete Flow through Reinforced Sections: a Porous Medium Analogy

Ein numerisches Modell für das Fließverhalten von selbstverdichtendem Beton in bewehrten Zonen: eine Analogie zu porösen Medien

An der Fakultät Bauingenieurwesen der Technischen Universität Dresden
zur Erlangung der Würde eines Doktor-Ingenieurs (Dr.-Ing.)
eingereichte

DISSERTATION

vorgelegt von
M.Sc. Ksenija Vasilić
aus Šabac, Serbien

eingereicht am 02. Dezember 2014
Tag der mündlichen Prüfung: 16. April 2015

Gutachter:
Prof. Dr.-Ing. Viktor Mechtcherine
Dr.-Ing. Nicolas Roussel

Preface

The work outlined in this dissertation was carried out during my time as a researcher at the BAM, Federal Institute for Material research and Testing, Berlin. I greatly appreciate a given opportunity to have a research position at the BAM and to start such an interesting project. The thesis is done in collaboration with and under supervision of Dr.-Ing. Nicolas Roussel (IFFSTAR, Paris), as well as Prof. Dr.-Ing. Viktor Mechtcherine's (TU Dresden) supervision.

I am deeply thankful to Prof. Dr.-Ing. Viktor Mechtcherine for supervising my thesis, for the invested time and for a valuable input during the most sensitive time of writing and completion.

I owe my greatest gratitude to Dr.-Ing. Nicolas Roussel for his tremendous support while he was guiding me through the PhD process. His ingenuity and willingness to unselfishly share his knowledge and ideas, have been an inspiration for me and helped me to persist during these years. I would like to thank Dr. Roussel for the time he invested in the visits, meetings, discussions and the proofreading.

The completion of my thesis and my employment would not be possible without the great support of Dr.-Ing. Hans-Casten Kühne, the head of the BAM division 7.4 and my supervisor. I would like to thank Dr. Kühne not only for his scientific input, but also for his understanding and for the eagerness to help me in any matter. I am thankful to Dr. rer. nat. Birgit Meng, head of the division 7.1 at the BAM and my supervisor during my first two years at the BAM, for her input and advice and for supporting this collaborative research project at the first place. I am also thankful to Dr.-Ing. Andreas Rogge, the head of the department 7 at the BAM, for his positive attitude towards our ideas and for supporting my employment and this project.

I would like to thank all my colleagues from the BAM 7.4 - their friendly support have been an irreplaceable asset to me. I am particularly grateful to Dr.-Ing. Wolfram Schmidt, for his engagement in the joint experimental studies and for his general readiness to help. I would also like to thank Dipl.-Ing. Frank Haamkens, the head of the concrete lab at the BAM 7.4, and the members of his team, for the great work done on the construction and the conduction of the large-scale experiments. I am also thankful to my dear fellow colleagues Nsesheye Susan Msinjili, Maria Barthel, Gilberto Nery de Araújo Neto and Nico Vogler for the proofreading.

Finally, I would like to thank all of my friends for their precious help and encouragement. Above all, I am thankful to my beloved family for supporting me in my choices with patience and compassion. I dedicate this modest contribution to them.

Summary

This thesis addresses numerical simulations of self-compacting concrete (SCC) castings and suggests a novel modelling approach that treats reinforcement zones in a formwork as porous media.

As a relatively new field in concrete technology, numerical simulations of fresh concrete flow can be a promising aid to optimise casting processes and to avoid on-site casting incidents by predicting the flow behaviour of concrete during the casting process. The simulations of fresh concrete flow generally involve complex mathematical modelling and time-consuming computations. In case of a casting prediction, the simulation time is additionally significantly increased because each reinforcement bar occurring in succession has to be considered one by one. This is particularly problematic when simulating SCC casting, since this type of concrete is typically used for heavily reinforced structural members. However, the wide use of numerical tools for casting prediction in practice is possible only if the tools are user-friendly and simulations are time-saving.

In order to shorten simulation time and to come closer to a practical tool for casting prediction, instead to model steel bars one by one, this thesis suggests to model zones with arrays of steel bars as porous media. Consequently, one models the flow of SCC through a reinforcement zone as a free-surface flow of a non-Newtonian fluid, propagating through the medium. By defining characteristic parameters of the porous medium, the influence on the flow and the changed (apparent) behaviour of concrete in the porous matrix can be predicted. This enables modelling of any reinforcement network as a porous zone and thus significantly simplifies and fastens simulations of reinforced components' castings.

Within the thesis, a computational model for SCC flow through reinforced sections was developed. This model couples a fluid dynamics model for fresh concrete and the macroscopic approach for the influence of the porous medium (formed by the rebars) on the flow. The model is implemented into a Computational Fluid Dynamics software and validated on numerical and experimental studies, among which is a large-scale laboratory casting of a highly reinforced beam. The apparent rheology of concrete within the arrays of steel bars is studied and a methodology to determine unknown input parameters for the porous medium is suggested. Normative tables defining characteristic porous medium parameters as a function of the topology of the rebar zone for different reinforcement cases are generated. Finally, the major contribution of this work is the resulting numerical package, consisting of the numerical solver and the parameter library. The thesis concludes on the ability of the porous medium analogy technique to reliably predict the concrete casting behaviour, while being significantly easier to use and far less time consuming than existing tools.

Zusammenfassung

Die Arbeit behandelt die numerische Modellierung des Fließverhaltens von selbst-verdichtendem Beton (SVB) in bewehrten Schalungselementen. Die numerische Simulation des Fließens von Frischbeton kann eine vielversprechende Unterstützung bei der Optimierung von Befüllvorgängen sein, indem diese bereits im Vorfeld vorhergesagt werden. Die Simulation des Fließens von Frischbeton verwendet komplizierte mathematische Modelle und zeitintensive Rechenoperationen. Darüber hinaus wird die Simulationszeit für die Vorhersage des Füllvorgangs zusätzlich deutlich verlängert, weil aufeinanderfolgende Bewehrungsstäbe einzeln zu berücksichtigen sind. Das ist insbesondere für die Simulation von SVB ein entscheidendes Problemfeld, da SVB oft gerade für hochbewehrte Bauteile verwendet wird. Dennoch ist ein weitreichender Einsatz von numerischen Hilfsmitteln bei der Vorhersage von Füllprozessen nur denkbar, wenn die Anwenderfreundlichkeit und eine Zeitersparnis gewährleistet werden können. Um die Simulationszeit zu verkürzen und näher an eine anwenderfreundliche Lösung für die Vorhersage von Füllprozessen zu kommen, wird als Alternative zur einzelnen Modellierung aller Stahlstäbe in dieser Arbeit vorgeschlagen, Zonen mit Bewehrungsstäben als poröse Medien zu modellieren. Infolgedessen wird das Fließen von SVB durch bewehrte Zonen als Strömung eines nicht-Newton'schen Fluides durch ein poröses Medium betrachtet. Durch die Definition charakteristischer Parameter des porösen Mediums kann das veränderte Verhalten des Betons in der porösen Matrix vorhegesagt werden. Dies ermöglicht die Modellierung beliebiger Bewehrungszonen und vereinfacht und beschleunigt folglich die numerische Simulation bewehrter Bauteile.

Im Rahmen der Arbeit wird ein Rechenmodell für das Fließverhalten von SVB durch bewehrte Schalungszonen entwickelt. Das Modell verkoppelt das Strömungsverhalten von Beton mit dem makroskopischen Ansatz für den Einfluss von porösen Medien, welche in diesem Fall die Bewehrungsstäbe ersetzen. Das entwickelte Modell wird in eine CFD-Software implementiert und anhand mehrerer numerischer und experimenteller Studien validiert, darunter auch ein maßstabsgetreues Fließexperiment eines hochbewehrten Balkens. Darüber hinaus wird die scheinbare Rheologie des Betons innerhalb der Anordnung der Stahlstäbe untersucht und daraus eine Methode zur Bestimmung unbekannter Parameter für das poröse Medium vorgeschlagen. Es werden hierfür auch normative Tabellen generiert, die die charakteristischen Eigenschaften der porösen Medien für unterschiedliche Bewehrungsanordnungen abbilden. Zuletzt ist der Hauptbeitrag dieser Arbeit das resultierende Numerikpaket, bestehend aus dem numerischen Solver einschließlich des implementierten Modells sowie der Parameterbibliothek. Im Abschluss werden die Verlässlichkeit der Vorhersage von Füllvorgängen durch die Analogie zu porösen Medien erörtert sowie Schlussfolgerungen zur deutlichen Ersparnis an Aufwand und Zeit gegenüber herkömmlichen Methoden vorgenommen.

Contents

1 Introduction

1.1 Motivation and objectives

Self-compacting concrete (SCC) is a highly fluid concrete that does not require any vibration during the placement process [1, 2]. It is able to flow and consolidate under its own weight, completely filling the formwork even in the presence of dense reinforcement, whilst maintaining homogeneity and without the need for any additional compaction effort [2]. It is a stable concrete that can spread readily into place and fill the formwork without any consolidation and without undergoing significant separation [3]. SCC has been described as "the most revolutionary development in concrete construction for several decades" [1]. Compared to the traditional vibrated concrete, SCC has numerous advantages: during the placement of SCC no vibration is needed, less manual effort is needed, the noise-level in the plants and construction sites is lower, it is easier to pump and it enables faster construction, it has an improved quality and durability and often higher strength then most of the conventional concretes [3].

Being introduced in the 1980s in Japan, this kind of concrete gained a great interest in the last decades, especially in the case of difficult casting conditions and complicated pours such as heavily reinforced sections [4-6]. Since 2001 SCC has been utilized in Germany but, despite all the advantages this concrete is still used sporadically and mostly for special applications [7]. The reason for the sporadic use is that the concreting sometimes results in segregation, sedimentation or even in showing no self-compacting properties at all. These malfunctions can even occur when the concretes were stable and positively approved at the initial tests, it can still happen that on the site concrete does not meet its key requirements. This is the key issue that prevented a faster and wider use of SCC in Europe, since it was not possible to ensure the proper filling of the building member based on the initial experimental tests and it was difficult to validate mix designs except by full-scale trials [8]. This type of concrete is still not used to its full potential, and in order to benefit from its unique properties, some additional tools able to predict the formwork filling are necessary. This sets the need for the use of numerical modelling of SCC, not only as a tool for form filling prediction, but in terms of determination of fresh concrete properties, mix design and casting optimisation.

During the last years numerical modelling of fresh concrete flow has gained importance and it is becoming an important tool for the prediction and optimization of casting processes [9-12]. The numerical simulation of fresh concrete flow is not a trivial task. The fresh concrete is a complex suspension with particles from micrometre to centimetre scale and it is not possible to build a precise numerical model of this material, even when using the most powerful computers. Thus simplified models are in use and the research

community still works on the development of the appropriate rheological and numerical approaches to simulate fresh concrete flow [12]. However, even when the approximate models are used, the modelling of SCC flow involves comprehensive mathematical calculations and leads to time consuming numerical simulations.

One of the main areas of application of SCC are building members with congested reinforcement [13]. Consequently, in addition to the complex rheological behaviour of SCC, the influence of reinforcement on the flow has to be taken into account and steel bars, which are always present in building members, have to be considered in the simulation. The necessary simulation time is therefore additionally increased when modelling castings, where concrete flows through highly reinforced sections. Modelling of the reinforcement bars (rebars) one by one makes the simulations more complex, significantly increasing the computational time. In order to overcome this problem, to decrease computational time and come closer to a practical simulation tool, the innovative approach of treating reinforcement as a porous medium is proposed here [14-16]. The basic idea of this approach is, instead to model rebars one by one, to present a reinforcement network as a homogenous porous zone (Figure 1).
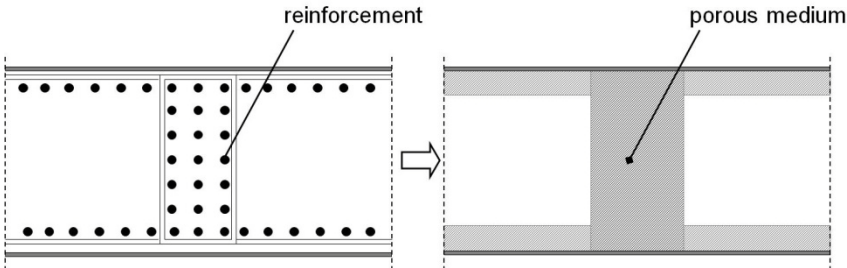
Figure 1:　Schematic representation of the basic idea, reinforcement modelled as a porous medium: real position (left), model (right).

SCC is a very flowable concrete with a fluid-like behaviour and it is here assumed that its flow can be modelled as a flow of a non-Newtonian fluid. Consequently it is suggested do model the flow of SCC through reinforced formwork zones as a free-surface flow of a non-Newtonian fluid through the porous medium. By defining characteristic parameters of the porous medium (permeability, porosity, etc.), its influence on the flow and the relationship between the viscometric behaviour and the observed behaviour in the porous matrix can be defined. Characterisation of the porous medium parameters for different reinforcement constellations enables modelling of any reinforcement network as homogenous zone and significantly simplifies mathematical and numerical modelling of reinforced sections.

Based on the proposed idea of treating reinforcement network as a porous medium, the objectives of the presented work are:

- to develop **a model** properly describing rheological properties and flow behaviour of concrete through a porous medium (reinforcement);

2

- to implement the model into a Computational Fluid Dynamics (CFD) numerical solver, obtaining **a numerical tool** able to forecast flow of concrete through porous medium;

- to **validate** the model and its applicability of flow of cementitious materials through formworks that contain reinforcement;

- to define **a parameter library** of porous medium parameters for different reinforcement cases.

In this thesis, the model development and the numerical implementation of this concept in a CFD software is described. A methodology allowing for the computation of the equivalent porous medium parameters for steel bars network is suggested. Finally, this numerical technique efficiency is evaluated through a comparison of numerical predictions with experimental results of model fluid and concrete castings in model formworks. It is to be shown here, that the resulting model is applicable to simulations of castings of reinforced sections and that it makes numerical simulations significantly simpler and far less time consuming.

1.2   Research steps

The aim of the presented thesis is development of a numerical model to simulate SCC flow through reinforced sections, coupling a model for concrete flow based on fluid dynamics and a mathematical model for propagation of non-Newtonian fluids through porous media (PM). A simplified scheme of the research steps done within this PhD study towards predefined goals is shown in Figure 2. The work is structured in five clearly defined tasks:

Model development:
I   development of the mathematical and numerical model for SCC flow through PM
II   implementation of the developed model in a numerical code.

Model validation:
III model testing through numerical case studies
IV model testing through experimental studies with a model material and with SCC.

Parameter library:
V   development of an industry oriented library of porous medium parameters for different reinforcement classes.

There are two expected final "products" of the study: a fully developed numerical model for the flow of SCC through reinforced zones modelled as porous media and a normative

library of the porous medium parameters for various reinforcement networks. The more detailed explanation of the research steps towards model validation can be found in Subchapter 3.4.
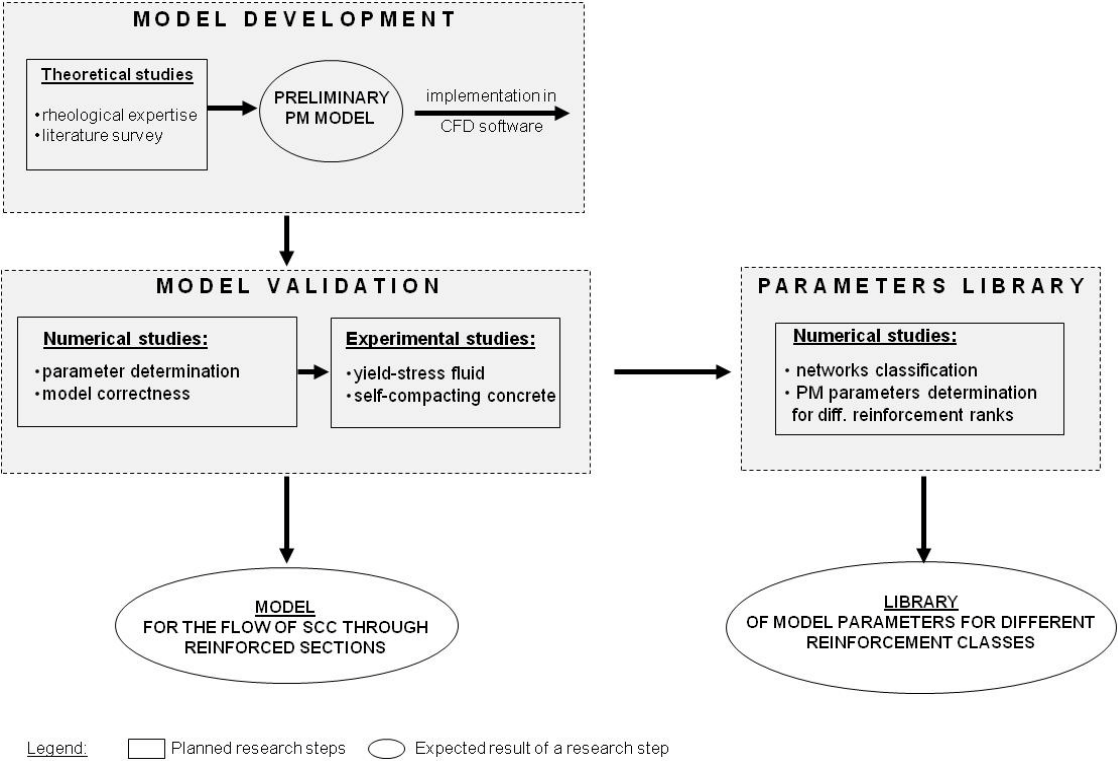
Figure 2: Simplified schema of the work structure in this thesis. The planned research steps as well as the expected products of these steps are shown.

1.3   Thesis structure

Overview of the state of the art in the related fields, namely numerical modelling of concrete flow and modelling of the complex materials flow through porous medium, is given in **Chapter 2.**

In **Chapter 3** details of the approach proposed for the modelling of concrete flow through reinforced sections are explained. The governing equations of the mathematical model for the flow of concrete, their coupling with the model for reinforcement treated as a porous medium as well as the methodology to determine unknown material parameters are given. Planned research steps towards the model validation are also explained.

Chapters 4 to 8 are devoted to the model validation and application.

The tests to confirm the applicability the utilized numerical code on the free-surface flows of cementitious materials and studies towards its calibration are shown in **Chapter 4**.

Chapter 5 focuses on the numerical studies done on Newtonian fluids. These studies were devoted to determine the unknown permeability and to prove the validity of the model on the arbitrary reinforcement network, when passed by Newtonian fluid.

In **Chapter 6** the validation of the model on the propagation of non-Newtonian fluid in porous media is presented. The methodology to determine remaining unknown model parameters is proposed and discussed.

The experimental validation of the proposed methodology on a model non-Newtonian fluid is presented in **Chapter 7** .

The experimental tests with concrete performed to prove the applicability of the model on flow of cementitious materials were topic of **Chapter 8**.

Chapter 9 discusses the classification of the reinforcement networks, presents studies on parameter determination and proposes a parameter library for the different reinforcement cases.

Finally, conclusions and outlook are given in **Chapter 10**.

2 State of the art

The present study focuses on numerical modelling of self-compacting concrete (SCC) casting in formworks that contain reinforcement. Numerical models of concrete flow are complex and the simulations of casting through reinforced sections are extremely time-consuming. In order to decrease computational time and to come closer to a numerical tool for practical applications, this thesis proposes to model the flow of concrete through a reinforcement zone as a flow of non-Newtonian fluid through porous media (PM). This means that this study enters two complex fields: modelling of fresh concrete flow and modelling of flow through porous media. Based on a research study on the existing methods and models in both areas, a model for SCC flow through arrays of bars treated as PM will be defined. In the chapters that follow, while giving a brief overview of the state of the art in two above mentioned fields, the author will try to answer the following questions:

- What are the difficulties in placement and characterisation of SCC, which imply that the use of numerical tools is necessary?
- Which phenomena are to be modelled and what are specifics and problems when modelling concrete flow?
- Which models for concrete flow are in use and which of them are feasible for SCC flow?
- Are there mathematical models focusing on the flow of concrete through reinforced sections in industrial casting processes?
- What are the benefits when using PM analogy instead of discrete rebars when modelling flow through reinforced zones?
- How the flow through arrays of cylinders can be treated as a flow through PM?
- Which phenomena are to be modelled within the PM?
- How can we classify the models of flow through PM and are they applicable to the flow of concrete?
- Which methods can be applied to determine the unknown parameters of the PM?

By answering these questions in two fields of interest, the author aims to demonstrate the necessity of developing a numerical model for concrete flow through reinforced sections. The study of the existing models and techniques in these two fields, should logically justify the choice of the models and approaches, which will be used in this thesis.

Subchapter 2.1 clarifies the difficulties in characterisation and placement of SCC and points out the need to use aid of numerical modelling in these issues. It will be shown that due to its complex behaviour, SCC cannot be properly characterised and the rheological properties cannot be properly determined using classical experimental methods and analytical tools. Furthermore, the casting behaviour on the site cannot be easily predicted.

This implies that the use of some numerical tools as an aid in material characterisation as well as for casting prediction is necessary.

Subchapter 2.2 is devoted to the recent studies on the modelling of concrete flow. It describes phenomena that occur during the flow and lists existing models and methods to model these phenomena. The studies on concrete rheological behaviour, explained in Section 2.2.1, show that on the macroscopic level and under some limitations SCC behaves as a non-Newtonian Bingham fluid. Evaluation of the existing numerical tools in Section 2.2.2 will show that the CFD models are most suitable to simulate flow of fluid concretes such as SCC. Furthermore, it will be shown that there is a lack of research on the flow through reinforced sections and it will be demonstrated that there is a need for research in this field: importance to study how the rebars influence the flow of concrete and to work on an upgrade to the existing numerical tools, which will be able to take the influence of rebars into account.

From Section 2.2.3 it can be concluded that industrial casting of SCC is actually a flow of non-Newtonian fluid through arrays of aligned cylindrical obstacles. The flows of complex fluids through arrays of aligned obstacles are studied in other engineering fields and it will be explained in Subchapter 2.3 what are the advantages when treating these arrays as fibrous porous media. Furthermore, this subchapter gives an overview of the models and methods used for flow through porous media in different engineering fields and discuss their applicability on the flow of concrete through reinforcement. It is to be seen, that the most appropriate model for the flow of SCC through PM is macroscopic approach, which defines apparent viscosity and apparent shear rate within the observed field.

2.1 SCC − basics, difficulties and need for numerical modelling

Due to their very complex rheological behaviour, the characterisation of cementitious materials is a difficult task. This subchapter points out which specific problems occur in design, testing and placement of SCC. The fact that a lot of issues are not solvable using existing experimental and analytical tools set the need for the use of numerical modelling in SCC technology. The following sections suggest and discuss how the implementation of numerical simulations can help to overcome the existing problems in measurements and casting with SCC.

2.1.1 Self-compacting concrete

2.1.1.1 General

Self-compacting or self-consolidating concrete (SCC) is a highly fluid concrete that is able to flow and consolidate under its own weight [1, 2, 6, 17]. It fills the formwork completely even in the presence of dense reinforcement, whilst maintaining homogeneity and without the need for any additional compaction effort. The concrete has to be homogeneous (regarding the paste composition), it has to fully fill the form, to envelop the reinforcement and it has to have a high quality surface without air voids.
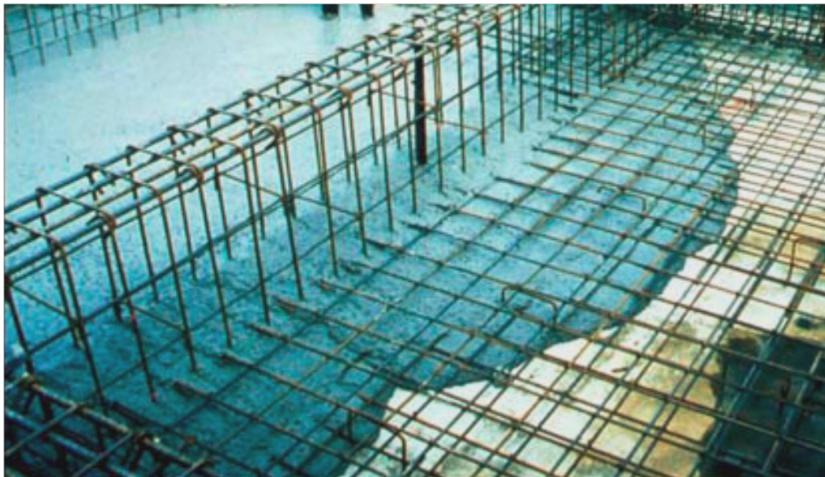
Figure 3:   An illustration of SCC fulfilling requirements on flowability, passing ability and stability [18].

SCC is described worldwide as one of the most important development steps in concrete materials technology during the last decades [1]. Since vibration is not needed, this type of concrete is suitable for casting of complex sections such as heavily reinforced elements, zones where compaction vibrators cannot access or in complex formwork

shapes, which may otherwise be impossible to cast using conventional vibrated concrete. There is a number of advantages of SCC when comparing it to the conventional concrete [3, 19]. These are for instance reduced in-place costs: since SCC increases productivity by increasing the speed of construction and since it improves formed surface finish and thus reduce repair and patching costs, reduce maintenance costs on equipment, and provide faster progress in construction. Furthermore, it provides an improved work environment and safety by eliminating the use of vibrators for concrete placement, thus minimizing vibration and noise exposures. It reduces fall hazards, as workers do not have to stand on forms to consolidate concrete. Improved aesthetics is also one of the advantages, since SCC provides unequalled formed surfaces with a far superior surface smoothness in comparison to conventional concrete.

The key properties that SCC has to possess are filling ability, passing ability and resistance to segregation [20]. Filling ability is the ability of concrete to flow freely under its own weight, both horizontally and vertically upwards, and to completely fill formworks of any dimension and shape without leaving voids. Passing ability is the ability of concrete to flow freely in and around dense reinforcement without blocking. Resistance to segregation is ability to stay homogenous during and after placement. There should be no separation of aggregate from paste or water from solids, and no tendency for coarse aggregate to sink downwards through the fresh concrete mass under gravity [20]. Figure 3 gives an illustration of an SCC mix, fulfilling the requirements of flowability, passing ability and resistance to segregation.
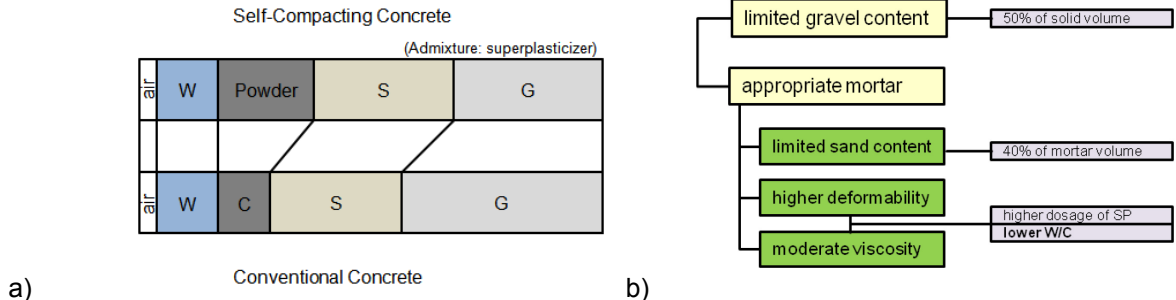
Figure 4: a) Proportions of constituent materials of SCC versus conventional concrete W = water, C = cement, S = sand and G = gravel; b) Methods for achieving self- compatibility [6].

There are several ways to obtain the above-mentioned properties of SCC mix [21]. The high flowability is achieved by using high-range water reducing admixtures, mostly based on (modified) polyacrylates (PA) or polycarboxylate ethers (PCE), also called "3rd generation" superplasticizers [22]. In order to achieve a sufficiently high resistance to segregation, the viscosity of the mixture must be increased compared to traditional concrete. This can be done in three ways: (1) using a higher powder content: "powder type SCC", (2) using a viscosity modifying agent (VMA): "VMA type SC", or (3) using both a higher powder content and VMA: "Combination type SCC".

Okamura and Ouchi in [6] compare the mix proportions of constituent materials for self-compacting and conventional concretes (Figure 4a). The authors also define the methods to achieve self-compatibility namely limited aggregate content, low water-powder ratio and use of superplasticizer (Figure 4b).

Most of the materials used for conventional concrete can be used for the production of SCC, but the main difference is that the properties of the produced fresh SCC can be allowed to vary only within much tighter limits [17]. For conventional concrete, deviations can be handled by varying the degree of compaction, but this is not possible with SCC. The properties of fresh SCC are also much more sensitive to variations in the quality and consistency of the mix constituents. Because of its greater sensitivity to variation, batching accuracy for all component materials is essential for SCC technology to be successful [17].

As a result, much more is demanded of SCC in the fresh state than of conventional vibrated concrete: the concrete has to be homogeneous (regarding paste composition), it has to fully fill the form and to envelop the reinforcement and it should have a high quality surface without air voids [9]. When proportioning such a mix, the prerequisites are indeed complex: one has to find a composite that is very flowable, but where the carrying fluid (mortar) is viscous enough to support coarse particles. If one increases fluidity, the risk of segregation will increase as well and there will be an increase in costs due to addition of more superplasticizer [9].

2.1.1.2 History and present of SCC – a brief overwiev

SCC was firstly developed in Japan in the late eighties in order to achieve durable concrete structures by improving quality in the construction process. It was conceptualized in 1986 by professor Okamura at University of Tokyo, Japan [5, 6]. A type of concrete that does not need vibration was a response to the lack of qualified skilled workers at construction sites and was a solution for achievement of durable concrete structures independent of the quality of construction work [6, 17]. The first prototype of SCC was completed in 1988 and performed satisfactorily with regard to drying and shrinkage, denseness after hardening etc. After the development of this prototype SCC, intensive research began in numerous institutes and construction companies in Japan and, as a result, SCC started being used in many practical applications.

After the pioneering studies in Japan in the eighties, it was found that this type of concrete offers economic, social and environmental benefits over traditional vibrated concrete so the technology spread rapidly to a number of other countries in Asia and Europe and finally to North America. The first significant publication in which 'modern' SCC was

identified is thought to be a paper from the University of Tokyo by Ozawa et al. in 1992 [23]. Research and development work into SCC in Europe began in Sweden in the 1990s [24]. The first research work to be published from Europe was at an International RILEM Conference in 1996 [25, 26] and the first RILEM TC with the objective of gathering, analysing and presenting a review of the technology of SCC was formed in 1997 [27]. After comprehensive research work in the 1990s in Sweden, SCC rapidly gained popularity and today nearly all countries in Europe conduct some form of research and development of this material.

SCC is used today on construction sites all over the world but, although it is obvious that SCC offers many advantages to conventional factory or cast-in-place concrete, it is still used only for special applications. Indicator for that is the SCC volume share of total precast concrete production, which is still in one digit percentage range. According to the annual report of "European ready mixed concrete organization" [28], the average share of SCC in Europe in 2011 and 2012 was respectively only 2.2% and 2% of the total ready mixed concrete production. Even in Germany, which is rich in innovative methods of concrete processing and applications, the applications of SCC is limited to the cases with specific demands and its volume share is about 1% of precast industry. Also in Japan, SCC is still regarded as special concrete because of its costs and difficulties of quality control.

The sections that follow will present and try to explain the missing links between rheology, mix design and casting as well as other practical issues that are the origin of the sporadic use of SCC. It will be talked about difficulties when proportioning such a mix as well as about the difficulties in utilisation of and measurements on SCC. It will be pointed out how the scientific approach can help to overcome these issues and how numerical modelling, in particular, can fill in the gap between the scientific work and practical applications.

2.1.2   Challenges in casting and rheological characterisation

2.1.2.1   Difficulties in practical applications

Before being used on a construction site, SCC should be approved through initial testing. Initial tests are simple experiments performed to verify if the SCC fulfils its key properties, namely filling ability, passing ability and resistance to segregation. In the last decades, more than 100 standardized tests to evaluate fresh concrete properties were developed [29]. The European guidelines for testing fresh SCC are provided in [20]. The experiments such as slump flow test, L-Box test, J-ring test and Sieve stability test are proposed as the reference methods to assess filling ability, passing ability and segregation resistance of the fresh SCC, respectively. Additionally, some simple tests (such as slump flow test) are

usually conducted directly at the construction site, giving a qualitative information about the material workability [30].

Nevertheless, even when the concrete is positively proved in initial tests and tests accompanying production, problems like bleeding, segregation or incomplete form filling can still occur during casting on a construction site. Or, although a stable, robust, non-segregating concrete with well-adjusted flow properties is used, improper filling of complex and heavily reinforced zones can occur. This means that the tests mentioned above are not always sufficient to characterise the material properly and to predict its behaviour on the construction site. This is also one of the main reasons why SCC is not used to its full potential.

Table 1:   Comparison of the experimental and numerical techniques to predict material flow behaviour [31].

Experimental measurements	Numerical simulations
Quantitative <u>description</u> of flow phenomena: - for one quantity at a time - at a limited number of points and time instants - for a laboratory-scale model - for a limited range of problems and operating conditions expensive, slow, sequential, single-purpose	Quantitative <u>prediction</u> of flow phenomena: - for all desired quantities - with high resolution in space and time - for the actual flow domain - for virtually any problem and realistic operating conditions cheap(er), fast(er), parallel, multiple-purpose

In [11] as one of the reasons for the limited success of SCC, the author named a lack of understanding of SCC in fresh state. Although very flowable, the rheology of SCC might vary significantly. To obtain required quality and performance of the structural element, a proper match between the rheological properties and the casting technique is essential. Although the understanding of concrete rheology is crucial for the successful casting, the use of rheometry is not a standard in the concrete industry and the typical measurements do not provide a proper link to the concrete behaviour during the casting. Therefore, for the expansion of SCC technology, it is significant to establish a new system that evaluates concrete fresh properties and links them to the flow behaviour. High requirements on the mix leave no place for trial and error and for correction of material properties through vibration; the mix has to be approved before its utilisation. The only solution to achieve this is a so-called scientific-based approach to concrete casting, where rheological and numerical investigations are employed together with the goal to take over control of casting process [11].

Therefore, to make use of SCC and other fluid concretes to their full potential, the utilisation of some numerical tools for casting prediction is necessary [9]. Table 1 shows a comparison of numerical simulations and experimental measurements in general and outlines some advantages if using numerical simulations to predict material flow behaviour. Models and simulations can be an aid in complex situations and may help to avoid expensive mistakes on site. Furthermore, simulations (such as CFD simulations for instance) can give us insight into patterns that are difficult, expensive or impossible to study using experimental techniques [31].

A numerical simulation of a casting process allows specifying a minimum workability of the fresh concrete that could ensure the proper filling of a given formwork. When using advanced models that take into account non-Newtonian behaviour, one should be able to correctly predict the final shape of material in concrete casting, i.e. of the hardened product. If one uses models that include the dispersed phase, not only the final shape of the filled forms but also the solid phase distribution within the form, eventual segregation, sedimentation or blocking (which is crucial for the strength of the final product) could be predictable.

The behaviour on site is affected by numerous external factors [22] and it can certainly not be expected that the laboratory experiments can account for all the possible influences. By integrating different physical models into the numerical model (e.g. for temperature influences, friction, wall-fluid interaction), these external influences can be accounted for so the simulation should be able to predict the behaviour on site. A beforehand possible problem detection gives valuable input data, allowing to make geometrical or mix design readjustments and to specify onsite workability tests acceptance criteria [10].

2.1.2.2   Difficulties in rheological characterisation

"A phenomenon is not properly understood unless it can be measured". Banfill in [32].

The empirical tests mentioned in Section 2.1.2.1 are mostly oriented to characterise material by trying to simulate field conditions on the laboratory scale. The next important point to discuss is the tests devoted to the measurement of the concrete material properties i.e. the rheological characterisation of concrete. The rheological characterisation is a key to understand the behaviour of fresh SCC and it is the first step to study the basic phenomena which are the origin of SCC stability [33].

We say that a material is rheologically characterised, if one can fully define its constitutive equations and their parameters [34]. The equations represent the evolution of variables such as viscosity and give quantitative relationships between deformations and stresses. Rheometry refers to standard experimental techniques used to determine the constitutive

14

equations and the unknown equations parameters [35]. The experiments themselves are performed with standard rheometer devices, such as for instance so-called very narrow-gap coaxial rheometers with $R_i \geq 0.99 \cdot R_o$, where R_i and R_o are radii of the inner and the outer coaxial cylinder respectively [34, 36].

Cementitious materials such as concrete are suspensions with particles up to several centimetres. Due to the restriction that the rheometer gap has to be at least 10 times greater than the coarsest particle and the dimension limits [32, 37] the narrow-gap rheometers cannot be constructed and for measurements with cementitious materials; therefore the so-called wide-gap rheometers are in use. The gap is here greater than $0.01 \cdot R_o$ and the condition $R_i \geq 0.99 \cdot R_o$ is not valid. Additionally, the concrete rotational rheometers usually have a modified geometry, which, instead of having two coaxial cylinders, consists of a cylindrical bowl with rotating impellers inside [29].

The rheometer measurements provide angular velocity–torque data which cannot be directly used for the parameter identification but have to be converted into stress–strain ones [38]. This conversion is uncomplicated when one uses narrow gap rheometers and the deformation state is uniform during the test. In this case, one can use analytical models to transform the experimental measurements (torques, forces, etc.) into stress–strain curves and the rheological parameters are then computed by graphical analysis [39].

Since concrete is noticeably inhomogeneous and the basis hypothesis of uniform strain is not valid for the wide-gap concrete rheometers, the direct analytical methods cannot be used to determine material parameters from rheometer measurements and approximate methods have to be applied [40-42]. There are a few studies concerning approximate methods to determine material parameters in concrete rheometry [21, 43]. In [21, 43] the authors applied the so-called integration method to determine material parameters from rheometer measurements, and some satisfactory results can be achieved. However, the application of these methods in concrete rheometry is limited and do not lead to a universal tool for parameter determination. All this implies that there is still no reliable technique to be applied to determine material properties (particularly plastic viscosity) from concrete rheometers and there is a necessity to develop a universal tool for parameter determination from concrete rheometer measurements.

In the last years, to deal with the problems of identifying rheological properties of complex materials, the so-called Computer Aided Rheology approach has been proposed [38-40, 44-46]. The basic idea of this approach is to perform both the experiments and numerical simulations, and to obtain the unknown parameters using inverse analysis, adjusting material parameters until the numerically calculated response matches the experimental result. This approach uses advanced experimental techniques such as shear stress

jumps, shear stress ramps and oscillation experiments to investigate complex phenomena such as wall slip, yield stress or steady state behaviour. Unknown properties of complex materials are then determined comparing the measured to the calculated responses by performing numerical simulations of the conducted experiments.

In the field of concrete technology the numerical models have also been developed to help interpret experimental results [29] and can be of great help to retrieve the flow curves and their parameters from the rheometer data. Furthermore, the simulations of simple tests, such as channel and slump flow, could, through inverse parameter fitting, be used to determine the unknown material parameters such as yield stress and plastic viscosity [11].

2.1.3   Conclusions

Although the advantages of SCC compared to traditional concrete are more than obvious, this material is still not used to its full potential. The main reasons for the limited use are the issues that still exist in mix proportioning, testing and casting of SCC.

This subchapter showed that the requirements on SCC mixes are more complex than on regular concrete and it is not an easy task to proportion such mixes. Since there is no possibility of correction of material properties by vibration, the mix has to fulfil the self-compacting criteria and to be approved before utilisation. Nevertheless, even in the cases where the material was positively proved at initial tests before utilisation, the casting sometimes end in segregation, sedimentation or showing no sufficient self-compacting properties, which implies that utilisation of the standard experiments only is not sufficient to evaluate self-compacting properties.

The understanding of concrete rheology is crucial for successful casting. Due to the complexity of the material behaviour and the concrete rheometers setups, it is nearly impossible to obtain the set of actual rheological parameters (plastic viscosity and yield stress) in fundamental units from rheometer measurements. Recently, some reliable methods have been developed to determine materials yield stress, from the slump and channel flow experiments [47, 48].

Mix design, testing and casting of SCC leave plenty of room for improvement and the key for the further progress lays in integration of experimental tests and numerical simulations. The recent developments go towards the so-called scientific approach in SCC technology, where one utilises both numerical simulations and experimental measurement to design and optimise concrete mix proportioning and casting. Numerical simulations can be employed as an aid in the following areas:

- to optimize the mix design;
- to determine unknown material properties from rheometer measurements;
- to predict casting behaviour, where a numerical simulation of casting should enable to analyse defects such as improper filling, segregation or blocking;
- to optimize casting process;
- to predict fiber orientation.

In this thesis, the focus will be placed on simulations of concrete castings devoted to predict form filling and the final shape of the casted element.

2.2   Modelling of concrete flow

Prior to starting a numerical simulation of a material flow, one has to fully understand the material structure and its rheological behaviour as well as to conclude which substantial phenomena are actually to be modelled. Section 2.2.1 deals with the rheological behaviour of fresh concrete and tries to explain its origins. It will indicate the complexity of the concrete micro- and mezzo-structure and try to explain the link between microstructure and macroscopic phenomena. A rheological i.e. mathematical model that describes material flow is a base for any numerical model. In Section 2.2.1.2 a survey on the rheological curves for suspension flows is conducted and their applicability on concrete flow is discussed.

Section 2.2.2 is devoted to the numerical modelling of concrete flow. Although being a suspension, concrete is, from the modelling point of view, far more complex than a regular suspension. At the beginning of the Chapter, the additional difficulties which occur when modelling concrete flow are indicated. It continues with the discussion on and classification of the existing numerical approaches to model concrete flow. Sections 2.2.2.1, 2.2.2.2 and 2.2.2.3 explain respectively the fluid dynamics, particle and multiphase approaches, give their brief historical development and examples of their application.

Subchapter 2.3 deals with the industrial casting processes and modelling of the flow through the arrays of rebars. It will be shown here that study of the flow through rebars arrays is still not exploited enough and that there are no mathematical models explaining the changed rheology in the zone formed by obstacles.

2.2.1   Rheology of fresh concrete

2.2.1.1 Flow behaviour and its origins

Cementitious materials are of great technological importance and, according to [32], their performance is satisfactory if one is able to transport and mould them successfully in the freshly mixed state. The processes such as transporting, pumping, pouring, injection, spraying, spreading, self-levelling, moulding and compaction depend on the rheology of the material. The rheology of concrete is one of the most difficult to study and the microstructure of concrete is the key to try to understand its rheology.

To get a closer insight of concrete inner structure, Figure 5 shows a computer tomography image of a concrete cube sample of about 108 x 108 x 108 mm in size [49]. On the first

level, one can say that concrete is a suspension of coarse aggregates in mortar. Mortar is yet again a suspension of dispersed sand particles in cement paste. Cement paste is not a simple homogeneous liquid, but it is a suspension of cement grains in water. All these particles have different shapes and a wide range of sizes, varying from tenths of nanometres (the smallest cement grains) to several centimetres (the largest coarse aggregates). The solid volume concentrations can be up to 50% in a cement paste and up to 90% in a high strength concrete.
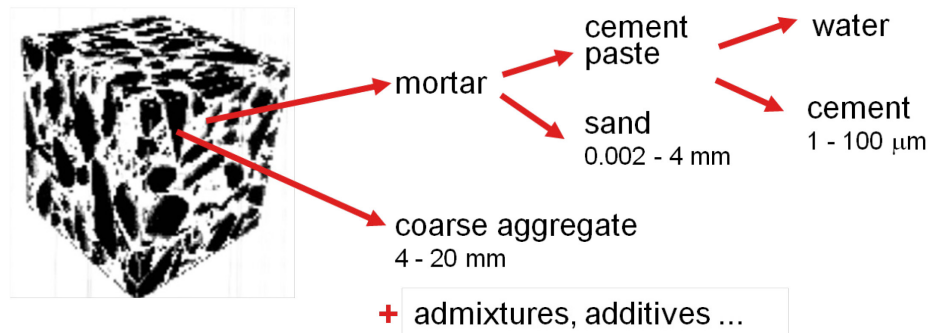
Figure 5:   A computer tomography image of concrete sample; concrete is a suspension with particles from micro- to centimetre scale. Image source: [49].

Although being a suspension on different scales, fresh concrete can be defined as a highly-concentrated (dense, flocculated) suspension of solid particles (aggregates) in a viscous liquid (cement paste) [50]. Highly-concentrated suspensions are defined as suspensions where the average separation distance between particles is equal to or smaller than the particle size [51]. As nearly all such systems of practical interest, cementitious suspensions are non-dilute, meaning that various forces are active in particle interactions. The interparticle forces acting in a suspension are: hydrodynamic effects, Brownian motion, electrostatic repulsion, polymeric repulsion and van der Waals attraction. More about this topic can be found in [34, 35, 52, 53]. Depending on the relative magnitude of these forces, the rheology of suspension can vary widely [54].

In [55] Banfill analysed the forces acting on cement, sand and coarse aggregate particles in concrete and discussed the effects of the internal structure changes caused by these forces on the macroscopic behaviour of the paste. He pointed out, that at the high concentrations typical for mortar and concrete, particles have strong interactions and the strength of this interaction depends on the shape of the particles, their size distribution, their concentration, their surface properties and the properties of the liquid [55]. When the attraction forces become larger than the repulsion, particles can remain together when they collide. The resulting agglomerates have a very complex structure, and the changes of this structure are believed to be the origin of the macroscopic effects that such suspensions exhibit. The net attraction between the particles causes their flocculation:

particles are randomly moving, coming together and sticking. They form flocs, where the size and architecture of the flocs play a major role in the rheology of the suspension. When shearing the material, the flocs are reduced to particles and the resistance to flow is reduced. When the suspension comes to rest, reflocculation occurs and one talks about the structural built-up. Material is now more resistant to flow (more viscous) and shows thickening behaviour. These shear-induced changes in microstructure are time dependent. Finally, additional influencing factor is the presence of dispersing admixtures, which can separate the flocs with significant effects on the rheology [56, 57].

After all, the interparticle forces and structural build-up and breakdown are responsible for the non-Newtonian and time dependent effects that occur during the flow of concrete: yield stress, shear thickening behaviour and thixotropy [32, 52, 58-62]. In addition, segregation and sedimentation of coarse aggregate also occur within the flow of concrete [63] [64].
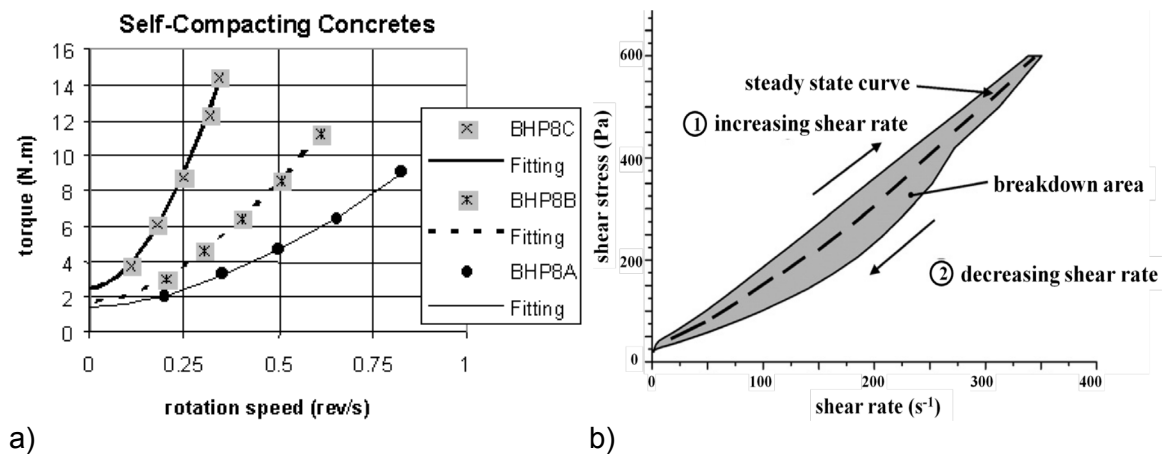
Figure 6:   a) Yield stress and shear thickening behaviour of three different SCCs [65]; b) Example of thixotropic loop obtained with a cement paste submitted successively to increasing and decreasing shear rate ramps [66].

Yield stress behaviour

In the physical sense the yield stress is assumed to act as a switch between the no-flow and the flow region, i.e. between solid-like and liquid-like behaviour [67]. It is the stress that has to be applied to the material to initiate flow. Below this stress, the material behaves as elastic solid. If the applied stress is higher than the yield value, the material flows and behaves as viscous fluid (Figure 6a). Cementitious systems are generally yield-stress fluids and it is believed that the yield stress is a consequence of the interparticle forces [32]. When shearing, the links between particles are broken so the yield stress depends upon time and previous shear history. In general, one can measure the yield stress value using controlled stress rotational rheometers [68], compressive testing [69], vanes [70] or capillary tube measurements [71]. In concrete technology, wide gap

20

rheometers are used to determine yield stresses. Recently Roussel in [48, 72] proposed analytical solutions to determine yield stress values from simpler experiments such as slump flow and channel flow.

Shear thickening behaviour

In the behaviour of fresh concrete paste, shear-thickening effects have been observed [43, 61, 73, 74]. A shear thickening material (also termed "dilatant" by analogy with the shear thickening behaviour of dry granular materials) is a non-Newtonian material in which (apparent) viscosity increases nonlinearly with the increasing shear rate. The diagram in Figure 6a shows an illustration of a flow curve of a shear thickening material. This effect is observed mostly for powder type SCC mixtures, it is a phenomenon that has been described only few times in literature [75]. This phenomenon can become dominant at high shear rates and is important for the processes such as pumping and mixing, where concrete is exposed to high shear rates. When not taken into account, the rapid increase of viscosity at high shear rates can lead to a possible rupture of the mixers, pumps or pipes.

In [74] the authors tried to describe the physical background of shear thickening behaviour in general, its physical causes and influencing factors. One of the theories applicable on concrete flow is that shear thickening is caused by formation of clusters, whereby grain inertia allows grains to come close enough to form clusters. It starts at a certain critical shear stress, at which the hydrodynamic forces start to dominate the repulsive forces between the particles allowing particles to stick together. This effect is reversible and fully hydrodynamic [74]. The shear thickening behaviour can be measured using shear rate ramps in rheometer measurements.

Thixotropy

The flow of concrete is thixotropic, meaning that the way concrete behaves also depends on time and stress history (Figure 6b) [66, 76]. Thixotropy is generally understood as the continuous decrease of apparent viscosity over time under shear and the subsequent recovery of viscosity when flow is reduced or stopped [77]. In [78] the authors claimed that, even though thixotropy and yield stress are considered as two entirely different phenomena, they show a tendency to show up together and they are indeed believed to be caused by the same fundamental physics. The microstructure of the fluid, which resists large rearrangements, is responsible for the yield stress, and the destruction of such a microstructure by flow is believed to be an origin of thixotropy [78].

The recent overview on constitutive equations for thixotropic dispersions can be found in [77], while thixotropy models for fresh concrete are discussed in [66]. In the later, the author pointed out that, in the case of cementitious material, situation is more complex since hydration process starts as soon as water and cement are mixed together. It was

however shown that these two effects have very different characteristic times and it is thought possible to have only thixotropy on short periods of time (approx. 30 min) during which the irreversible changes caused by hydration can be neglected. In practical applications, thixotropy is important when analysing effects such as formwork pressure or multi-layer casting. For these cases, measuring the rate of structuration (i.e. the rate at which apparent yield stress increases over time) is often sufficient from a practical point of view. In literature, however, the standard experiment is a so-called hysteresis loop experiment. Here, the sample is subjected to a systematic increase of shear rate and the decreasing shear rates are imposed (Figure 6b).

<u>Segregation and phase separation</u>

Although fresh SCC must be stable and must ensure the uniform mechanical properties over the structure, problems like segregation or settlement can occur during flow. Particle segregation remains one of the major problems for traditional and self-compacting concrete. Segregation of the particles can appear during placing (referred to as dynamic segregation) or afterwards, during the dormant stage, when the coarsest aggregates segregate under the effect of gravity forces (referred to as static segregation or sedimentation) [33, 63, 64, 79, 80]. In the plastic state, concretes with insufficient segregation resistance show a reduced ability to flow and blocking between reinforcement bars can occur [63]. Later on, in the hardened state, the foregoing segregation of particles leads to non-uniform distribution of solid phase and consequently of properties within the material. The non-uniform apparent viscosity affects the future hardened properties of the material and can result in insufficient strength of the final hardened product, as well as of its durability and serviceability. The uneven distribution of strength and uneven modulus of elasticity over the cross section lead to a reduced bond strength in areas where there is less coarse aggregate. Furthermore, segregation could increase the local porosity and, as a result, the permeability of the concrete to aggressive substances [9].

2.2.1.2   Mathematical models to describe concrete flow behaviour

<u>Suspension rheology – models in use</u>

Fresh concrete is a suspension and rheological equations typical for suspension flows are used to mathematically describe the material flow behaviour. These equations give the evolution of stresses and deformations in the material. The rheological behaviour of suspensions with a low solid content is well known and can be easily characterised using standard rheometry. On the contrary, fresh concrete as well as the most of the suspensions of practical interest is highly concentrated and exhibits complex non-Newtonian flow behaviour (Section 2.2.1.1) [34]. The theories for such suspensions are less developed and models to describe rheological properties are mostly empirical or semi-empirical. The overview of different rheological equations to describe suspension

flows can be found in [34] and those used for cementitious materials are given in [32, 50, 52].

Table 2 shows the mostly used rheological equations to describe suspension flows, while the illustration of the rheological curves is given in Figure 8. The viscous fluids and low concentrated suspensions of non-interacting particles (with solid content less than few percents) mainly show Newtonian flow behaviour where the shear stress τ is proportional to the shear rate $\dot{\gamma}$ and the constant of proportionality is the viscosity η (Equation 1). For the behaviour of pure viscous materials in the non-linear range, Ostwald and de Waele proposed a shear-rate dependent approach [81] where shear thinning as well as shear thickening fluids can be represented (Equation 2). In this equation, k is the fluid consistency index and m is the flow behaviour index.

Table 2:   Flow and viscosity curves to describe suspension rheology.

Newtonian:	$\tau = \eta \cdot \dot{\gamma}$	$\eta = \dfrac{\tau_0}{\dot{\gamma}}$	(1)
Ostwald-de Waele:	$\tau = k \cdot \dot{\gamma}^m$	$\eta = k \cdot \dot{\gamma}^{m-1}$	(2)
Herschel-Bulkley:	$\tau = \tau_0 + k \cdot \dot{\gamma}^m$	$\eta = \dfrac{\tau_0}{\dot{\gamma}} + k \cdot \dot{\gamma}^{m-1}$	(3)
Bingham:	$\tau = \tau_0 + \eta_{pl} \cdot \dot{\gamma}$	$\eta = \dfrac{\tau_0}{\dot{\gamma}} + \eta_{pl}$	(4)
Modified Bingham:	$\tau = \tau_0 + \eta_{pl} \cdot \dot{\gamma} + c \cdot \dot{\gamma}^2$	$\eta = \dfrac{\tau_0}{\dot{\gamma}} + \eta_{pl} + c \cdot \dot{\gamma}$	(5)

For the yield stress fluids, the Newtonian and the Ostwald-de Waele law turn into the Bingham [82, 83] and the Herschel-Bulkley laws [84], respectively. The Bingham model (Equation 3) assumes occurrence of the yield stress and linear behaviour if the applied stress is higher than the yield value. In the Bingham equation τ_0 denotes yield stress, η_{pl} is the plastic viscosity and $\dot{\gamma}$ is the shear rate. Herschel-Bulkley (H-B) approach assumes that the material behaves non-linearly if the stresses are above yield value (Equation 4). In the H-B equation τ_0 is again yield stress, k is the consistency index and m is the flow behaviour index. If the factor m > 1 material is shear-thickening and if m < 1 the material shows shear-thinning behaviour. If the value m = 1 the equation reduces to the Bingham model. To model shear-thickening behaviour some authors use the modified Bingham equation shown in Equation 5 [85, 86].

Table 3:   Viscosity as a function of solid volume fraction, models in use.

Dilute suspensions	Einstein	$\eta = \eta_L \cdot (1 + 2.5 \cdot f_s)$	(6)
Semi-dilute suspensions	Krieger Dougherty	$\eta = \eta_L \cdot (1 - 2.5 \cdot f_s / f_{s,max})$	(7)

All above mentioned equations represented stress and viscosity as a function of shear rate. The parameters of the equations are not constant, but depend on local properties of the material, namely solid volume fraction. According to Coussot in [52] the critical parameter that characterises the behaviour of a suspension is the solid volume fraction f_s. The solid volume fraction is the ratio of the total volume of the dispersed phase (particles) to the total sample volume.
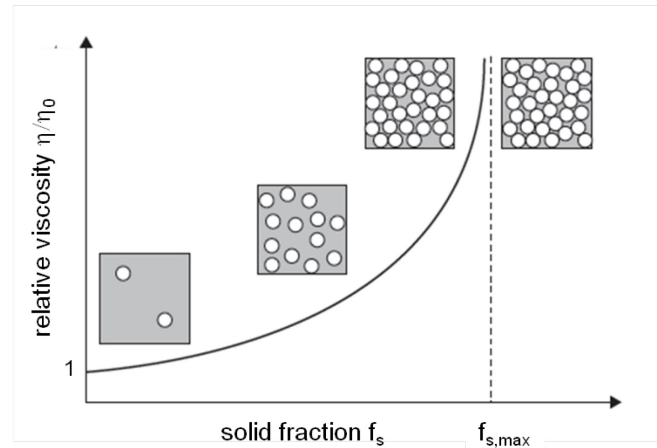
Figure 7:   Relative viscosity of suspensions of uniform spheres in a Newtonian liquid as a function of solid fraction. From left to right: dilute, semi dilute, concentrated and compact suspensions [52].

Based on solid volume fraction, suspensions are classified as dilute, semi-dilute, concentrated and compact. As an illustration, Figure 7 shows relative viscosity of suspensions of uniform spheres in a Newtonian fluid according to [52]. To include the influence of the volume fraction of the dispersed phase, the viscosity of low concentrated suspensions (up to 1% by volume) can be approximated using a simple Einstein equation (Table 3, Equation 6) where the viscosity is directly proportional to the solid fraction and to the viscosity of the surrounding liquid [34]. For semi-dilute and up to some extend for the concentrated suspensions (up to 55%), the Krieger-Dougherty approach can be applied (Table 3, Equation 7). In this equation, the parameter $f_{s,max}$ the maximum solid fraction that can be reached using mono-sized grains. In the case of cementitious materials, where we have different particles and where the size of grains varies from few microns to a few millimetres, the maximum packing density may be up to 90 – 95%. For such systems, there is no explicit equation that defines the viscosity as a function of solid concentration [52].

Rheology of fresh cementitious materials – models in use

The rheology of fresh cementitious materials has been studied extensively in the last decades, in order to predict fresh properties and to be able to design materials and processes with the required performances [32]. In this study, we will focus on the rheological equations to describe concrete flow, where there is still disagreement among the authors, which model is the most appropriate to describe flow of concrete. In [50] the

24

author classifies the approaches to describe flow of cementitious suspensions: either they try to relate the concentration of the suspension to the viscosity or they try to correlate shear stress to shear rate, thus assuming that there is only one value for the viscosity of the whole system. The first ones could be used to describe cement paste, but due to materials complexity they are not applicable to concrete. For instance, although considering only the influence of the solid content and not taking into account non-Newtonian phenomena, the Einstein model and its extensions have been still used by some authors to describe the flow of the cement paste [50].

a: shear-thickenning; b: Bingham; c: shear-thinning
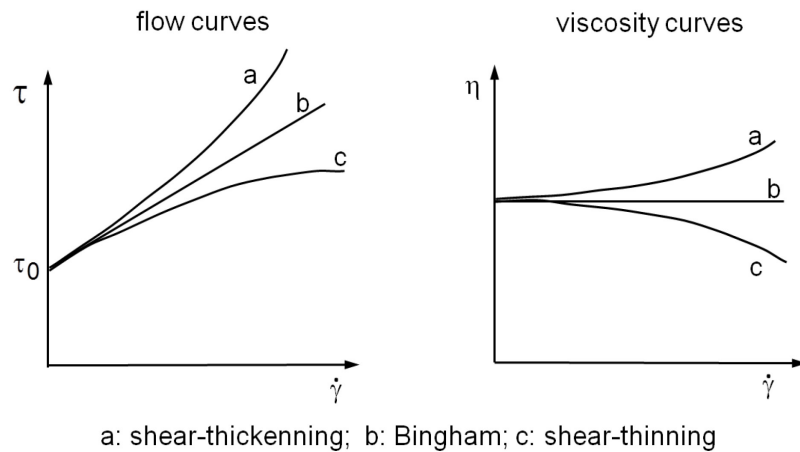
Figure 8:   A sketch of flow and viscosity curves illustrating Bingham, shear-thinning and shear-thickening behaviour.

To describe the non-Newtonian flow behaviour of concrete, most authors use the Bingham and Herschel-Bulkley models, which are shown in Equations 3 and 4 and illustrated in Figure 8. The most commonly used equation today is the Bingham equation, which assumes occurrence of yield stress and linear behaviour at the shear stresses higher than the yield value. The reasons for the widespread acceptance of this model are mostly practical: the model parameters can be measured independently and the flow of real concrete seems to follow this equation fairly well in most cases [50].

It has been though shown by some authors [43, 61, 65] that, for some concretes such as SCC, the Herschel-Bulkley equation better describes their behaviour than the Bingham one. In [43] the authors concluded that, for some SCCs of powder type, when using the Bingham model to fit the rheometer measurements, the model results in negative values for the yield stress, which of course has no physical meaning. The effect is more noticeable when the higher superplasticizer contents are added to the SCC mix resulting in a lower yield stress. The authors suggested that, in order to avoid the appearance of a negative yield stress, a shear-thickening model must be used to describe this flow behaviour. Similar results were obtained in [61].The Herschel–Bulkley approach is mostly used to approximate the shear-thickening flow behaviour of concrete at high shear rates

[43]. Some authors use also the modified Bingham approach shown in Equation 5. This model assumes yield stress, and non-linear behaviour beyond the yield stress value [74].

Although considering both yield stress and shear-thickening behaviour, the Herschel-Bulkley model cannot take time-dependent structural changes such as thixotropy into account [78]. The literature on thixotropic models was reviewed by Barnes in [87] and more recently by Labanda and Dullaert [77, 88]. All models can be divided into three groups: models based on structural parameters, direct structure theories and simple viscosity theories. In the first approach, the structural changes are described using a general description of the degree of structural built-up in the microstructure, denoted by a scalar parameter, usually called λ. The value of λ is equal 1 for the fully built-up structure and its value equals 0 for the fully destroyed structure. The models based on structural parameter λ are the most developed models to mirror the phenomena occurring during internal structure breakdown and build-up by formulating equations of state, termed constitutive equations, and kinetic equations which take into account the time-dependence of viscosity under constant shear rate conditions [88]. Other researchers attempt a direct description of the temporal changes related to the number of bonds between particles (so-called direct structure theories), while the third approach uses the viscosity time data itself to base a theory. In [66] Roussel discussed methods to measure and model thixotropy and proposed a thixotropy model for fresh concretes. He used structural parameter λ to describe structural kinetics and proposed the evolution equation to describe the change of λ over time.

2.2.2 Numerical simulations of fresh concrete flow

Recent developments in the field of SCC technology go towards a scientifically based approach to concrete casting where both experimental studies and numerical simulations are utilised to achieve an optimal mix design and an effective casting.

Numerical simulations have been used in various engineering fields, where suspension flows have been successfully simulated (e.g. flow of metallic suspensions in forming processes, polymer flows, etc.) [89]. For instance, numerical tools have been used to predict flow-filling of moulds and eventual subsequent hardening process, for mould design and process optimisation [90]. It is to expect that simulations can be a powerful tool for prediction and optimisation of concrete casting processes as well as for parameter determination. Computational modelling of concrete flow could be used to predict particle migrations within the material and for simulation of total form filling. Additionally, since the complex material behaviour disallows the rheological characterisation of concrete using classical rheometry, the use of numerical simulations is required to determine material unknown parameters as well. Therefore, computational modelling of the flow could be a

tool both for understanding the rheological behaviour of concrete and for mix proportioning.

The problem to be modelled is quite complex, one deals here with a free-surface flow of a dense suspension with a wide range of particle sizes. Similarly to most of suspensions of practical interests, concrete shows non-Newtonian flow behaviour, yield stress, shear-thickening behaviour and thixotropy. What distinguishes concrete from other suspensions is the high solid fraction and the range of particle sizes. The particles may differ by a factor of 10^6 in size and the solid fraction is up to 85% [32]. During flow, migration of particles, such as segregation and blocking, can occur. Trapped air in concrete represents the next, gaseous phase to be modelled. Due to the fact that flow of SCC is a free-surface flow, the treatment of the interface and its position represents another important numerical modelling issue.

The computational models used in other fields do not involve such a wide range of particles and the volume fraction of the solid phase is far lower than in concrete, so the experience from the other fields cannot be directly applied to the simulations of concrete flow. Thus in the field of concrete technology, the numerical modelling is a relatively new method, which potentials are still not fully exploited. The first work in the field of numerical modelling of concrete flow started in Japan in the 1980s, but it actually has gained importance in the last decade. A comprehensive overview of the previous and current numerical studies on concrete flow can be found in [9-11] and most recently in [12].

A complete, discrete description of concrete from the cement particles to coarse aggregate is impossible with any computer model [91] since accounting for broad particle size and shape distributions exceeds the computational limits of even the best super computers. An exact multiphase model of such a complex system like concrete does not exist and approximate models are in use. Instead of modelling the exact structure, the authors have to simplify the inner structure, but to include the complex non-Newtonian phenomena occurring within the flow in the model. In the last years, a lot of research work has been done in this field but there is still disagreement in the research community which rheological and numerical approach is the most suitable one [11, 12]. The basic classification of all the methods to model concrete is whether they are based on fluid dynamics (concrete is assumed to be a fluid) or on solid mechanics (concrete is assumed to be a collection of single solid particles). Figure 9 shows a classification and the schematic representation of the fluid and particle methods. Furthermore, we could classify the models whether or not they take the dispersed phase into account to one-phase models and two-phase models.
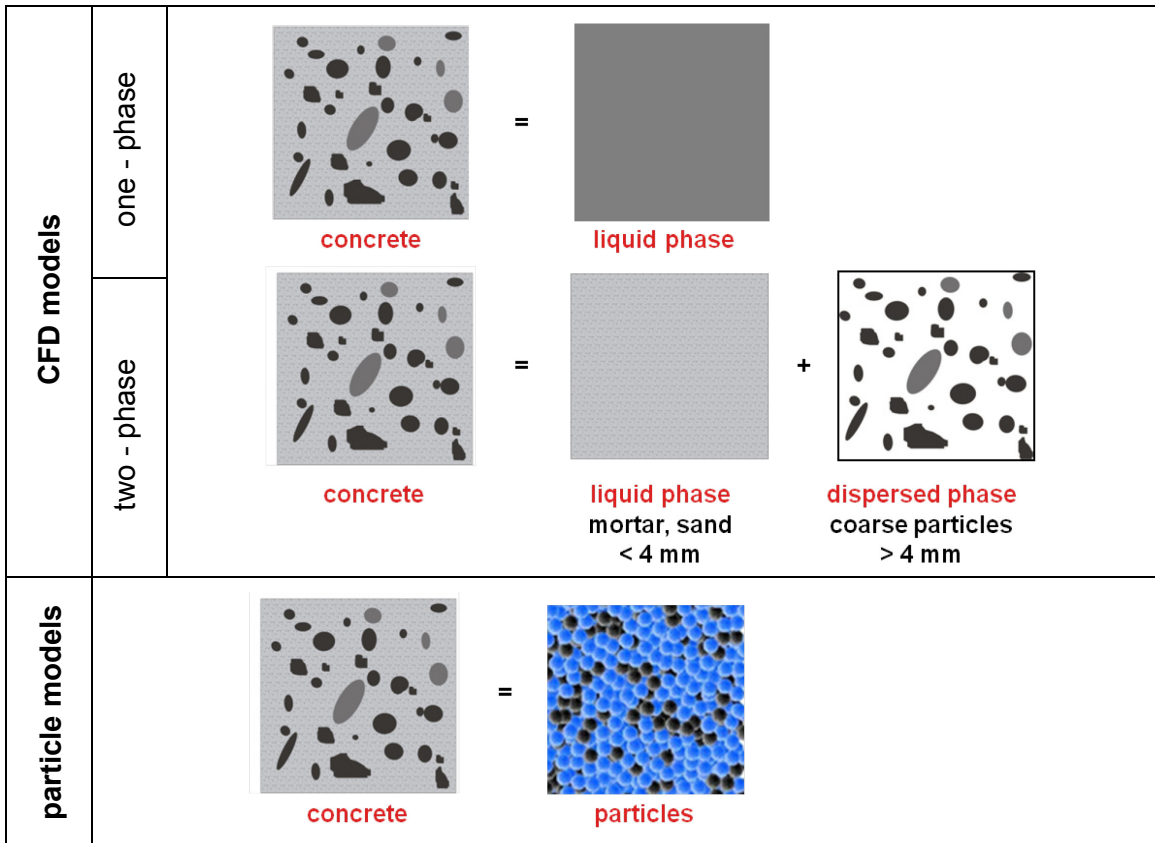
Figure 9: Schematic representation of the model classification: CFD models (above) and particle models (below).

The following sections will give an overview of the numerical techniques used to simulate concrete flow and provide some examples of applications. In Section 2.2.2.1 the basics of computational fluid dynamics are explained followed by a brief historical development and some application of CFD methods in concrete technology. Section 2.2.2.2 is devoted to the particle methods, explaining the basics of DEM and its applications. Section 2.2.2.3 gives examples of studies, where concrete is simulated as a suspension and proposes some future trends.

2.2.2.1 Models based on fluid dynamics

Governing equations of fluid dynamics

Using the approach based on fluid dynamics, concrete is represented as a fluid and its flow is governed by a system of equations named Navier-Stokes equations [92]. The governing equations are partial differential equations (PDE) which represent conservation laws for the mass, momentum, and energy. Computational Fluid Dynamics (CFD) is the method of replacing such PDE systems by a set of algebraic equations which can be solved using digital computers [31].

The governing equations are mathematical statements for the following three physical laws: mass is conserved, Newton's second law and energy is conserved. Equations 8 and 9 represent the general form of the mass and momentum conservation equations respectively (the energy conservation is omitted, since relevant only if flow is compressible and thermodynamics is to be included).

$$\frac{\partial \rho}{\partial t} + \underline{\nabla} \cdot (\rho \underline{v}) = 0 \tag{8}$$

$$\rho \frac{D \underline{v}}{D t} = \underline{\nabla} \cdot \underline{\underline{\sigma}} + \rho \underline{g} + \underline{F} \tag{9}$$

Here ρ is density, $\underline{v}$ is the local velocity vector, $\underline{\nabla}$ is so called nabla (del) operator, symbol D stands for convective derivative, t is time, g denotes gravity and $\underline{F}$ are external body forces. $\underline{\underline{\sigma}}$ is the so called Cauchy stress tensor, a symmetric second order tensor defined as:

$$\underline{\underline{\sigma}} = \begin{bmatrix} \sigma_x & \tau_{xy} & \tau_{xz} \\ & \sigma_y & \tau_{yx} \\ & & \sigma_z \end{bmatrix} \tag{10}$$

where σ_i are normal stress components and τ_{ij} are shear stress components. Causchy stress tensor can be written as:

$$\underline{\underline{\sigma}} = -p\underline{\underline{I}} + \underline{\underline{T}} \tag{11}$$

where p is pressure, $\underline{\underline{I}}$ is the second order identity tensor and $\underline{\underline{T}}$ is the deviatoric stress tensor. The stresses in $\underline{\underline{\sigma}}$ arise from a combination of pressure p and viscous friction, which are prescribed by constitutive relations between stresses and velocity gradients [92].

Approximate solution of governing equations using CFD

CFD is based on the approximate solution of the differential flow equations in fluid continuum. More about the CFD can be found in [93-95]. CFD algorithms use a wide range of different mathematical models and discretisation methods to macroscopically solve flow differential equations. The CFD provides a qualitative and quantitative prediction of fluid flows by means of mathematical modelling (partial differential equations), numerical methods (discretisation and solution techniques) and software tools (solvers, pre- and post-processing utilities). Generally, one can define the phases of a CFD simulation as:
- preprocessing phase, where the problem and mathematical model are defined, the grid is generated and the flow and material parameters as well as the boundary conditions defined;
- computation, where the software solves i.e. calculates the flow equations until the convergence criteria is fulfilled;

- post-processing phase, which is devoted to the analyses of the results, visualisation and output of the quantities of interest.

Brief historical overview

The earliest numerical solution was probably the Thom's solution for flow past a cylinder in 1933 [96]. Kawaguti obtained a solution for flow around a cylinder in 1953 by using a mechanical desk calculator, working 20 hours per week for 18 months [97]. The modern CFD, as we know it today, was firstly introduced during the 1960s by the NASA scientists at Los Alamos lab in the USA. During that time, this theoretical group contributed basics of numerical methods that are used in CFD today [98]. In the 70s the group at the Imperial College, London paid the next important contribution to CFD, by developing numerous codes and equations that are still in use now (as for example Parabolic flow codes, Vorticity-Stream function based codes, the SIMPLE algorithm and the TEACH code, as well as the form of the k - e equations that are used today) [99].

In the early 80s various commercial CFD codes came to the market and some of them are still available. The industry started using the commercial software soon and CFD is routinely used today in many disciplines and industries such as aerospace, automotive, power generation, chemical engineering, polymer processing, petroleum engineering, medical research and meteorology. In his analysis on the use of CFD in the process industries in [90], Davidson concluded that the use of CFD has led to cost and time reductions of product and process development and optimization, it reduced the need for experimentation, improved design reliability, and facilitated the resolution of environmental, health, and right-to-operate issues. It follows that the economic benefit of using CFD has been substantial.

Applications in concrete technology

If assuming that material is homogeneous, concrete can be treated as a one-phase fluid and simulated using CFD. Here, the scale of observation is of great importance, to choose whether or not the homogenous approach is suitable [11]. The order of magnitude of a formwork smallest characteristic size is around 20 - 30 cm while the order of magnitude of the size of the coarsest particles is 1 – 2 cm. This means, that if as a first approximation the presence of the steel bars is neglected, the flow in a typical formwork can be considered as the flow of a homogeneous fluid [14]. A comprehensive overview of the history and present of CFD simulations in concrete technology can be found in [9-11, 100]. The CFD simulations were employed to simulate basic concrete tests (such as slump flow and L-box), rheometer measurements, casting and mixing. The mostly used software are ANSYS Fluent©, FLOW-3D© and FIDAP©.

30

In 1986 Tanigawa and co-workers were the first to simulate the slump of concrete, modelling concrete as a homogeneous continuum, using their developed finite element program [101] and later using so called Viscoplastic Finite Element Method (VFEM) [102]. In [103] Christensen enhanced their slump flow simulation material model using finite elements and the software FIDAP©. Ever since numerous authors used CFD to simulate standard concrete tests such as slump flow and L-Box [48, 104-111]. In [112] the authors used CFD code Flow 3D© to simulate slump flow experiment for different yield stresses. The comparison with analytical results validated that the final shape of the material at stoppage depends only on yield stress and density of material. This is however not valid for the experiments where the kinetic energy plays an important role, like for example with low viscosity concretes in L-box.

In 1990 Hattori and Izumi suggested to model viscoplastic fluid, also by introducing a continuum particle that holds a collection of particles in matrix. The original Hattori-Izumi theory was modified to include for example yield stress in [59]. Here, the thixotropic behaviour of the mortar phase is related to coagulation, dispersion and re-coagulation of particles. Fresh concrete flow in the viscometer has been studied in detail by [59] using a conglomeration and deconglomeration algorithm.

The examples of simulations of concrete casting can be found in [9, 107, 109, 113-116]. In [115] a full-scale SCC wall casting using the Galerkin Finite Element formulation of the Navier-Stokes equations is conducted. Test methods and full scale castings of walls with and without reinforcement were simulated with the software FIDAP©. It has been shown in the presented examples, that the CFD is able to predict the form filling and the final shape of the material when the flow stops.

2.2.2.2 Particle methods

The particle methods are mainly based on the Distinct Element Method, also called Discrete Element Method (DEM). DEM is a family of numerical methods proposed originally by Cundall in 1971 [117] for problems in rock mechanics and computation the motion of large number of particles (such as grains or sand). It models the movement and interaction of particles, allows displacements and rotations of these discrete bodies, which may attach to or detach from each other.

Using DEM concrete is represented as a large ensemble of single granular particles, which are interacting through contact laws. The overview of studies that used DEM to simulate concrete flow is recently given in [118, 119]. The particles are defined to be rigid. Their interaction is treated as a dynamic process with a developing state of equilibrium whenever the internal forces are in balance. The contacts between neighbouring particles occur only at one point at a given time. The motion of each solid particle is determined by

the application of Newton's second law and the contact forces between them are modelled artificially. The contact points between particles are usually modelled by a set of normal and shear springs, normal and shear dashpots, normal and shear no tension-joints and shear sliders (Figure 10).
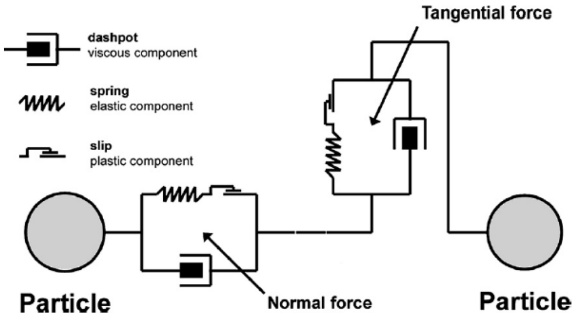
Figure 10: A standard contact law between two particles in DEM; according to the separating distance and relative velocity of the particles, normal and tangential interaction forces between particles can be calculated [9].

The interactions constituents for the normal and tangential direction are shown in Figure 11. They consist of the basic rheological elements spring, dashpot, and slider, which respectively represent the elastic, viscous and friction components of the particles interaction.
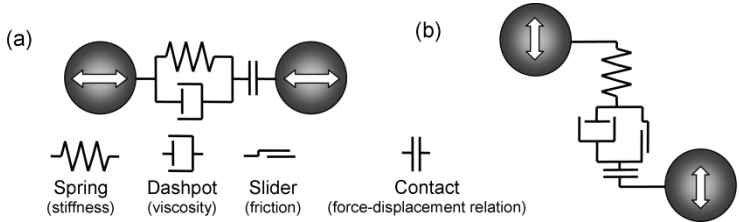
Figure 11: Model for particle interaction: (a) normal direction and (b) tangential direction [119].

The particle methods should be applied when the situation to be simulated is in "discrete regime" i.e. when the scale of observation no longer allows us to neglect the difference in velocity between the particles and surrounding fluid [9, 119]. Concrete technology processes and phenomena such as mixing, compaction, de-airing, sedimentation, fibre distribution and orientation etc. can be analysed using particle methods [119].

The first simulations of concrete using particle methods were done beginning of 1990s in Japan. For instance Chu and Machida [120, 121] simulated a funnel test with software PFC©, showing the build-up of granular arches (blocking) in the funnel during flow. 1999, also in Japan, distinct element simulation with separate particles was employed for visualization of SCC flow [122].

Based on work by Chu et al. [120, 121], a 3D DEM using a 3D particle flow code program, PCD3D©, was applied in a preliminary study by Noor and Uomoto [122]. In order to simulate the flow of SCC during various standard tests: slump flow test, L-box and V-funnel. The material was divided into mortar and coarse aggregates (larger than 7.5 mm). The method proposed by Noor and Uomoto was also adopted in [123, 124] to simulate SCC flow during L-box, slump flow test and J-ring test, respectively. They found both 3D and 2D simulations to be appropriate.

In the last years, the simulations of fresh concrete flow based on DEM are developed thoroughly by Schwabe et al. [125-127], Mechtcherine and Shyshko [118, 128-131]. Schwabe and Kuch in [125] employed DEM to model and analyse the blending of the grain ingredients within a concrete mixer. The different grain fractions are filled successively into the mixer and the analysis of the mixture quality is realized by a virtual extraction of a probe (sampling) within the mixing box. Experimental analyses with different construction designs in planetary mixers at real scale confirmed the simulations.

It has been shown by Mechtcherine et al. [118, 129-131] that this numerical approach allows to simulate the behaviour of fresh concrete with different consistency during transport, placement and compaction. Processes such as casting, compaction of ordinary concrete, wet spraying and extrusion have been simulated. The correlation between mix design and rheology was also investigated through the effect of large aggregates. Furthermore, first attempts towards modelling air inclusions and de-airing were carried out. Mechtcherine and Shyshko were first who used PFC3D© to include fibres in the model [129]. The mostly used commercial codes today are PFC2D©, PFC3D© and EDEM©.

2.2.2.3   Multiphase modelling

The one-phase methods described in 2.2.2.1 are able to predict casting to some extent, but cannot depict segregation, sedimentation and blockage occurring during flow. On the other hand, the distinct element methods described in 2.2.2.2 did not take into account the presence of both liquid and solid phases in the system, and describe concrete as distinct elements interacting through complex laws. A reliable numerical model of a multiphase material behaviour shall take both phases (solid and liquid) into account. From the numerical point of view, concrete flow should be seen as the free-surface flow of a highly-concentrated suspension of rigid particles in a liquid. The common approach in the field of concrete technology is to consider concrete as a two phase suspension: the "liquid phase" made of either cement paste or mortar and the dispersed phase made of the coarser particles (Figure 9).

When solving multiphase flows by means of CFD, numerical solutions of the Navier-Stokes equations require a substantial amount of computation even for simple cases. It is evident that for simulation of complex flows some sort of averaging has to be applied, where focus is not on the detailed and exact description of the phases but on the momentum interaction between the phases. Using the CFD approach, the suspended particles can be included into computations using two different approaches namely Euler-Euler and Euler-Lagrange approach. The Euler-Euler approach describes both the liquid phase and the dispersed particles as a continuum. The second one, called Euler-Lagrange, assumes that there is a continuous liquid phase (Euler phase) and dispersed phase (Lagrange phase) in the form of solid particles. The model is based on the solution of constitutive equations for continuous liquid phase, and then the amount of single particles is introduced into the field and their trajectories are tracked. When the Lagrangian model is applied, the disperse phase should not exceed a volume share of 10%, because otherwise the added particles strongly influence the continuous phase, so that the equations for the continuous phase are not valid anymore and cannot describe the material correctly. Additionally, for higher content of solid particles (for example for laminar flows typical for SCC casting), a very high computing power is necessary. Therefore, Euler-Lagrange approach is suitable only when particle size and their volume fraction are small. Euler-Euler averaged description in which both phases are treated as continua, is though appropriate for larger particles and dense systems [89].

Examples of application

The multiphase models try to capture the suspension nature of concrete (particles in a matrix phase) [11]. Some examples of multiphase modelling can be found in concrete technology, where authors aimed to study heterogeneities, particle migration, blocking or fibre orientation. The recent overview can be found in [11, 91].

The first work where concrete is modelled as a suspension was done by Mori and Tanigawa in [132] where they used the so-called viscoplastic suspension element method to simulate concrete as a suspension of coarse particles in mortar. In 2005 a finite element method with Lagrangian integration points (FEMLIP) was used by Dufour et al. [133]. The method actually allows the simulation of a heterogeneous material made of mortar and aggregate. Modigell et al. [134] suggested to model concrete in the L-box experiment as a two-phase suspension with continuous liquid matrix and a disperse, solid phase. The simulations were performed using non-commercial software code PETERASOFT© and the dispersed phase was treated as a continuum.

Recently Spangenberg et al. [135] coupled a CFD simulation of casting process with numerical modelling of the segregation of the coarse particles, while trying to predict dynamic segregation (flow induced heterogeneities) using the software FLOW3D©. The position of the particles is calculated explicitly with a one-way momentum coupling

between the continuous phase and the particles (i.e. the particles "feel" the continuous phase but not vice versa). Also, no interaction between the particles is assumed.

An entirely different approach was applied by Martys in [136]. The author applied multi-scale model that takes information (rheological properties) corresponding to one length scale as input into the next higher scale. In a multi-scale approach for suspensions, one starts at the smallest scales, defining a suspension by a matrix or embedding fluid that contains solid inclusions. This suspension now becomes the matrix fluid for larger solid inclusions (typically ten times the size of the particles in the matrix fluid). This process can again be repeated over and over until the final macroscopic fluid of interest is attained. To study fluid flow behaviour corresponding to the different length scales, Martys has developed several computational models based on Dissipative Particle Hydrodynamics (DPD) [136], Smoothed Particle Hydrodynamics (SPH) [137] and alternate approaches like Lattice Boltzmann [138]. Both DPD and SPH can be thought of as a Lagrangian formulation of the Navier-Stokes equations. The DPD can be thought of as a simplified version of SPH that is useful when the particles are of order of a micrometer in size. In these approaches a fluid phase is represented by a set of points that carry the fluid properties. Solid inclusions are represented by "freezing" a set of the fluid particles so that they move together as a rigid body [139].

2.2.2.4   Comparison of fluid and particle methods

A complete description of concrete from the cement particles to coarse aggregate is impossible with any computer model since accounting for broad particle size and shape distributions exceeds the computational limits of even the best super computers [136, 140]. Therefore the approximations are in use. The best and nearest possible approximation of concrete would be the use of suspension models. These models are still being developed and there is still no a multiphase model to include such a high concentration of solid particles. This means that the researchers have to choose between the CFD and DEM models [53]. This choice depends on the concrete application, and based on the process itself and on the type of concrete utilised, one chooses which approach (continuous/particle) is appropriate and whether flow of concrete is closer to the flow of a liquid or movement of granular media.

It was shown in Section 2.2.1.1 that the scale of observation plays an important role. In general it can be assumed that concrete shows the fluid-like behaviour when casting and the use of the CFD approach is then more appropriate for this application. However, concrete granular media behaviour is dominant when mixing, so the use of particle methods is more suitable for optimisation of mixing procedures.

Furthermore, which model is to be applied, depends also on the type of concrete. Some high-performance concretes such as SCC are very flowable and the amount of coarse particles is lower than in conventional concrete. It can be assumed that these concrete behave like fluids (or fluid suspensions) and it is fully legitimate to describe their behaviour by use of fluid dynamics. However, in case of ordinary concretes, such as for example a no-slump concrete, the amount of coarse particles is higher, so the behaviour is predominated by the granular nature of the material. The utilisation of particle methods is therefore reasonable in this case.

Anyway, the applied numerical methods should lead to development of practical simulation tools, which are to be utilised by engineers to solve real problems occurring at construction sites. This means that the numerical tools should be user-friendly and as fast as possible and that the computational time is one of the decisive factors for the method choice. Although being able to predict rotation and movement of single granular particles, the simulations based on DEM are extremely processor intensive. This limits the number of particles and number of different particle classes that can be used in actual computation, so the use of this model could be though reasonable only with use of very powerful computers in parallel processing. Additionally, the parameters of the spring-damper models used for the contact between the particles are based on trial and error – a qualitative determination from measured material properties is possible but not straight forward [130, 131].

On the contrary, the CFD simulations are far less time consuming then the ones based on DEM (for instance, the total time needed for a slump flow simulation using a DEM code is around 70 hours and using CFD software ANSYS Fluent© is a couple of hours). So, even though using simplified models, the CFD simulations are faster and in the case of flowable concretes as SCC more adequate then the particle method, and therefore more in use. Another advantage of CFD methods is that one can measure the material properties (such as yield stress and plastic viscosity), which are needed as input for numerical simulation to model its macroscopic behaviour.

2.2.3   Industrial casting processes

Traditional procedure of concrete casting by using vibration energy to compact (consolidate) fresh concrete had remained unchanged for decades. The introduction of SCC has radically changed the way a formwork is filled and eliminated the need for compaction. A comprehensive survey on SCC casting can be found in [18]. In this report was shown, that SCC is well suited for pumping, which can be optimised on the basis of fluid mechanics and give improved control of pump pressures and feeding rates. New pump generations are likely to consider the specifics of SCC, where the pumps for flows into several hoses and inlets to forms will be further developed [18]. Casting of SCC can

be made both with pressure, i.e. pumping through valves and traditional filling from above. The elimination of manual compaction during casting makes very high casting rates possible which, in combination with the high flowability, might cause high formwork pressures. If the concrete is designed accordingly, thixotropic effects can significantly reduce the formwork pressure.

Figure 12: An example of congested reinforcement: an ideal application for SCC [17].

The development of SCC strongly supports an increased industrialisation of the concrete construction process. The fact that concrete can be handled as a fluid also gives additional process improvement possibilities. The possibilities of utilising complex formwork systems have improved and an increased use of permanent formwork of high-quality sheet materials are going in the direction of the enhancing further the possibilities of industrialisation [18].

As already discussed in Subchapter 2.1, the SCC is particularly suitable and is often being utilised for casting of densely reinforced sections. An example of a congested reinforcement, which is an ideal application for SCC, is shown in Figure 12. It is certain that the presence of the reinforcement influences the flow in different ways and up till now, some studies concerning the flow through reinforced zones are conducted already [80, 141-143]. However, these studies dealt only with the aspect of coarse particles blocking.

If the characteristic size of the gaps between the bars is in the order of magnitude of the size of the coarsest particles, a granular blocking may occur and granular arches may appear. In [141] the authors theoretically studied probabilistic passing ability of fresh concrete. They introduced a so-called blocking parameter P, a dimensionless factor depending on volume of concrete, volume fraction of the aggregate particles, maximum diameter and shape of the coarse aggregates and gap between the bars. This parameter can capture the transition between the blocking and passing, showing that for tested concretes no blocking appears for P lower than 0.1. Accordingly, for each particular filling case the corresponding parameter P should be calculated and used as a limiting criterion determining whether yield stress or blocking dominates the flow. If the gaps between the

bars are not much larger than the size of the coarsest particles it is most probably that the blocking occurs; this limits the proper form filling. If the bar distance is increased and the blocking parameter is higher than the critical value, no blocking occurs and the yield stress is the limiting factor for the form filling. The passing ability and blocking tendency could be proved experimentally by J-Ring and L-Box tests [20].

Even in the cases when blocking does not occur, the influence of the reinforcement on the flow is still significant and has to be taken into account. Most of the applications shown in the previous subchapters have focused on the setups with no or only little reinforcement. When dense reinforcement systems are applied, the viscous flow resistance is increased and the assumption to neglect the reinforcement is not valid anymore. To our knowledge, up to now, there is no rheological expertise dealing with concrete macroscopic behaviour in presence of obstacles and no modelling research studies dealing with the flow of concrete through reinforced zones. This sets the need to study the rheology of SCC within the reinforcement networks and to define a mathematical model able to describe it. As mentioned above, the research community still searches for the most appropriate numerical model and benchmark method to simulate concrete flow. After the benchmark method is established, an upgrade that includes the reinforcement influence on the flow will be necessary.

The geometry of a reinforced zone is actually similar to the up-scaled geometry of fibrous porous media. In [144] Nguyen studied permeability of reinforced sections through experiments with test fluids. To the author's knowledge, aside from [144] there are no other attempts to study and model the flow of cementitious materials through reinforcement as a flow of a non-Newtonian fluid through porous media.

2.2.4   Conclusions

The rheology of fresh concrete is one of the most difficult to study. Concrete is a suspension of different particles (aggregate, sand, cement) dispersed in liquid, at very high concentrations (up to 85%). It is believed that the structural changes are the cause of the non-Newtonian macroscopic effects occurring during the flow. Thus the macroscopic behaviour has its origin in the interaction of liquid matrix and of dispersed phases and depends on properties of the both liquid matrix and dispersed phases. It depends on the type of mortar and aggregate, dispersed phase volume fraction, particle shape and particle size. In case of SCC, the additives also play an important role since they are influencing the viscosity and yield stress greatly. Additionally, the concrete behaviour and performance on site is influenced by numerous external factors such as temperature, interaction with the structure, time and stress history.

Due to the computational reasons, it is not possible to build an all-encompassing numerical model which will include all the particle classes into account. Most authors aim to model the macroscopic behaviour of fresh concrete and to find a rheological equation that would fit this behaviour in best way. However, this is also not a trivial task and an "all-inclusive" model for concrete flow should account for the following phenomena and influences:

- yield stress;
- shear thickening behaviour at high shear rates;
- thixotropic behaviour;
- changes in behaviour due to the sedimentation, segregation, blocking;
- external influences (temperature, casting conditions, fluid-structure interaction, etc.);
- hydratation process.

Although there have been numerous studies on concrete rheology in the last decades, it is still difficult to develop a complete model that would be able to account for all the phenomena simultaneously. Concrete is instead approximated as one of known non-Newtonian materials such as Bingham or Herschel-Bulkley fluid. It depends on the process to be modelled and the effects which predominate the process, which of these two models is more suitable. For instance, for the processes such as pumping, where the high shear rates are likely to happen, the shear-thickening behaviour can occur and the Herschel-Bulkley model could be more suitable one. In case of a slow laminar flow, that occurs for instance at the end of the typical casting process, where one is interested in the final shape of the material, the values of the shear rates are rather low. In both the Herschel-Bulkley and Bingham equation the contribution of the second part of the equation is negligible and in such cases the yield stress practically dominates the flow. This means, it is not relevant if the material behaves linearly or non-linearly at the higher shear rates, and to predict the final shape, the material can be modelled as a yield-stress fluid (Bingham fluid).

To simulate concrete flow, most authors use either particle methods or CFD methods. Since being much faster than particle methods, the CFD methods are more in use. Here the scale of observation, the process to be simulated and the type of concrete are decisive factors for the choice of the method. For instance, the particle methods might be appropriate for no-slump concretes (concrete of stiff or extremely dry consistency) but in the case of extremely flowable concretes (such as SCC) the CFD method is more adequate to depict concrete flow behaviour and to predict the form filling.

In this thesis, the fluid dynamics approach is used and concrete is described as a one-phase non-Newtonian (Bingham) fluid.

2.3 Modelling of complex materials flow through porous medium

In a typical casting process, the fresh SCC is pumped into the formwork and it propagates through the arrays of steel bars until the form is filled. In a numerical simulation of a casting process, one simulates the flow through the arrays with a goal to forecast if the filling will be successful. This thesis assumes that the bars form a sort of porous media and our aim is to study the macroscopic influence of the reinforcement on the flow and to connect the PM properties with the changed fresh rheology of concrete within the PM zone. The essentials on modelling of flow of cementitious materials are discussed in Subchapter 2.2. The second complex field that will be tackled in this thesis is the modelling of flow of complex fluids through porous media.

The next section will present the available models of flow of complex fluids through PM and discuss their applicability on the reinforcement networks. Fluid flow through porous media plays an important role in a variety of engineering systems. In these applications, the porous materials may generally be divided into two classes: granular media and fibrous media. Section 2.3.2 will focus on the second class of porous media, namely fibrous PM. The last subchapter will discuss the methods to determine unknown parameters of the porous media in the model equations.

2.3.1 Flow of complex fluids through porous medium

Flow of complex fluids through porous media occurs in many subsurface systems and in a wide range of technical applications. These fluids display complex non-Newtonian behaviour such as time and shear rate dependency (shear-thinning/thickening effects, elasticity, anisotropy, yield stress, thixotropy, etc.) [145-147]. Early studies on the flow in porous media were focusing on Newtonian fluids, while studies on the flow of non-Newtonian fluids in porous media exist from the early 1960s. Due to its importance in various engineering fields (petroleum, pharmaceutical, food, cosmetic, textile, paper and polymer composite industries) flow of complex fluids through periodic porous medium was thoroughly studied in the last years and some sophisticated models were developed. A detailed overview of the earlier work was presented by Sorbie at al. [148], by de Boer [149] and more recently by Lopez at al. [147].

The studies have focused mainly on flow through isotropic porous media considering generalised Newtonian fluids, yield stress fluids and viscoelastic fluids (overview in [150]). The general conclusion of the studies is that the flow through PM is far more complex than any other regular rheometric flow and there is little agreement on how to model and predict complex fluid flow through PM. The complex geometric nature of PM makes the

formulation of accurate predictive flow of them difficult, and the detailed pore-scale simulations almost impossible, so the scientists focus on approximate methods [151].

All the approximate models can be classified into two groups. First one are macroscopic models, where single-phase, single-species flow through porous media has been modelled using either the linear Darcy's law or some empirical nonlinear relationship between the pressure gradient and the Darcy velocity as an approximation to momentum conservation. The second group, which appeared recently, are models based on microscale conservation laws and averaging techniques to methodically derive a macroscale momentum equation appropriate for more complex flow scenarios [152].
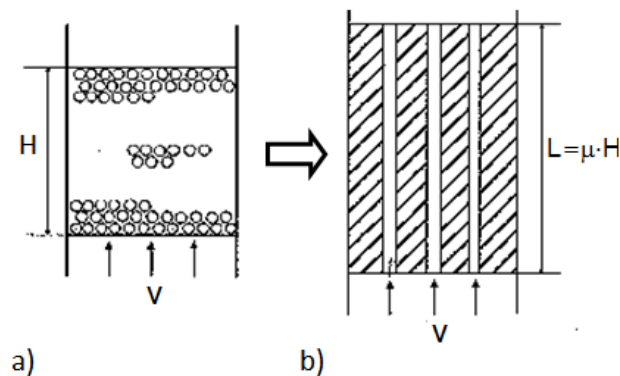
Figure 13: Schematic representation of a capillary model: a) packed bed, b) capillary model [153].

Based on the geometry used for approximation, the macroscopic averaging methods can be classified as:

-    capillary models
Here, the PM is represented as a bundle of parallel capillary tubes (Figure 13b) and analytical expression is then derived from Stokes law [153]. The calculation is based on definition of average capillary radius and is dependent on porosity and absolute permeability [153]. Random distribution of capillaries with circular or rectangular cross sections and capillary networks (in three directions) are available as well [145, 146, 154].

-    pore-network models
This approach is an extension of the capillary model and it is used for complex fluids in topologically complex PM. Here PM is presented as a collection of interconnected elements, pores and throats (Figure 14). Extended from Newtonian fluid the equations are developed for non-Newtonian, Bingham, thixotropic [147, 148, 155, 156] and yield stress fluids [157]. This method can use some statistical methods for network pore distribution.

Figure 14: An illustration of a pore network model: a) porous medium, b) pore network model [147].

Modelling flow in porous media at the engineering scale usually employs equations such as the Ergun equation, Darcy's law or the Carman-Kozeny equation. Common for these equations is a view of the porous medium as a continuum, meaning that velocity is a spatially averaged, superfici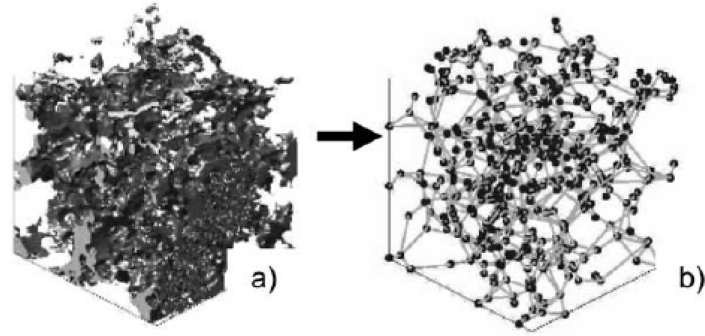al velocity. Accordingly, all the complexities of the microscopic pore structure are lumped into terms, such as permeability. To include the influence of porous medium on the flow, the common practice is to use continuum macroscopic models, e.g. to modify model equations to account for presence of the porous matrix as a continuous medium [158]. The resulting macroscopic flow laws look like modified version of Darcy's law and the relationship between macroscopic pressure gradients and flow rate is similar to constitutive relation between the stress and the strain rate in the flowing fluid at the pore scale [150, 158]. The Darcy's law in general form can be empirically derived as:

$$\underline{v} = -\frac{\underline{\underline{k}}}{\eta} \nabla p \tag{12}$$

where $\underline{v}$ is Darcy's velocity vector (which equals the volume flow rate q), $\underline{k}$ is the permeability tensor and ∇p is the pressure gradient. For a Newtonian fluid, the viscosity η in Equation 12 is constant. In the case of non-Newtonian fluids, this viscosity is bulk non-Newtonian viscosity which depends on the shear rate in the porous medium.

The rheological models developed in fluid mechanics for non-Newtonian fluids cannot be directly applied to the porous media. As a result, many laboratory studies were undertaken in an attempt to relate the rheological properties of a non-Newtonian fluid to the flow velocity or the imposed pressure drop [145]. Even when the bulk rheology of the fluid is known, there is still an issue of how this relates to the in situ rheology of the fluid, i.e. the effective rheology within the porous medium, referred to as the "apparent viscosity". Therefore, some equivalent or apparent viscosities η_{app} are required in the Darcy's equation:

$$\underline{v} = -\frac{\underline{\underline{k}}}{\eta_{app}} \nabla p \tag{13}$$

42

Since it is practically impossible to determine distribution of shear rate within a PM, one defines an effective or apparent shear rate approach, which is based on use of a shifted, modified shear rate in the porous medium. For non-Newtonian fluids the flow rate is correlated with the in-situ shear rate within the porous medium, which is frequently expressed as [159]:

$$\dot{\gamma}_{PM} = \frac{\alpha q}{\sqrt{k\phi}}$$

(14)

where $\dot{\gamma}_{PM}$ is apparent shear rate in porous medium, q is flow rate, k is permeability, ϕ is porosity and α is a medium dependent 'shift factor' also called 'shape factor'. Apparent viscosity is a function of flow rate through the porous medium, i.e. it is expressed in terms of apparent shear rate where overall shape of $\eta_{app}(q)$ is similar to the bulk $\eta(\dot{\gamma})$ [147]:

$$\eta_{app}(q) = \eta(\dot{\gamma} = \frac{\alpha q}{\sqrt{k\phi}})$$

(15)

Strictly speaking, Darcy's law holds only for a Newtonian fluid over a certain range of flow rates. As the flow rate increases, a deviation from this law is noticed [160]. It has been experimentally and mathematically observed that this deviation is due to inertia, turbulence, and other high-velocity effects. The observed deviation starts from the Reynolds' number of about one, and a correction to Darcy's law for high flow rates can be described by a quadratic term [160].

Other effects that introduce additional complexity in the Darcy's equation are non-Newtonian phenomena, such as for example the occurrence of yield stress. There is a limited number of papers indeed which deal with convection of a yield-stress fluid in a porous medium [161, 162]. In [162] Rees discusses in detail the modelling of the flow of a Bingham fluid in a porous medium and presents the models which have appeared in the literature so far. Several generalized equations have been developed for Bingham fluids that are analogous to Darcy's law, such as Pascal model or Buckingham-Reiner model:

$$v = \begin{cases} -\dfrac{k}{\eta_{pl}}\left[1 - \dfrac{G}{|\nabla p|}\right] \cdot \nabla p & \text{if } \nabla p > G \\ 0 & \text{if } \nabla p \leq G \end{cases}$$

(16)

$$v = \begin{cases} -\dfrac{k}{\eta_{pl}}\left[1 - \dfrac{4}{3}\dfrac{G}{|\nabla p|} + \dfrac{1}{3}\left(\dfrac{G}{|\nabla p|}\right)^4\right] \cdot \nabla p & \text{if } \nabla p > G \\ 0 & \text{if } \nabla p \leq G \end{cases}$$

(17)

where G denotes the threshold gradient. Recently, through experiments with yield stress fluids flowing through confined packing of glass beads of different sizes, Chevalier et al. derived a general expression for the pressure drop vs. flow rate curve through a porous medium as a function of the flow rate and the characteristics of the system [163].

2.3.2   Flow through arrays of cylinders – fibrous porous media

Flow of concrete through a typical formwork containing reinforcement can be referred to as flow through arrays of aligned cylinders or cylinder clusters. The flow of Newtonian and non-Newtonian fluids through periodic arrays of aligned cylinders has been studied extensively for a range of applications [164]. Studies on the flows of non-Newtonian fluids have primarily explained the roles of shear-thinning or shear-thickening rheological behaviour, viscoelasticity or development of elastic instabilities.

Less well documented is the flow through arrays of cylinders of materials that exhibit yield stress and show a transition between 'solid' and 'liquid' type rheological behaviour [165]. Some examples on studies on flow of Bingham fluids through cylinder arrays may be found in [165, 166]. In [166] Nieckele et al. studied the flow of viscoplastic materials through tube bundles in staggered arrangement; they analysed the effects occurring and the flow field, high and low viscosity regions, the critical pressure drop below which the material does not flow anymore. In [165] numerical studies were carried out applying bi-viscosity model for Bingham plastics, whereby the velocity as a function of regularisation parameter, or the drag force (drag coefficient c_d) as a function of Bingham number B_n were investigated. It can be concluded that most of the studies on yield-stress fluid flow through arrays of obstacles were concentrated on the local phenomena such as drag force or visualisation of the flow field.

Generally speaking, from the geometrical point of view, a zone with clusters of cylinders can be considered as a porous medium, and there are some examples where the clusters of cylindrical obstacles were treated as porous media [167]. The approaches which idealize such arrays as fibrous porous media are however more interesting for this thesis, since they are mainly devoted to determination of macroscopic properties of the media. Advantage of this approach enables to connect the macroscopic rheology of the flow with the influence of the rebars on concrete rheology.

Phenomena of fluid flow through fibrous porous media play important role in various engineering fields such as for example resin transfer and moulding process or industrial filters materials. An overview of experimental and theoretical studies on fibrous porous media can be found in [168]. Due to anisotropic properties of fibrous materials, the laminar flow through such media is modelled by using a generalized form of Darcy's law [168]. The knowledge of permeability which characterizes the ability of fluid to penetrate the fibres is an important matter in design of the above-mentioned processes and devices.

2.3.3 Parameters of porous medium

Each porous medium is fully defined by its geometrical properties namely porosity and permeability. In the case of non-Newtonian fluids the additional parameter that partly depends on the porous medium topology is the shift factor α. In the following sections we describe these parameters and the methods of their determination.

2.3.3.1 Porosity

The porosity (or void fraction) of any medium is defined as a fraction of the volume of voids over the total volume:

$$\phi = \frac{V_V}{V_T} = 1 - \frac{V_s}{V_T} \tag{18}$$

where V_V is the volume of void-space (such as space between the obstacles in reinforced zone) and V_T is the total or bulk volume of material, including the solid and void components, V_s is the volume of solid components. Porosity has a value between 0 and 1.

2.3.3.2 Permeability

Permeability is a measure of the ability of a porous material to allow fluids to pass through it. The permeability of porous media has been a subject of numerous experimental and numerical studies since decades and a literature review on permeability of fibrous media has been presented in [168] and [169]. For a random anisotropic porous media the permeability is a tensor of the second rank with 9 components:

$$\underline{\underline{k}} = \begin{bmatrix} k_{xx} & k_{xy} & k_{xz} \\ k_{yx} & k_{yy} & k_{yz} \\ k_{zx} & k_{zy} & k_{zz} \end{bmatrix} \tag{19}$$

where the components k_{ij} (i, j = x, y, z) are the permeabilities for flows in i direction as driven by gradient in j direction. It was firstly proved in [170, 171] that the permeability tensor is symmetric and positive definite. This means that the permeability tensor has three principal directions and three positive principal values.

For an arbitrary homogeneous (uniform distribution of pores) anisotropic porous medium one can select the Cartesian frame of reference (x, y, z) in such a way that its axes are parallel with the three mutually orthogonal principal axes of the anisotropic porous medium, assuming they exist. Then the permeability tensor becomes diagonalized [172, 173]:

$$\underline{\underline{k}} = \begin{bmatrix} k_{xx} & 0 & 0 \\ 0 & k_{yy} & 0 \\ 0 & 0 & k_{zz} \end{bmatrix} \qquad\qquad (20)$$

where k_{xx}, k_{yy} and k_{zz} are the three principal components of permeability. If these three elements in each of the above matrices are known quantitatively, then the anisotropy of the medium is fully specified with respect to fluid flow [174]. In case of fibrous porous media it is common practice to assume that the z-axis is parallel to fibres axes, so k_{xx} and k_{yy} are the components of the permeability tensor in the principal directions perpendicular to the fibres and k_{zz} is the component of the permeability tensor in the direction parallel to the fibres. For a uniform bundle of fibres it is usually assumed that the filtration properties are equal in each direction perpendicular to the z-axis, which translates in $k_{xx} = k_{yy}$, the characteristic permeability of such a porous medium [174].

The permeability of any media can be experimentally determined or numerically calculated through a single flow of a Newtonian fluid through the media by means of Darcy's law. In case of fibrous porous media, numerous authors however tried to derive analytical expressions to connect the value of permeability with the geometrical properties such as porosity and diameter of the fibres [168, 174-180]. One of the early works by Neale in 1977 [174] provides several expressions for permeability of porous media composed of parallel circular monosized cylindrical fibres. The equations are given for Cartesian coordinates and it is assumed that the z-axis is parallel to the fibres axes and there is a same distance between the fibres in x and y direction. The first approach in [174] was suggested by Happel et al. [175] for the creeping Newtonian flow and gives the equations for the permeabilities perpendicular and parallel to the cylinder axis as:

$$k_x = -\frac{r^2}{8(1-\phi)}\left[\ln(1-\phi) + \frac{\phi(2-\phi)}{\phi^2 - 2\phi + 2}\right] \qquad k_z = -\frac{r^2}{8(1-\phi)}\left[2\ln(1-\phi) + 2\phi + \phi^2\right] \qquad (21)$$

where k_x is the permeability in the direction perpendicular to the bars, k_z is permeability in the direction parallel to the bars, r is the radius of the bar and ϕ is porosity. The second, alternative prediction was developed at the same time independently by Kuwabara et al. [176]:

$$k_x = -\frac{r^2}{8(1-\phi)}\left[\ln(1-\phi) + \phi + \frac{\phi^2}{2}\right] \qquad\qquad k_z = 2 \cdot k_x \qquad (22)$$

In one of the recent studies [177], Boutin investigated permeability of fibrous porous media using both method of homogenization of periodic media (HPM) and self-consistent method (SCM). The HPM method derives the macroscopic Darcy's law from the Navier-Stokes equation at the pores scale. It also gives the theoretical expression of the Darcy's tensor, whatever the periodic microstructure. The SCM method computes the permeability from analytical solutions in simplified configurations. Dissimilar to HPM the microstructure

is not identified accurately, and if the basic analytical solution is correct, the application of the result to real porous media is generally conjectured. Boutin combined the HPM and SCM approaches in order to obtain results for permeability of classes of porous media with an explicit description of their microstructures. Applying the method to the fibrous media, the paper defined the values for the lower and upper bounds of permeability of fibrous materials, i.e. fluid-solid inclusions where flow is parallel or perpendicular to immersed parallel cylinders. These lower and upper bounds for permeability of a periodic configuration of parallel cylinders when the flow is perpendicular or parallel to the axis are given as:

$$k_{x_{bound}^{lower}} = -R_B \left(\ln(\rho_B) + (1-\rho_B)^2 / (1+\rho_B)^2 \right)/4 \qquad k_{z_{bound}^{lower}} = -R_B^2 \left(\ln(\rho_B) + (1-\rho_B)^2 / (1+\rho_B)^2 \right)/2 \qquad (23)$$

$$k_{x_{bound}^{upper}} = -R_B \left(\ln(\rho_B) + (1-\rho_B^4)/2(1+\rho_B^4) \right)/4 \quad k_{z_{bound}^{upper}} = -R_B^2 \left(\ln(\rho_B) + (1-\rho_B)^2 \cdot (3-\rho_B)^2/4 \right)/2 \qquad (24)$$

where R_B is half the distance between the centres of the cylinders and ρ_B is the ratio between the radius of the cylinders and R_B.

Most recent studies concerning the permeabilities of fibrous porous media can be found in [178-180]. In [178] the authors studied the permeability of ordered fibrous media for normal and parallel flow analytically. Several fibre arrangements including touching and non-touching arrays were considered. In [179] the same authors studied the flow parallel to ordered fibres analytically. The considered fibrous media were made up of in-line (square), staggered, and hexagonal arrays of cylinders. Starting from the general solution of Poisson's equation, compact analytical solutions were proposed for both velocity distribution and permeability of the considered structures. The permeability for the squared array of cylinders for the flow perpendicular and parallel to the array is given as:

$$k_x = \frac{d^2 \cdot 0.16}{\sqrt{1-\varphi}} \cdot \left[\frac{\pi}{4\varphi} - 3\sqrt{\frac{\pi}{4\varphi}} + 3 - \sqrt{\frac{4\varphi}{\pi}} \right] \qquad k_z = \frac{d^2}{16\varphi} \left[-1.479 - \ln\varphi + 2\varphi - \frac{\varphi^2}{2} - 0.0186\varphi^4 \right] \qquad (25)$$

where k_x is the permeability in the direction perpendicular to the bars, k_z is permeability in the direction parallel to the bars, d is the diameter of the bar and φ is the solid volume fraction (of the porous medium) defined as $\varphi = 1 - \phi$, where ϕ is porosity.

2.3.3.3 Shift factor α

For non-Newtonian fluids, flow rate is correlated with the in-situ shear rate within the porous medium [159] and this correlation is frequently expressed as:

$$\dot{\gamma}_{pm} = \frac{\alpha v_d}{\sqrt{k\phi}} \qquad (26)$$

where α is a medium dependent shift factor, also called shape factor. Shift factor is function of the topology of the porous medium, as well as of the flow and the properties of

the propagating fluid. This quantity is usually found by experiment [181], but it is also possible to calculate it using pore-scale modelling approaches [147]. An early work by Sorbie et al. [148] gave an overview of the theoretical and empirical models for the functional relationship between the equivalent shear rate and Darcy's velocity for the single flow of various polymers in porous media. Although by different approaches, all the authors showed that the average in situ shear rate in the network (which corresponds to $\dot{\gamma}_{pm}$) actually varied linearly with the flow velocity and was a linear function of $v_d/\sqrt{k\phi}$. When using 2D bundle capillaries model, the dependency factor α is said to be equal $4/\sqrt{8}$ for the bundle of capillaries of uniform diameter. The experimentally determined values lied in the range of 1.5 to 2.5 for packed glass beads and in the range of 4 to 7 for sand.

Pearson and Tardy [158] reviewed the different mathematical approaches used to describe non-Newtonian flow in porous media. They concluded that none of the present continuum models gives accurate estimates of macroscopic transport properties: α is a function of both the bulk rheology and the pore structure and currently there is no theory that can predict its value reliably. Reported values of α vary from 1 to 15. Nevertheless, the fact that the empirically obtained value is always $\alpha \geq 1$ implies that the shear rate in the porous medium is underestimated, and empirical parameter has to be used to match up the data between the bulk and porous medium measurements.

Lately some sophisticated studies were performed using 3D pore scale models [147, 155] to model various sand packing. In [155] Valvatne et al. numerically studied the relation between the flow rate and the viscosity for the polymer solutions. The bulk rheology was well-described using a truncated power law. The authors used an adjustable scaling factor α to fit the analytical solutions with experimental and numerical data. Reported values for α were in the range 1 to 5.2 and varied with different porous media and fluid systems.

2.3.4   Conclusions

To model the flow of complex fluids through the porous media, approximate models are in use. The most common approach is to use macroscopic averaging methods and to define the apparent shear rate and the apparent viscosity within the medium and in Darcy's equation. The arrays of cylindrical obstacles such as rebars in a formwork can be approximated as fibrous porous media and modelled using the macroscopic approach.

The unknown parameters of the porous media are porosity, permeability and shift factor. The porosity can be easily calculated from the known PM geometry. The permeability of a medium is a tensor with 6 independent components. For the case of fibrous porous media, the permeability tensor can become diagonalized and can have three independent

permeabilities. The components of the permeability tensor can be calculated either from the experimental measurements or from the numerical simulations with a given Newtonian fluid and applying Darcy's law. Numerous authors studied parallel and perpendicular permeability of fibrous media and developed analytical expressions correlating the permeability to diameter of the bars and porosity. A common result for all the analytical solutions is that the permeability is directly proportional to the square of the bar diameter, where the coefficient of proportionality is dependent on porosity.

The determination of the shift factor α is a difficult task, and there is no established method for its calculation. A number of authors tried to determine this factor experimentally and numerically: values of α were found to vary from 1 to 15.

3 Model for SCC flow through reinforced zones – the porous medium analogy

The brief overview of the state of the art in concrete industry presented in Chapter 2 pointed out the main difficulties during characterisation and placement of SCC. It also showed that the fresh concrete workability (its ability to fill the mould properly without reducing the concrete quality) cannot be always predicted using standard experimental techniques. This emphasised the need to have a numerical tool able to predict concrete behaviour during casting. Such a tool should help engineers to avoid expensive mistakes on site and therefore has to be praxis oriented, user friendly and as fast as possible.

Since most concrete structural elements are (often heavily) reinforced, the focus when developing such a tool has to be placed on the modelling of the flow of concrete in presence of rebars. In any computer simulation of concrete casting, if one models steel bars one by one, the total time needed for the simulation will be very high. However, the geometry of the arrays of rebars corresponds to a scaled geometry of a typical fibrous porous medium. Thus, in order to reduce computational time and to come closer to a practical tool to simulate concrete casting, this thesis suggests to model the network of steel bars as a homogeneous porous zone [14-16]. The illustration of the idea is shown in Figure 15, which provides a 2D representation of a rectangular box containing arrays of aligned rebars and its porous medium analogy.
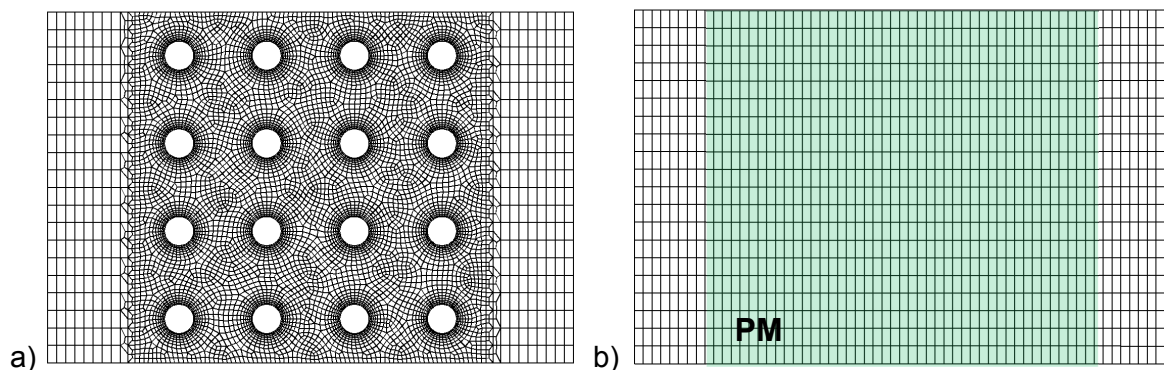
Figure 15: Schematic representation of a) steel bars reinforcement b) reinforcement treated as a porous medium [14-16].

In order to demonstrate the expected decrease in simulation time, which can be achieved if one uses the porous medium analogy instead of the real geometry with all the rebars, one has to consider the duration of all numerical simulation phases. As explained in Section 2.2.2, the total time needed for a numerical simulation includes two key phases: the pre-processing phase and the computational phase. During the pre-processing, the geometry is built and the mesh is generated, i.e. the whole domain is discretised into a finite number of elements (cells, volumes). During the computational time the fluid

governing equations are numerically solved for each finite element (volume, node) within the domain and the properties of the whole domain are evaluated by superposing the properties of the elements.

The example in Figure 15 shows that the geometry to be modelled is obviously far simpler in the case of the porous medium analogy than in the case with bars. As a consequence, the pre-processing time (needed to build up the geometry and to generate the mesh) will be strongly reduced in the case of homogeneous porous medium. However, it is difficult to estimate exactly to what extent the time needed for geometry and mesh generation will decrease. As some symmetric geometries are considered here, it is possible to assume that the pre-processing time shall decrease by a factor 10 between the cases with and without steel bars (if ten is being the number of obstacles in one direction, the use of copy-paste functions will allow for a fast meshing of the rest of the domain). It is also obvious that the number of elements needed to generate PM (around 1200 cells) is significantly lower than on the geometry with discrete representation of rebars (approx. 8700 cells). As the number of mesh elements decreases, the number of equations that have to be solved also decreases, and it is to be expected that the computation time will also be significantly reduced (a rough approximation is that this time will be 8 times lower in the case of porous medium geometry). Thus the expected reduction in total time can be around 80 percent, which, as a first assumption, justifies the idea to treat the reinforced zone as a PM.

In addition to this simplification of the geometry, where the rebars zone is modelled as a homogenous porous medium, the second major approximation in the presented work is that fresh SCC is assumed to be a homogenous material and proposed to be modelled as a one-phase non-Newtonian fluid. According to [182], from a physical and modelling point of view, fresh concrete can be considered as a fluid when the granular nature of the material can be neglected compared to the hydrodynamic interactions within the material. This assumption is in general fulfilled for stable materials with lower than average contents of coarse aggregates such as concretes with slumps higher than 15 cm and SCC [6, 183].

Moreover, identifying concrete as a homogeneous fluid means that, in any two parts of the observed volume, we should find similar ensembles of components [35]. According to [62], the scale of observation is thus of great importance to choose whether or not a homogeneous fluid approach is legitimate. The order of magnitude of a formwork characteristic size is of the order of decimetres while the size of the coarsest particles is of the order of centimetres. This means that, if, as a first approximation, the presence of the steel bars is neglected, the flow in a typical formwork can be considered as the flow of a homogeneous fluid [62].

If the steel bars are present, segregation and blocking of coarse particles can occur, leading to non-homogeneities within the material and influencing the final shape of the flow and the quality of the final product. Although the yield stress of concrete allows for filling of reinforced formworks and determines the material final shape [48], the blocking of coarse particles cannot be ignored. As mentioned in 2.2.3, in [141], while studying probabilistic passing ability of fresh concrete, Roussel et al. introduced a so-called blocking parameter P, a dimensionless factor that can capture the transition between the blocking and passing. Accordingly, for each particular filling case, the corresponding parameter P should be calculated and used as a limiting criterion determining whether yield stress or blocking dominates the flow.

The changes in the material structure caused by blocking and segregation can be numerically fully described only when using multiphase models, which take both liquid and dispersed phase into account. In Section 2.2.2 it was shown that such a comprehensive model able to simulate concrete as a multiphase suspension is still not developed [9, 10, 184]. In the present thesis, the author does not aim to develop such a multiphase model that takes into account particles and their migrations, but solely to study the macroscopic influence of a reinforcement network on the concrete flow behaviour. The modelling is strictly restricted to the cases where the probability that some of the coarse aggregates form granular arches within the flow is negligible and one can assume that yield stress only determines the flow behaviour through the obstacles [80, 142]. We assume that blocking does not occur and our model is therefore limited to stable, non-segregating and non-blocking concretes. Most fluid concretes in standard industrial casting satisfy the above-mentioned constraints and their flow can therefore be described as a flow of homogeneous non-Newtonian fluids.

Consequently, based on the two above-mentioned simplifications of concrete and reinforcement, this thesis suggests to model the flow of concrete through a reinforced zone as a free-surface flow of a yield-stress fluid through a continuous porous medium. This chapter will describe the proposed model and its governing equations. We start in Subchapter 3.1 with the flow constitutive and continuity equations, which depict fresh concrete as a Bingham fluid. Subchapter 3.2 is devoted to the porous medium analogy used to describe arrays of steel bars. It gives the equations valid within the medium and proposes the method for calculation of unknown parameters in these equations. Subchapter 3.3 will provide a short description of the standard ANSYS Fluent© models for Bingham materials, it will explain the implementation of our porous medium model into this software and point out the modifications that have to be made to original ANSYS Fluent© equations. Eventually, the proposed approach and the implemented model have to be evaluated and validated. In Subchapter 3.4, the planned research steps, employed to numerically and experimentally validate the proposed model, are explained.

3.1   Governing equations of concrete flow

3.1.1   Constitutive equations

The rheological behaviour of a material is mathematically sublimated in its constitutive equation. In the studies concerning concrete rheology [32, 58, 60, 184-187], several authors pointed out that the Bingham equation is the most suitable approach to describe the rheological behaviour of flowable concretes (Section 2.2.1.2). Based on this assumption and on the conclusion of the previous paragraphs, in this thesis SCC will be described as a non-compressible Bingham fluid. The viscosity of a Bingham fluid is not constant, but is dependent on the local shear rate $\dot{\gamma}$ [82, 83]. Bingham fluid exhibits a finite yield stress at zero shear rate: for applied stresses lower than the yield value, the material behaves as an elastic body; for applied stresses greater than the yield value, the viscosity changes linearly. A constitutive equation defining viscosity of a Bingham fluid writes:

$$\eta(\dot{\gamma}) = \frac{\tau_0}{\dot{\gamma}} + \eta_{pl} \tag{27}$$

where $\eta(\dot{\gamma})$ is the apparent bulk viscosity, $\dot{\gamma}$ is the shear rate and τ_0 and η_{pl} are respectively the yield stress and the plastic viscosity of the material. For a general 3D flow, the shear rate $\dot{\gamma}$ can be defined as:

$$\dot{\gamma} = \sqrt{2D_{II}} = \sqrt{2tr(\underline{\underline{D}}^2)} \tag{28}$$

where D_{II} is the second invariant of the strain rate (deformation rate) tensor $\underline{\underline{D}}$ and tr denotes trace of a tensor. The strain rate tensor $\underline{\underline{D}}$ is a second order tensor defined as:

$$\underline{\underline{D}} = \frac{1}{2}\left(\nabla \underline{v} + \nabla^T \underline{v}\right) \qquad D_{ij} = \frac{1}{2}\left(\frac{\partial v_i}{\partial x_j} + \frac{\partial v_j}{\partial x_i}\right) \tag{29}$$

where $\underline{v}$ is the velocity vector, ∇ is so called nabla operator, D_{ij} is the ijth component of the strain rate tensor and v_i is the component of the velocity in the direction x_i.

The Bingham equation takes into account the yield stress behaviour of fresh concrete. There are however two more phenomena occurring during concrete flow that should be discussed, namely shear-thickening behaviour and thixotropy (details in section 2.2.1.1). As already mentioned in 2.2.1.1, the shear-thickening behaviour is important for the processes where concrete is exposed to high shear rates such as, for example, pumping and mixing. Thixotropy, on the other hand, is important when analysing effects such as formwork pressure or multi-layer casting.

In this thesis, the flow of concrete through reinforced formworks during casting is studied, with the goal to predict if the material will properly fill in the form (i.e. to predict its flow distance and the free-surface final shape). Thus we are particularly interested in the flow at stoppage, which is a slow, laminar flow, where high shear rates are not likely to occur. Consequently, shear-thickening is not expected to play a dominant role. Furthermore, thixotropy can occur when shear is high, for example during pumping. At the end of the casting, which we focus on here, the flow velocity is reduced and the viscosity is recovered. Finally, both thixotropic and shear-thickening effects influence predominantly the plastic viscosity of the material and not the yield stress [21, 61, 65, 66, 74, 76, 182]. In this thesis, the focus is not placed on the casting velocity (which depends on material plastic viscosity), but on the final shape of concrete when it stops flowing. Since the final shape and the flow distance of the material are determined only by yield stress [47, 48, 188], the viscosity changes caused by shear-thickening and thixotropy shall not influence the final result.

Therefore, as a first approach, thixotropy and shear-thickening behaviour are not taken into account in the model. Nevertheless, the model leaves open the possibility to include these effects into the model equations. The viscosity equation can be easily extended from Bingham to the Herschel-Bulkley (Equation 3), so that shear-thickening behaviour is taken into account. Thixotropy can, without difficulty, be included into system equations as well, by extending the viscosity equation by some of the well-known thixotropy models (as for example the model of Roussel [66]). This however will not be topic of this work and implementation of Herschel-Bulkey model or a thixotropy model is not planned in this thesis.

3.1.2   Conservation equations

The cornerstone of the computational fluid dynamics are the fundamental governing equations of fluid dynamics - the mass, momentum and energy conservation equations (see 2.2.2.1 for details). The mass conservation equation of concrete flow is the continuity equation of an incompressible fluid and writes:

$$\underline{\nabla} \cdot \underline{v} = 0 \qquad (30)$$

where $\underline{v}$ is the local velocity vector and $\underline{\nabla}$ is so called nabla (del) operator. For the Cartesian coordinate system the mass conservation equation writes:

$$\sum \frac{\partial v_i}{\partial x_i} = \frac{\partial v_x}{\partial x} + \frac{\partial v_y}{\partial y} + \frac{\partial v_z}{\partial z} = 0 \qquad (31)$$

where v_i is the component of the velocity in the direction x_i; v_x, v_y and v_z are components of the velocity vector in the directions x, y and z respectively.

The general form of conservation of momentum is given by:

$$\rho \frac{D\underline{v}}{Dt} = -\underline{\nabla} p + \underline{\nabla} \cdot \underline{\underline{S}} + \rho \underline{g}$$ (32)

where D is the so called convective derivative, t is time, ρ is density, p is pressure and $\underline{g}$ denotes gravity. In the Cartesian coordinate system, for each direction i, the momentum conservation equation writes:

$$\rho \left(\frac{\partial v_i}{\partial t} + v_i \frac{\partial v_i}{\partial x_i} + v_j \frac{\partial v_i}{\partial x_j} + v_k \frac{\partial v_i}{\partial x_k} \right) = \frac{\partial p}{\partial x_i} + \eta \left(\frac{\partial^2 v_i}{\partial x_i^2} + \frac{\partial^2 v_i}{\partial x_j^2} + \frac{\partial^2 v_i}{\partial x_k^2} \right) + \rho g_i$$ (33)

The viscous dissipation and non-Newtonian effects are reflected in the definition of the extra stress tensor $\underline{\underline{S}}$, which depends on bulk viscosity following:

$$\underline{\underline{S}} = 2 \cdot \eta(\dot{\gamma}) \cdot \underline{\underline{D}}$$ (34)

Where $\underline{\underline{D}}$ denotes the strain rate tensor (defined in Equation 29) and $\eta(\dot{\gamma})$ is the bulk viscosity of the material which depends on shear rate $\dot{\gamma}$ following the Bingham model given in Equation 27. The conservation of energy has to be taken into account only if the flow leads to compression of the fluid, then one must consider thermodynamics. Since concrete flow can be assumed incompressible, the conservation of energy does not have to be derived here.

3.2   Model of flow through porous medium

The proposed model approximates a zone in a concrete formwork formed by arrays of rebars as a fibrous porous medium. As mentioned in Subchapter 2.2, the fibrous PM are thoroughly studied in other engineering fields and the common approach to include the influence of porous medium is to use continuum macroscopic models, e.g. to modify model equations to account for presence of the porous matrix as a continuous medium. In this thesis a macroscopic approach is chosen, where one includes the influence of PM on the flow by defining so-called apparent shear rate and apparent viscosity within the porous medium. Consequently, the constitutive and conservation equations have to be modified to include these apparent properties.

From a mathematical point of view, the influence of the PM formed by rebars on the flow is included in the model by the addition of a momentum source term to the standard momentum flow equations (right side of Equation 32). Since the flow in industrial casting of concrete is mostly laminar, the inertial loss term can be neglected and the source term is only composed of a viscous loss term. The pressure drop then reduces to Darcy's law [189] (details in Subchapter 2.3), which in 3D general form can be written as:

$$\underline{v} = -\frac{\underline{\underline{k}}}{\eta}\nabla p \qquad \text{i.e.} \qquad \begin{bmatrix} v_x \\ v_y \\ v_z \end{bmatrix} = -\frac{1}{\eta}\begin{bmatrix} k_{xx} & k_{xy} & k_{xz} \\ k_{yx} & k_{yy} & k_{yz} \\ k_{zx} & k_{zy} & k_{zz} \end{bmatrix} \cdot \begin{bmatrix} \dfrac{\partial p}{\partial x} \\[4pt] \dfrac{\partial p}{\partial y} \\[4pt] \dfrac{\partial p}{\partial z} \end{bmatrix} \tag{35}$$

where $\underline{v}$ is Darcy's velocity, $\underline{\underline{k}}$ is permeability and ∇p is the pressure gradient. The permeability tensor $\underline{\underline{k}}$ is symmetric so it holds: $k_{ij} = k_{ji}$. If x, y and z coincide with axes of permeability (for porous media formed by cylindrical obstacles if one of the coordinate axes is parallel to the cylinder axes) it can be written:

$$\begin{bmatrix} v_x \\ v_y \\ v_z \end{bmatrix} = -\frac{1}{\eta}\begin{bmatrix} k_x & & \\ & k_y & \\ & & k_z \end{bmatrix} \cdot \begin{bmatrix} \dfrac{\partial p}{\partial x} \\[4pt] \dfrac{\partial p}{\partial y} \\[4pt] \dfrac{\partial p}{\partial z} \end{bmatrix} \tag{36}$$

where the k_x, k_y and k_z are principal values of permeability (details in 2.3.3.2). Equation 36 holds only for the parallel or perpendicular bars, when the principal axes coincide with the coordinate axes. For the other bar arrangements, a local transformation or a prior determination of the principal axes has to be carried out. Nevertheless, the reinforcement steels are usually either in parallel or perpendicular arrangement, so it can be considered that Equation 36 is valid for the reinforcement bars. Introducing the apparent viscosity η_{app} in Equation 35, Darcy's law writes:

$$\underline{v} = -\frac{\underline{\underline{k}}}{\eta_{app}}\nabla p \tag{37}$$

Accordingly, the added momentum source term, which includes the extra pressure drop within the porous zone and which is modelled applying Darcy's law, is given as:

$$S_i = -\frac{\eta_{app}}{k_i}v_i \tag{38}$$

where S_i is the source term in the direction i, η_{app} is the apparent viscosity, k_i is the permeability coefficient in the direction i and v_i is Darcy's velocity in the direction i. For Newtonian materials, the apparent viscosity is the constant Newtonian viscosity of the material. For Bingham materials, apparent viscosity depends on the local strain rate in the flowing material. Since the local strain rate is unknown and is a complex function of the geometry and disposition of the steel bars, one has to define a so-called "apparent" shear rate $\dot{\gamma}_{app}$ within the medium as:

$$\dot{\gamma}_{app} = \frac{\alpha_i \cdot v_i}{\sqrt{k_i \cdot \phi}} \tag{39}$$

where α_i is the shift factor in the i direction and ϕ is the PM porosity (the volume of the voids divided by the volume of the porous zone). If we assume that the apparent viscosity is a function of the apparent shear rate as given in Equation 27 and then implementing this apparent viscosity into the Equation 38, the source term in the momentum equation writes:

$$S_i = -\frac{1}{k_i}\left(\frac{\tau_0 \cdot \sqrt{k_i \cdot \phi}}{\alpha_i} + \eta_{pl}v_i\right) \tag{40}$$

The source term will be finally added to the right side of the momentum equation (Equation 32) as

$$\rho\frac{D\underline{v}}{Dt} = -\underline{\nabla}p + \underline{\nabla}\cdot\underline{\underline{S}} + \rho\underline{g} + \underline{S} \tag{41}$$

where $\underline{S}$ is the added source term. For the Cartesian coordinates $\underline{S}$ is defined as:

$$\underline{S} = \begin{bmatrix} S_x \\ S_y \\ S_z \end{bmatrix} \tag{42}$$

The final expression for the ith component (i being x, y or z) of the momentum conservation equation for concrete flow within the porous medium formed by rebars is given as:

$$\rho(\frac{\partial v_i}{\partial t} + v_i\frac{\partial v_i}{\partial x_i} + v_j\frac{\partial v_i}{\partial x_j} + v_k\frac{\partial v_i}{\partial x_k}) = \frac{\partial p}{\partial x_i} + \eta\left(\frac{\partial^2 v_i}{\partial x_i^2} + \frac{\partial^2 v_i}{\partial x_j^2} + \frac{\partial^2 v_i}{\partial x_k^2}\right) + \rho g_i + S_i \tag{43}$$

The final momentum equation contains five unknown parameters:
-   two material parameters, namely plastic viscosity η_{pl} and yield stress τ_0 and
-   three unknown parameters of porous medium: porosity ϕ, permeability k_i and shift factor α_i.

The overview of the determination of material and porous medium parameters is given in Sections 2.2.1 and 2.3.3 respectively.

At this stage, it can however be worth noting that the yield stress of concrete τ_0 can be relatively reliably determined from the rheometer measurements and through simpler test such as LCPC box [47] or slump flow [48]. In this thesis, the values of yield stress will be determined from LCPC box and slump flow measurements and verified by corresponding numerical simulations.

The determination of plastic viscosity of concrete is a more delicate issue and there is still no reliable universal technique to determine the value of plastic viscosity in absolute units from rheometer measurements [184]. In this thesis, this issue will be tackled by trying to determine the plastic viscosity of SCC from experimental data with the help of numerical simulations (see Section 8.4.1). The porosity ϕ can be easily calculated from the topology

of the PM (see Section 2.3.3.1). The permeability of any medium can be directly experimentally measured or numerically computed by a single steady-state measurement on a sample of given geometry crossed by a Newtonian fluid. The thesis proposes to determine values of permeability k numerically from the single flow simulations of Newtonian fluid flow through the particular rebars zone (see Subchapter 5.1). Then, again, there is no defined technique to calculate the unknown shift factor. Here a numerical method to estimate values of shift factor α, appropriate for modelling of slow concrete flow through PM (see Subchapter 6.1) will be suggested.

3.3   Model implementation into the CFD code

As a general CFD solver, ANSYS Fluent© provides four options for modelling viscosity of non-Newtonian flows: power law model, Carreau model, Cross model and Herschel-Bulkley model for Bingham plastics [190]. Since the Herschel-Bulkley (H-B) equation becomes Bingham if the value of the power law parameter is equal 1, the H-B model will be used in this thesis. In the Bingham viscosity equation (Equation 27), when shear rate approaches zero, the viscosity strive towards infinity. From the numerical point of view, this means that for the very low and zero shear rates, the model becomes invalid. In order to be able to use it in a numerical code, the Bingham equation has to be modified (i.e. regularised [191]). For the regularisation of the Bingham equation in ANSYS Fluent© the so-called bi-viscosity model is used [192]. This model introduces a so-called critical shear rate as:

$$\dot{\gamma}_{\text{crit}} = \frac{\tau_0}{\eta_0} \tag{44}$$

where $\dot{\gamma}_{\text{crit}}$ is the critical shear rate, τ_0 is the yield stress and η_0 is the initial value of viscosity, which should be assumed very high. Then, the regularised Bingham equation is given by:

if $\dot{\gamma} < \dot{\gamma}_{\text{crit}}$ $\qquad \eta = \eta_0$ $\qquad\qquad\qquad\qquad \tau = \eta_0 \dot{\gamma}$

$$\text{If } \dot{\gamma} \geq \dot{\gamma}_{\text{crit}} \qquad \eta = \frac{\tau_0}{\dot{\gamma}} + \eta_{\text{pl}} - \frac{\tau_0}{\eta_0 \cdot \dot{\gamma}} \qquad\qquad \tau = \tau_0 + \eta_{\text{pl}} \dot{\gamma} - \frac{\tau_0}{\eta_0} \tag{45}$$

For strain rates lower than $\dot{\gamma}_{\text{crit}}$, the "rigid" material acts like a very viscous fluid with viscosity η_0. As strain rate increases and the yield stress threshold τ_0 is passed, the fluid behaviour is linear for the Bingham fluid. The schematic representation of the bi-viscosity model is given in Figure 16.

The conservation equations for the incompressible fluid used by ANSYS Fluent© correspond to Equations 30 - 33 [190]. In this study, the viscosity equation and the mass conservation equation will not be modified; the only one to be modified is the momentum conservation equation. The source term that describes the extra pressure drop in the

rebars zone has to be added on the right side of the momentum equation as shown in Equation 43.
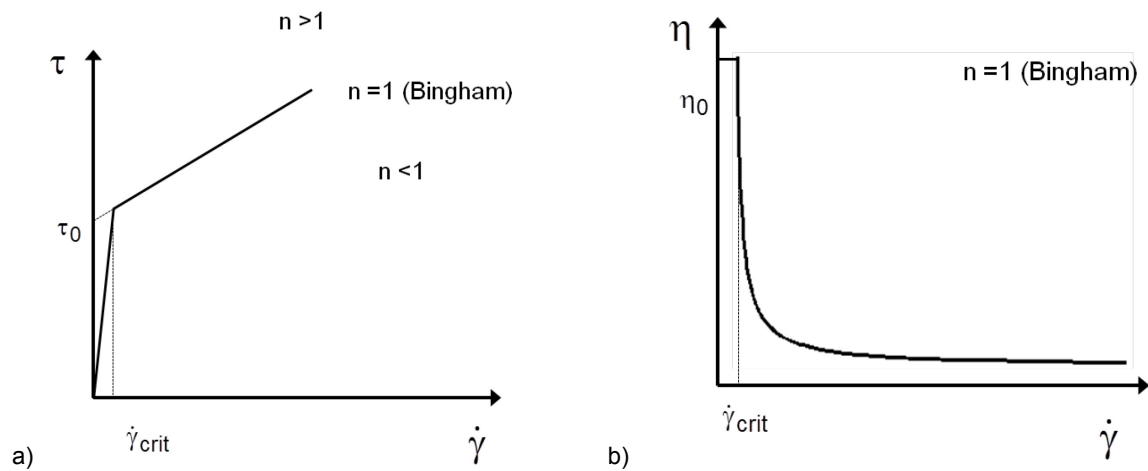

Figure 16: An illustration of the bi-viscosity model for Herschel-Bulkley and Bingham fluid used by ANSYS Fluent©: a) shear stress as a function of shear rate, b) viscosity as a function of shear rate.

To implement this term into the program code, one has to write a so-called User Defined Function (UDF) for the source term in x, y and z direction. The UDF is a short code written in C programming language, which is compiled and hooked to ANSYS Fluent© (for details refer to [193]). In this particular case, a short code is written to calculate the value of the source term S_i for the porous zone according to Equation 40.

definition of exact geometry of PM (size, boundaries)

implementation

UDF for source term:

$$S_i = -\frac{1}{k_i}\left(\frac{\tau_0 \cdot \sqrt{k_i \cdot \phi}}{\alpha} + \eta_{pl}v_i\right)$$
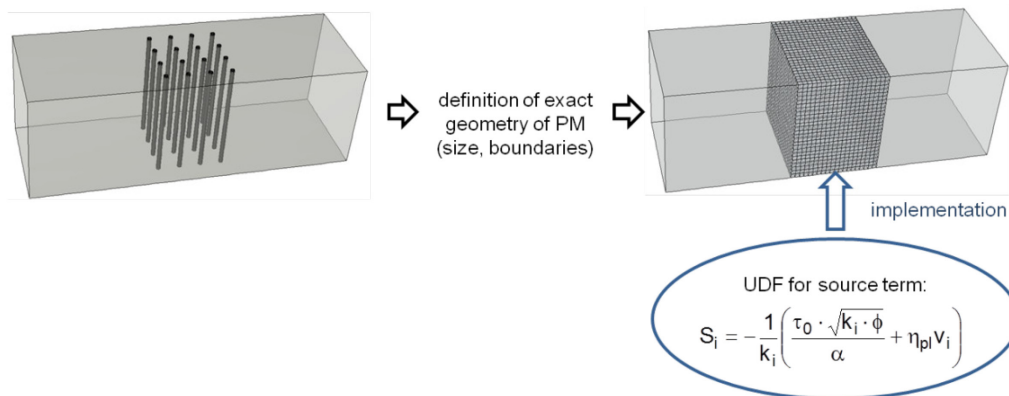
Figure 17: An illustration of implementation of the model into ANSYS Fluent©. Geometry with rebars (left), a porous medium analogy (right).

In Section 2.2.2 it was indicated that each CFD simulation consists of pre-processing, calculation and post processing phase. Figure 17 shows an illustration of the actual pre-processing steps needed to implement the model into the programme code, which enables to simulate an exact geometry as the corresponding PM geometry. Firstly, the exact geometry has to be fully defined meaning that one has to know the dimension of the formwork, the size of the bars and their distance, size of the zone etc. In order to be able to build the geometry and mesh for the PM case, the exact dimensions and boundaries of

the porous zone has to be defined. For details on how to define the exact boundaries of the PM see Subchapter 5.3. After the geometry of the zone is defined, the mesh is built (in the present case using the software Gambit©). As the next step, the boundary conditions for the porous zone have to be set up. Here one has to choose "source terms" in the boundary conditions menu and to choose the user defined momentum source term. An UDF to define this source term has to be written and implemented in ANSYS Fluent©. With this, the extra pressure drop in x, y and z direction, caused by the presence of rebars, is added. The computation and post processing procedure are the same as for any other CFD simulation.

3.4 Programme of the research steps towards model validation

The PM approach to simulate SCC casting through the reinforced formworks and the mathematical model, which is the core of the proposed approach, have to be validated. This means that it has to be demonstrated that, within defined limitations, the numerical tool proposed in Chapter 3 works correctly when used to simulate concrete flow. Since the material and the model themselves are complex (including complex non-Newtonian behaviour, several model approximations, several hypotheses to check and various unknown parameters), it is not reasonable to start directly with numerical simulations of SCC industrial casting. The model validation is therefore done stepwise, whereby each step is devoted to prove only one point (i.e. one hypothesis at a time). Each research step that follows iteratively includes one additional hypothesis to be demonstrated. The model validation is divided in three clearly defined phases and five work packages (WP).

Phase 1: Preliminary phase

WP 1: Software calibration – concrete flow, no obstacles (Chapter 4).
The mathematical model shown in preceding equations is to be implemented into a CFD software. Before implementation of the computational model and before starting calculations with porous media analogy, one has to be sure that the chosen software ANSYS Fluent© is an appropriate code for this task, by proving that the code is able to properly simulate the free-surface flow of concrete. In order to verify that, numerical simulations of standard concrete experiments such as slump and channel flow (without obstacles) will be performed. Concrete is here modelled as a non-Newtonian fluid. Besides, in this phase, some sort of software calibration is performed, where it is tested which type of mesh, flow conditions, boundary conditions as well as software options and numerical parameters are the best choice for numerically stable and yet correct simulations of free-surface flow of concrete.

Phase 2: Model validation

WP 2: The Newtonian fluid flow with obstacles – numerical validation (Chapter 5).

At this point, cylindrical obstacles are included. In the present approach, it is assumed that the permeability of the zone with obstacles (rebars) can be calculated from the numerical simulations with Newtonian fluid. It will be proved that this holds through the simulations of Newtonian fluid channel flow with cylindrical obstacles, by comparing the numerically obtained values of k with analytical ones. Moreover, numerical simulations of several different channels with obstacles are performed and compared with their PM analogies, where the permeability k is calculated numerically. Within this step, we prove that numerically calculated k is correct and that it can be used for PM simulations of the flow of random Newtonian material arrays of rebars.

WP 3:   Non-Newtonian fluid flow with obstacles, numerical validation (Chapter 6).
In this phase, the non-Newtonian effects are included. The second unknown parameter of the porous medium equation is shift factor α, which should be calculated numerically. Simulations with non-Newtonian fluids through various channels with cylindrical obstacles are performed to calculate α for a wide range of Bingham numbers. The proposed numerical technique for α calculation is afterwards validated on non-Newtonian fluid on several numerical case studies. The flow of yield stress fluids through channels with different disposition of vertical rebars are simulated using exact geometry and using the PM approximation and the results are compared.

WP 4:   Free-surface non-Newtonian fluid flow with obstacles, experimental validation (Chapter 7).
At this point the free-surface is introduced into the study. With proposed methods to calculate k and α the model is complete and can be applied to simulate real flow of non-Newtonian fluids through arrays of cylindrical bars. Experiments with model yield stress fluid Carbopol® are performed, and the model is validated through the comparison of the experimental results with numerical simulations of exact geometry with rebars and the simulation with porous medium approximation. This should prove that the developed model is valid for the free-surface flow of yield stress materials and it can be used to predict real castings of yield stress materials.

Phase 3: Model application

WP 5:   Free surface flow of concrete with obstacles, experimental validation (Chapter 8).
This phase is devoted to application of the model. Here it has to be finally proved that the model can be applied on realistic casting of cementitious materials. To come closer to the real casting conditions, a large-scale experiment is conducted, where concrete is poured in a highly reinforced beam. The experiment is simulated using the proposed porous medium model. The comparison of the experimental and numerical results and their good congruence should ensure that the proposed model and the methods for parameter determination provide reliable results.

3.5   Conclusions

This chapter presented the proposed model for SCC flow through the arrays of obstacles in a typical formwork and the scientific methodology chosen in the thesis to develop and validate this model. The model couples fluid dynamics approach for concrete flow and a porous medium approach to approximate geometry of the reinforced zones. Two major approximations are made here: the concrete is assumed to be a homogenous yield-stress fluid and reinforced zone is assumed to be a fibrous porous media. The first approximation is valid for flowable concretes such as SCC and when blocking do not occur. The proposed model is therefore limited to stable, non-blocking and non-segregating concretes.

Bingham constitutive equation is chosen to describe rheology of SCC. Since not relevant for the flow at stoppage, the model does not take into account thixotropy and shear-thickening behaviour, but can be easily upgraded to account for these effects. The flow of concrete in the formwork is governed by standard mass and momentum equations of incompressible fluid. Within the porous medium, the conservation equations are modified to include the influence of the bars. The extra source term based on Darcy's law is added to the right side of momentum conservation equation. The model is implemented into the CFD software ANSYS Fluent© by writing a UDF for the source term and adding this term to the standard momentum conservation equation.

The final equation for the flow through PM contains five unknown parameters: yield stress and plastic viscosity of the fluid, and permeability, porosity and the shift factor of the porous medium. In this chapter, the methods for calculation of the unknown parameters were also proposed. The proposed model has to be validated stepwise. Chapters 4 to 8 will be devoted to validation of the proposed model and to the description of the proposed methods to determine unknown model parameters.

4   Calibration of the numerical code

The model that was selected for the simulation of SCC flow is based on fluid dynamics and assumes that the fresh concrete is a non-Newtonian fluid. When using the fluid dynamics approach, the fluid flow is described by its fundamental governing equations explained in Chapter 3. The system of flow governing equations cannot be solved analytically for the whole flow domain; it has to be solved numerically by use of a Computational Fluid Dynamics (CFD). Available commercial CFD software are able to numerically solve the governing equations of a given flow and, by using various material models, to depict the material flow by means of simulation. The numerical solvers usually have most of the standard material and flow models integrated. Besides, some of the solvers offer the users a possibility to implement new user models and to customize existing models for some variables. In this thesis, to depict concrete's rheology within the porous zone formed by rebars, some apparent properties are to be defined within this zone. These equations, defining the apparent viscosity and shear rate in the porous medium, are to be implemented into such a CFD solver.

The CFD software ANSYS Fluent© was chosen in this thesis [194]. The ANSYS Fluent© is one of the most comprehensive software packages for CFD modelling available today, with wide range of physical modelling capabilities. Although being widely used for various engineering applications and being approved as a fast and accurate CFD solver, prior to implementation of the model, the software still has to be tested and "calibrated" for the specific problem to be modelled. Here, it should be verified that this code is appropriate for our study by proving its ability to depict the flow of cementitious materials, by demonstrating the general correctness of performed simulations.

All the flows of the cementitious materials are free-surface flows, where the large free surface can predominate the flow. It is actually the main point of interest to observe the propagation of this free surface and to determine its final shape and position when the material stops flowing. Therefore, a calibration of the software on a Hagen-Poiseuille flow of a Newtonian fluid is not reasonable, and the software should be adjusted by simulating the free-surface flows of non-Newtonian materials. For this purpose, we choose to simulate two benchmark concrete experiments: channel flow and slump flow. These are standard concrete testing procedures and their advantage is that they are analytically calculable: knowing material properties (such as yield stress and plastic viscosity) one can analytically calculate the flow length for a given material when it stops flowing [48, 72]. This in turn allows for an easy comparison between analytical and numerical results.

Thus two case studies are conducted, where propagation of yield-stress (Bingham) fluid in channel flow and Abram's cone experiment are calculated analytically according to [48] and [72], respectively, and simulated numerically using ANSYS Fluent©. At the end the

final shape of the flow front is compared. The results of these studies will be shown in 4.2 and 4.3. Before the channel and slump flow simulations, some preliminary studies on the boundary conditions and parameters of modified Bingham model had to be performed. The discussion on this topic is given in 4.1.

4.1   Boundary conditions and regularisation of the model

As explained in Subchapter 3.2, the CFD solver ANSYS Fluent© uses a regularised Herschel-Bulkley model for Bingham plastics. Generally, in numerical studies, the Bingham rheological model is replaced by a regularized model, that allows a-posterior determination of the yield surface and the use of a well-defined rheological description throughout the entire domain [165]. For the regularisation of Bingham equation ANSYS Fluent© uses the bi-viscosity model [190]. The bi-viscosity model introduces the critical shear rate, defined as a ratio between the yield stress τ_0 and the initial Newtonian viscosity [191]. For the strain rates lower than the critical one, the "rigid" material acts like an extremely viscous fluid with very high viscosity η_0. For the shear rates higher than critical one, when the yield stress threshold is passed, the material acts as a Bingham fluid with viscosity $\eta = \eta_{pl} + \tau_0 / \dot{\gamma}$.

This practically means that, when simulating Bingham fluid flow with ANSYS Fluent©, one has to define a third material parameter namely the initial Newtonian viscosity η_0. The viscosity η_0 is an artificial constant and to choose its value is a delicate task. It has to be high enough to keep the value of the critical shear rate low and to provide the simulated material behaviour, which is as close as possible to the real behaviour of the material. When flowing under its own weight with no external forces present, as soon as the shear stress is lower than the yield stress the Bingham plastic behaves as a solid body and completely stops flowing. Strictly speaking, at stresses lower than yield stress, a bi-viscous material would never stop flowing. That means that one has to choose sufficiently high value of η_0, so that at the low stresses occurring at the end of the flow, the material almost does not flow and its velocity tends to zero. This is however from a numerical point of view rather tricky, since very high viscosities can cause numerical instabilities.

Before starting the numerical case studies of the standard experiments, preliminary studies on channel flow were performed, where we tested different values of η_0 and its influence on the flow. Since yield stress and initial viscosity define the value of critical shear rate, the value of the initial viscosity should be chosen with respect to yield stress. For the channel flow to be presented here (see Figure 21), the values of initial viscosity that were chosen to be 10, 100, 1000 and 10000 times higher than the value of yield stress. The numerical tests showed that, from the numerical stability point of view and

regarding the flow stoppage, the best results were obtained when the ratio η_0/τ_0 was 1000 s, i.e., when the value of critical shear rate is $\dot{\gamma}_{crit} = 0.001$ s^{-1}. The diagram in Figure 18 shows the results for the shape of the flow front for the material with following properties: $\tau_0 = 50$ Pa, $\eta_0 = 50000$ Pa·s and $\eta_{pl} = 50$ Pa·s after 20, 30 and 50 s of flow time. One can see that the difference between the flow front after 30 s and 50 s is negligible and it can be assumed that material stopped flowing. This approves the chosen value of the initial viscosity η_0. In the simulations that follow, the initial value of viscosity will be always chosen as $\eta_0 = 1000 \cdot \tau_0 \cdot 1$s (or higher) whereby the critical shear rate is $\dot{\gamma}_{crit} = 0.001$ s^{-1} (or lower).
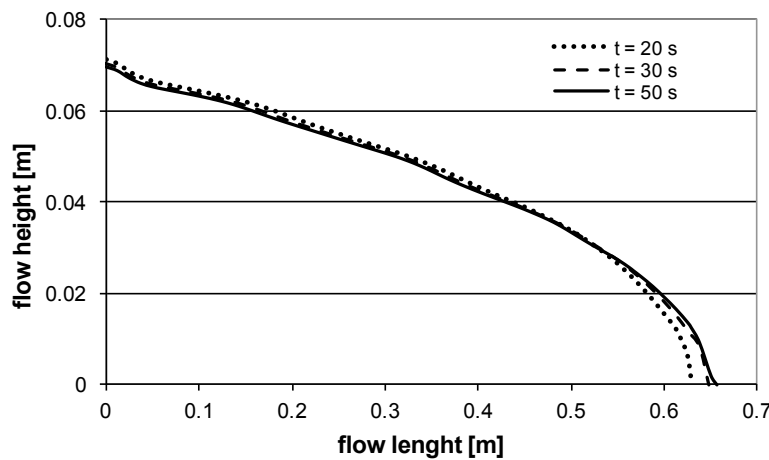

Figure 18: The preliminary tests on channel flow: comparison of the flow profile after 20, 30 and 50 seconds for the modified Bingham material with $\eta_{pl} = 50$ Pa·s, $\tau_0 = 50$ Pa and $\eta_0 = 50000$ Pa·s.

The next issue to discuss is the choice of the boundary conditions for the solid walls (in the particular cases studied in this chapter these are the slump flow base plate or the walls of the LCPC box, Figures 19 and 24, respectively). For an isothermal one-phase flow the ANSYS Fluent© offers two options for the contact between the material and the wall: no-slip and specified shear boundary condition [190]. In fluid dynamics, the no-slip condition for viscous fluids states that at a solid boundary, the fluid will have zero velocity relative to the boundary. The fluid velocity at all fluid–solid boundaries is equal to that of the solid boundary. Conceptually, one can think that the outermost molecules of the fluid are stuck to the surfaces, which come in contact with this flowing fluid [195]. In addition to the no-slip wall, one can model a slip wall by specifying zero or non-zero shear [196]. For non-zero shear, the shear stress is to be specified at the wall by the fluid, by entering x, y and z components of the shear stress. If the specified shear in all the three direction equals zero, we talk about full-slip wall boundary condition.

For the numerical studies performed in this thesis, the most correct approach for the wall-fluid interaction would be to use specified shear boundary condition and to specify the

exact values of the shear stress caused by friction between the fluid and the wall surface. This is however almost unfeasible, since one would have to determine the exact values of the friction coefficients for each single concrete and the specific material of the wall. Although there are some studies concerning tribology in concrete science, there still are no consistent methods to easily determine the friction coefficients [197, 198]. In this thesis, the aim is not to study the friction between different concrete types and different surfaces. Since it is not possible to determine the friction coefficients, the specified shear condition at the wall boundaries cannot be used. This basically means that we have to choose between the no-slip and full-slip condition for the base plate and the walls of the channel flow (as well as for the further studies in this thesis).

The LCPC box (as well as typical concrete formworks) is usually made of wooden plates while the base plate for the slump flow experiment is made of metal tin. During experiments, the fresh concrete flows smoothly and slowly along the surface but usually without slipping (at least none can be visually detected). So these surfaces are not slippery and, as a rough first approximation, we can say that the concrete behaviour in contact with these surfaces is closer to no-slip then to full-slip condition. Therefore in the following numerical studies, the full-slip boundary is applied only at the surfaces where no sticking is desired (for example in the funnel in Figure 20, where it is desired that entire material outflows the funnel). All the other walls and plates are though assumed to be no-slip walls.

4.2   Channel flow

Flow of fresh concrete through a horizontal channel is typical for standard experiments such as L-Box and LCPC-Box experiment [20, 47, 72, 104]. The L-box experiment is used around the world as a reference test for passing ability, flow rates and filling ability of SCC in confined spaces [20]. The L-box consists of concrete reservoir, slide gate, three parallel obstacles and horizontal test channel (Figure 19a). The vertical section is filled with concrete and subsequently the gate is lifted to allow concrete to flow into the horizontal section. When the flow stops, one measures the reached height of fresh SCC after passing through the specified gaps of steel bars and flowing within a defined flow distance. With this reached height, the passing or blocking behaviour of SCC can be estimated. The LCPC box test is shown in Figure 19b. The experimental setup is a simple cubic container and instead of flowing from the vertical container, the material is slowly poured directly into the horizontal box and the flow length is measured. It was proposed by Roussel in [47] as a simple method to determine yield stress of tested concrete. The author provided the analytical solution that enables determination of the yield stress when the final length of the material in the box is known.

In the first calibration study to be presented here, the channel flow as in LCPC box is calculated analytically and simulated numerically and the results are compared. The poured concrete volume is V = 6 l and the material properties are: yield stress τ_0 = 50 Pa, plastic viscosity η_{pl} = 50 Pa·s and density ρ = 2300 kg/m^3.
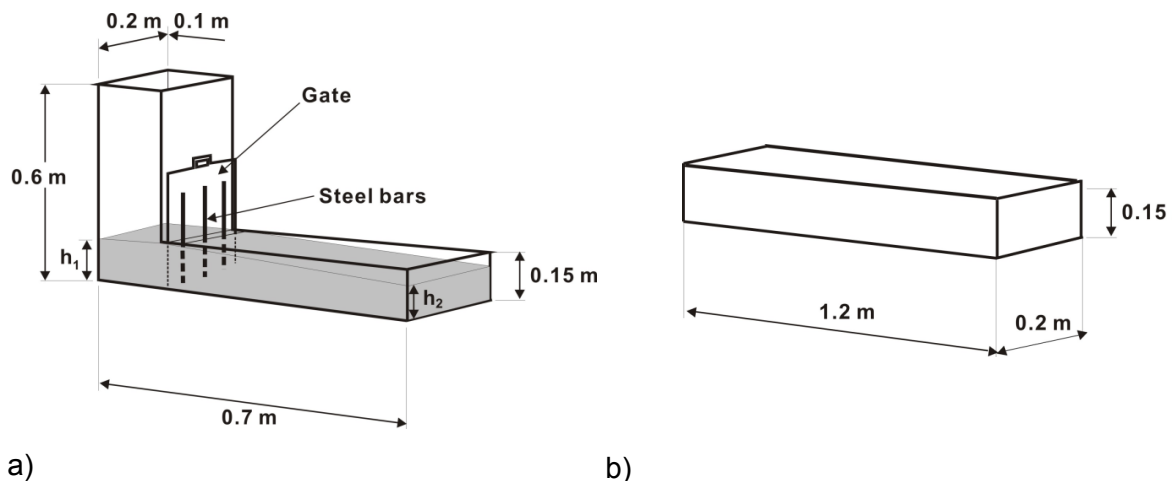

Figure 19: Drawings of the channel flow concrete experiments: a) L-box experimental setup [20], b) LCPC box experimental setup [47].

4.2.1 Analytical solution

In [72] the authors provided an analytical solution of the L-Box flow in the spreading regime (i.e. for the cases when the flow length is much greater than the thickness of the of the sample). They showed that it is possible to calculate the flow length of the material by knowing the material yield stress and vice-versa. The proposed method also applies to calculation of the channel flow spread and in this thesis will be fully taken from [72]. In the following paragraphs a short insight into the proposed analytical method is given.
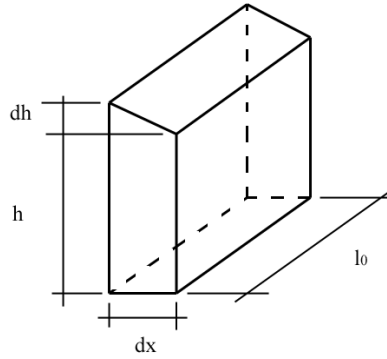

Figure 20: The elementary volume to calculate forces equilibrium in Equation 46 [72].

In [72], it was considered that the material is poured slowly into the box, so that inertia effects are negligible. The flow stops when the shear stress at the walls reaches the value of the yield stress of the material. Writing the force equilibrium on the elementary volume shown Figure 20 one obtains:

$$\rho g l_0 \frac{(h+dh)^2}{2} - \rho g l_0 \frac{h^2}{2} + \tau_0 l_0 dx + 2\tau_0 h dx = 0 \tag{46}$$

where g denotes gravity, ρ is density and τ_0 is the yield stress. The dimensions h, dh, dx and l_0 are depicted in Figure 20. By conserving the first order terms, the previous equation becomes:

$$\rho g h \frac{dh}{dx} = -\tau_0 - 2\tau_0 \frac{h}{l_0} \tag{47}$$

Furthermore, by replacing A = $2\tau_0/\rho g l_0$ and u = $2h/l_0$ one gets:

$$\frac{u}{1+u} \frac{du}{dx} = -\frac{2A}{l_0} \tag{48}$$

The solution of this differential equation is:

$$h_0 - h + \frac{l_0}{2} \ln(\frac{l_0 + 2h}{l_0 + 2h_0}) = Ax \tag{49}$$

where h_0 is the thickness of the sample at x = 0. This relation allows for calculating the overall shape of the sample. The total volume V of the sample is equal to:

$$V = \frac{l_0^3}{4A} \left(\ln(1+u_0) + \frac{u_0(u_0-2)}{2} \right) \tag{50}$$

70

With $u_0 = 2h_0/l_0$, Equation 50 allows for the computation of h_0 for a given tested volume V. The spread length in the channel may then be calculated using:

$$L = \frac{h_0}{A} + \frac{l_0}{2A} \ln\left(\frac{l_0}{l_0 + 2h_0}\right)$$

(51)

This relation allows the prediction of the spread length L when the yield stress τ_0 is known for a given concrete. In the further study, the equations 49 and 51 are used to calculate the final slope h(x) and length L, respectively.

4.2.2   Numerical simulation

The numerical simulation of the channel flow is conducted using two geometry variations depicted in Figure 21. In the first case, material is placed behind a gate and starts flowing when the gate is lifted. In the second case, the material flows under its own weight into the channel from a pouring funnel. Either way, the material flows slowly into the form, propagates under its own weight and eventually stops. At the moment of stoppage, the final flow length and shape are observed.

a)   b)
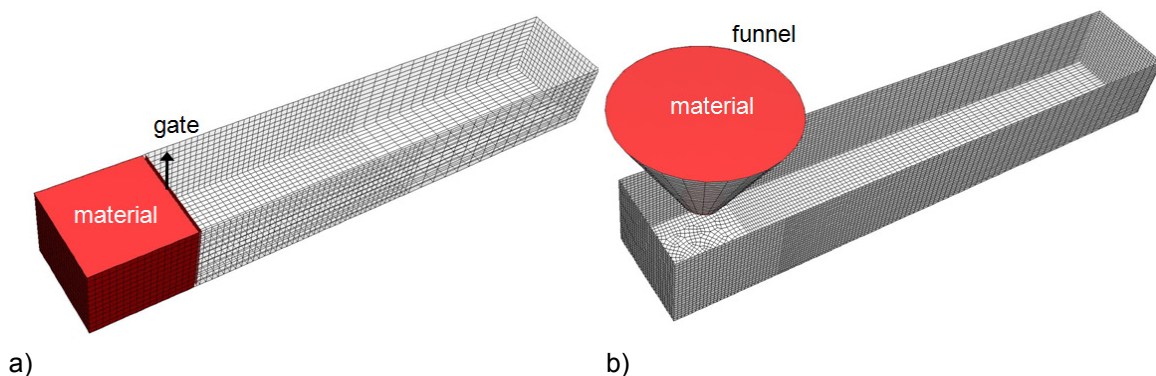
Figure 21:   Channel flow, mesh and initial position of the material: a) material placed behind the gate (channel 1); b) material poured through a funnel (channel 2).

All the numerical results were obtained using ANSYS Fluent© version 6.3.26 [194]. Before the simulations were finally conducted, to find the optimal solver and boundary settings, influences of different factors on the solution were investigated. The mesh was changed from coarse to fine in order to find the necessary fineness, which lead to a stable solution. As explained in Subchapter 4.1, the studies concerning the material parameters of the regularised Bingham model were conducted. Boundary conditions at the wall (full-slip or no-slip condition), at the inlet and the outflow (both the pressure and the mass flow inlet/outlet) were tested. 2D and 3D simulations were also compared.

Finally, the following settings were used for the simulations:
- 3D, implicit, pressure based solver;
- mesh is based on hexahedral mesh elements (around 27000 elements in the channel) ;
- concrete is modelled as an incompressible Bingham material;
- flow is set to be laminar;
- no-slip boundary conditions are used at the walls of the container;
- for the pouring case (Figure 21b), full slippage is used for the funnel walls;
- Volume of Fluid (VOF) model is used for the free surface calculation.

4.2.3   Comparison of analytical and numerical data

The comparison of the analytically and numerically obtained results is shown in Figure 22. The diagram shows the thickness of the material plotted as a function of the flow length at stoppage. For the numerical simulations, the shape is measured in the middle line of the channel. A good agreement between the analytical and numerical results can be seen, with the maximal difference in the final length being of 5%. This proves the correctness of the numerical solution: of the used solver as well as of the chosen boundary conditions, material and numerical settings. Figure 23 illustrates the flow shape in both simulations (with gate and with the funnel). The total computation time needed to obtain the final shape in Figure 23 left was 1 hour and 18 minutes. It can be observed that the way of pouring concrete in the horizontal channel has no influence on the final flow length, confirming that there are no inertia effects when carefully pouring the material or lifting the gate slowly.
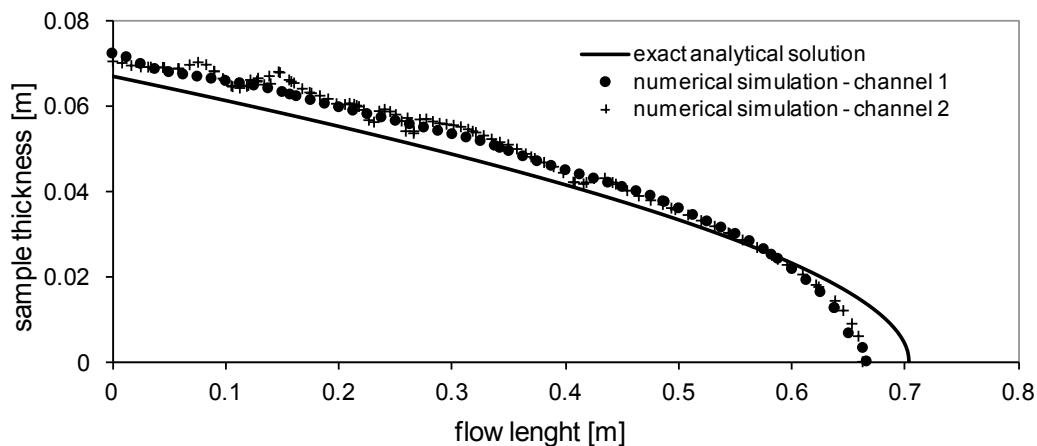

Figure 22:   Channel flow – profile of the material when the flow stops: a diagram comparing analytical solution with two numerical simulations. Channel 1 refers to the geometry with the gate and channel 2 to the geometry with the pouring funnel.
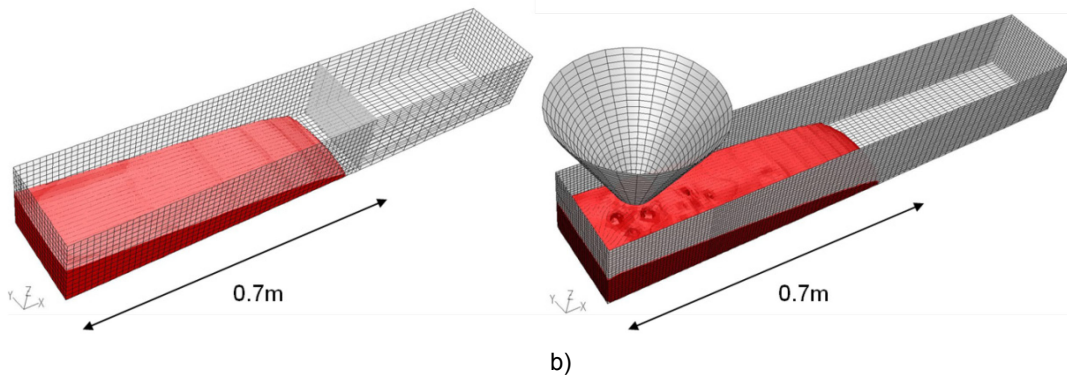
Figure 23: Simulation of the LCPC box, final shape of the material when the flow stops: a) numerical simulation with the gate (channel 1), b) geometry with the pouring funnel (channel 2).

4.3 Slump flow

Slump flow is the most widely used test in SCC technology [199]. Due to its simplicity, it is used in every day practice and on-site to measure the filling ability of SCC. It measures two parameters: flow spread and optionally flow time t_{50}. The former indicates the free deformability and the latter indicates the rate of deformation within a defined flow distance [20]. In the experiment, the Abrams cone is placed on a non-absorptive surface and filled with fresh concrete without any tampering, see Figure 24. Then the cone is lifted and the concrete flows out under its own weight. Two perpendicular measurements of the final diameter are taken across the spread of concrete and the average is reported. The flow diameter is a criterion of concrete's sufficient flowability [20, 199]. For instance, slump flow spread diameter values of 500 to 650 mm are considered satisfactory according to [200]. Khayat in [201] distinguishes between regular SCC and highly viscous SCC and sets a flow value of at least 570 mm spread diameter with a time T_{50} of 5 and 15 seconds, respectively.
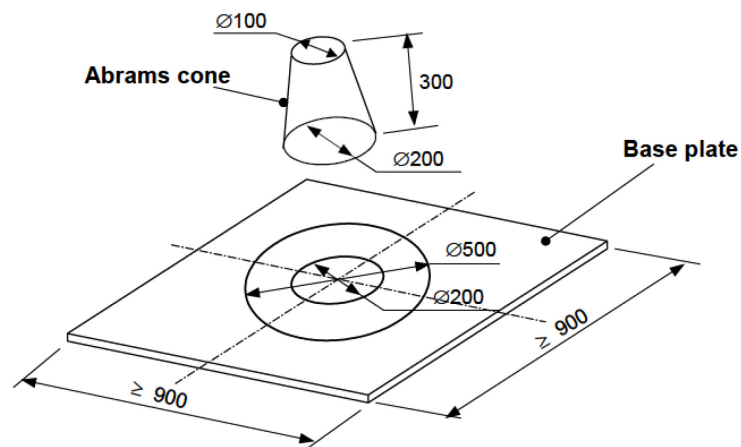

Figure 24: A drawing of the slump flow experiment showing the dimensions of the cone and the base plate [20].

In the second calibration case study, the analytical and numerical solutions of the spread flow are compared. The classical Abrams cone is used (Figure 24), where the dimensions of the cone are: 300 mm height, 200 mm lower diameter and 100 mm upper diameter. Base plate is of size at least 900 mm x 900 mm, made of impermeable and rigid material. SCC used for this study was again the same concrete with following properties: yield stress τ_0 = 50 Pa, plastic viscosity η_{pl} = 50 Pa·s and density ρ = 2300 kg/m^3. The total volume of the material is V = 5.5 l.

4.3.1 Analytical solution

The analytical solution for the flow length of the slump flow experiment is fully overtaken from [48]. In [48] Roussel et al. showed that is possible to predict the spread of the slump flow, if yield stress is known and when in the spreading regime (i.e. when the thickness of the flow is far smaller than the radius of the sample). To analytically find the relation between the fluid thickness h at stoppage as a function of the distance r, one uses the cylindrical coordinates (r, θ, z), see Figure 25.
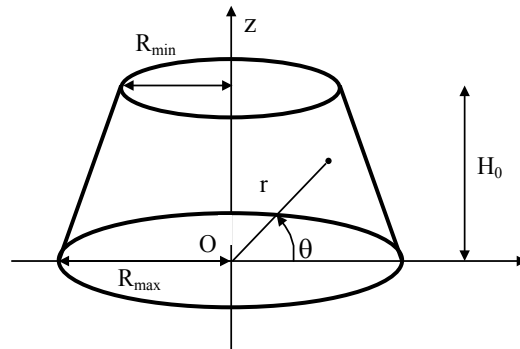

Figure 25: Analytical solution of the slump flow experiment: initial cone shape and the cylindrical coordinates [48].

Since the problem is symmetric, there is no tangential motion ($v_\theta = 0$) and the variables do not depend on θ. Thus the strain rate tensor has the following general form:

$$\underline{\underline{D}} = \frac{\partial v_r}{\partial r} \underline{e}_{rr} + \frac{v_r}{r} \underline{e}_{\theta\theta} + \frac{\partial v_z}{\partial z} \underline{e}_{zz} + \frac{1}{2}\left(\frac{\partial v_r}{\partial z} + \frac{\partial v_z}{\partial r}\right)\left(\underline{e}_{rz} + \underline{e}_{zr}\right) \tag{52}$$

where $\underline{\underline{D}}$ is the strain rate tensor, v_r and v_z are radial and vertical velocity, respectively and e_{ij} are unity vectors (where i, j = r, θ, z). In the "spread" regime, the radial velocity is expected to be much higher than the vertical velocity (v_z <<v_r) and the variations of flow characteristics in the vertical direction to be much more rapid than in the radial direction flow ($\partial/\partial r << \partial/\partial z$). In this case, the strain rate tensor simplifies as:

$$\underline{\underline{D}} = \frac{1}{2}\frac{\partial v_r}{\partial z}\left(\underline{e}_{rz} + \underline{e}_{zr}\right) \tag{53}$$

When inertia effects can be neglected, only the tangential stress component τ_{rz} is significant in the extra-stress tensor, so that the momentum equation simplifies to:

$$0 = -\frac{\partial p}{\partial r} + \frac{\partial \tau_{rz}}{\partial z} \quad 0 = -\rho g - \frac{\partial p}{\partial z} \tag{54}$$

where p is pressure and ρ is density. Integrating the second equation of Equation 54 between 0 and z leads to the hydrostatic pressure distribution:

$$p = \rho g\bigl(h(r) - z\bigr) \tag{55}$$

When integrating from 0 and h, Equation 54 gives:

$$\rho g h \frac{dh}{dr} = -\tau_{rz}(0) \tag{56}$$

At stoppage the shear stress approaches yield stress $\tau_{rz}(0) \to \tau_0$, so the boundary condition in Equation 55 is $h(R) = 0$. The shape of the material at stoppage is described by:

$$h(r) = \left(\frac{2\tau_0(R - r)}{\rho g}\right)^{1/2} \tag{57}$$

The total volume of the sample V is given as:

$$V = \int_0^{2\pi} \int_0^R h(r)\,r\,dr\,d\theta \tag{58}$$

From Equation 55 one can compute the expression for the spreading distance R as a function of the yield stress and material volume:

$$\tau_0 = \frac{225\rho g V^2}{128\pi^2 R^5} \quad \text{i.e.} \quad R = \sqrt[5]{\frac{225\rho g V^2}{128\pi^2 \tau_0}} \tag{59}$$

The expressions 57 and 59 are used to calculate the material shape h(r) and spreading radius R at stoppage for the given material in the presented analytical study of slump flow.

4.3.2   Numerical solution

The numerical simulation of the slump flow (geometry and material properties are shown in 4.2) is conducted with CFD software ANSYS Fluent© 6.3. As preliminary studies the influences of different factors on the solution are investigated. The solver options are varied and their effect on the stability of the solution is studied. The impact of the mesh refinement on the solution is tested as well, starting with coarse mesh and increasing the number of elements until a stable solution is achieved. Here, a special attention is paid to refinement of the particular zones (see Figure 26). Furthermore, the different boundary conditions (such as slip and no-slip condition on the base plate, pressure/mass flow inlet) on two-dimensional and three-dimensional simulations are also compared. To prove that the spread length depends on yield stress solely, material properties are varied and

simulations are performed for materials with different plastic viscosities. Based on these preliminary tests, 3D solver is used. The used mesh is shown in Figure 26. The mesh with 67770 hexahedral elements is chosen (due to the symmetry, only one quarter of the whole domain was calculated). Laminar flow conditions are assumed and concrete is modelled as an incompressible Bingham material. To calculate the free surface position, which in this case dominates the problem, the VOF model for the free surface is employed, with no additional interaction between concrete and air.

a)

b)

c)

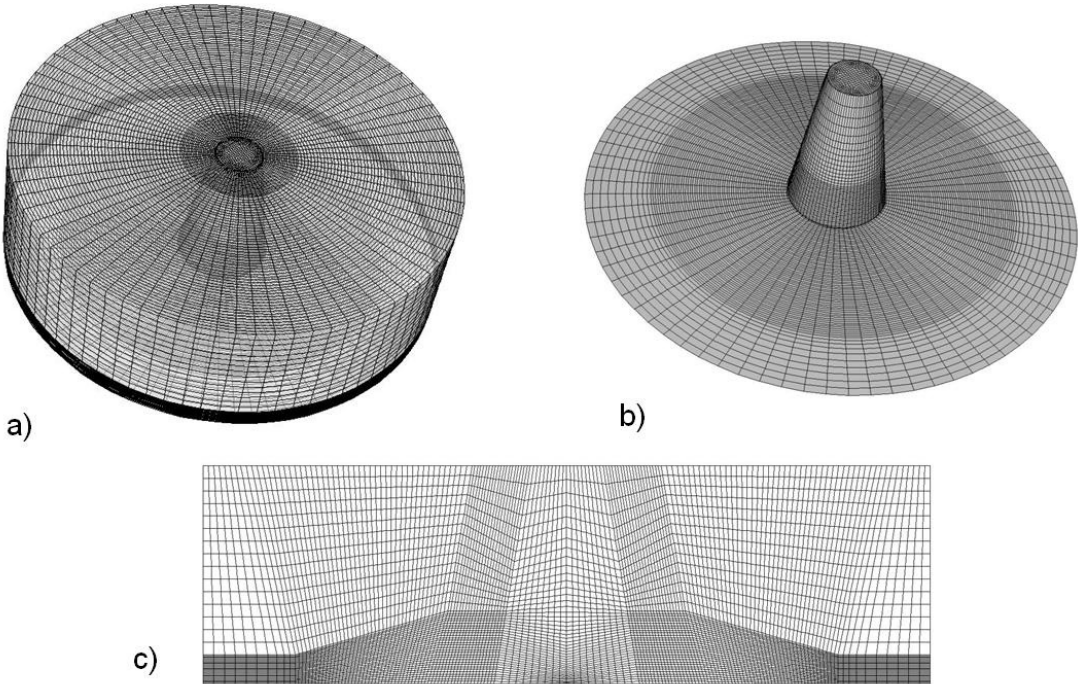Figure 26: Numerical simulation of the slump flow, details of the mesh: a) whole domain meshed, b) plate and initial shape of concrete, c) symmetry plane. Some zones required finer meshing.

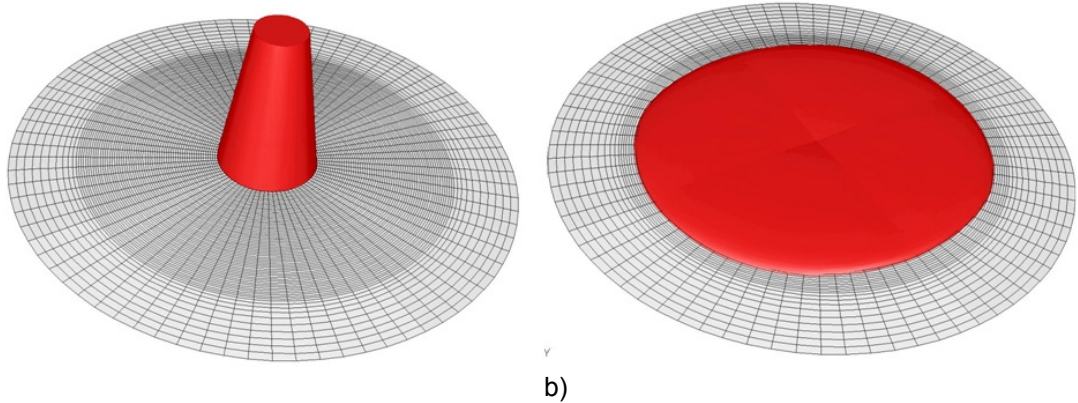a)   b)

Figure 27: Numerical simulation of the slump flow: a) beginning of the flow, b) the end of the flow. Concrete shown in solid colour, the base plate shown meshed.

4.3.3 Comparison of analytical and numerical data

Figure 27 depicts the material shape at the beginning and at the end of the flow. The flow stops after 3.2 seconds (real time) and the whole simulation takes 62 minutes. In Figure 28, analytical and numerical solutions for the flow profile at stoppage are compared. The diagram shows the relation h(r), where h is thickness of the sample and r is the spread distance. A perfect match between the analytically calculated and simulated flow distance can be observed in terms of the maximum spread distance. This in turns proves the correctness of the chosen solver and its ability to simulate the free surface flow of a Bingham material. A slight discrepancy in shape of the curve can be noted at r = 0. Here is to be noted, that the numerical solution is more accurate, since at the stoppage the flow does not move and the forces have to be in equilibrium. This means that the resulting forces and stresses at the symmetry plane have to be zero, which is not the case for the approximate analytical solution.
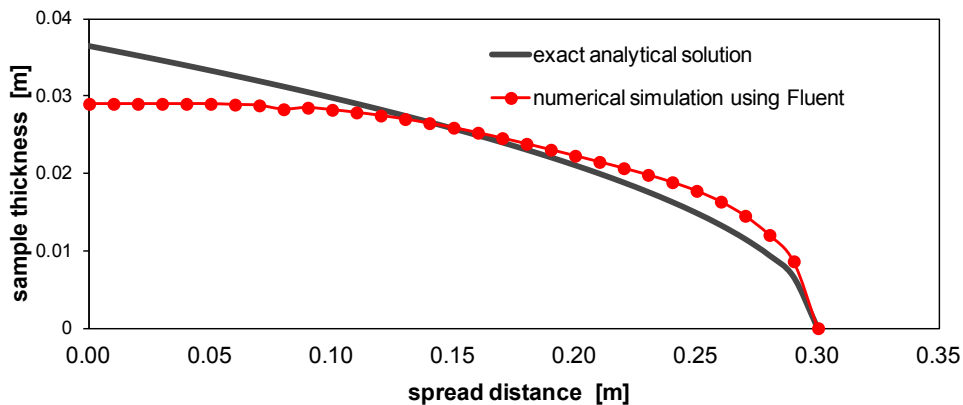

Figure 28: Slump flow, the material shape when the flow stops: comparison between the exact analytical solution according to [48] and numerical simulation using ANSYS Fluent©.

4.4   Conclusions

Chapter 4 showed the "calibration" studies of the software ANSYS Fluent© on two basic concrete flows: channel flow and slump flow. Within these studies, the software ANSYS Fluent© is proven to be numerically stable when solving these free-surface problems. This is certainly an important finding, since all concrete flows are free-surface flows. The software is moreover suitable for numerical simulations of the non-Newtonian flows, with several non-linear material models (such as Bingham, Herschel-Bulkley, polynomial, etc.) built-in. The comparisons of analytical and numerical results showed that the selected software with all the chosen settings (such as flow models, initial conditions, boundary conditions, material properties, numerical parameters etc.), is able to provide a numerical

solution very close to the analytical solution and herewith justify the use of Fluent© for the further numerical studies.

When choosing the material parameters of the bi-viscosity Bingham model (Subchapter 4.1), one should choose the value of initial viscosity so that the critical shear rate is 0.001 s^{-1} or lower. The wall boundary conditions to be used for standard walls and plates are no-slip while the full-slip condition should be used when modelling pouring funnels or cones.

Additionally, some simple tests (which were not presented here) confirmed that ANSYS Fluent© allows relatively uncomplicated implementation of user defined variables into the code. These are implemented as so called "user defined functions". User-defined functions allow for the implementation of new user models and the extensive customization of existing ones. One can define for instance momentum sources, mass sources, variables such as velocity profiles, temperature or material properties such as viscosity, thermal properties etc. [193].

Finally, the low computational time needed for both presented case studies (78 and 72 minutes for channel and slump flow respectively), proved once more the great advantage of CFD when compared with time consuming particle methods.

5   Flow of Newtonian fluids through porous media

In Chapter 3 the details of the proposed approach and the governing equations for the SCC flow through reinforced zones were presented. The model is based on the theory of propagation of non-Newtonian fluid through porous media. The model equations are to be implemented into the CFD software ANSYS Fluent©, which calibration is shown in Chapter 4. Prior to implementation and validation of the non-Newtonian model, the numerical studies on propagation of Newtonian fluid through reinforcement are to be conducted (see Subchapter 3.4 for the planned research steps). The goal of these numerical studies is to prove the validity of the idea of treating reinforcement network as a fibrous PM, when arbitrary Newtonian fluid is flowing through it. Additionally, a method to determine the intrinsic parameters of porous medium formed by reinforcement bars has to be established.

The permeability of any medium can be directly experimentally measured or numerically computed by a single steady-state measurement on a sample of given geometry crossed by a Newtonian fluid [158]. The presented thesis suggests calculating the permeability numerically by performing channel flow simulations where Newtonian fluid crosses reinforcement zones. To validate this method, the permeability of several reinforcement networks is determined numerically using Fluent© (Subchapter 5.1). The values of numerically determined permeabilities are then compared with analytically calculated ones. If the comparison of the analytical and numerical results shows a good congruence, this proves the correctness of permeability calculation method. This would justify the idea that the permeability of any reinforcement network can be calculated numerically, performing simple Newtonian fluid simulations.

Hypothetically speaking, every reinforcement network can be represented as a porous zone, where the permeability of the zone is determined as proposed above. In order to verify this statement, the numerical case studies, where Newtonian fluid is propagating through different reinforcement geometries, are conducted (Subchapter 5.3). Then, the simulations of the equivalent porous medium geometries are carried out, where the zone with rebars is represented by homogeneous porous zone with permeability k. The results for the pressure drop within the zone for both simulations with the bars and with the PM are compared. Their good match will confirm the correctness of the permeability computation and prove that the reinforcement network can be modelled as a porous medium with permeability k.

In order to be able to represent and simulate a reinforcement zone using the proposed model, the exact boundaries of the corresponding PM have to be precisely determined. Subchapter 5.2 will discuss the interfaces of the porous medium with the surrounding

fluid, boundaries between two different PM as well as interfaces determining the wall influence.

5.1   Unknown model parameters: studies on permeability

The final equations (Equations 39-43) of the proposed model for the influence of PM formed by rebars on the concrete flow contain two unknown PM parameters: the permeability k and the shift factor α. The permeability on any porous medium depends only on its geometry and topology and is mathematically represented as a permeability tensor $\underline{k}$ (details in Section 2.3.3.2). In case of fibrous porous media studied here (or more precisely of arrays of cylindrical obstacles), if the coordinate axes are parallel/perpendicular to the axes of the cylinders, the permeability matrix becomes diagonalized with three principal values of permeability, namely k_{xx}, k_{yy} and k_{zz}. Let us name these three principal permeabilities k_x, k_y and k_z for simplicity reasons. If the z coordinate axis is parallel to the bars axes, then the principal permeabilites k_x and k_y become the "perpendicular" permeability while the k_z is the "parallel" permeability. As mentioned before, these three permeability values can be determined from a measurement on the given geometry crossed by a Newtonian fluid. Knowing the inlet velocity of the fluid and measured/calculated pressure drop within the network, the unknown permeability in the direction i is calculated from the Darcy's law as:

$$k_i = v_i \cdot \eta_n \cdot \frac{\Delta L_i}{\Delta p_i} \tag{60}$$

where η_n is viscosity of the Newtonian fluid, v_i is the Darcy velocity of the fluid, ΔL_i is the length of the PM and ΔP_i is the calculated pressure drop between the inflow and outflow interfaces of the PM in the direction i respectively.

In this thesis, it is proposed to calculate perpendicular and parallel permeability numerically from ANSYS Fluent© simulations of a Newtonian fluid flow through a sample of the observed reinforcement zone. An illustration of the proposed calculation method for k_x is shown in Figure 29. A laminar flow through a channel (no free-surface) is simulated, where the zone with the obstacles is placed in the middle of this channel. For the given inlet velocity, the pressure drop within the zone is calculated (the difference between the static pressure at the beginning and at the end of the bars' zone). Knowing the inlet velocity and the length of the porous zone, the permeability is calculated according to Equation 60. To validate the proposed method and the chosen numerical settings, the numerically obtained values of permeability are here compared with the analytically determined ones for the same networks.
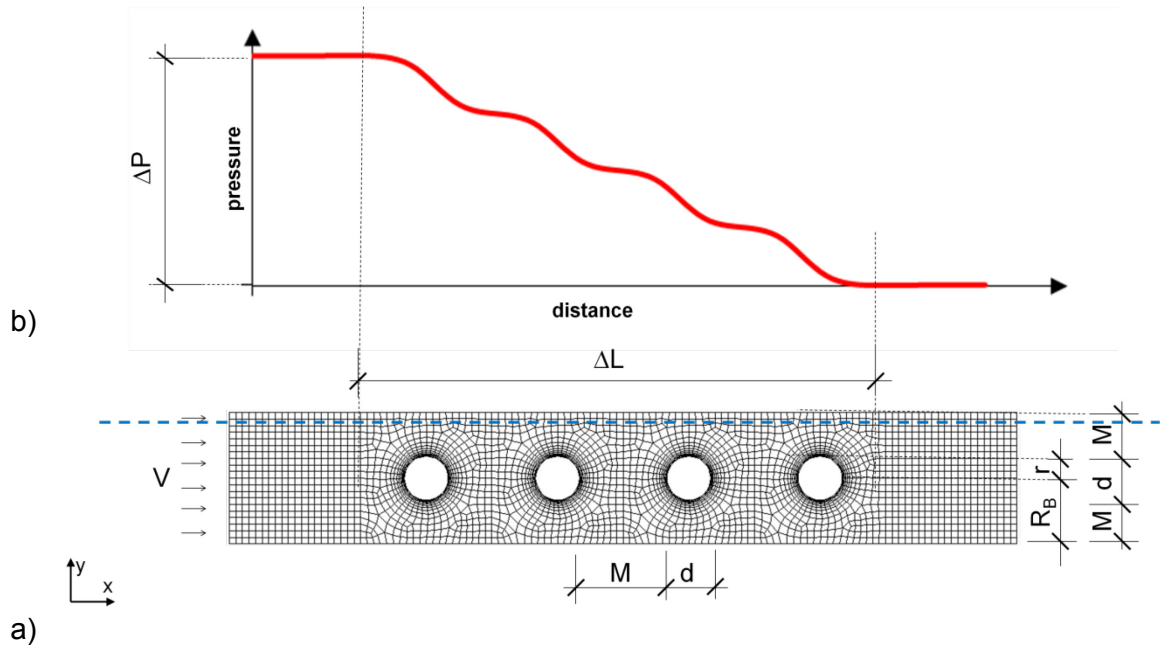
Figure 29: a) An array of four cylindrical obstacles b) the diagram showing the pressure drop along the horizontal dashed line marked on the array. The pressure drop Δp along the distance ΔL are shown at the diagram.

The analytical solutions for the permeability of reinforcement network are overtaken from Neale [177], Boutin [174] and Tamayol et al. [178]. As explained in Section 2.3.3.2, the method of Boutin [174] gives the lower and upper bounds for permeability of a periodic configuration of parallel cylinders as given in Equations 23 and 24. The values for d and R_B are taken as shown in Figure 29. Furthermore, to ensure the correctness of our solutions, we compare the results with two more approaches from [174], namely solutions by Happel et al. [175] and by Kuwabara et al. [176]. The equations for the permeabilities perpendicular and parallel to the cylinder axes of Happel and Kuwabara are respectively given in Equations 21 and 22 of Section 2.3.3.2. Recently, Tamayol and Bahrami in [179, 180] proposed solutions for transversal and parallel permeability of fibrous porous media as given in Equation 25. The following sections will show the comparison of numerical and analytical studies on permeability, where the analytical solutions are calculated according to Equations 21 - 25.

5.1.1 Permeability in the direction perpendicular to the cylinder axes

In order to save computational time, the numerical simulations to study perpendicular permeability are performed with 2D geometries simplifications. However, to make sure that the 2D representation provides accurate results, two of them are compared with the exact 3D geometries. It was shown through this comparison that the results for

permeability are absolutely the same for 3D geometries and corresponding 2D simplifications. The geometries used for the numerical determination of the perpendicular permeability named k_x or $k_\perp$ are shown in Figure 30. The figure shows rectangular channels with arrays of vertical cylindrical obstacles. The diameter of the obstacles is d = 4 mm and the distance between the bars was M = 8, 16, 24, 32 and 40 mm, making the relative distance between the bars X = 2, 4, 6, 8 and 10.
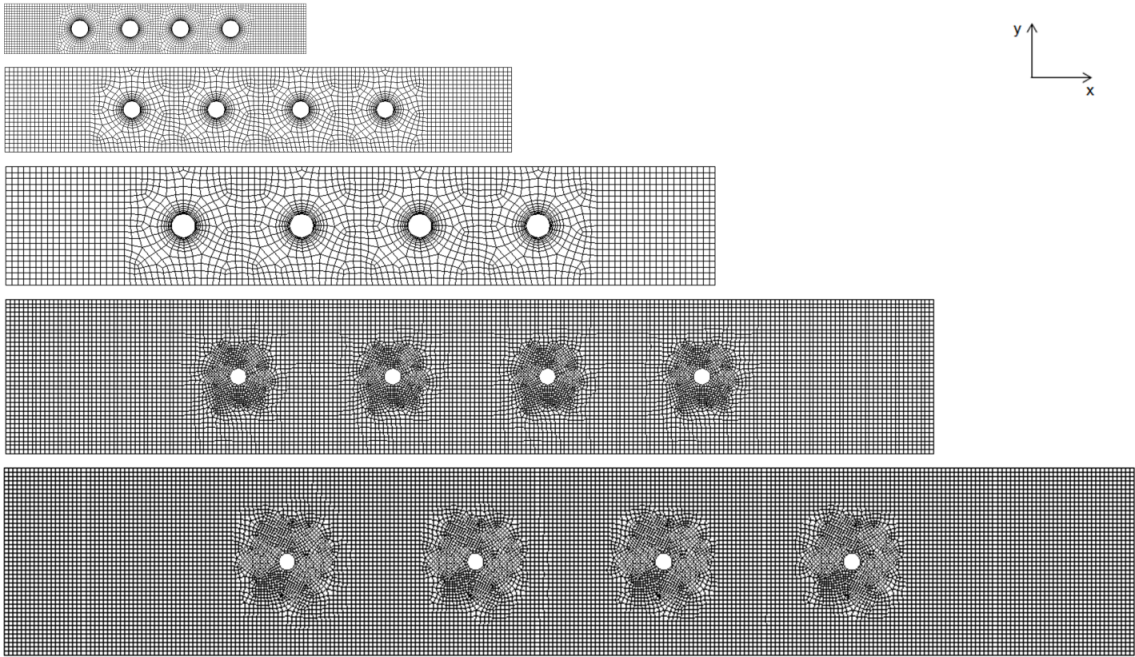

Figure 30: 2D geometries used for the numerical simulations with Newtonian fluid to calculate permeability k_x.

Figure 31 shows the comparison of the analytically and numerically calculated permeability k_x plotted versus X, where X is so-called relative distance between the bars defined as the ratio of the distance between the bars to the diameter of the bars as X = M/d. The obtained numerical results prove to be in a good agreement with the analytical ones and perfectly fit within the bounds given by [177]. Comparing with other two analytical solutions, it can be noticed that the results have the same order of magnitude, while a nearly perfect match between the numerical permeabilities and the analytical solution of Kuwabara [176] is observed. This can be assumed satisfactory and justifies the proposed simple numerical method for calculation of permeability in the direction perpendicular to the rebars.
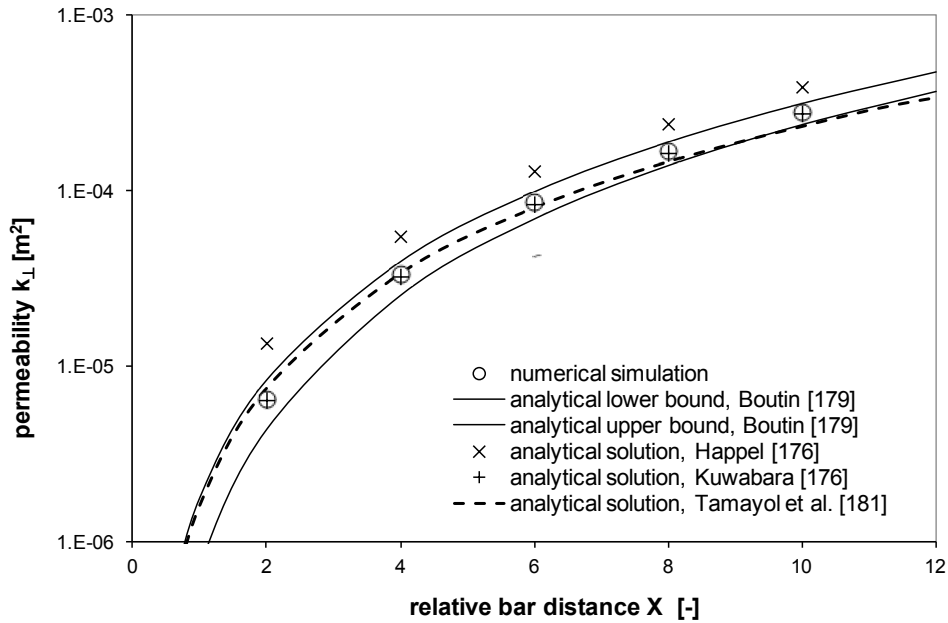
Figure 31: Perpendicular permeability $k_\perp$ (also called k_x). The results of the numerical simulations compared with four analytical solutions from [177], [174] and [179]. The permeabilities are plotted as a function of the relative bar distance X.

As mentioned in Subchapter 2.3, numerous researchers dealt with analytical, experimental and numerical solutions to determine permeability of cylinder arrays, as a function of porosity and bars diameter or as a function of the bar diameter and the distance between the bars. The obtained equations (such as for instance in [174]) show that the permeability is directly proportional to the square of the bar diameter. Let us plot the permeabilities obtained for a case study similar to the ones shown in Figure 30, as a function of distance between the bars M. Figure 32 shows that the permeability curve can be expressed as a function of the square of the clear distance between the bars called M. Since, in this case M = X·d, it can be written:

$$k = c \cdot M^2 = c \cdot X^2 \cdot d^2 \qquad\qquad (61)$$

where c is a dimensionless factor, which value in this particular case is found to be 1/12. This coefficient is presumably dependent on porosity, i.e. distance between the bars, and its universal value cannot be easily directly determined. The study however confirms the finding of the analytical studies, that the permeability is directly proportional to the square of the distance between the bars.
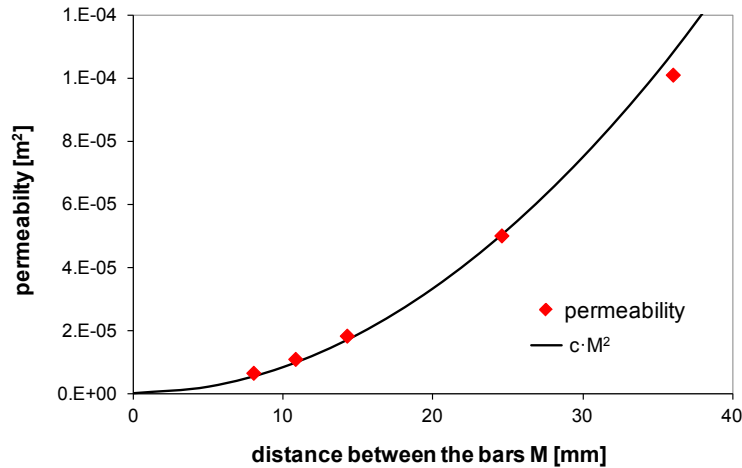
Figure 32: Permeability as a function of the distance between the bars. The coefficient c = 1/12 in the specific case.

5.1.2 Permeability in the direction parallel to the cylinders axes

To calculate the principal permeability in the direction parallel to the cylinders axes (named k_z or $k_{||}$), the same numerical approach that is applied for perpendicular permeability in 5.1.1 is utilised. The geometries used in simulations are shown in Figure 33. Unlike the simulations devoted to the k_x determination, the permeability k_z cannot be determined using 2D simplifications, since they would not make physical sense. The used 3D setups consist of a rectangular sample with one single or four parallel cylinders. The diameter of the bars is d = 4 mm and their relative distance in both x and y direction is X = 2, 4, 6, 8 or 10. The length of the bars is 10 cm and the distance to the outlet is 5 cm. To avoid the influence of walls, it was assumed that the flow is indefinite in the x and y directions and the symmetry conditions are chosen on all the external boundaries, except on the inlet and outlet.

The test Newtonian fluid is flowing through the sample with a constant velocity in the positive z direction, parallel to the cylinders' axes. The flow is kept laminar and continuous (channel flow with no free surface). For each of the geometries and for three different values of velocity, the pressure drop between the beginning and the end of the zone is calculated. The "numerical" permeability k_z is then calculated according to Equation 60, while the analytical solutions are calculated again according to Equations 21 - 25 (note that for k_z, both the solutions of Happel and Kuwabara give the same equation).
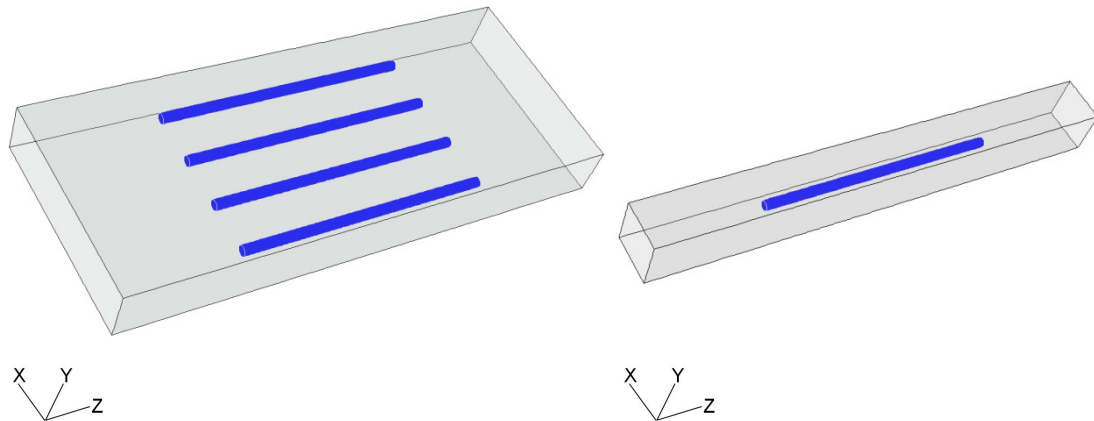
Figure 33: 3D numerical setups used to calculate the permeability k_z. Rectangular channels with cylindrical obstacles, the material flows continuously in z direction. The distance between the bars is varied.

Figure 34 shows the numerically determined and analytically calculated values of permeability k_z plotted versus the relative distance between the bars X. The numerical values fit comparatively fine between the boundaries given by Boutin [177] and again perfectly match with the values calculated according to Kuwabara [174]. The good congruence proves that the proposed numerical method is able to calculate correct values of the permeability of cylinder arrays for the direction parallel to the cylinder axis.
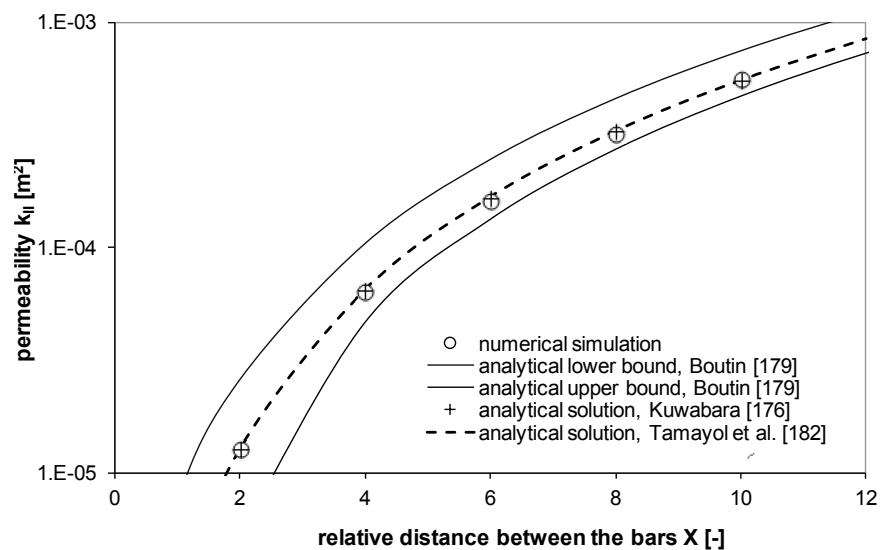
Figure 34: Parallel permeability k_z from numerical simulations of the flow of a Newtonian fluid as a function of the ratio of the distance between the bars to the diameter of bars.

Finally, the comparison of numerically obtained k_x and k_z values plotted versus X is shown in Figure 35. It is obvious that the parallel permeability is always twice larger than perpendicular one and that the following relation always holds:

$$k_z = 2 \cdot k_x \tag{62}$$

This finding also corresponds to the analytical solutions found in [174]. Therefore, within this study, the permeabilities parallel to the axes of the rebars will be calculated either numerically as suggested above using simulations of Newtonian fluid or from Equation 62, if transverse permeability is already known.
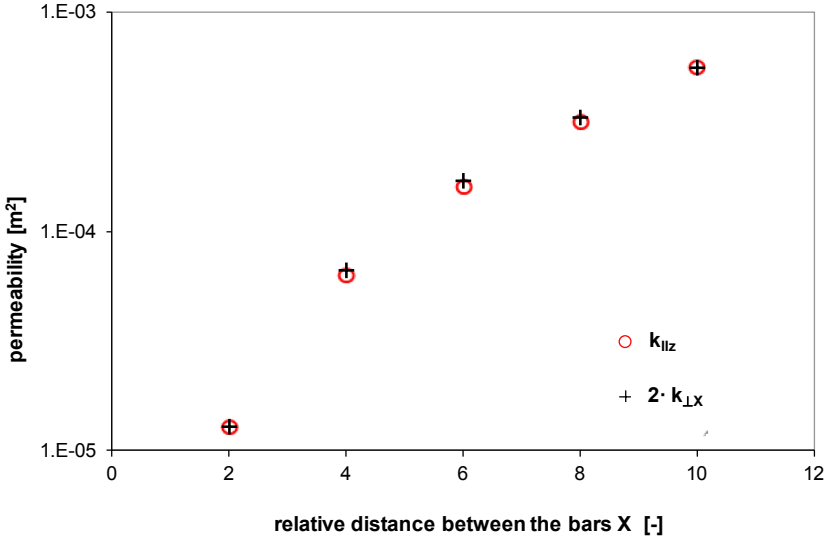
Figure 35: A diagram showing the comparison between the numerically calculated permeabilities $k_{\|z}$ and $k_{\perp x}$. It holds: $k_{\|z} = 2 \cdot k_{\perp x}$.

5.1.3   Permeability as a function of bars arrangement

In the studies shown in Sections 5.1.1 and 5.1.2, the permeability as a function of the distance between the bars was discussed, where the bars were positioned in equidistant aligned arrays with squared arrangements. In the practical applications it can happen that the reinforcement bars are positioned in distorted arrays as shown in Figure 36.

$$X = M / d$$

$$\phi = 1 - \frac{\pi}{(1 + X)^2}$$

Figure 36: a) Squared and b) staggered arrangement of the bars.

The figure shows a basic element of a squared and a staggered bar disposition, which have the same distance between the bars M and the same value of porosity ϕ (shown for

86

a representative cell marked with dashed lines). Thus, the next issue that has to be discussed is the influence of the bars arrangement on permeability.

Some studies concerning this topic can be found in [178-180]. In [178, 179] Tamayol and Bahrami provided analytical solutions for the perpendicular permeability of square, staggered and hexagonal arrangements and discussed results for some given range of porosities. The relative permeability k_x^* (defined as transverse permeability k_x divided by square of the bar diameter d) for the squared and staggered arrangement of the bars is given as:
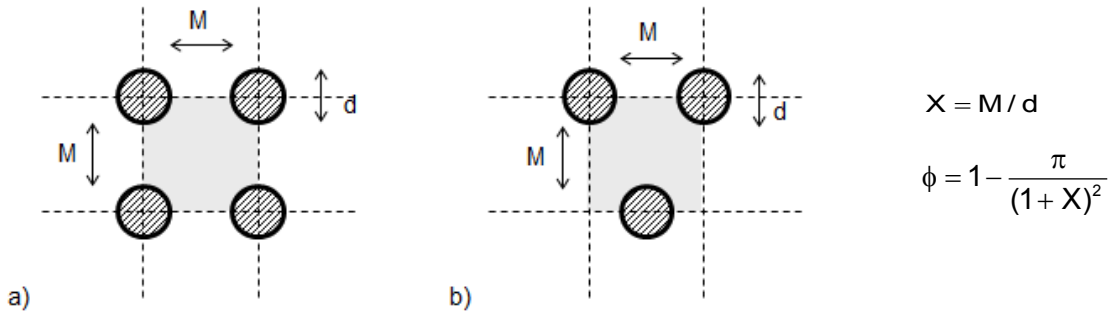
squared:
$$k_x^* = \frac{k_x}{d^2} = 0.16\left[\frac{\pi}{4\varphi} - \sqrt{\frac{\pi}{4\varphi}} + 3 - \sqrt{\frac{4\varphi}{\pi}}\right]\bigg/\sqrt{1-\varphi}$$

(63)

staggered:
$$k_x^* = \frac{k_x}{d^2} = 0.16\left[\frac{\pi}{2\sqrt{3}\varphi} - 3\sqrt{\frac{\pi}{2\sqrt{3}\varphi}} + 3 - \sqrt{\frac{2\sqrt{3}\varphi}{\pi}}\right]\bigg/\sqrt{1-\varphi}$$

where φ is solid fraction of the porous medium defined as 1-ϕ, where ϕ is porosity.

In [180], while studying parallel flow through the ordered fibres, the authors provide an analytical solution for the permeability as:

squared:
$$k_z^* = \frac{k_z}{d^2} = \frac{1}{16\varphi}\left[-1.479 - \ln\varphi + 2\varphi - 0.5\varphi^2 - 0.0186\varphi^4\right]$$

(64)

staggered:
$$k_z^* = \frac{k_z}{d^2} = \frac{1}{16\varphi}\left[-1.478 - \ln\varphi + 2\varphi - 0.5\varphi^2 - 0.0186\varphi^6\right]$$

where k_z^* is relative parallel permeability (defined as parallel permeability k_z divided by square of the bar diameter d) and φ is solid fraction of the porous medium defined as above.

In order to study the influence of the bar arrangement of the permeability, numerical simulations are performed and subsequently compared with the analytical solution of Tamayol and Bahrami, shown in Equation 62. Both 2D and 3D simulations are presented here.
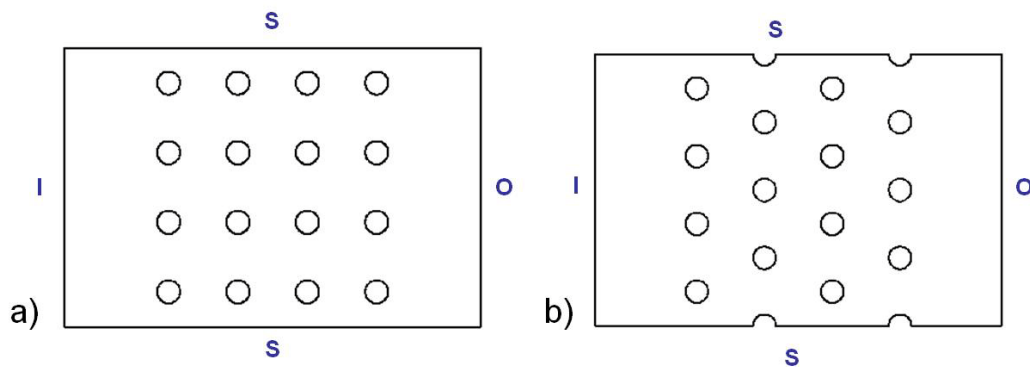

Figure 37: The 2D geometries used to demonstrate the influence of the bars disposition on the values of permeability.

The 2D geometries used in numerical simulations to demonstrate the influence of the disposition of the rebars on the values of perpendicular permeability are shown in Figure 37. The figure shows a 2D representation of a rectangular channel with vertical cylindrical obstacles. The obstacles with the diameter d = 4 mm are positioned in square arrangement or distorted arrangement. The relative distance X between the bars for the both geometries is varied from 2 to 10. The letters i, o and s denote inlet, outlet and symmetry boundary condition respectively. The permeability is determined through simulations with Newtonian fluid as explained in Subchapter 5.1.

The diagram in Figure 38 shows the results of the 2D numerical simulations. The value of relative permeability k^*_x for both arrangements is plotted versus relative distance between the bars X. The relative difference between the $k^*_{x,squared}$ and $k^*_{x,staggered}$ values is also shown. For all the tested porosities, the permeability of squared arrangement is slightly higher than the permeability of the staggered disposition, but this difference is relatively low (less than 5.5 %). With higher X and higher porosity this difference decreases.
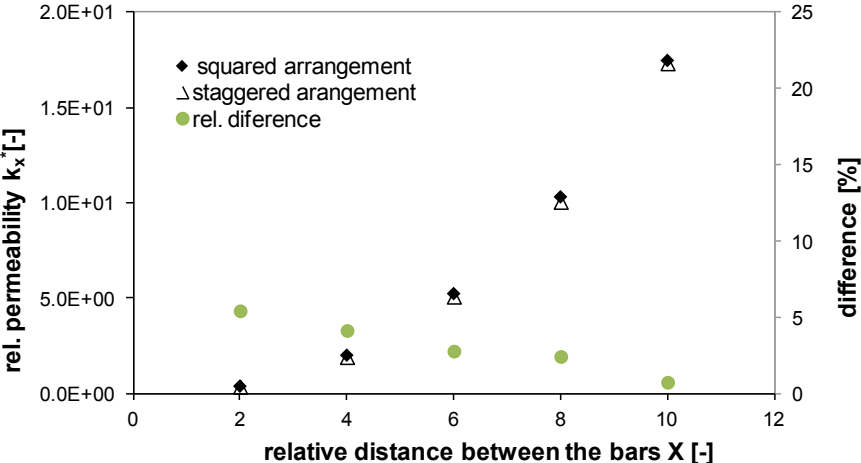
Figure 38: Comparison of numerically calculated values of k_x^* for squared and staggered arrangement of the rebars. For the same X, the square arrangement has a slightly higher permeability then the staggered one.

In order to prove these findings, the influence of the bars arrangement on k_x is studied once again, through 3D numerical simulations of Figure 39. The figure shows segments of approx. 60 x 20 x 20 cm^3 rectangular samples, where the rebars zone is placed in the middle of the channel. The detail of a horizontal projection of a typical periodic cell is also shown. Six different cases are considered with 9x9, 14x14 and 17x17 equidistant bars (d=3 mm) in both aligned or distorted arrangement.
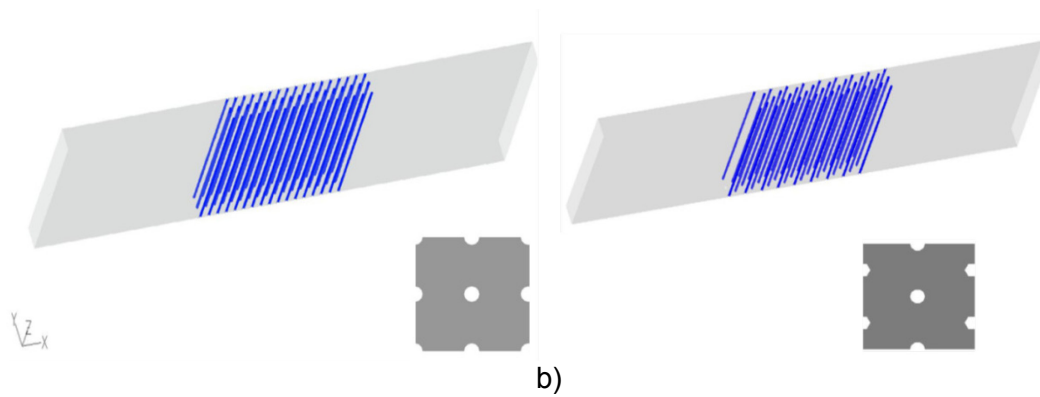
Figure 39: The 3D geometries used to study the influence of the bars distribution to the values of permeability: a) squared distribution and b) staggered distribution.

The results are shown in Figure 40. The numerically determined permeability values show that the difference between the $k_{x,squared}$ and $k_{x,staggered}$ is lower than 3% and therefore not significant.
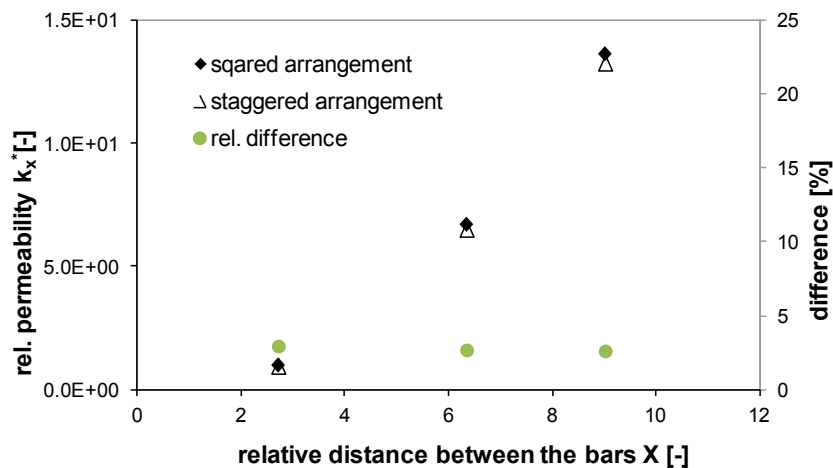
Figure 40: The results of 3D numerical simulations with uniform and non-uniform bar disposition. The permeability is a function of the distance between the bars; the influence of the bar arrangement can be neglected.

Let us now study the analytical solution for parallel and perpendicular permeability for the squared and staggered bars arrangement, calculated according to [178-180] for the porosity range typical for concrete elements, for instance slabs. According to the Eurocode 2 [202], the distance between the bars in concrete slabs has to be larger than 2 bars diameters and smaller than 400 mm, which means that the relative distance between the bars X can vary from 2 to 67. On the other hand, according to [203], where the norms for practical use are given, the value of X is between 2 and 48.

The results for k^*_x and k^*_z that are calculated analytically according to Equations 63 - 64 for X = 2 to 48 are shown in Figure 41. The diagram shows that the permeability k^*_x of uniform (squared) is always smaller than the permeability of non-uniform (staggered)

arrangement, where the difference is significant and is between 16% and 30%. The difference decreases for higher X and increasing porosity. Figure 41b shows the analytically calculated values of the permeability k_z for squared and irregular distribution of the bars. In this case, the difference in k_z^* between regular and irregular bars disposition is rather low, and for X between 2 and 48 this difference is between 1.9% and 0.3%.
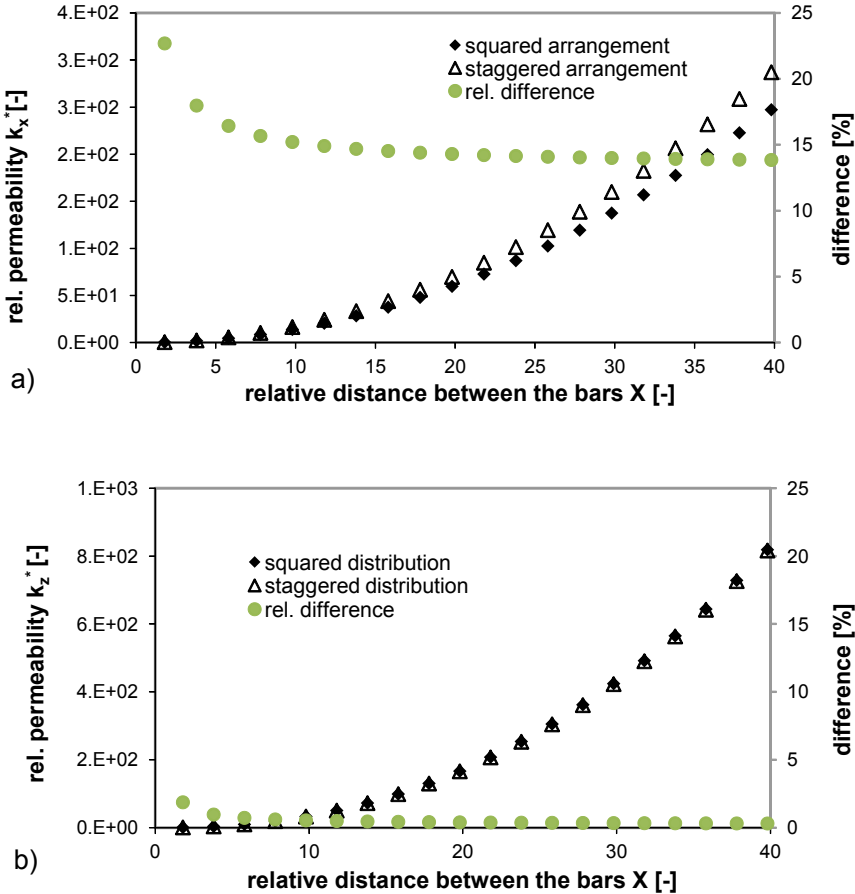
Figure 41: Comparison of the a) relative perpendicular permeability k_x and b) relative parallel permeability k_z for squared and staggered arrangements of the bars. The analytical solution from [179].

The conclusion of the analytically calculated permeabilities is that the bars distribution has no significant influence on the k_z but it has significant difference on the k_x. This finding could be in contradiction with the well-established relation between k_x and k_z ($k_z = 2k_x$, see Equation 22 or Figure 35). This implies that such a large relative differences between the squared and staggered arrangement for k_x and very small differences between squared and staggered k_z, might not be plausible. Furthermore, by comparing the numerical and the analytical results for the same range of X, one can see that the results of the analytical studies shown in Figure 41, are in contradiction with the results of numerical studies shown in Figures 38 and 40. The analytically calculated difference between $k_{x,squared}$ and $k_{x,staggered}$ was significantly larger than the simulated one. However,

since the results of numerical studies have been proved on the several different examples and geometries, we could assume that the findings of the [178-180] for transverse permeability are not relevant for the studied cases. Consequently, for the purpose of this study the influence of the bar arrangement can be neglected and the permeability remains at first order only a function of the relative distance between the bars X and the bar diameter d.

5.2   Boundaries and interfaces

A periodic porous medium is a porous medium having the property that the fixed solid particles are identical and the whole media is a periodic system of cells, which are replicas of a standard (representative) cell [204]. In case of an array of cylindrical obstacles (as for instance the ones shown in Figures 29 and 36a), one can say that the rebar is a fixed solid particle (obstacle) and a representative cell is the area (volume) around the bar with dimensions $(d+M)^2$. The entire zone is a periodic system of these cells. This holds also for the bars in distorted arrays, where the representative cell can look like the ones shown in Figures 36b or 40b. Basically, as long as in the observed zone the size of the bars and their separating distances are identical to the ones in the neighbouring cells, one talks about a homogeneous periodic porous medium. As soon as the cell is not identical to the neighbouring cell, we reach the interface of the media either to a surrounding liquid, to a neighbouring porous medium or a channel formed between the wall and the media.

5.2.1   Boundaries between porous zone and flowing fluid

When dealing with "standard" porous media (such as saturated media, or soil) it is not problematic to determine the boundaries of the media. In case of the zone formed by cylindrical obstacles or typical fibrous media, the boundaries are not strictly defined and it is to be discussed what is the area of the flow influenced by the porous medium as well as how the interfaces are to be treated. Strictly speaking, the last bar array determines the interface of porous medium and the surrounding fluid (see for instance the dashed line in Figure 45). It is however questionable if this line can be taken as a boundary of the porous medium in the numerical simulations.

In the literature, several studies focusing on the interfaces between the fibrous porous media and the surrounding fluid can be found [205-208]. In [205] the authors focused on the determination of boundary conditions at the interface between fluid layer and fibrous medium. When a fluid flows through a channel bounded by a porous medium, or flows around a porous body, the no-slip condition at the surface of the porous medium generally does not apply. There is an effective slip velocity at the surface. This is schematically

shown in Figure 42, which depicts a pressure driven flow of a fluid in a channel formed between a porous medium and a wall. The total velocity at the interface is a sum of Darcy's velocity in the medium and slip velocity at the interface. The recent studies of interfacial flow [205] have focused on the dependence of this velocity on the characteristics of the medium and the external flow.
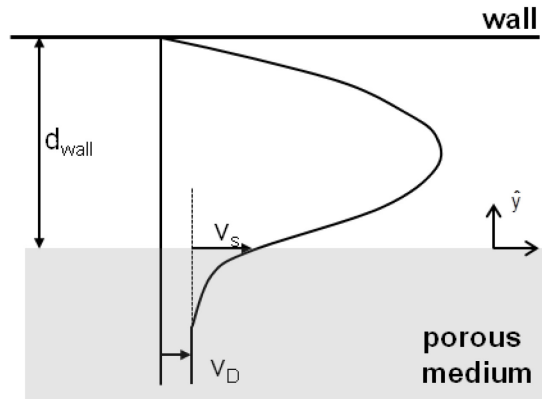
Figure 42: The velocity profile for pressure driven planar flow in a channel and adjacent porous medium. v_D is Darcy's velocity and v_s is slip velocity [205].

To determine the exact boundaries of the zones formed by rebars, we again perform simulations of simple flow of Newtonian fluids, through channels with rebars. Figures 43 and 44 show examples of these geometries. The diameter of the bar in both cases is $d = 4$ mm and the distance between the bars is $M = 8$ mm. A slow laminar flow of a Newtonian fluid ($\eta = 1$ Pa·s) in positive x direction is simulated. In both presented cases, the symmetry boundary conditions are used, except on inlet and outlet. The results studied are the pressure drop, the strain field and the velocity profiles.

In order to determine the boundaries and to analyse the interface between the medium and the fluid, which is parallel to the flow, let us analyse the results shown in Figure 43. The figure shows the velocity profiles for two cuts (lines) perpendicular to the flow as well as a detail of the velocity profiles near the interface between the medium (rebars zone) and the surrounding fluid. The velocity profiles for lines a and b show that the influence of the medium in the direction perpendicular to the flow starts at a given distance from the last bars. The analytical studies mentioned above showed that there is always a slip velocity at the PM fluid interface at $\hat{y} = 0$. However, in the detail shown on the right hand side of Figure 43, one can observe that, at the interface defined by the last bar (at $\hat{y} = 0$), the velocity varies from $v_a = 0$ and $v_b \neq 0$. Thus, there is not one single value of the slip velocity as in the case of idealised PM profiles and one has to search for the distance $\hat{y}$ at which the value of the slip velocity is the same for the both lines a and b. It is found out that the distance is equal to $\hat{y} = M/2$ where M is the distance between the bars. This

suggests that, when using the porous medium analogy, the porous media boundary parallel to the flow shall be positioned at M/2 from the last rebar.
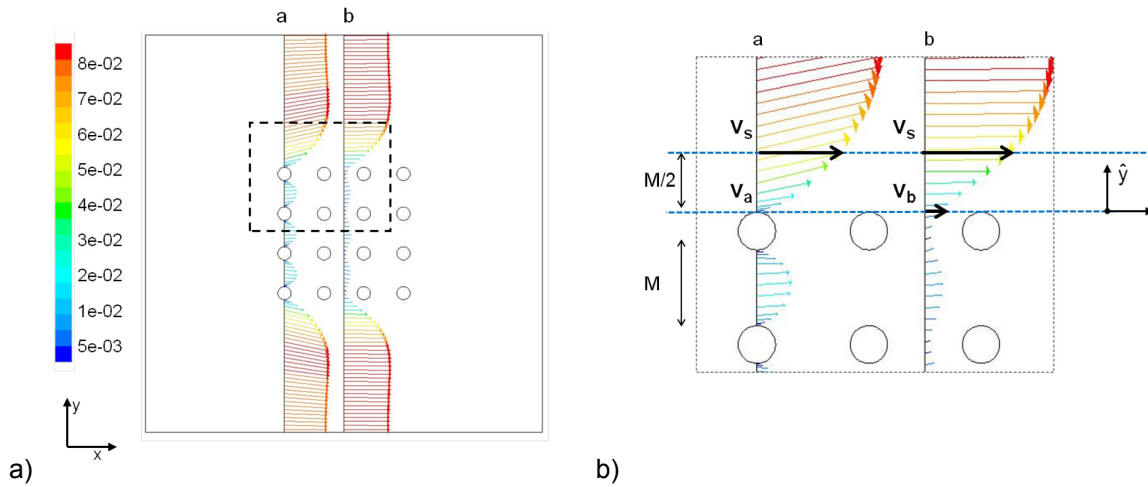
Figure 43: a) The velocity vectors along two lines in y direction, when flow is in x direction and b) the detail of the interface between the PM and fluid.

To determine the influence of the porous medium in the x direction, let us analyse the results shown in Figure 44: the pressure drop along a horizontal line and the strain rate contours for the whole channel. The pressure is plotted versus the distance for three different inlet velocities, while the strain rate is shown for one velocity v = 0.05 m/s. The black vertical lines on the diagram mark the position of the first and last rebar in the zone. It can be seen that the pressure is constant near to inlet and outlet and that the pressure drop caused by the presence of the obstacles starts at a given distance from the first and the last bar. From the diagram, it can be read that this distance is again approximately M/2 (see black dashed line). The strain rate contours show a similar effect: the strain rate is very low near the inlet and the outlet; the influence of rebars on the strain rate field starts at a distance M/2 from the last bars. Since this finding is additionally proved in several numerical studies within this thesis, the boundary of the media in the direction of the flow will be determined at $\hat{x}$ = M/2 distance from the last bar.
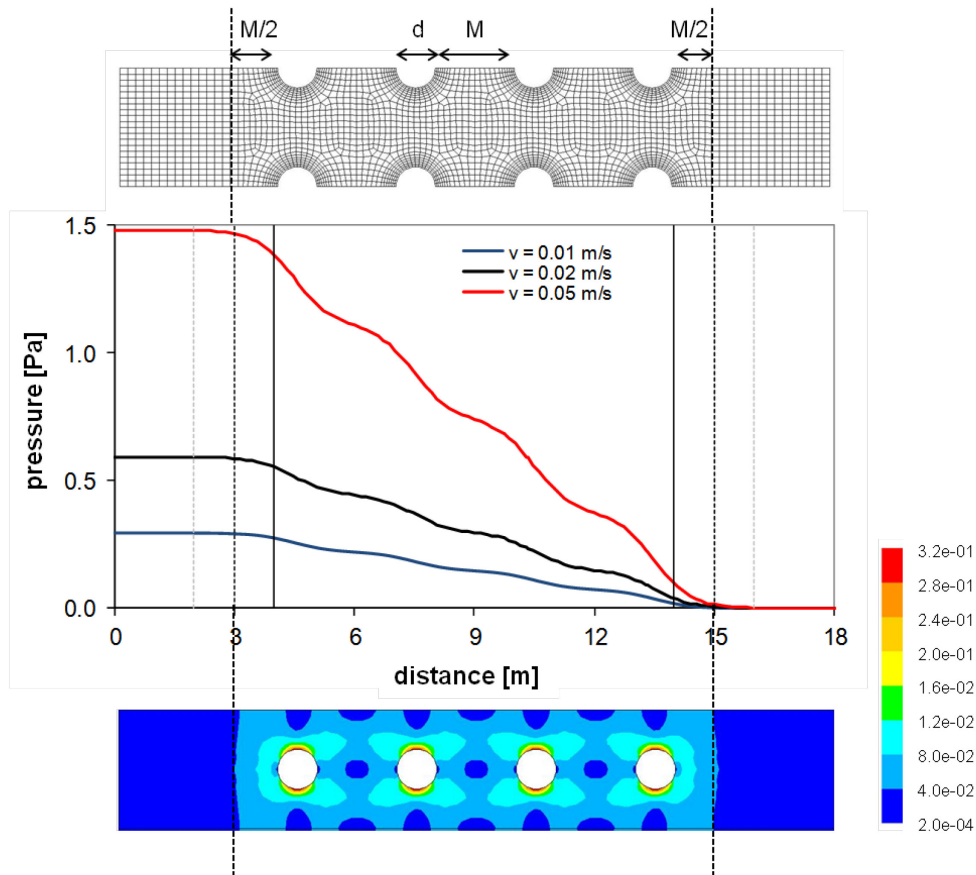
Figure 44: Case studies performed to determine the boundaries of the porous medium in the flow direction. The geometry (above), the pressure-distance diagram for different inlet velocities (middle), the strain rate contours (below).

5.2.2 Wall influence

The previous paragraphs suggest that, when using PM analogy to simulate a reinforced zone, the dimensions of the PM analogy are $(a+M_x) \cdot (b+M_y)$, where a and b are the length and the depth of the rebars zone respectively while M_x and M_y are the distances between the bars in directions x and y respectively. The next question, arising from the fact that in the real casting situations the walls are always present, is how to treat the interface/contact between the wall and the PM.

Up to now, while determining permeability, we always used symmetry boundary conditions on the surfaces of the sample. Let us now study the influence of the wall distance from the bars on the flow. A numerical setup to study the wall influence is shown in Figure 45. Six different case studies are performed, whereby the measures (arrangements of the bars, their diameter and the distance between the bars) are kept the same and the distance from the last rebar to the wall is varied from 1 to 32 M. Two different inlet velocities (v = 0.01 m/s and v = 0.03 m/s) are used. The numerical influence of the wall distance on pressure drop is observed.

94
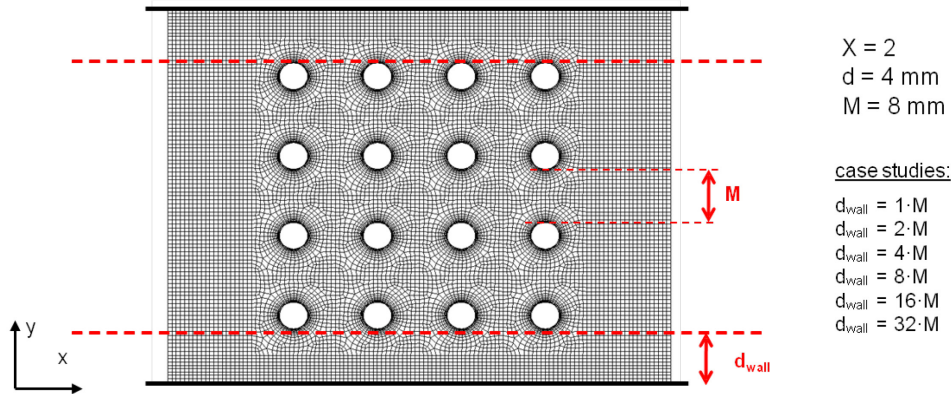
Figure 45: Numerical setup to study the influence of the distance between the wall and the medium on the flow. The thick black lines represent walls.

Figure 46 shows the pressure along the rebars zone for different values of d_{wall}. The pressure drop obtained from the simulations with two different inlet velocities is plotted versus relative wall distance defined as d_{wall}/M. One can note that for the higher wall distance the pressure is lower and there is, as expected, a big difference between the particular cases. The wall distance plays an important role and it is necessary to study how to treat a "channel" formed between the bars zone and the wall, and the interface between the bars zone and this channel.
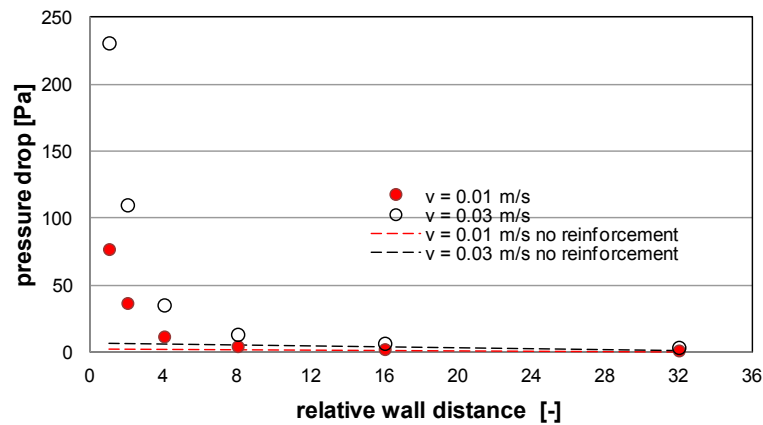
Figure 46: Pressure drop within the bars zone (for the cases where the distance to the wall is varied) plotted versus the relative distance to the wall.

Additional information that can be gained from Figure 46 is that, when the distance between the reinforced zone and the wall is high (for instance when d_{wall} = 16 M or d_{wall} = 32 M), the pressure drop becomes equivalent to the pressure drop that would occur if the reinforced zone would not exist (dashed lines in the diagram). This is however an interesting observation for the cases where the distance to the wall is much greater than

the size of the rebars zone (let us say 20 times greater); in this case the influence of the rebars zone could be neglected.
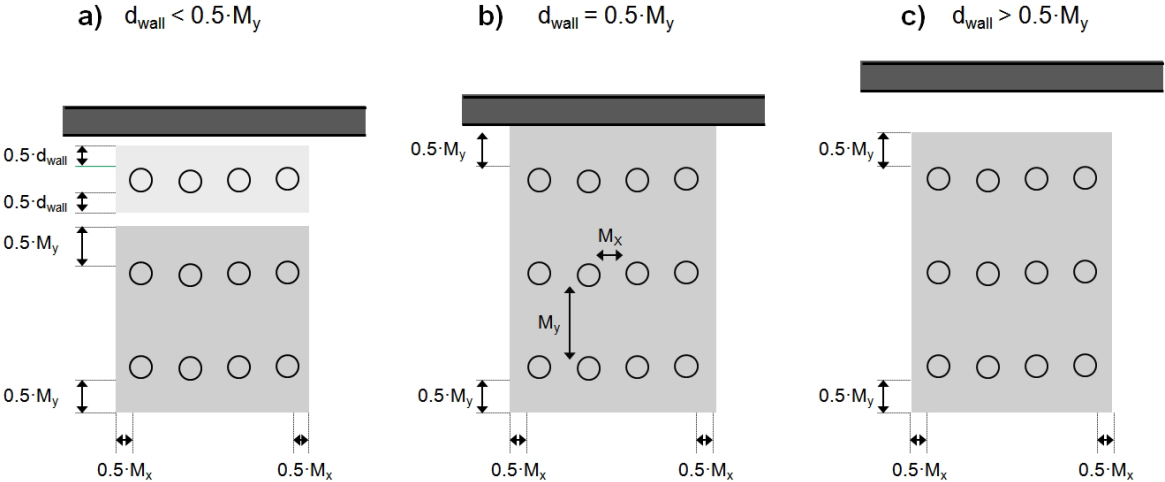
Figure 47: The real position (rebars) and corresponding porous media (grey area) for three different cases of distance between the rebars and the wall.

Since it was previously shown that the influence of the PM stops/ends at a distance of $0.5 \cdot M$ from the last bar of the array, it is logical to conclude the following:

- If the distance d_{wall} is smaller than M/2, one has to define 2 different porous media: one near to the wall with smallest characteristic distance being d_{wall} and the second PM zone in the middle, with characteristic distance M (see Figure 47a);
- if the distance d_{wall} is equal to M/2, the porous medium is spreads from wall to wall (Figure 47b);
- if the distance d_{wall} is greater than M/2, one has to define one porous medium as shown on the Figure 47c.

Finally, to prove the above findings, the numerical studies are performed, in which the results of the exact geometry simulations are compared with porous medium case studies, in which the size of porous medium is varied. The case studies are shown in Figure 48 and the results of the simulations are shown in Figure 49.
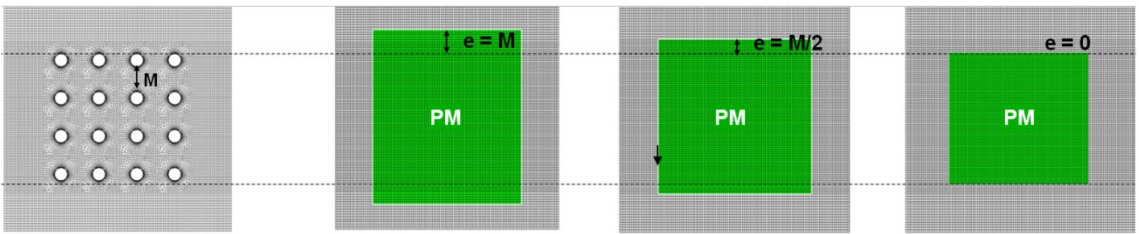
Figure 48: Geometry with rebars and the setups for the corresponding PM numerical simulations, where porous medium size is varied.

The results show that the best match between the results with rebars and results with porous media are obtained for the case b, where the dimension of the porous medium is equal to the area occupied by bars plus M (one half of M added to the each side of the reinforcement zone).
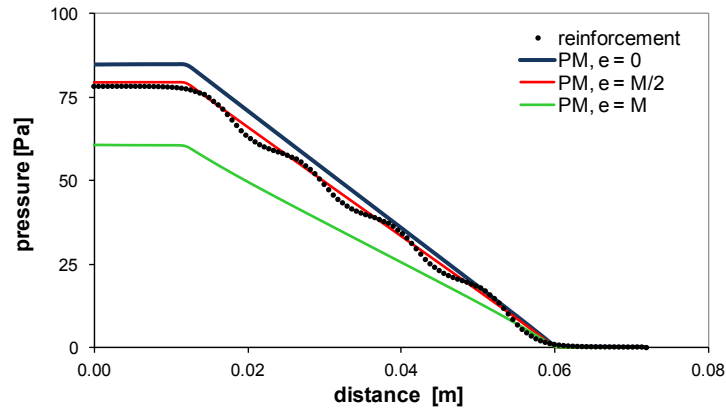
Figure 49: Results of the numerical simulations with the rebars and with the three versions of porous medium. Pressure drop along the middle horizontal line.

5.3   Numerical case studies with Newtonian fluid: bars vs. PM

In the previous subchapters, it was proved through the comparison of numerical and analytical results, that the permeability can be numerically calculated from the single simulation of the flow of a Newtonian fluid through the geometry of interest. It was also discussed how to determine exact borders of the PM. In this subchapter, the reinforcement zones are modelled as PM zones, where permeability is calculated as described in Subchapter 5.1 and dimension of the PM zone determined as shown in Subchapter 0. The goal of this step is to prove through the comparisons of the simulation results of the exact and PM geometries, that the obtained k value is correct and that the developed model is valid for the Newtonian flow through rebars zones.

Some of the 2D geometries are schematically shown in Figure 50. Similarly to all the previous studies, the setup consists of a rectangular channel with vertical rebars, in which a test Newtonian fluid is injected with a constant velocity through the inlet (left) and flows in the direction of the outlet (right). The bar diameter is d = 3 mm and the configuration of the rebars is varied so that the distance between the bars M is varied from 6 mm to 10.8 mm, so the relative distance between the bars X is from 2 to 3.6. All the test-material properties are set to the unity-values. The simulations are performed for different inlet velocities and the pressure drop is calculated. The corresponding porous medium geometry is also shown. The simulations for the reinforcement and PM cases are compared in terms of flow front and pressure drop within the reinforcement/porous zone.
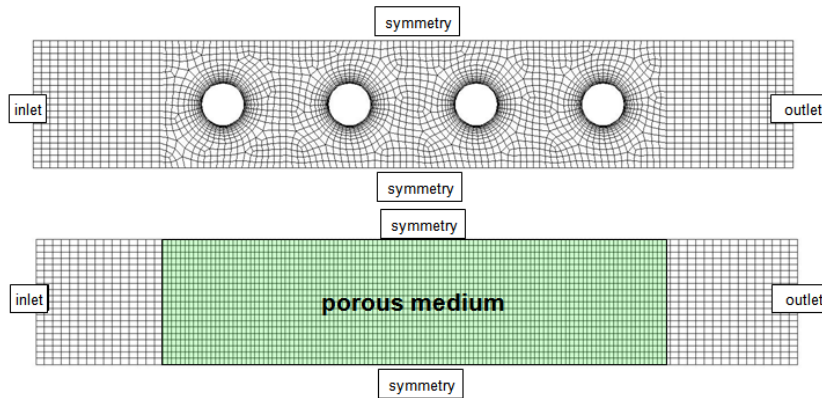
Figure 50: One of the geometries used for numerical simulations: a box with the array of reinforcement bars (above), the porous medium analogy (below).

Results of the numerical simulations with the 2D geometry and Newtonian fluid are shown in Figure 51. The diagrams show an excellent agreement when comparing the reinforcement and PM geometry, where the maximal discrepancy for the calculated pressure drop between reinforcement and PM case is found to be less than 0.4%.

It is interesting to note that the PM analogy works perfectly fine in the case of a Newtonian fluid. Independent of the geometry, the Newtonian viscosity or the inlet velocity, as long as the flow remains laminar, pressure drop and flow-rate are linearly related showing that, as expected in the case of simple Newtonian fluids, the reinforcement bars can be treated as a porous medium. The calculated permeability will be used further as an input parameter in the case of yield stress fluids propagating in identical PM.
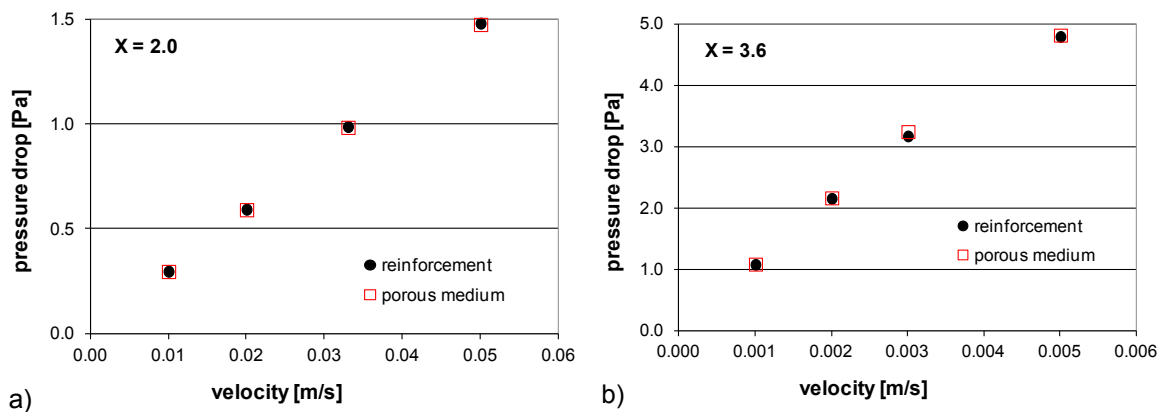
Figure 51: Results of the numerical simulations, reinforcement vs. porous medium for the relative distance X between the bars a) 2.0 and b) 3.6.

5.4   Conclusions

The permeability of any reinforced zone can be determined form a numerical simulation with a Newtonian fluid. The numerically calculated values of permeability k_x and k_z shown in this Chapter are in good agreement with the analytical solutions. This proves that the necessary permeabilities can be calculated from a numerical simulation of a flow of a Newtonian fluid through the rebars zone. The perfect match is observed between the numerical values and the permeabilities calculated according to Kuwabara in [174, 176]. That means that both analytical and numerical methods can be used to calculate permeability of periodic arrays of the rebars. It was furthermore shown that there is a constant relation between the permeabilities in the direction perpendicular and parallel to the axes of the bars. This makes the calculation of the parameters for the reinforcement zones easier, since the permeability parallel to the rebars can be simply calculated as: $k_{\|z} = 2 \cdot k_{\perp x}$.

Permeability is only a function of the bar diameter and the distance between the bars. The bars disposition (regular or irregular arrangement) at first order has no influence on the permeability values.

The study on boundaries and interfaces showed that the porous medium zone should start/finish at the distance M/2 from the first/last bar. The determination of the wall/porous medium interfaces is more delicate and should be carried out as explained in Subchapter 5.2.

Based on the case studies with Newtonian material shown in 5.3, one can note that the PM analogy works perfectly fine in the case of a Newtonian fluid. Independent from the geometry, the Newtonian viscosity or the inlet velocity, as long as the flow stays laminar, pressure drop and flow-rate are linearly related showing that, as expected in case of Newtonian fluids, the arrays of reinforcement bars can be treated as a porous medium.

6   Propagation of non-Newtonian fluids in porous media

When a flowable concrete is passing through a reinforced zone, if blocking does not occur, it can be assumed that the yield stress of concrete is a first order factor for the final flowing length and slope of the surface. Consequently, in this study, fresh SCC flow is approximated as a flow of non-Newtonian yield stress fluid (Chapter 3). This chapter is devoted to the numerical studies on the flow of yield stress fluids through arrays of parallel cylindrical obstacles and corresponding porous media. The objective of this research step is to propose a method for determination of remaining unknown parameters of the porous medium and to evaluate if the proposed numerical model is capable to handle the flow of non-Newtonian fluids through PM formed by rebars.

It was stated in the previous chapter that the permeability k depends only on the PM geometry and can be calculated from the numerical simulations with an arbitrary Newtonian fluid. Chapter 5 was devoted to numerical calculation of the permeability and to the validation of the obtained permeability values. The shift factor α, the second unknown PM parameter in the model equations (Equations 39 - 43), is a function of both the PM geometry and the material properties of the propagating fluid (for details on α see Section 2.3.3.3). In this study, the author proposes to calculate α numerically, from the numerical simulations of flow of yield-stress fluid through the observed reinforced zone. This method is explained in Subchapter 6.1. At this point, numerous numerical studies are performed to determine dependence of α on geometry and material parameters and the most appropriate value of α for slow concrete flows is estimated.

It was previously shown in Subchapter 5.3 that, when a Newtonian fluid is propagating, a reinforcement network behaves as a porous medium and can be modelled using the proposed approach. However, the studies on Newtonian fluid do not fully validate the proposed model. The core of the model is namely the definition of the apparent shear rate within the PM (Equation 39). When simulating flow of Newtonian fluids through PM, viscosity is constant; the apparent shear rate has no influence on viscosity and is not included in the governing equations. On the contrary, viscosity of non-Newtonian fluids depends on shear rate and the apparent shear rate definition has to be included in the model equations. Therefore, the proposed approach must be validated on flows of non-Newtonian fluids. For this purpose, the ANSYS Fluent© built-in governing equations are changed by implementing the equation for extra momentum source within the PM, which is based on the definition of the apparent shear rate and the apparent viscosity as explained in Chapter 3. After implementation, various 2D and 3D numerical studies with non-Newtonian materials are conducted, where flow through reinforced geometries is simulated and compared with corresponding PM geometry simulations (Subchapter 6.2). These simulations should show that, when using the proposed model for apparent

viscosity within the PM, the reinforcement and PM simulations provide comparable results.

6.1   Unknown model parameters: numerical studies on shift factor

6.1.1   A numerical method to determine values of shift factor α

When a non-Newtonian fluid is propagating through a PM, the local apparent shear rate can be computed from the value of the macroscopic Darcy velocity of the fluid, the porosity, the permeability and the so-called shift factor α (discussed in Subchapter 3.1). The shift factor α depends on the flow conditions, on the properties of the propagating material and on the topology of the porous medium (Section 2.3.3.3). This factor might be determined experimentally or numerically but a fully established method for its calculation does not exist [158]. In this thesis the shift factor for arrays of cylindrical obstacles is studied by performing numerical simulations of non-Newtonian fluids propagating through the bars arrays. The aim is to compute the values of α and particularly to examine its dependency on the Bingham number.

The Bingham number is a dimensionless quantity, which is, for the specific cases studied here, defined as:

$$B_n = \frac{\tau_0 \cdot M}{\eta_{pl} \cdot v}$$

(65)

where again τ_0 is yield stress, η_{pl} is plastic viscosity, M is the distance between the bars and v is velocity [209]. The Bingham number expresses the relative contribution of yield stress and plastic viscosity to the flow. For instance, high Bingham numbers are associated to flow regimes, in which the contribution of yield stress exceeds and dominates the contribution of plastic viscosity.

In order to determine values of α for a large range of Bingham numbers, a number of numerical case studies in various configurations is conducted. A slow laminar channel flow of a test Bingham fluid through a reinforced sample is simulated and, for each given inlet velocity, the pressure drop within the bars zone is numerically calculated. The macroscopic apparent shear rate in the PM (to be distinguished from the local apparent shear rate defined in Equation 39) is calculated from the computed pressure drop as:

$$\dot{\gamma}_{app}^{MACRO} = \frac{\tau_0}{\dfrac{k}{v_D}\dfrac{\Delta p}{\Delta L} - \eta_{pl}}$$

(66)

where k is permeability, v_D is Darcy's velocity, Δp is pressure drop within the PM and ΔL is the length of the zone. We furthermore assume that the macroscopic apparent shear rate equals the local shear rate:

$$\dot{\gamma}_{app}^{MACRO} = \dot{\gamma}_{app} \tag{67}$$

The value α is calculated so that the local apparent shear rate obtained from Equation 39 equals the macroscopic apparent shear rate calculated from Equation 66 on a wide range of Bingham numbers as:

$$\alpha = \frac{\sqrt{k \cdot \phi} \cdot \dot{\gamma}_{app}^{MACRO}}{v_D} \tag{68}$$

Since the shift factor depends on the medium topology, which, in the specific case of a fibrous medium formed by cylindrical obstacles, is anisotropic, it can be expected that the shift factor alpha will be different for the transversal and longitudinal flow direction. Therefore, the values of the shift factor for the flow normal to the bars axes named α_x and for the longitudinal flow, namely α_y, are determined.

6.1.2   Numerical studies

The simulated geometry used to determine α_x is shown in Figure 52. The figure shows 2D approximation of cuboid samples with arrays of rebars. The inlet and outlet are placed on the left and right edge respectively and the symmetry boundaries are positioned on the remaining outer edges. A slow laminar flow of a test Bingham fluid in x direction is simulated, where the material flows from the inlet through the bars arrays without free surface. Inlet velocity, distance between the bars and material properties are varied to obtain data for Bingham numbers ranging from 0.001 to 10000. The diameter of the bars is either d = 4 mm or d = 1 m, and the relative distance between the bars is X = 2, 4, 6, 8 and 10. The yield stress τ_0 and plastic viscosity η_{pl} of the test Bingham material are also varied: τ_0 = 1, 10 and 100 Pa and η_{pl} = 1, 10 and 100 Pa·s. The simulations are performed for various inlet velocity values in the range v = 0.00001 - 0.05 m/s.

Figure 53 shows a typical geometry used to calculate the values of α_z. The diameter of the bars was d = 4 mm and the relative distance between the bars is varied X = 2, 2.7, 4, 6, 8, 10. The length of the bar is 10 cm and the total length is 20 cm. The yield stress and plastic viscosity of the Bingham material are varied as described in the previous paragraph. The simulations are performed for several different inlet velocity values in the range v = 0.001 - 0.05 m/s. The flow is laminar and parallel to the axis of the bar. The symmetry boundary conditions are assumed at outer faces of the sample.

From the numerical simulations, the pressure drop is obtained. The values of both α_z and

α_x are then calculated according to Equation 68. The values of B_n are calculated according to Equation 65. Finally, the dependence of α_x and α_z on B_n is discussed.
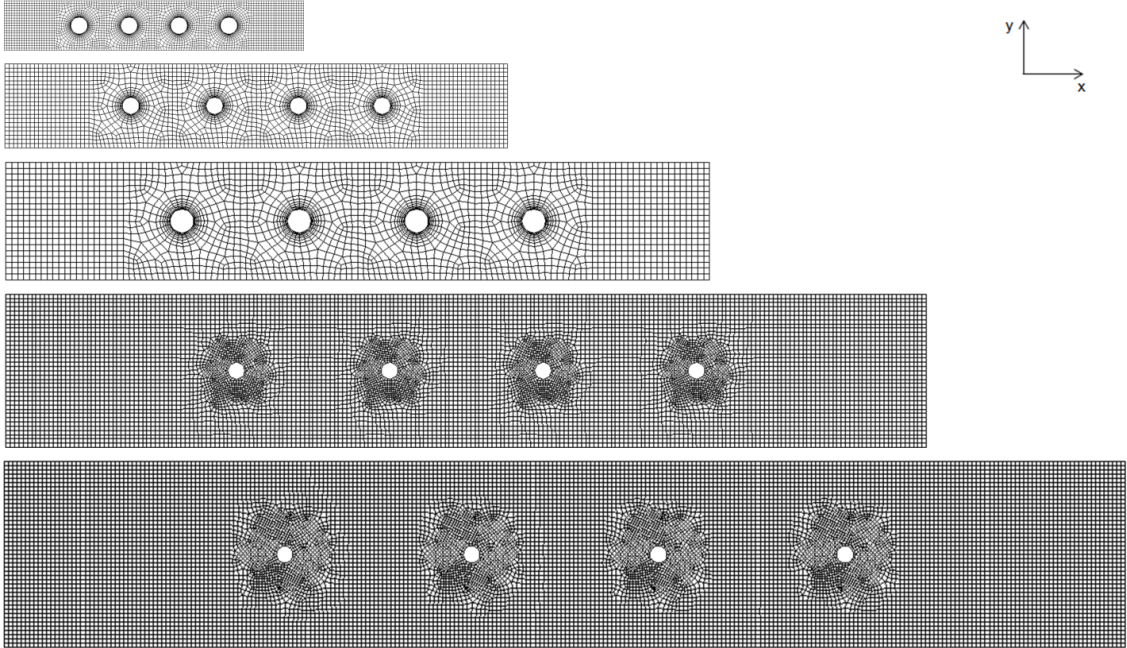
Figure 52: The geometries used for the simulations with non-Newtonian fluid to calculate the value of shift factor α_x when the flow is transversal i.e. perpendicular to the cylinder axes.
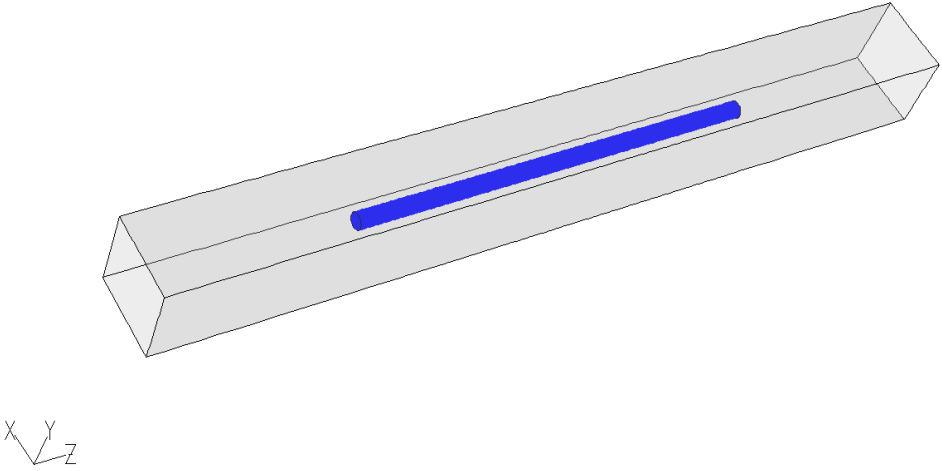
Figure 53: A detail of a typical geometry used to calculate α_z. The diameter of the bar is either d = 4 mm, while the distance between the bars is varied.

6.1.3   Results of numerical studies

The results of the numerical simulations for the shift factor in perpendicular direction α_x are shown in Figure 54. The diagram shows the numerically calculated values of α_x plotted versus Bingham number in the range of 10^{-3} to 10^5. On the studied range, it can be noted that α_x does only weakly depend on Bingham number as it varies between 1 for the lowest Bingham numbers and 1.5 for the highest ones.
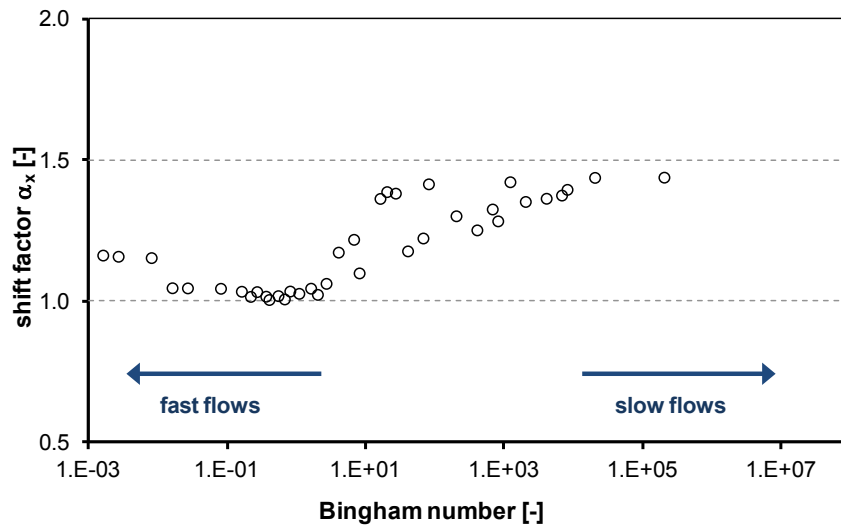
Figure 54:   Shift factor in transversal direction α_x as a function of the Bingham number Bn. The value of α_x varies from 1.0 to 1.5, the dashed lines represent the limit values.

The results of numerical studies on shift factor in parallel direction are shown in Figure 55, depicting α_z as a function of Bingham number Bn. Similarly to α_z, the values of α_z show only a weak dependency of the Bingham number so that again no dependency function can be developed. On the studied range of Bingham number (Bn = 0.001 to 100000), α_z varies between 0.05 for the lowest Bingham numbers and 3 for the highest ones.

As mentioned above, the high Bingham numbers are associated to flow regimes in which the contribution of yield stress exceeds and dominates the contribution of plastic viscosity. In the industrial practice, yield stress of fluid concretes (which are studied in this thesis) is of the order of several tens of Pa. Their plastic viscosity is of the order of a couple tens of Pa·s. As a consequence, the above values for shift factor are adequate as long as local apparent shear rate stays lower than a few hundreds of s^{-1} and higher than few hundredths of s^{-1} [14]. These limit values are respectively well above and below the range of shear rates that are often considered during industrial casting (i.e. between 1 and 10 s^{-1} [66]). However, the lower boundary of this shear rate range prevents from the full prediction of flow stoppage during which shear rate slowly tends towards zero (Bingham

number becoming infinite). It can be noted that, in most practical cases, first order data are the ones dealing specifically with what happens when flow stops. These are the situations of interest when one wants to predict whether a given concrete will fill a given formwork or stop flowing before the mould is filled, leaving voids in the final structure. Therefore, in the following, the focus will be on the shape of the concrete in the mould when flow stops. In order to ensure that the numerical tool presented in this paper is able to predict flow stoppage with the highest accuracy, the following limit values of the shift factor will be used in the range of high Bingham numbers: α_x = 1.5 and α_z = 3.0.
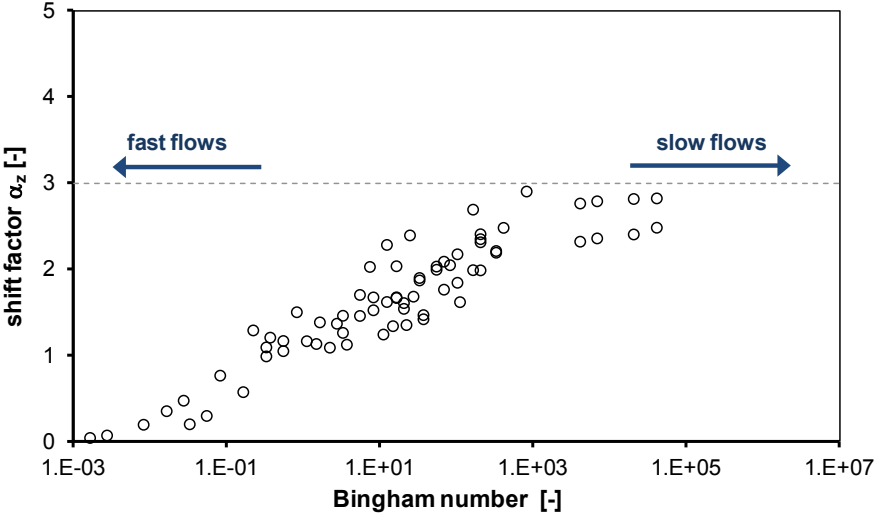
Figure 55: Shift factor α_z as a function of the Bingham number. The dashed line represents the upper limit α_z = 3 which the function approaches.

6.2   Numerical validation: case studies with non-Newtonian fluid

The permeability k and the shift factor α can be determined numerically as proposed in subchapters 5.1 and 6.1, making Equation 40 for the influence of the PM on the flow fully defined. This equation is implemented in ANSYS Fluent© as an UDF function and applied to PM zones. In this subchapter, we compare the simulations of the flow of non-Newtonian fluid through arrays of rebars with the simulations of flow through the corresponding PM geometry. The goal is to prove if the determined values of α are correct and if the model could in general be applied on yield stress fluids propagating through arrays of rebars.

In the first case study to be presented here, simulations with the 2D geometry depicted in Figure 56 and a test Bingham material are conducted. The bar diameter is d = 3 mm and the distance M between the bars is varied from 6 mm to 8 mm (whereby the relative distance X between the bars is X = 2 and X = 2.7). Inlet and outlet are placed at the left and right outer edge, respectively, while all the other outer edges have a symmetry

106

boundary condition. The material properties are set to unity values: yield stress τ_0 = 1 Pa, plastic viscosity η_{pl} = 1 Pa·s and density ρ = 1 kg/m^3.
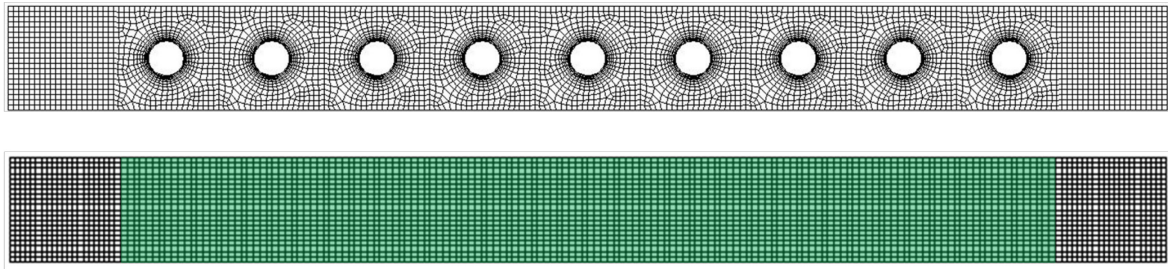
Figure 56: The 2D geometries used in the case study. Exact geometry (above): the diameter of the bar is d=3mm and the distance between the bars is varied from 2d to 2.7d. The porous medium analogy (below).

The second and more "realistic" 3D study is performed using a concrete-like Bingham fluid, having material properties typical for self-compacting mortar: τ_0 = 5 Pa, η_{pl} = 5 Pa·s and ρ = 2700 kg/m^3. The test geometry in Figure 57 has the following dimensions: the box dimensions are 25 x 25 x 75 cm^3, the bar diameter is d = 1 cm and the distance between the bars is M = 4 cm. The material flowing from the inlet on the left towards outlet on the right, whereby remaining four outer faces are walls with no-slip boundary condition.

a)   b)
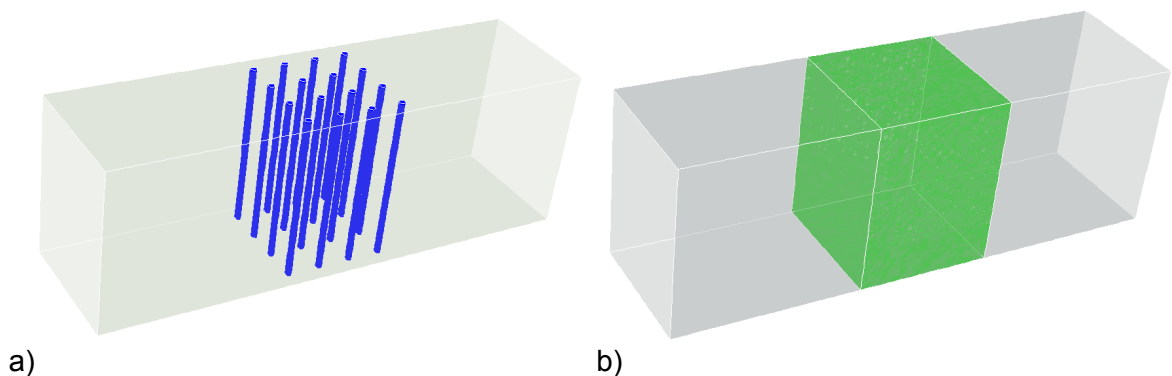
Figure 57: The 3D case study: a) exact geometry and b) the porous medium analogy.

The simulations with the PM geometry are conducted by implementing the porous media model explained in Chapter 3 into ANSYS Fluent©. Since this is a pure channel flow with only one flow direction, the pressure drop is added only in the flow direction, i.e. in the direction x. The unknown permeability is computed as explained in 5.1 and the value of α_x is taken to be 1.5. The simulations for the reinforcement and PM cases are compared in terms of pressure drop within the reinforcement/porous zone.

The results of the numerical simulations with the 2D geometry and unity Bingham fluid are shown in Figure 58. The simulations are performed for different inlet velocities and the pressure drop is calculated. The diagrams show the pressure drop within the

reinforcement/porous medium zone plotted versus the inlet velocities. For both cases under investigation (X = 2 and X = 2.7), an excellent agreement when comparing the reinforcement and PM geometry is achieved. The maximal discrepancy for the calculated pressure drop between reinforcement and PM case is found to be 1%.
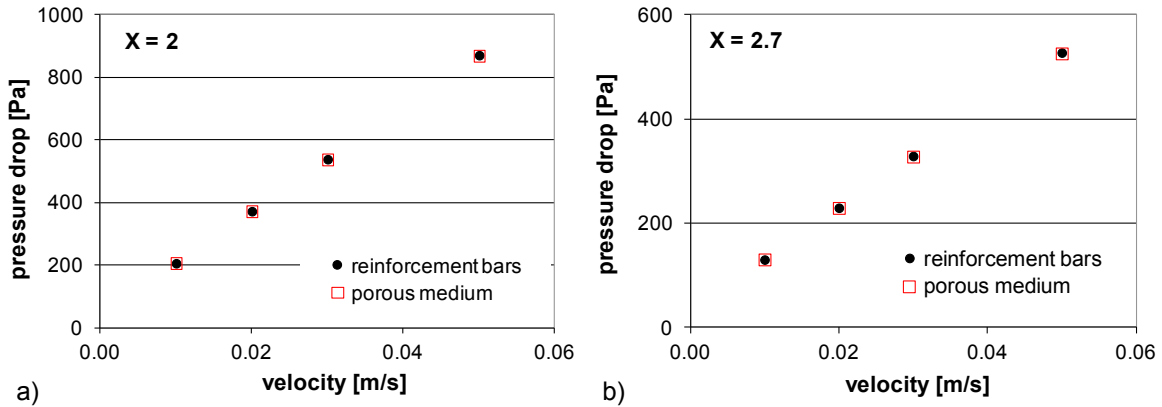
Figure 58: 2D case study: comparison of the model with rebars and PM model, pressure drop as a function of inlet velocity for a) X = 2, b) X = 2.7. X is the relative distance between the rebars.

The results of the 3D simulations with the concrete-like material are shown in Figure 59. The diagram shows the comparison of the pressure drop for the reinforcement and porous medium geometry for three different inlet velocities.
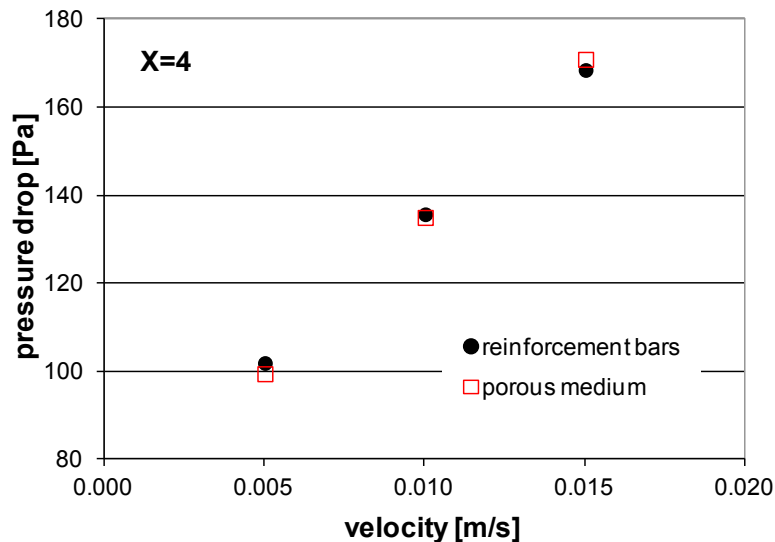
Figure 59: 3D case study: comparison of the model with bars and PM model, pressure drop as a function of inlet velocity.

The comparison shows good match between the numerical results for the reinforcement and corresponding porous medium. This validates that propagation of the non-Newtonian fluid through arrays of rebars can be modelled as a PM.

6.3   Conclusions

The studies on the shift factor α calculation in 6.1 showed that its determination is not a simple task since this parameter is influenced by several factors. The numerical simulations performed for the wide range of Bingham numbers B_n demonstrated however that the dependency of α on Bn is weak. Since, in this study, the shape of the material when flow stops is of the main interest, it is to be emphasized that the values of α for slow flows (i.e. flows with very high Bingham numbers) are relevant for our study. Therefore, in the numerical simulations that follow, the following limit values for α are used:

- for the flow perpendicular to the bars α_x = 1.5 and α_y = 1.5;
- for the longitudinal flow, parallel to the bars axes α_z = 3.

In the case studies presented in 6.2, the results obtained when using reinforcement geometry and its porous medium equivalent were compared. The results showed a good match, suggesting that the chosen values of the shift factor are reasonable and can be used for further simulations. The good congruence also proved that the model is so far able to represent the flow of a yield stress fluid through a channel (with walls) with arrays of bars, considering these as porous medium.

The results shown in this chapter validate the basic postulate of this thesis: when crossed by a yield stress fluid, the reinforcement network behaves as a porous medium and can be mathematically modelled as one. Hereby the free surface is not considered. For that reason the next step towards practical application of the model should be to test the proposed method and parameters on the free-surface flow of yield stress fluids through reinforced formworks.

7 Experimental validation: experiments with model material

Chapters 3 to 6 presented a mathematical model to describe the flow field within the PM, showed a methodology to determine unknown parameters in the model equations and its implementation into the numerical code. The performed numerical studies moreover proved that the approach is applicable on channel flow of Newtonian and non-Newtonian fluids through arrays of rebars, where these are modelled as porous medium. The next step, which will bring us closer to full practical validation of the model, is an experimental validation of the numerically proved postulates on free surface flows of yield stress fluids.

In order to recognize porous medium behaviour of the reinforcement network and to make general conclusions about propagation of yield stress fluids through the reinforcement zone, experiments with model material on a small scale are carried out. This experimental survey is a part of a doctoral thesis conducted by the project partner and results are published in [144]. The experimental setup and obtained experimental results are fully overtaken from [144] and, within this research step, these experiments are simulated.

In the sections that follow, the model material and experimental setup of the experiments performed in [54] are explained. We start with the test material Carbopol® gel that is used in this study, pointing out why this material is suitable to be a "representation" for cementitious materials. We continue with a detailed depiction of experimental and numerical setups and a description of the experimental procedure. In conclusion, experimental results are compared with the corresponding simulations. The experiment is modelled both as reinforcement geometry and the geometry with equivalent porous medium instead of rebars. The results will show that the simulation of Carbopol® works fine and that the experimental and numerical results for the flow front and the pressure drop are in a good agreement. This moreover proves that the proposed model is able to simulate casting of a yield stress fluid in reinforced formworks.

7.1 Model material and experimental setup

7.1.1 Model material

From the rheological point of view, fresh cementitious materials are thixotropic yield stress fluids (see Section 2.2.1). This means that these suspensions flow when the applied stress is higher than a critical value called yield stress and that this yield stress strongly depends on the flow history of the material [32, 58, 59, 61, 66, 182, 185, 187]. Moreover, cementitious materials are submitted to a non-reversible chemical evolution (i.e. the hydration process), which strongly affects the rheological behaviour on longer times of

observation [210]. All these phenomena are of interest for researchers trying to understand their physical origin and practitioners trying to ensure that the casting process will result in the proper filling of a given formwork. However, these phenomena mixed together in one material and occurring simultaneously prevent researchers and practitioners from understanding or predicting the material behaviour properly [14]. That is why model materials, which show flow behaviour similar to the one of the cementitious materials but less complex, are of very high interest.

In this thesis, the focus is placed only on one aspect of the flow: the yield stress behaviour. Nevertheless, in nature or industry, most yield stress fluids are also thixotropic. Two materials, which display pure yield stress behaviour, can however be found in literature: water/oil emulsion and Carbopol® suspension. As the preparation of emulsion is highly time consuming as soon as volumes higher than a few litres are needed, in [144] the author chose to focus on Carbopol®. The polymer used in this work is Carbopol® Ultrez 10, a transparent material that disperses in water faster than other conventional grades. Carbopol® of 0.3% volume fraction is used. As rheology of polymer solutions is very sensitive to the chemical composition of solvent in order to achieve a better reproducibility of the results, distilled water is chosen as the solvent. The manufacture of a suspension of Carbopol® is divided in two stages: dispersion of the powder and neutralization of the solution.
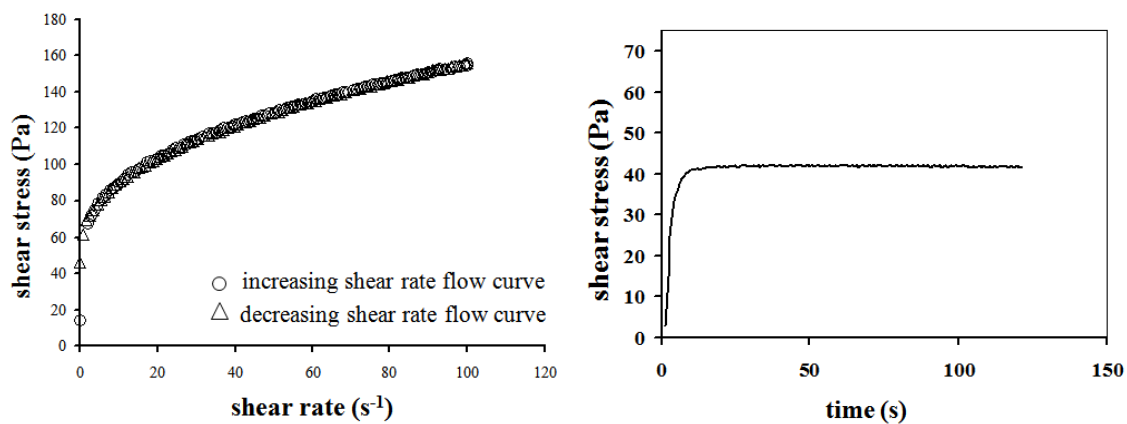
a) b)

Figure 60: Rheological behaviour of the Carbopol® suspension used in [144] and presented in this thesis. a) Shear stress as a function of shear rate for increasing/decreasing shear rates, b) yield stress measurement at a constant shear rate of 0.08 s^{-1} [14, 144].

The dehydrated Carbopol® powder is slowly added to distilled water through a fine metal mesh using a variable speed mixer. The solution is then neutralized by sodium hydroxide. A mixing period of six hours follows this neutralization phase. Finally, the products are conserved at 25° C during 2 days. The prepared Carbopol® suspension can then be diluted in distilled water in order to produce mixtures with yield stresses between 15 and 125 Pa. Before use, air bubbles are removed by a slow manual shearing [144].

The Carbopol® suspension used in [144] presents neither thixotropic characteristic nor irreversible evolution. This is shown by the superposition of the curves of increasing and decreasing rotating shear rate ramps in Figure 60a and by the plastic plateau in Figure 60b. These curves are obtained using a HAAKE ViscoTester VT550 equipped with coaxial cylinders, the inner cylinder of diameter 18.9 mm being in rotation whereas the outer cylinder of diameter 20.5 mm remains fixed. Both cylinders surfaces are covered with sand paper in order to avoid wall slip. In the following, we fit the behaviour of all Carbopol® suspensions with the Bingham model.

7.1.2 Experimental setup

The experimental setup used in [144] and in this study is shown in Figures 61. The setup consists of a 20 x 20 x 60 cm³ container made of transparent Plexiglas, enabling observation of the flow front of the poured fluid. The adaptable plate in the middle of the box, holds a variable number of vertical steel bars with diameter d = 3 mm. This system allows for easy modification of the number of bars and their configurations. Figure 62 shows the details of this plate with the bars.
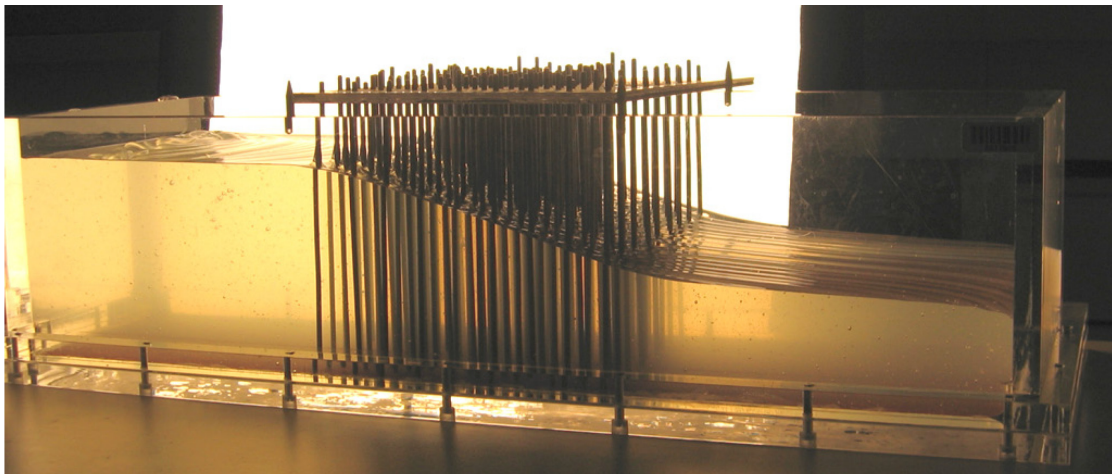
Figure 61: Experimental setup: the transparent container with the adaptable modulus holding the reinforcement bars, shown here with Carbopol® gel at the end of casting [14, 144].

Between 11 and 12 litres of Carbopol® suspension are slowly poured at one side of the form to avoid any inertial effect [112]. The Carbopol® suspensions used in this project have the following material properties: density ρ = 990 kg/m³, plastic viscosity η_{pl} = 1 Pa·s and yield stresses τ_0 = 15 or 40 Pa. When the flow stops, the image analysis allows for the measuring of the final shape of the material
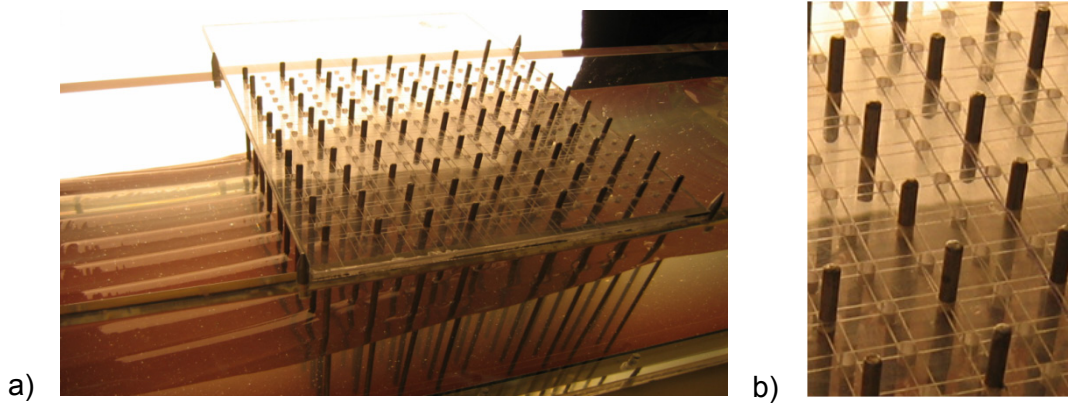
Figure 62: a) The adaptable module holding the reinforcement bars and b) the detail of the module [14, 144].

7.2 Comparison of numerical and experimental results

7.2.1 Determination of boundary conditions

Since the interaction between Carbopol® suspensions and the Plexiglas wall of the model formwork is unknown, numerical studies on wall-fluid interaction are first conducted using the CFD software Fluent©. As mentioned in 4.1, this software enables two models for the fluid-wall interaction: wall slippage or no-slip condition. The experiments are performed by pouring the material into the model formwork without any steel bars and by recording the shape of the free surface when flow stops. The Carbopol® suspension used in this section has the following properties: density ρ = 990 kg/m^3, plastic viscosity η_{pl} = 1 Pa·s and yield stress τ_0 = 15 Pa.

Figure 63: Numerical setup for the calibration of the boundary conditions. Intermediate position of the fluid flowing into the box with no obstacles [14].

The experiments are simulated using either full-slip or no-slip boundary condition at the lateral walls of the channel. The numerical setup is shown in Figure 63. The material is numerically poured in the formwork using a pouring funnel. Since jamming and sticking of the material is to be prevented in the funnel, the funnel walls are assumed to have full-slippage boundary condition. Figure 64 shows the comparison of the experimentally obtained values with numerical studies, taken at the middle line of the container. It can be observed that the best agreement is obtained when the no-slip condition is used on the bottom and the lateral walls of the formwork. This boundary condition is used in the rest of this study for the channel walls.
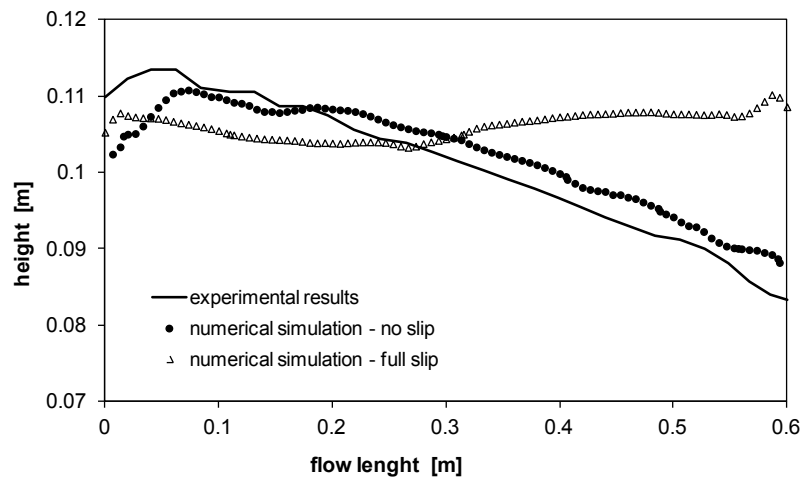
Figure 64: Comparison of the experimental shape with the numerical simulations for the two types of boundary conditions at the channel lateral walls [14].

7.2.2   Numerical simulation with steel bars and with PM

The numerical setups used here are shown in Figure 65. Numerical simulations of casting of Carbopol® suspensions in the model formwork with various steel bars configuration are carried out using the software ANSYS Fluent© (Figure 65a). The comparison between the predicted final shape and experimental measurements is plotted in Figure 66. As expected, it was shown that, when using the exact geometry with each bar being implemented, CFD is able to predict the free surface flow of a yield stress fluid in a complex formwork.

In order to demonstrate applicability of the approach proposed in this paper on the reinforced sections, the same experiment is simulated using PM model. The PM model is implemented in ANSYS Fluent© as a User Defined Function (UDF) by adding a momentum source term in the porous medium (see Subchapter 3.3). Since the flow in this case is dominantly in one direction, in order to simplify the simulations, the extra source term is added only in one dominant flow direction (x). The permeability is obtained from

numerical studies with Newtonian material (see Subchapter 5.1), and the value of shift factor used in the simulations is $\alpha_x = 1.5$ (see Subchapter 6.1).
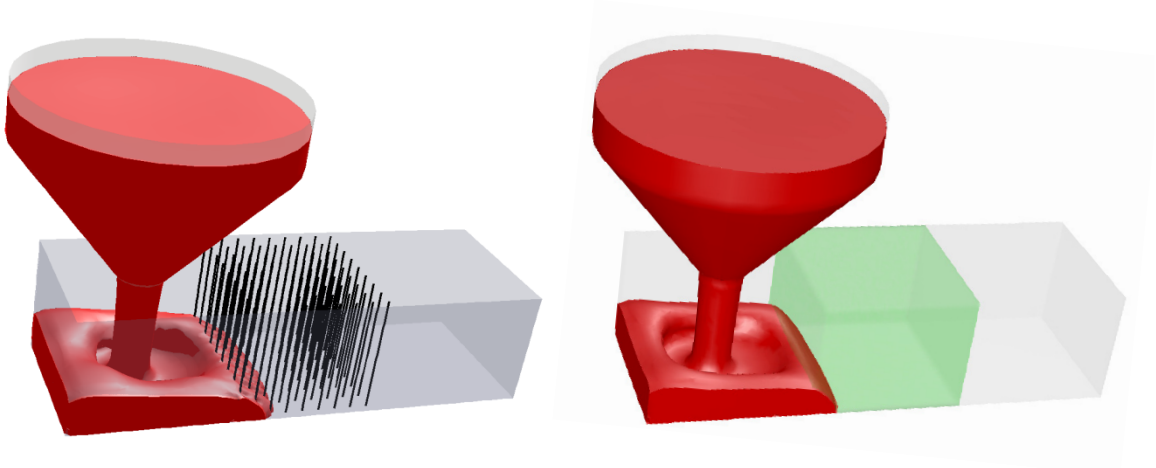
Figure 65: a) The numerical setup for the simulations with steel bars and b) porous medium analogy. The intermediate state of the flow is shown.

Figure 66 shows a comparison of the final shape of the material between experimental results, numerical simulation with the steel bars and numerical simulation for the corresponding PM case, for a 15 Pa Carbopol® suspension crossing a network of 3 mm steel bars located on a 22 mm x 22 mm grid. The total number of bars was 81. Figure 67 gives only a visual representation of both experimental and numerical results obtained.
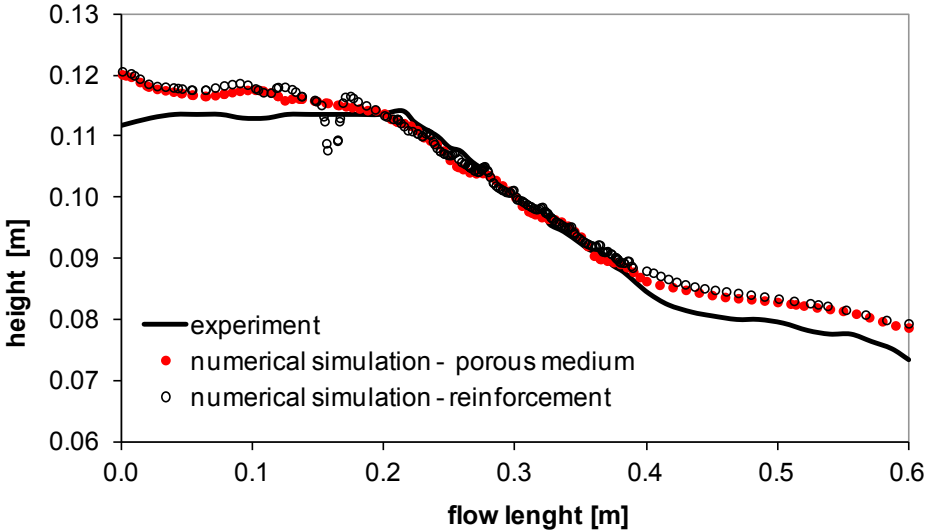
Figure 66: Comparison between the experimental measurements, numerical simulation with steel bars and numerical simulations with porous medium - the final shape when the material stops flowing.

A good correlation between experimental and numerical results shows that, although considering the steel bars network as a porous medium is a rough approximation, similar

116

results are obtained for the final shape of the material after casting. The discrepancies that can be observed near the front and the back wall of the container, might be result of the used wall boundary conditions. Nevertheless, more important for this study is that the slope of the flow front within the porous zone is in perfect congruence for both numerical solutions and experimental results. This result validates the basic postulate of this study: when casting a yield stress fluid, the reinforcement network behaves as a porous medium and can be mathematically modelled as one.
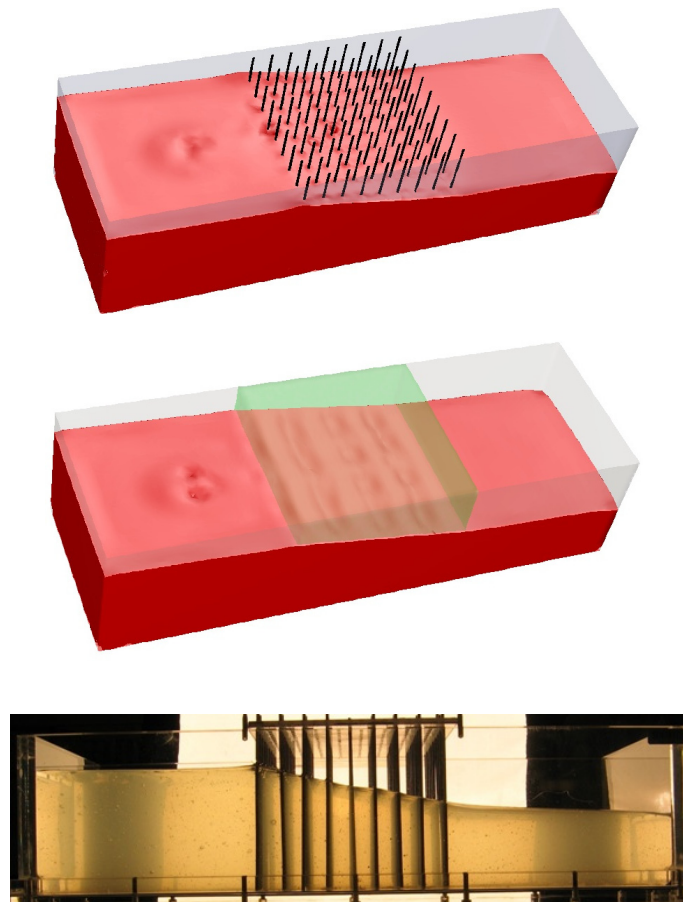
Figure 67:   Visual illustration of experimental and numerical results with steel bars and with porous medium.

Figure 68 shows a comparison between numerical simulations with steel bars or porous medium and experimental results in the terms of pressure drop. The results are shown for a range of relative distances between the bars between 2.5 and 7 and various yield stresses between 15 and 40 Pa. In order to gather all results in one graph, it was chosen here to plot the "apparent permeability" defined as $k_{app} = (M \cdot \tau_0 \cdot \Delta x)/(\rho\, g \cdot \Delta h)$ where τ_0 is the yield stress of the tested material, Δh is the thickness variation in the porous medium and Δx is distance. It can be noted that, in some cases, the material was not able to fully cross the porous medium both in the experiment and in numerical simulations. So the distance

Δx is equal to 0.2 m if the material crossed the porous medium or is equal to the propagating distance in the porous medium if it was not able to fully cross the porous medium. From the diagram it can be seen that, in the range of configurations tested here, there is a good congruence between the experimental and the numerical results.
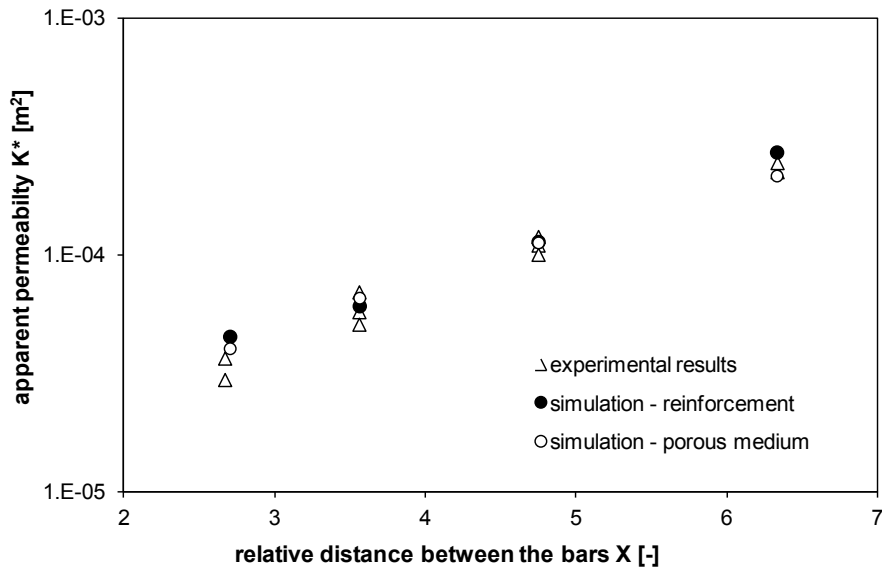
Figure 68: Comparison between the experimental measurements, numerical simulation with steel bars and numerical simulations with porous medium - permeability k_{app} as a function of X.

It can be noted that, in order to obtain the final shapes shown in Figure 67, the following pre-processing times and computation times on the same computer were needed:

A) Numerical simulation with steel bars :
   Number of calculation cells: 170000 cells (this mesh is, in theory, too coarse but had to be chosen in order to limit the computation time);
   Pre-processing time: 2 hours;
   Computation time: 10 hours;
   Total time: 12 hours.

B) Numerical simulation with porous medium:
   Number of calculation cells: 60000 cells (this mesh is finer than actually needed);
   Pre-processing time: 20 minutes;
   Computation time: 3.5 hours;
   Total time: 3 hours 50 minutes.

Although 70% reduction of total time is reached here, it can be noted that it would still be possible to reduce the number of calculation cells in the case of PM by a factor 3 decreasing therefore the total time to 1.5 hours (88% reduction) bringing it in the range of potential industrial applications.

7.3   Conclusions

This Chapter presented the experimental and the numerical studies on casting of Carbopol® gel into model formworks. The experimental results are compared with the simulations with bars as well with PM analogies. The comparison of experimental and numerical results suggested that the proposed model showed a good congruence with experiments in terms of pressure drop and flow front. In the range of configurations tested here, the technique based on porous medium analogy is fully able to predict the shape of the cast material when flow stops. The time needed for the numerical simulations with PM model was significantly shorter than for the simulations with reinforcement. The average reduction in the total simulation time (both pre-processing and computation times) is 70%.

The results shown in this Chapter validate the basic postulate of this study: when crossed by a free-surface flow of yield stress fluid, the reinforcement network behaves as a porous medium and can be mathematically modelled as one. So our model is valid for castings of non-Newtonian fluids into reinforced formworks. The next step towards the model's final validation, is application of the model to simulate casting of SCC into reinforced formwork.

8   Experimental validation: large scale experiments with SCC

This chapter is devoted to the application of the proposed numerical model to simulate SCC casting in a model formwork.

In the preceding studies, the model for SCC flow between the rebars was developed and implemented into the CFD software Fluent©. The preliminary experimental validation on the small scale experiments with Carbopol® gel described in Chapter 7 proved that the implemented model is able to successfully simulate the flow of non-Newtonian fluids through reinforcement networks. It was also proved that the implemented model lead to a significant decrease in total computational time.

The first approximation of the model, where the rebars zone is simplified as a homogeneous PM, was proved valid in the previous chapters. The second major simplification of the chosen approach is that we assume that concrete is a continuous yield stress fluid. In this Chapter, it will be proved that, under certain limitations, this approximation is valid also for SCC i.e. that at a macroscopic level behaves as a Bingham fluid and its flow between the rebars can be modelled using the approach based on propagation of yield stress fluids through porous media. For this purpose, a large-scale form-filling experimental setup is built and experiments are performed. Through comparison of the experimental results and the results of corresponding numerical simulations, the applicability of our mathematical and numerical model for the flow of cementitious materials in presence of reinforcement should be finally proved.

To choose an appropriate experimental setup, it was necessary to perform series of numerical studies with different geometries of the filling form and reinforcement dispositions, tuning them until optimal ones are found. Once the geometry is decided on, the experimental setup is built and the experiments with SCC are performed using several different concrete mixes. Subsequently to the experiments, the numerical simulations when using exact geometry (rebars) and numerical simulation using approximate porous medium geometry and model are conducted. Similarly to the case studies with Carbopol® gel, the developed numerical tool is validated through the comparison of experimental results, numerical results when using exact geometry and numerical simulation using the equivalent porous medium. The experimental and numerical data are compared in terms of flow front. The observed good congruence between numerical and experimental results proves that the model is able to depict behaviour of different concretes through various reinforcement zones.

Subchapter 8.1 will give the details on the preliminary numerical simulations which are performed in order to choose the optimal experimental geometry. Subchapter 8.2 is devoted to the studies concerning the choice of concrete mixes. In Subchapter 8.3, the

experimental setup, experimental procedure and performed steps needed for material characterisation are described. Subchapter 8.4 gives insight into the numerical simulations performed in this step: the simulations to determine material and PM parameters and simulations of the main experiment. Subchapter 8.5 presents the experimental and numerical results and their discussion.

8.1   Numerical studies to choose an optimal experimental setup

The experiments with SCC should serve as a final step to prove that the model can be applied on simulations of real castings and its design is not a trivial task. The experiment should be designed and carried out so that one can observe different behaviour when concrete is propagating through diverse bars arrays, while the unwanted effects are avoided. It should be a form-filling experiment, where concrete is poured in a geometrically simple form, which contains reinforcement bars. The experimental setup and procedure have to fulfil the following prerequisites:

- The experiment is to be constructed as realistic as possible: as long as dimension limits allow, one should use concrete mixtures, rebar size and distances that are actually used on construction sites.

- In order to be able to see different flow behaviour through reinforcement zones, the form should contain at least three sectors, in which the rebars are arranged differently and which will consequently influence the flow of concrete in dissimilar ways.

- It is necessary to have a 3D distribution of the bars, so that the material is offered a possibility to bypass the reinforcement zone, whereby this can be observed during the experiment.

- Within the experiment, one should be able to observe flow front from the side and from above. Therefore the front wall should be constructed from a transparent material such as Plexiglas. The Plexiglas plate should be thick enough to support a high pressure that concrete creates on formwork.

- One has to choose an appropriate material for the walls of the formwork, so that both the eventual slippage and high friction are avoided.

- Since the proposed model is limited to non-blocking concretes, one has to choose the maximum diameter and minimum distance between the bars to assure that no blocking occurs during the experiment.

- According to the blocking criteria [211] the minimum distance between the bars cannot be less then d_{bar} + 5mm and not less than d_{max} + 5mm (where d_{bar} is the diameter of the steel bar and d_{max} is maximum particle diameter in the utilised concrete).

- Since the dispersed particles cannot be included as a second phase in the simulation, the used concrete should neither bleed nor segregate.

- In the casting situations observed in this thesis, the flow of concrete is laminar and should be accordingly kept laminar within the experiment (no turbulences, waves etc.)

Due to the complexity of formwork geometry, the quantity of concrete to be utilised (hundreds of litres) and the related high costs, it was not possible to perform preliminary full-scale experimental studies to determine the optimal experimental setup. Therefore, analytical calculations as well as a series of preliminary numerical studies are conducted where, by testing several different setups, the optimal test geometry and procedure, which will fulfil all the above-mentioned prerequisites, were tried to be found.
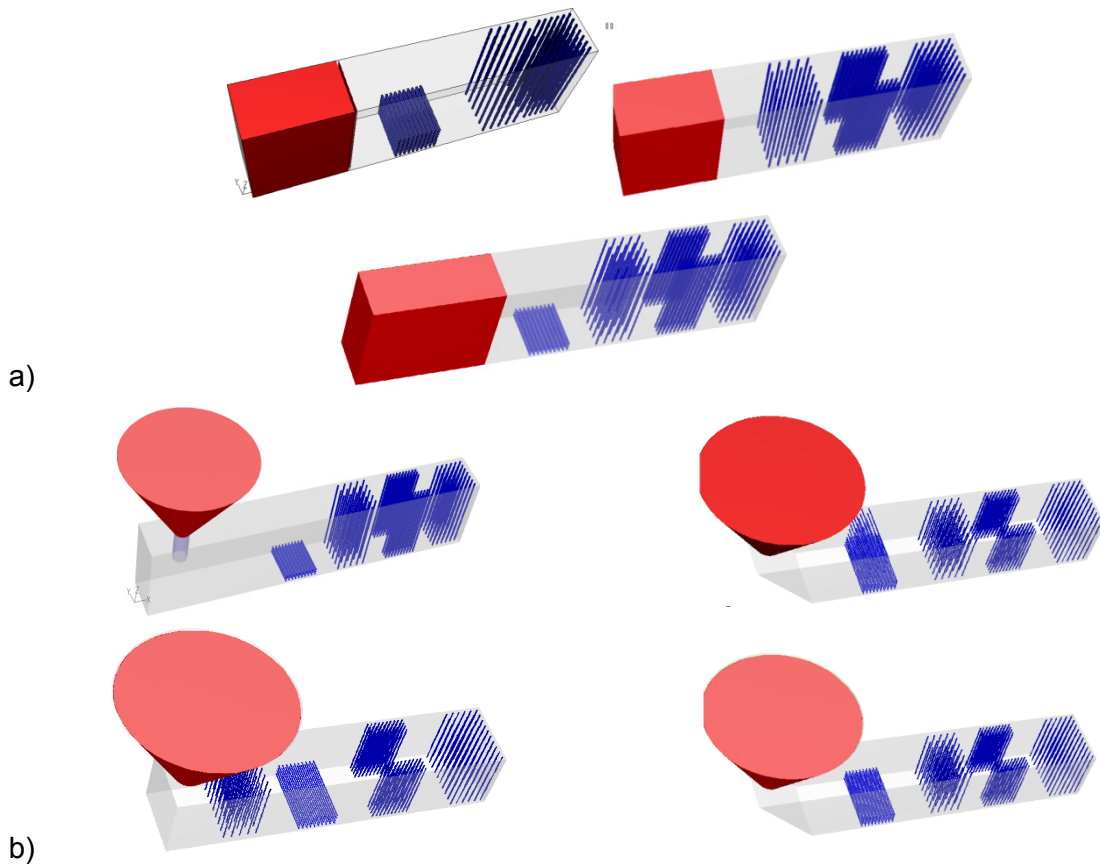
Figure 69: Preliminary numerical studies to determine the optimal experimental geometry. a) Three geometries with a gate and b) four different forms with a pouring funnel. The initial position of concrete is also shown.

Figure 69 shows several different geometries that were taken into consideration. To determine settings and boundary conditions for the formwork itself, the flow of concrete into a form without steel bars was simulated (the inlet flow rate, the optimal inlet height, ways to avoid turbulences and waves, wall boundary conditions, solver settings etc. were tested here). Afterwards, the obstacles are introduced into the form and both reinforcement positions and form geometry were altered in order to find one geometry, where we can observe the wanted effects and avoid undesirable behaviour. The tested channels were up to 3 m long and approx. 300 - 400 litres of concrete was poured in. Both setups with pouring funnels and setups with a gate were tested. It was found out, that placing the material behind the gate will cause a very high pressure of the concrete on the gate and, in the experiment, it would be difficult to prevent the gate from rolling over or to

lift such a highly loaded and relatively big plate slowly. It was therefore decided that the pouring from a funnel suits better for the main experiment, so the different shapes of the funnel and its opening are also tested. It was shown that, in order to avoid high kinetic energy of concrete falling from the funnel, the channel itself should have a ramp on the pouring side and that the funnel gate opening should be between 2.5 and 6 cm.

Based on all the prerequisites and the conclusions of the preliminary numerical studies the final geometry is chosen as shown in Figure 70 and Table 4. It consists of a rectangular container with dimensions of 2980 x 500 x 700 mm^3, where the concrete is poured in. A 45° ramp is constructed on the pouring side of the box, so that concrete can flow slowly into the form. There are four different reinforcement zones within the box; the diameter of all the rebars is d_{bar} = 10 mm, while the distance between the bars is 50, 20, 20 and 40 mm in the zones 1, 2, 3 and 4, respectively.
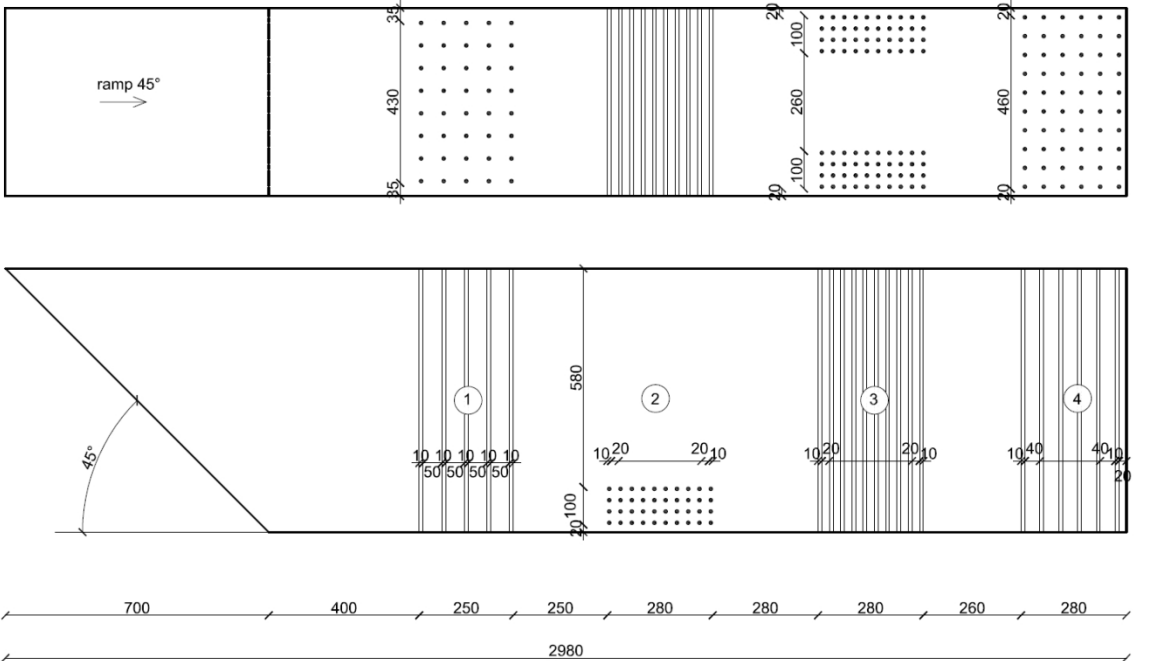
Figure 70: A sketch of the container geometry chosen for the experimental setup, top view and front view. All the measures are given in mm.

Table 4: The geometrical parameters of the four reinforcement zones depicted in Figure 67.

ZONE NR.	1	2	3	4
D, bar diameter [mm]	10			
n, number of the bars [-]	5x8	10x4	2x (10x4)	6x10
M, distance between the bars [mm]	50	20	20	40

Figure 71 shows the filling formwork, which is built according to the drawings in Figure 70. The walls of the form are made of smooth wooden plates while the front wall is made of 2.5 mm thick Plexiglas plate. Metal clamps are used to secure Plexiglas and wooden plates tightly together and prevent movement or separation through the high formwork pressure. The adaptable module (with a 10x10 mm grid) in the zones 1 - 4, hold a variable number of vertical steel bars. This system allows for easy modification of the number of bars and their configurations. Within the experiment, the material is to be poured from a funnel along the ramp (left corner of the form in Figure 68) and let flow under its own weight through the reinforcement zones.
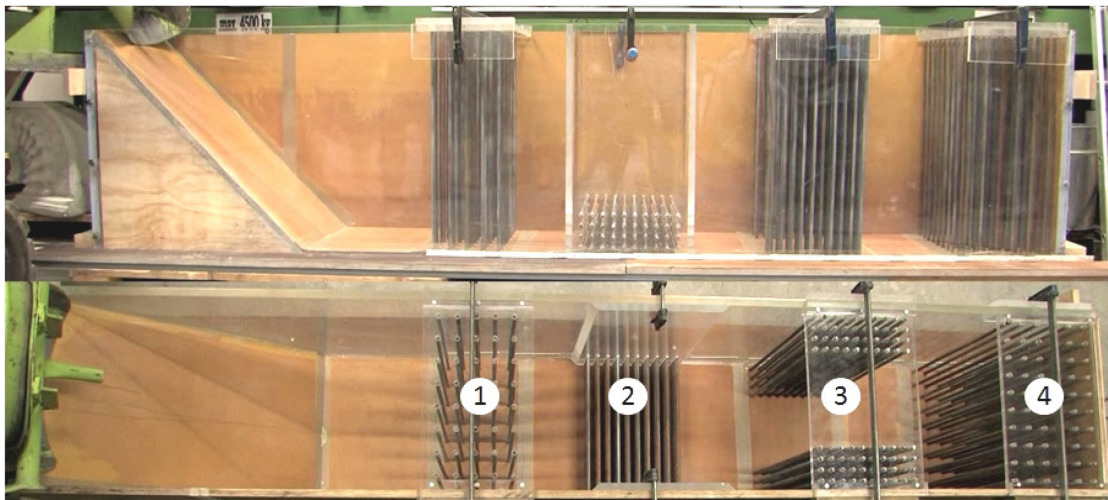
Figure 71: The front and the top view of the Plexiglas container with four different reinforcement zones, built according to the drawings in Figure 67.

8.2 Concretes under investigation

During the experiment, the concrete is poured into the form shown in Figure 71. The total volume of the box is 930 litres. In order to be able to observe material's flow front, to avoid overflow as well as high pressure on the formwork walls, approximately one third of the container should be filled. Thus 350 litres of concrete is utilized in the main experiment. The minimum distance between the steel bars is M_{min} = 20 mm, so taking into account the blocking limitations, the maximum particle diameter is d_{max} = 8 mm.

To demonstrate the applicability of the model on concretes with different rheologies, the concretes under investigation should vary from very flowable to stiffer ones (which are in fact almost not self-compacting). When blocking does not occur, the yield stress of concrete is the determining parameter for the final shape of the material. The aim is therefore to test the mixtures that have very different values of yield stress. Before the whole experimental procedure started, preliminary tests on concrete mixtures were

performed, where investigated SCCs were adjusted in order to achieve required parameters.

To make sure that no influences of different volumetric ratios of paste to aggregates occur, the same mixture composition was chosen for all concrete mixes. Since within certain boundaries, the addition of polycarboxylic superplasticizers (PCE) predominantly affects the yield stress without having crucial effects on the plastic viscosity, the superplasticizer addition can be used as a controlling parameter for the yield stress adjustment [22]. However, the amount of PCE also strongly affects the workability retention, and for the good conduction of the experiment a long workability time had to be adjusted. Thus, high PCE dosages are required in order to provide sufficient open time and therefore a mixed approach is preferred, in which the rheological properties are adjusted by PCE and stabilising agent. Due to its strong effect on yield stress, stabilising agent based on potato starch was used. Table 5 shows the mix design for the four concretes tested, which only differ in the addition of superplasticizer and stabilising agent. The main experiment is performed for these four concretes, named SCC1 to SCC4.

Table 5:   Mixture composition for the basic SCC mixtures used in the experiments.

		SCC1 very low yield	SCC2 low yield	SCC3 medium yield	SCC4 high yield
Constituent	Specific Gravity [-]	Net weight per 1 m^3 of concrete [kg/m³]			
Cement	3.12	296			
Limestone filler	2.74	296			
Water	1.0	180			
Sand (0 - 2.0)	2.60	662			
Aggregate (2.0 - 8.0)	2.60	891			
		admixture adjustment			
Superplasticizer	1.07	2.79%	2.15%	2.15%	2.15%
Stabilising agent		-	-	0.017% bwo water	0.47% bwo water

8.3   Experimental setup and procedure

The experimental procedure involves several (overlapping) phases: mixing of concrete, parameter determination, slow pouring of concrete into the form and measurements when the material stops.

At first, 400 litres of concrete were mixed over a period of 10 minutes in a TEKA rotational mixer with an effective mixing volume of max. 500 litres. The material is then divided into

two portions: 350 litres were used for the main flow experiment and the remaining 50 litres were used for the investigation of the material properties.

The first share of 350 litres is filled from the mixer into a mobile hopper, poured into a funnel and transported to the position above the left corner of the Plexiglas container using a forklift (Figure 72). The funnel gate is opened (so that the inlet opening is kept constant i = 5 cm) and the concrete is allowed to freely flow into the Plexiglas container. During flow, the flow front development was videotaped from aside and from above. When the flow stops, the final shape of the flow front was measured.

a)   b)

Figure 72: Main experiment: a) filling of the pouring funnel with concrete and transport of concrete to the position above the form; b) the Plexiglas form and the funnel filled with concrete. The experiment starts by pulling a gate on the bottom of the funnel.

The second portion i.e. the remaining 50 litres of concrete is used for the determination of the material properties. The tests to determine the material properties are performed twice: after the mixing, two minutes before the funnel gate is opened and during the main experiment. Here the slump flow, the LCPC-box flow distance and the V-funnel efflux time were measured and the G-yield and H-viscosity are determined using the Rheometer-4SCC (Figures 73 - 75 respectively). The material parameters to be determined from these measurements are the yield stress and plastic viscosity of concrete. The results of the measurements for SCC1 - SCC4 and the determined values of yield stress and plastic viscosity for the given concretes are given in Table 6.

The yield stress values were derived from the correlation curves between the G-Yield values determined by the Rheometer-4SCC and the values obtained analytically from the slump flow and the LCPC box measurements according to [47].

Figure 73: Material testing. LCPC Box: a) equipment, b) final flow shape for the material tested (right). L = 600 mm for SCC3.

Figure 74: Material testing. Slump flow: a) equipment, b) final shape for the SCC3. D = 570 mm.

Figure 75: Material testing. a) V-funnel test, b) ConTec Rheometer-4SCC [212].

The values of plastic viscosity were estimated by the correlation factors between the Rheometer-4SCC and the ConTec Viscometer 5 provided by the producer (row "measured" pl. viscosity, Table 6). However, the reliability of the estimated values is rather questionable and cannot be proved. As mentioned before, the yield stress is responsible for the final length and shape of the flow and the viscosity value does not play a decisive role. Therefore, based on this fact and on the preliminary numerical simulations, the viscosity was estimated to be around several tens of Pa·s (row plastic viscosity, Table 6). In this study only the final shape of the material at the stoppage is of interest. Since the final shape at the end of flows where inertia can be neglected depends only on yield stress [48], an approximate value of viscosity is considered sufficient. This will be further discussed in Section 8.4.1.

Table 6:   The experimental results for SCC1 - SCC4.

	Very Low Yield Stress		Low Yield Stress		Medium Yield Stress		High Yield Stress	
	SCC1		**SCC2**		**SCC3**		**SCC4**	
Slump flow [mm]	825		720		570		480	
LCPC-box [mm]	935		770		600		470	
Rheometer data G-yield, H-Viscosity [-]	257	3410	311	4195	621	5876	1728	9435
V–funnel time [s]	5		6		9		11.5	

yield stress τ_0 [Pa]	**29.3**		**35.5**		**70.8**		**166.4**	
"measured" pl. viscosity η_{pl} [Pa·s]	47.2		58.9		84.1		137.5	
pl. viscosity η_{pl} [Pa·s]	**20 - 40**							

8.4   Numerical simulations

8.4.1   Simulations to determine unknown parameters

Before starting the numerical simulations of the main experiment, the unknown material properties as well as the unknown parameters of the porous medium formed by the steel bars in zones 1 – 4 have to be determined. This section gives an insight into the numerical studies devoted to the parameter determination.

8.4.1.1   Material parameters

The material parameters needed as an input for the numerical simulations of the main experiment are the yield stress and the plastic viscosity. The yield stress values were

determined from the rheometer measurements, and analytically calculated based on slump flow and LCPC box flow values according to [48] and [47] (the values are given in Table 6).

It is though not easy to determine the values of viscosity reliably, since there is no sound transformation method of the V funnel and rheometer measurements to the values of viscosity in Pa·s. Although there values of plastic viscosities can be estimated from the factors given by manufacturers (Table 6, "measured pl. viscosity"), as a first approximation for the simulation of the form filling experiment, it was assumed that the value of viscosity is around 30 Pa·s. In this step, we try to determine the plastic viscosity numerically, through the numerical simulations of LCPC-box and V-funnel. The idea behind it is to firstly perform the simulations of the V-funnel experiment (where the material has experimentally determined yield stress and estimated plastic viscosity) and to compare the experimental results with the numerical data. At the same time, we will try to prove here, that the values of plastic viscosity of 20 - 40 Pa·s are acceptable for the specific flows studied here. Furthermore, numerical simulations of channel flow will be performed, in order to show that plastic viscosity has no influence on the flow length and to confirm that the measured values of the yield stress are correct.

a)   b)   c)
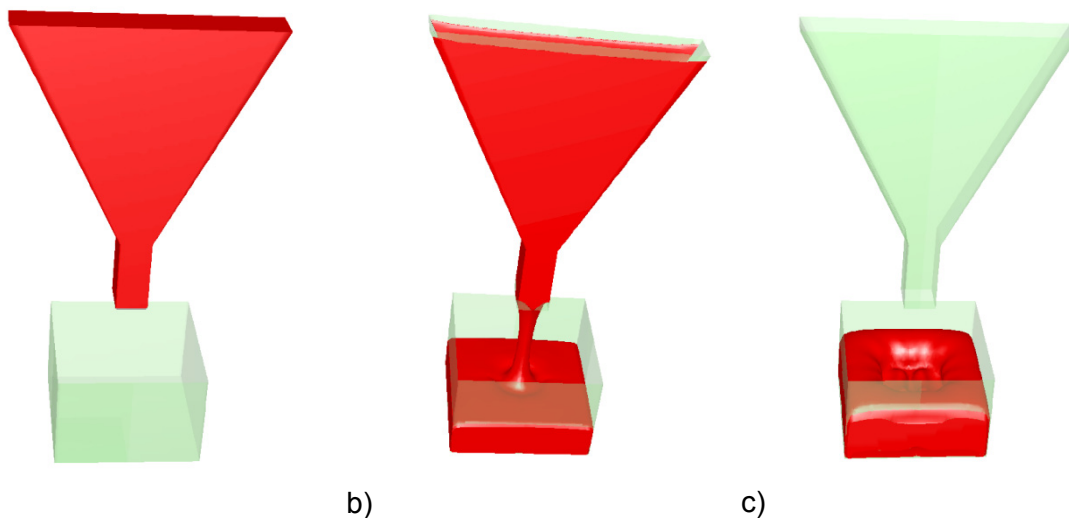
Figure 76: Numerical simulation of V-funnel experiment: a) initial shape of concrete, b) flow after 10 s for the case when no-slip boundary condition at the funnel is assumed, c) flow after 1 s when full-slip at the funnel assumed (right).

Figure 76 shows the numerical setup for the V-funnel simulation. This simulation is performed for SCC1 and SCC3, where the yield stress and the plastic viscosity values are taken from Table 6. Two cases are considered for the funnel wall boundary: full-slip and no-slip. For both simulations, the time needed for the material to flow out of the funnel are considered and compared with the experimental values. The comparison of the experimentally and numerically obtained flow times are shown in Table 7. One can see

that the difference between numerical results with full-slip condition and results when using no-slip condition is huge and neither of them fits the experimental results.

Table 7: V-funnel experiment. Time needed for outflow: measured time, numerically obtained when full-slip condition is assumed and the when the no-slip condition is assumed.

t [s]	experiment	simulation no-slip	simulation full-slip
low yield SCC1 τ_0 = 29 Pa, η_{pl} = 47.2 Pa·s	5	10	1.1
medium yield SCC3 τ_0 = 71 Pa, η_{pl} = 84.1 Pa·s	9	21.2	1.65

In the next step, numerical simulations of the V-funnel experiment with SCC3 are performed, where one tries to fit the experimentally measured flow time by fitting the plastic viscosity value. So the simulations of the V funnel experiment are performed for τ_0 and several values of plastic viscosity η_{pl} = 20, 40, 80 and 160 Pa·s and for both full-slip and no-slip boundary condition.
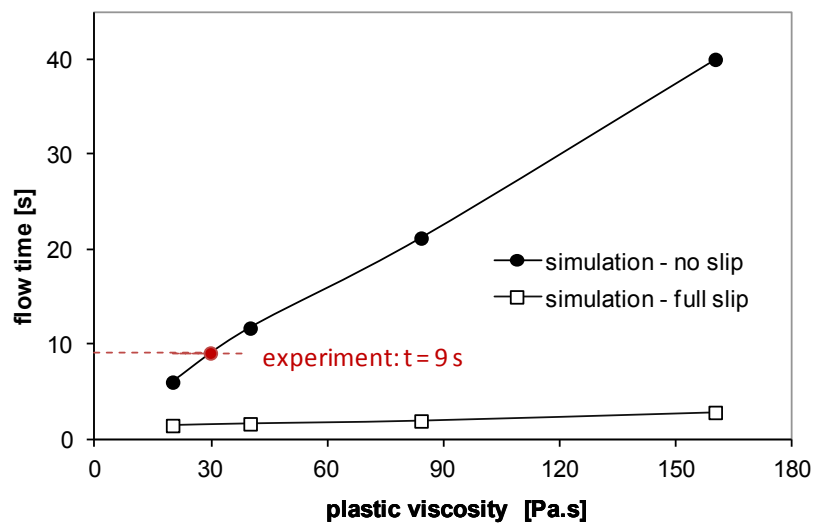
Figure 77: Numerical simulation of V-funnel experiment for SCC3, flow time for several values of plastic viscosity and no-slip and full-slip boundary condition.

The results are shown in Figure 77, where the time that material needs to flow out of the funnel is plotted versus plastic viscosity. The diagram shows that the full-slip condition is definitely not the correct setting to use, since it leads to very low values of flow time t, so that unrealistically high values of plastic viscosity would have to be used to fit the experimental results. The results obtained with no-slip boundary condition on the other hand are more realistic and lead to slightly low (when compared with the typical viscosity values from [32]) but reasonable values of plastic viscosity. It can be also read from the diagram, that in order to numerically obtain the experimentally measured value of t = 9 s,

one should use no-slip boundary condition and the value of η_{pl} = 30 Pa·s for numerical simulation of this particular setup.

Nevertheless, it is obvious that the wall boundary condition and the friction between the wall and the material has a significant influence on the flow time, and, although a no-slip condition gives reasonable results, neither of the used conditions fits the reality perfectly. For a successful simulation of the V-funnel experiment, the shear stress boundary conditions should be used at the walls of the funnel, meaning that the exact values of the wall friction coefficients are needed. The determination of wall friction parameters is a complex task and is not a topic of this study. As a consequence, it is unfortunately not possible to determine the correct values of plastic viscosity by mean of V-funnel numerical simulations. Therefore it is assumed, that the value of plastic viscosity is in order of 20 to 40 Pa·s.
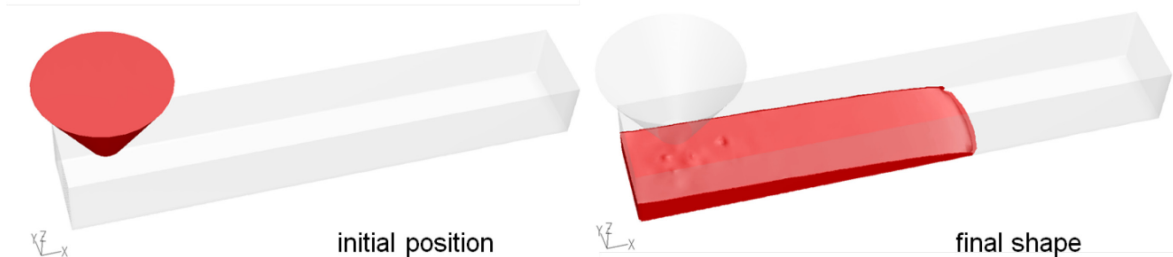
Figure 78: Numerical simulation of LCPC-box. Initial and final shape of concrete.

To prove the latter value of plastic viscosity and to prove that the influence of plastic viscosity on the flow length in the cases of interest can be neglected as well as to confirm the experimentally calculated values of yield stress, the simulations of the LCPC-Box experiment are performed. The values of yield stress for SCC1 - SCC4 are taken from Table 6 and the plastic viscosity is assumed to be 20 or 40 Pa·s.

Table 8:   LCPC-Box, measured and numerically determined values of flow length (in mm) for different concretes.

Flow lenght [mm]	SCC2, low yield τ_0 = 36 Pa	SCC3, medium yield τ_0 = 71 Pa	SCC4, high yield τ_0 = 166 Pa
experiment	770	600	470
simulation η_{pl} = 20 Pa·s	759	597	464
simulation η_{pl} = 40 Pa·s	749	599	462

Figure 78 shows a numerical setup for the simulation of the LCPC box flow. The full-slip boundary condition is chosen at the funnel walls and the no-slip condition is assumed at the walls of the channel. The material is slowly poured into the channel and the simulation is run until the material stops. The flow length is compared with the measured one and the

results for concretes SCC2, SCC3 and SCC4 are shown in Table 8. The experimental and numerical studies show a fairly good congruence in flow length, which confirms the correctness of the measured yield stress values. Although the value of plastic viscosity is a rough approximation, it had no influence on the flow length, confirming that, the value of 20 - 40 Pa·s is sufficiently fine for this study.

8.4.1.2 Porous medium parameters

The performed experiments are to be simulated in two ways: once using the exact geometry with rebars and once using the PM approximation. If rebars are modelled as PM, the unknown parameters of PM needed as input for simulation are the permeability k and the shift factor α. The values of the shift factor α do not have to be calculated but are to be taken as explained in Subchapter 6.1. The principal permeabilities k_x, k_y and k_z have to be determined numerically as proposed in Subchapter 5.1 for each of the four reinforcement zones shown in Figure 70.

One of the numerical setups for the permeability determination is shown in Figure 79: a rectangular specimen with the corresponding rebars zone in the middle. Since the zones are symmetric, only a half of the zone is taken into account for the simulation. The rectangular sections are kept longer so that the inlet/outlet has no influence on the pressure drop within the zone. The boundary condition at the outer faces is symmetry one. The slow laminar channel flow is simulated for three different values of inlet velocity. The permeability is calculated according to Equation 60 where the pressure values are the area-weighted average pressures at the surfaces perpendicular to the flow at the beginning and at the end of the zone (more precisely at the distance of M/2 from the zone).

a)   b)
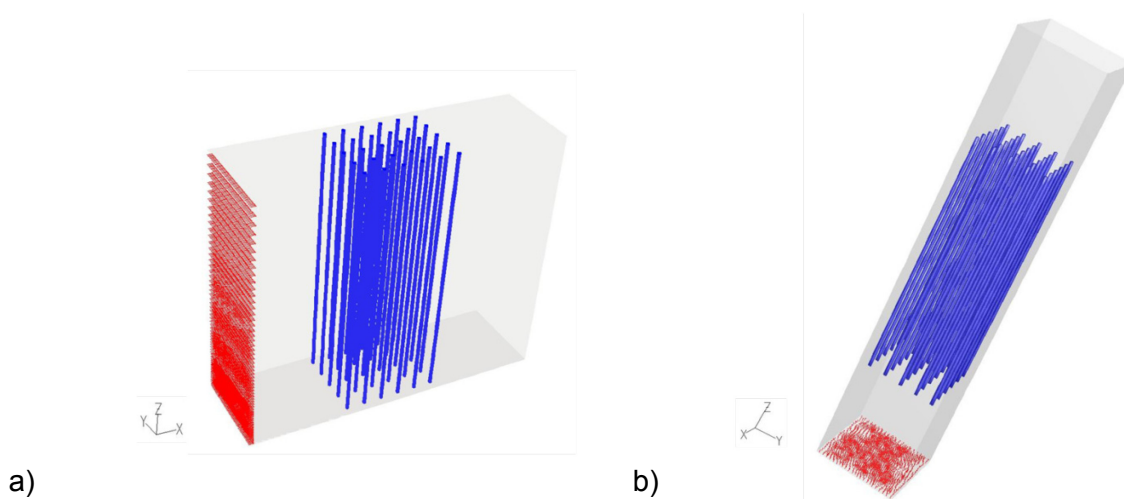
Figure 79: Numerical setup to determine unknown permeabilities for Zone 4: a) k_x and b) k_z. The markers indicate the position of the inlet.

Table 9 shows the permeability values in x, y and z direction obtained from the numerical simulations as well as the analytical solutions according to [176]. A good congruence between numerical and analytical results is found. The numerical values shown in the table will be used for the simulation of the main experiment.

Table 9:   Numerically and analytically calculated values of permeability for Zones 1 - 4.

	k_x [m^2]		k_y [m^2]		k_z [m^2]	
	num.	analyt.	num.	analyt.	num.	analyt.
zone 1	3.6E-04	3.4E-04	3.6E-04	3.4E-04	6.8E-04	6.8E-04
zone 2	4.7E-05	4.0E-05	1.1E-04	8.0E-05	4.7E-05	4.0E-05
zone 3	4.1E-05	4.0E-05	4.7E-05	4.0E-05	1.1E-04	8.0E-05
zone 4	2.2E-04	2.0E-04	2.2E-04	2.0E-04	5.2E-04	4.0E-04

8.4.2   Simulations of the form-filling experiment

Numerical simulations of SCC casting in the model formwork are carried out using the software Fluent©. The numerical setups are shown in Figure 80.
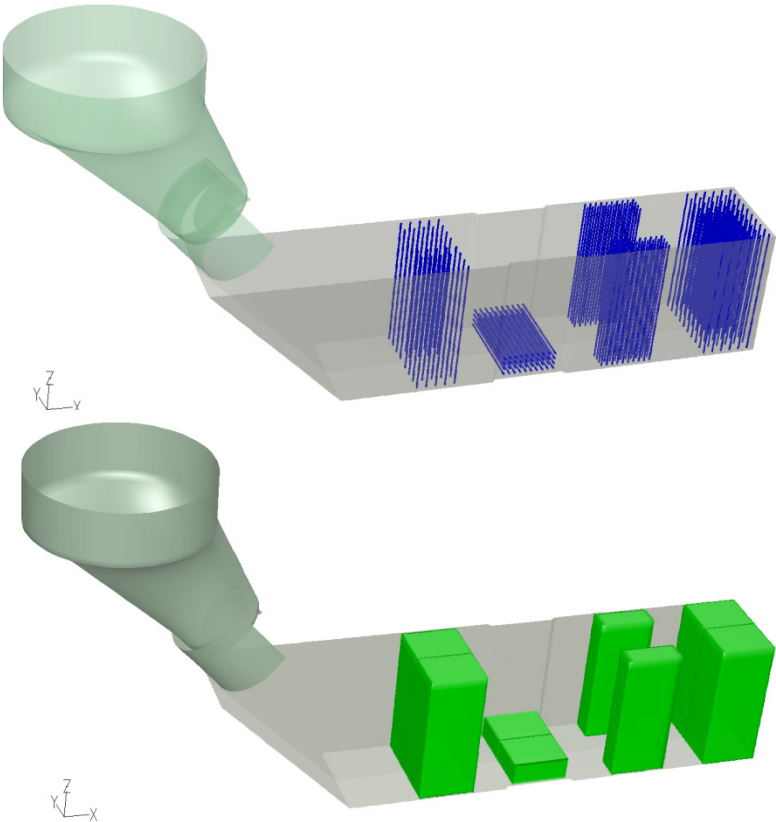
Figure 80: Numerical setup. Exact simulation with rebars (above) and the porous medium analogy (below).

134

The structured grids are generated using Gambit© 2.4.6. The hexahedral elements are used, where the numerical grid aspect ratios (the ratios of the sides of the hexahedral elements) are kept in the range of 1 to 1.5. The constant pressure boundary condition is applied on the computational domain outlet. The full slip boundary condition is assumed at the walls of the funnel, while the no-slip boundary condition is assumed for the reinforcement and the walls of the Plexiglas container. To prove the chosen numerical settings, the experiments are simulated using the exact geometry with reinforcement bars. To demonstrate the applicability of the proposed PM approach, the same experiment is simulated using PM model. The PM model is implemented in Fluent© as a User Defined Function (UDF) by adding a momentum source term in the porous medium to the momentum equation (see Chapter 3, Equation 43). The pressure drop caused by PM in the main flow direction is dominant and much higher than the pressure drop in other two directions. Additionally, the numerical simulations of Carbopol® experiments presented in Chapter 7, showed that satisfactory results are obtained if a source term is added only for the dominant flow direction. In order to save computational time, the code implemented here is written in such a way that it firstly decides which direction is dominant (by comparing the strain rates and velocities for these directions) and then it adds only the pressure drop in the dominant direction.

The material properties yield stress and plastic viscosity taken for the simulations are shown in the grey marked rows in Table 6. The value of plastic viscosity is taken to be η_{pl} = 30 Pa·s. The permeability values of the porous zones are shown in Table 9. The value of the shift factor used in the simulations is α_x = 1.5, α_y = 1.5 and α_z = 3.0 (see Subchapter 6.1). The material is initially placed in the funnel and then let flow through the funnel outlet (2.5 - 5 cm small opening at the bottom of the funnel) under its own weight and into the Plexiglas container. Simulation is run until the flow stops, then the final shape is observed.

8.5   Comparison of the experimental and numerical results

The experimental results for four different concretes are shown in Figure 81.

The figure shows the final shape of the material. It can be seen that yield stress influences the final shape of the material in the expected way: the higher the yield stress the higher the pressure drop within the rebar zone and the steeper the flow front. SCC1 with the very low yield stress fills the form nicely and the flow front is almost levelled. SCC4 with the highest value of yield stress has a very steep flow front and the material does not even reach the end of the form. This demonstrated that yield stress determines the final shape, the flow length of the material and proper filling of the form in practical applications.

SCC1, τ_0= 29 Pa

SCC2, τ_0= 36 Pa

SCC3, τ_0= 71 Pa
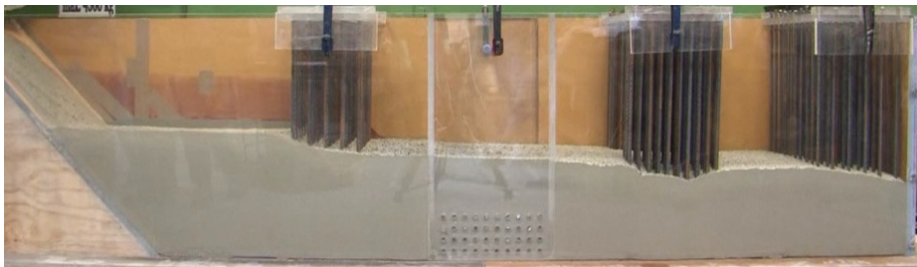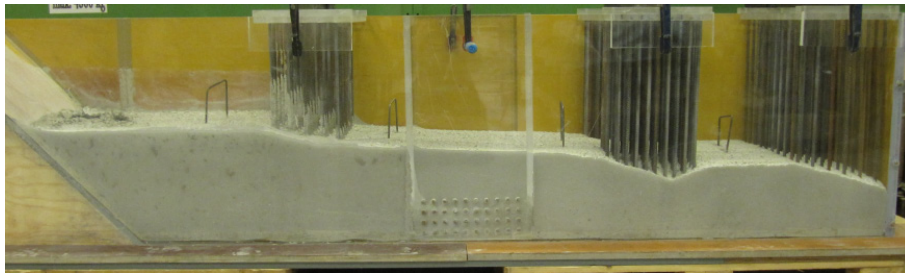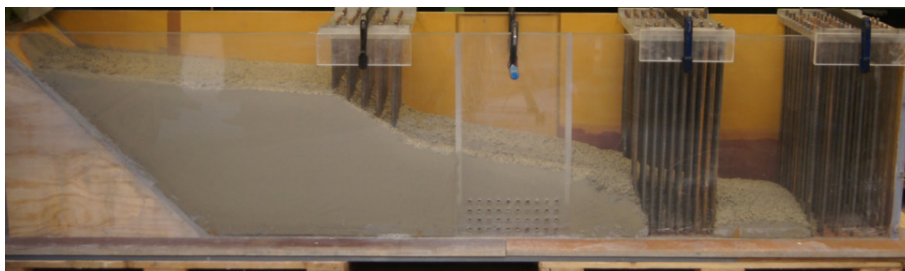
SCC4, τ_0= 166 Pa

Figure 81: Experimental results: the final shape of the material for four SCCs under investigation. The influence of yield stress on the final shape is noticeable.
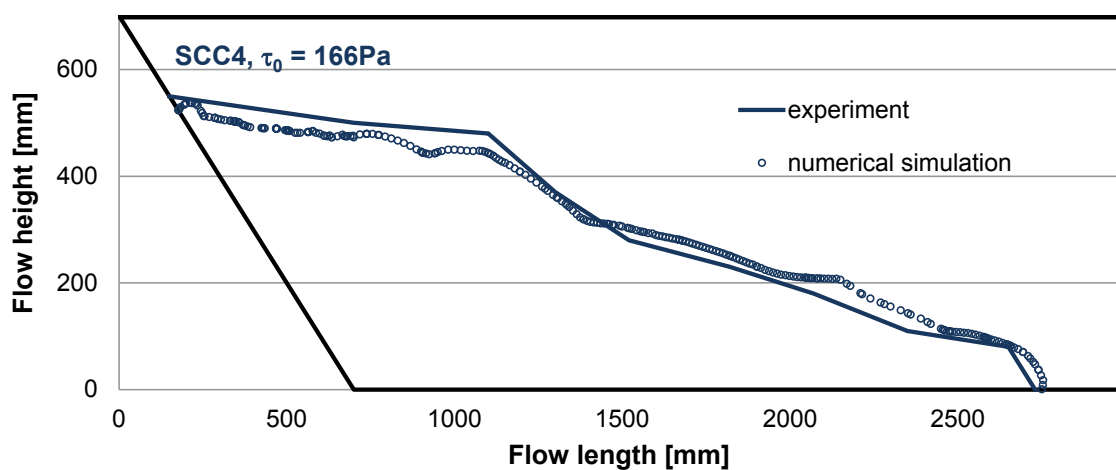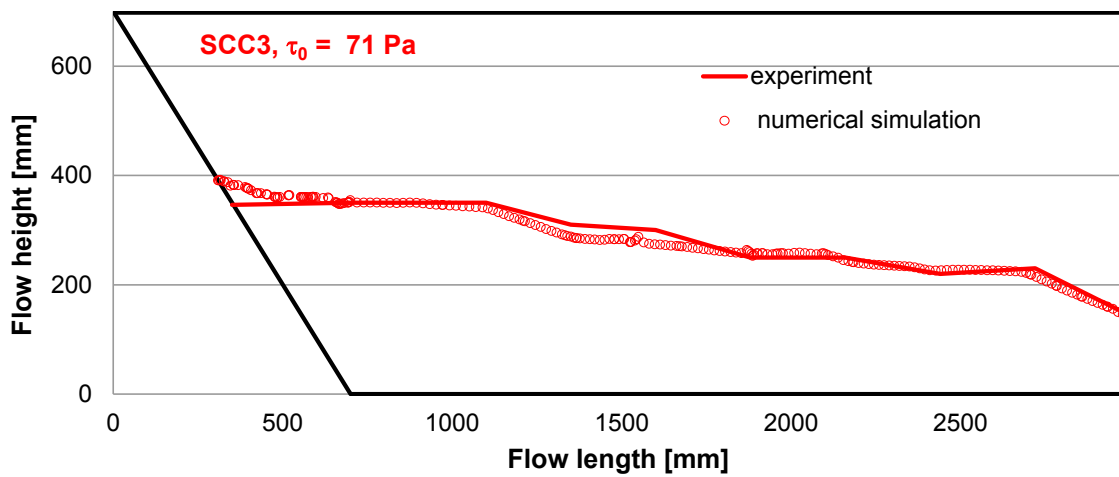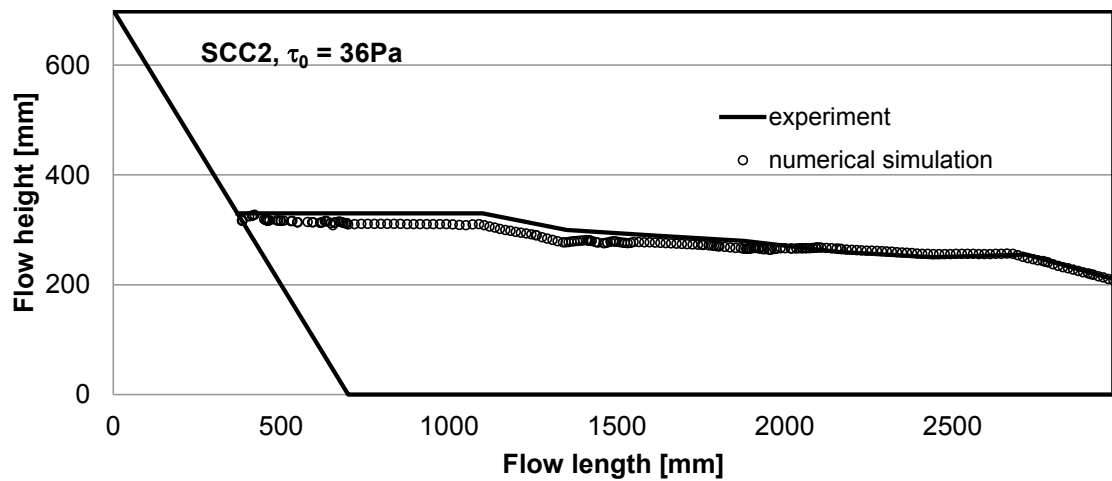
Figure 82: The material shape when the flow stops: experiment versus numerical simulation for SCC2 with τ_0 = 36 Pa (above), SCC3 with τ_0 = 71 Pa (middle) and SCC4 with τ_0 = 166 Pa (below).

Figure 82 shows a comparison of the experimentally and numerically obtained flow front when the material stops for SCC2, SCC3 and SCC4. Figure 83 gives a visual illustration of both experimental and numerical results obtained for SCC2 and SCC3. The results show a comparatively good congruence between the numerically and experimentally obtained flow fronts. The results also showed that the model is able to predict the behaviour of different SCC, having different rheological properties, since the same effects (in terms of slope and length) in the final shape of the flow are observed in both numerical and experimental studies.

a)   b)
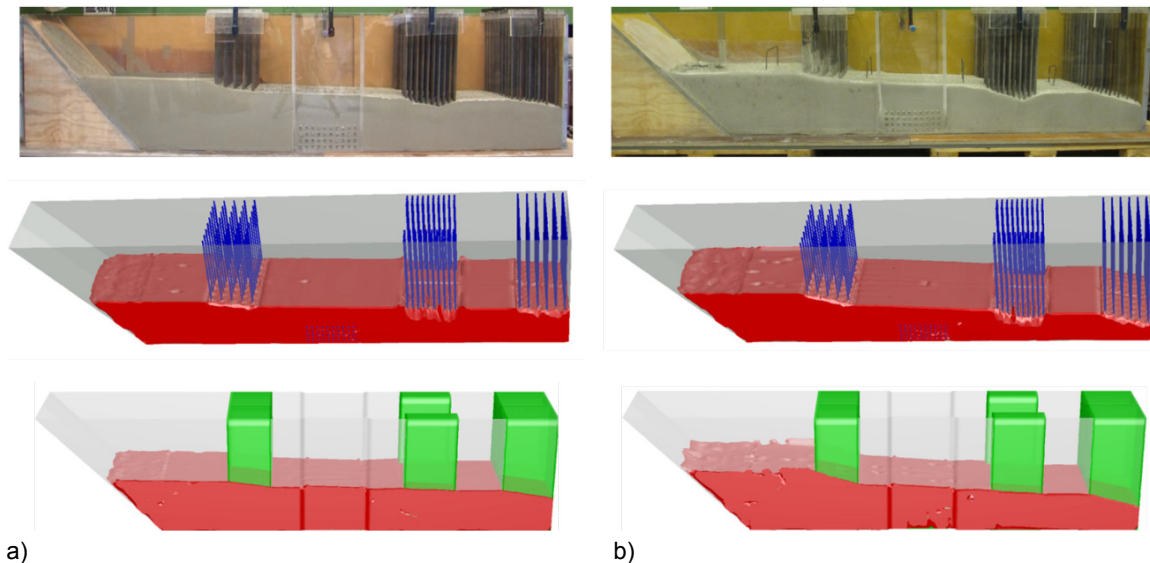
Figure 83: The material shape when the flow stops: experiment versus numerical simulation for a) SCC2 with τ_0 = 36 Pa and b) SCC3 with τ_0 = 71 Pa.

To obtain the final shapes shown in Figure 83, the following pre-processing times and computation times on the same computer were needed for simulation of the experiment with SCC2:

A) Numerical simulation with steel bars :
Number of calculation cells: 482000 cells (this mesh is, in theory, too coarse but had to be chosen in order to limit the computation time);
Pre-processing time: 10 hours;
Computation time: 116 hours;
Total time: 126 hours;

B) Numerical simulation with porous medium :
Number of calculation cells: 187000 cells (this mesh is actually finer than actually needed) ;
Pre-processing time: 2 hours;
Computation time: 18.5 hours;
Total time: 20.5 hours.

138

83% reduction of total time is reached here, bringing it in the range of potential industrial applications. This proves once more that, when using porous medium model, the simulations are significantly simpler and faster than when using reinforcement bars. It has to be noted here, that, in order to achieve good quality figures, the mesh of the PM case was finer than necessary and it would still be possible to reduce the number of calculation cells in the case of PM decreasing therefore the total time.

9 Extrapolation of an industry-oriented library of porous medium parameters

The aim of the present study is to propose a model for flow through reinforcement that could be an upgrade for any CFD numerical model for concrete flow. This upgrade should include both the numerical tool, able to solve the flow of SCC through reinforced zones, and a methodology defining all the parameters necessary for the computation. To make this possible, one has to calculate the unknown model parameters (namely porosity ϕ, permeability k and shift factor α in the model equations 39 - 41) for different reinforcement geometries. The parameters in the model equations have to be defined for different reinforcement categories, covering most of the cases appearing in practice of construction. As a final product, a user-friendly table is expected, where the user can read the corresponding PM parameters for a given reinforcement density. This Chapter is dedicated to the determination of such a porous medium parameters library.

The subchapter that follows will give some examples of reinforced sections and engineering standards to be respected. Existing classifications will be discussed and the possible classification of the reinforcement networks for the library of parameters will be suggested. Subchapter 9.2 will present the numerical studies, devoted to the determination of the parameters. Finally, in Subchapter 9.3 the normative tables of porous medium parameters will be proposed.

9.1 Classification of reinforcement networks

In the previous research steps the model for SCC flow through reinforced formworks was developed. It was implemented into the CFD software ANSYS Fluent© and validated on several numerical and experimental studies. The methodology for determination of the unknown porous medium parameters porosity ϕ, permeability k and shift factor α is proposed as well. The values of porosity can be easily analytically calculated from the geometry measures while the values of the shift factor α are already defined in Subchapter 6.1. At this point, the determination of permeability for different reinforcement dispositions has to be discussed. The permeability can be calculated numerically from the simulations with Newtonian fluid (as explained in Subchapter 5.1). Previous studies showed that the numerically calculated values of permeability k correspond to the analytical ones and that k is a function of the bar diameter and spacing between the bars. Depending on the constructive element type and on the structural loading applied, the reinforcement bars in the constructive members can be placed in an infinite number of different ways and it would certainly not be possible to calculate permeability for each particular case observed. Instead, it will be tried here to find the categories of

reinforcement zones, which have the same (order of magnitude of) permeability value. It will be discussed what is the best way to classify the reinforced concrete members, with respect to reinforcement and to the value of permeability of the porous zones formed by the bars.

Up to the author's knowledge, there are very few works on classification of SCC structures based on the density of reinforcement utilised in a member. In the work of Nagataki et al. [213], while studying self-compatibility, based on the geometry and reinforcement conditions the authors suggested the following classification of SCC members:

−   Rank 1: Self-compactability into members or portions having large cross sectional areas and a small amount of reinforcement with a minimum steel clearance of more than 200 mm. The maximum steel content is less than 100 kg/m^3.
−   Rank 2: Self-compactability into reinforced concrete structures or members with a minimum steel clearance in the range of 60 to 200 mm. This normally corresponds to a steel content of 100 to 350 kg/m^3.
−   Rank 3: Self-compactability into members or portions having complicated shapes and/or small cross-sectional areas with a minimum steel clearance in the range of 35 to 60 mm and with the steel content more than 350 kg/m^3.
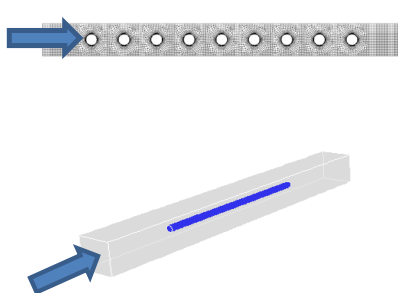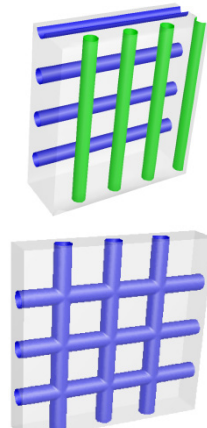
		class A arrays	**class B** networks
RANK 1	ρ_{reinf} < 100 kg/m^3 M > 200 mm		
RANK 2	ρ_{reinf} = 100 -350 kg/m^3 M = 60 - 200 mm		
RANK 3	ρ_{reinf} =350 - 500 kg/m^3 M = 35 - 60 mm		
RANK 4	ρ_{reinf} > 500 kg/m^3 M < 35 mm		

Figure 84:   A possible categorization of reinforcement in SCC, similar to the classification suggested in [213].

To define the reinforcement permeability classes, the categorization of concrete members according to [213] as illustrated in Figure 84 seems to be generally appropriate. Since the SCC is particularly suited for members with congested reinforcement, it might be useful to define Rank 4 as well, for the constructive elements with the steel content higher than 500 kg/m^3. Moreover, one has to distinguish between the arrays of the bars (class A) and the reinforcement networks (class B).

142

When classifying the building members as shown in Figure 84, one has either to find one permeability value valid for all the reinforcement densities in one rank or to subdivide the rank in several sub-categories having a single permeability value. Thus, the next issue to be discussed is how to determine the appropriate value of permeability for the certain rank or which change in k can be neglected within one sub-category.

Let us analyse the concrete members of Rank 2 for the bars with diameter d = 14 mm. To achieve ρ_{reinf} = 100 - 350 kg/m^3 the clearance M between the bars should vary between 60 and 110 mm, meaning that the relative distance X between the bars is 4 to 8. If we would use the classification as in Figure 84, the arrays with the relative distance X between the bars from 4 to 8 would have the same value of permeability.
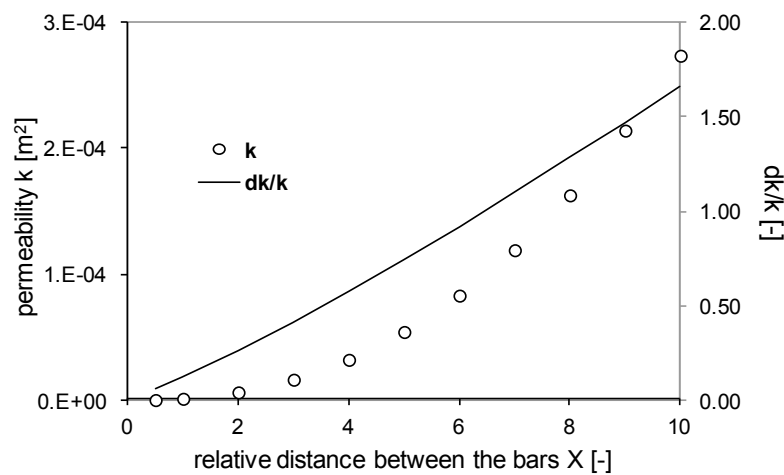
Figure 85: Analytical values of permeability and relative change in permeability dk/k as a function of X for the bars with d = 14 mm.

To check if this is physically meaningful, we analyse the relative change of permeability as a function of X. For this purpose the perpendicular permeability of the arrays of the 14 mm bars for the values of X between 0.5 and 10 is analytically calculated according to [176]. The diagram in Figure 85 shows the analytically calculated permeability values k and changes of relative difference dk/k (ratio of the permeability change and permeability value for X_i and X_{i+1}). From the diagram it can be seen that there is significant difference between the permeability of X = 4 and X = 8 (k(X = 8) is five times higher than k(X = 4)), thus it is not reasonable to place these two cases in the same rank with the same permeability. It can be seen that for the studied values of X, the dk/k is significant and it is not easy to determine the dX (range of the bars densities) for which the permeability change dk can be negligible. Thus if using categorization of concrete members according to their reinforcement density as suggested in Figure 84, it would be rather difficult to determine an appropriate value of permeability for one rank, since, within this rank, values of X and d and consequently values of permeability can vary significantly. It will be instead discussed here, what the realistic values of X and d typical for SCC constructive elements are and how to determine permeability values for possible X and d combinations.

The minimum percentage of the reinforcement required and minimum clearance between the rebars for specific structural elements are defined by the European norms Eurocode 2 [202] and the German standard DIN 1045-1 [211]. The bounds defined by these standards are summarized in Table 10. The minimum clearance between the bars should be greater than 20 mm, greater than the bar diameter and aggregate size + 5 mm. The maximum distance between the rebars should be less than 400 mm for the principal reinforcement. Since the typical bar diameter of steel rebars is from d = 6 mm to d = 40 mm, according to the Table 10 the values of M and X can vary from 1 mm to 400 mm and from 1 to 67, respectively.

Table 10: Standards for spacing and quantity of reinforcement in concrete members according to [202, 203, 211].

	DIN 1045-1	Eurocode 2	
		slabs	beams
Minimum spacing	20 mm 1 x bar diameter aggregate size plus 5 mm (if aggregate d_p > 16 mm)	20 mm 1 x bar diameter aggregate size plus 5 mm	
Maximum spacing	according to Table 21 [211]	principal reinforcement: 3h but < 400 mm secondary reinforcement: 3.5h but < 450 mm	-
Minimum cross-section area of reinforcement required	according to Table 9-10 [211]	$0.26 \cdot f_{ctm} \cdot b_t \cdot d / f_{yk}$ $0.0013 \cdot A_c$ (0.13 – 0.25%)	$0.26 \cdot f_{ctm} \cdot b_t \cdot d / f_{yk}$ $0.0013 \cdot A_c$ (0.13 – 0.25%)
Maximum cross-section area of reinforcement allowed	$0.08 \cdot A_c$	$0.04 \cdot A_c$	$0.04 \cdot A_c$

h - slab thickness, F_{cd} - design value of concrete compressive strength, A_c – cross-sectional area of concrete, f_{ctm} - mean value of axial tensile strength.

It has to be mentioned that the bounds for X calculated above are rather wide, since in practical applications it is not likely to have the limit cases such as a bar with d = 6 mm and M = 400 mm distance. Nevertheless, the practical guidelines for engineers given in [203] provide tables with the typical dimensions for slab and beam reinforcement used in practice (example in Figure 86). The tables provide the values of the typical reinforcement grades, given as a function of the diameter of the bar and the distance between the bars, for the steel BSt 500. The reinforcement grade is calculated as a reinforcement cross-section area per meter of length (for the slabs) or per square meter (for beams and columns). The bar diameters varies as d = 6 - 28 mm and the distance between the bars as M = 50 - 250 mm.

From the previous considerations, it can be thus concluded that the most convenient and precise way for the parameter library, would be to provide a table similar to the one given in [203] and Figure 86, where the specific values of permeability would be listed for certain bar diameter d and certain distance between the bars M. In the following subchapter, the numerical simulations to determine the values of permeability for the typical bar arrangements with d = 6 - 28 mm and M = 50 - 250 mm are performed.

Querschnitte von Flächenbewehrungen a_s in cm²/m

Stab-abstand s in cm	Durchmesser d_s in mm									Stäbe pro m
	6	8	10	12	14	16	20	25	28	
5,0	5,65	10,05	15,71	22,62	30,79	40,21	62,83	98,17		20,00
5,5	5,14	9,14	14,28	20,56	27,99	36,56	57,12	89,25		18,18
6,0	4,71	8,38	13,09	18,85	25,66	33,51	52,36	81,81	102,63	16,67
6,5	4,35	7,73	12,08	17,40	23,68	30,93	48,33	75,52	94,73	15,38
7,0	4,04	7,18	11,22	16,16	21,99	28,72	44,88	70,12	87,96	14,29
7,5	3,77	6,70	10,47	15,08	20,53	26,81	41,89	65,45	82,10	13,33
8,0	3,53	6,28	9,82	14,14	19,24	25,13	39,27	61,36	76,97	12,50
8,5	3,33	5,91	9,24	13,31	18,11	23,65	36,96	57,75	72,44	11,76
9,0	3,14	5,59	8,73	12,57	17,10	22,34	34,91	54,54	68,42	11,11
9,5	2,98	5,29	8,27	11,90	16,20	21,16	33,07	51,67	64,82	10,53
10,0	2,83	5,03	7,85	11,31	15,39	20,11	31,42	49,09	61,58	10,00
10,5	2,69	4,79	7,48	10,77	14,66	19,15	29,92	46,75	58,64	9,52
11,0	2,57	4,57	7,14	10,28	13,99	18,28	28,56	44,62	55,98	9,09
11,5	2,46	4,37	6,83	9,83	13,39	17,48	27,32	42,68	53,54	8,70
12,0	2,36	4,19	6,54	9,42	12,83	16,76	26,18	40,91	51,31	8,33
12,5	2,26	4,02	6,28	9,05	12,32	16,08	25,13	39,27	49,26	8,00
13,0	2,17	3,87	6,04	8,70	11,84	15,47	24,17	37,76	47,37	7,69
13,5	2,09	3,72	5,82	8,38	11,40	14,89	23,27	36,36	45,61	7,41
14,0	2,02	3,59	5,61	8,08	11,00	14,36	22,44	35,06	43,98	7,14
14,5	1,95	3,47	5,42	7,80	10,62	13,87	21,67	33,85	42,47	6,90
15,0	1,88	3,35	5,24	7,54	10,26	13,40	20,94	32,72	41,05	6,67
16,0	1,77	3,14	4,91	7,07	9,62	12,57	19,63	30,68	38,48	6,25
17,0	1,66	2,96	4,62	6,65	9,06	11,83	18,48	28,87	36,22	5,88
18,0	1,57	2,79	4,36	6,28	8,55	11,17	17,45	27,27	34,21	5,56
19,0	1,49	2,65	4,13	5,95	8,10	10,58	16,53	25,84	32,41	5,26
20,0	1,41	2,51	3,93	5,65	7,70	10,05	15,71	24,54	30,79	5,00
21,0	1,35	2,39	3,74	5,39	7,33	9,57	14,96	23,37	29,32	4,76
22,0	1,29	2,28	3,57	5,14	7,00	9,14	14,28	22,31	27,99	4,55
23,0	1,23	2,19	3,41	4,92	6,69	8,74	13,66	21,34	26,77	4,35
24,0	1,18	2,09	3,27	4,71	6,41	8,38	13,09	20,45	25,66	4,17
25,0	1,13	2,01	3,14	4,52	6,16	8,04	12,57	19,63	24,63	4,00

Figure 86: The values of the typical reinforcement grades in cm²/m, given as a function of the diameter of the bar and the distance between the bars. Source: [203], in German.

9.2   Numerical studies

9.2.1   Studies to determine permeability

The goal of the numerical studies presented in this section is to determine parallel and perpendicular permeability for all the reinforcement grades listed in Figure 86. If one conducts the numerical simulation to determine the permeability for each of the reinforcement/distance combinations in the table, it would make around 500 simulations in total, what would be very time consuming. However, it was shown in 5.1 that on the tested range the numerically calculated permeabilities matched perfectly with the analytical solutions of [176]. Thus, in principle, the values of permeabilities in the normative tables

can be also calculated analytically. To prove that the analytical solution is also applicable to the typical reinforcement cases, the numerical and analytical solution for permeabilities of some typical reinforcement combinations will be compared. Their agreement would justify the intention to determine the values of the permeabilities for the normative tables analytically.
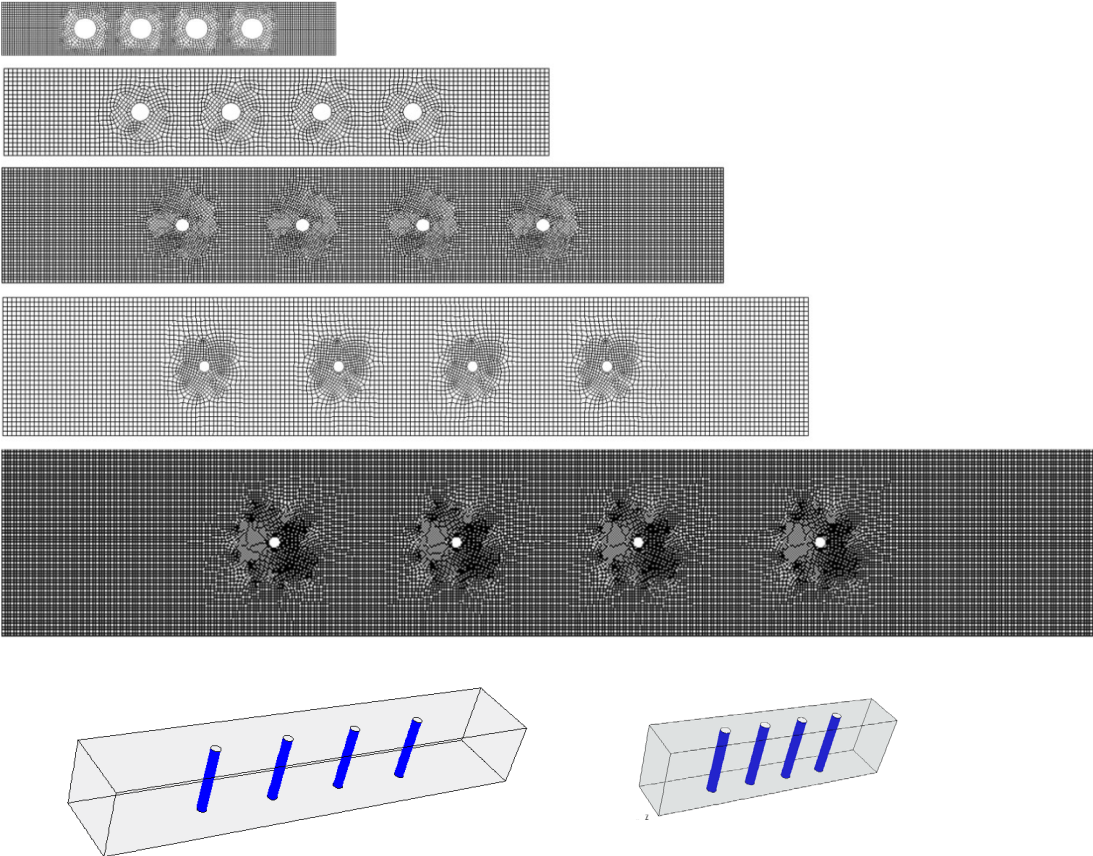
Figure 87: Test rebars arrays used to calculate permeability values for different reinforcement cases with d = 14 mm and M = 50 - 250 mm.

Numerical setups to determine the perpendicular permeabilities of several typical reinforcement arrays are shown in Figure 87. The numerical simulations are performed for the bars with diameter d = 14 mm and distance between the bars M = 20, 50, 100, 150 and 250 mm. From the simulations with Newtonian test fluid ($\eta = 10\,\text{Pa} \cdot \text{s}$), the values of k_x are calculated as explained in Subchapter 5.1. For M = 20 mm and M = 50 mm 3D simulations are performed and compared with 2D approximations. The same values obtained from 3D and 2D simulations showed that, for the determination of the permeability in direction perpendicular to the rebars k_x, one can use 2D approximations of the real geometries. Therefore, the 2D setups are used here to calculate the values of permeability and to compare them with the analytical values.

The results of the numerical simulations and analytical calculations according to [176] are shown in Figure 88. There is a very good match between analytical and numerical values, with a maximum relative difference of 5%. Therefore, for the further studies, the values of

permeability k_x will be calculated according to [176] and Equation 22. The values of permeability parallel to the rebars are calculated as $k_z = 2 \cdot k_x$. According to the conclusion of Chapter 5, the irregular distribution of the bars can be assumed to be equivalent to the regular one with the same porosity (i.e. values of d and M).
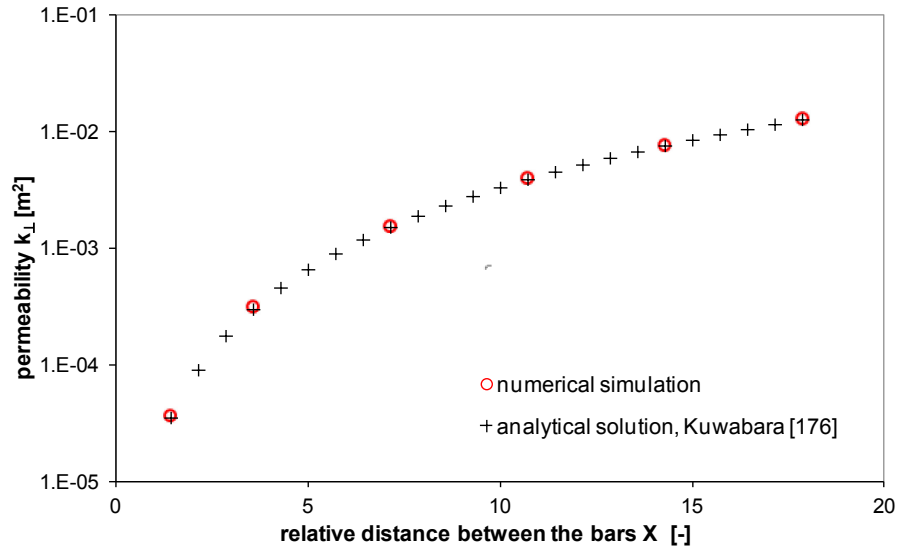
Figure 88: The comparison of the numerical simulations and analytical calculation for the perpendicular permeability of test reinforcement arrays shown in Figure 87.

9.2.2 Influence of web reinforcement and bar laps on the permeability

9.2.2.1 Bar laps

In reinforced concrete members, forces are transmitted from one bar to another by lapping of bars, welding or mechanical devices assuring load transfer [202]. A typical bar lap is shown in Figure 89. According to the Section 5.89 in [203] the minimum required length of the lap between two bars depends on the concrete quality, the bar diameter and the position in the concrete member. The minimum lap is given as:

$$ l_s = \alpha_1 \cdot \alpha_a \cdot (A_{s,req} / A_{s,prov}) \cdot (d/4) \cdot (f_{yd} / f_{bd}) \tag{69} $$

where l_s is the length of the lap, α_1 and α_a are dimensionless parameters (α_1 = 1, 1.4 or 2 while α_a = 0.7 or 1), $A_{s,req}$ is the cross-sectional area of reinforcement required, $A_{s,prov}$ is the actual area of the reinforcement, d is bar diameter, f_{yd} is the value of the steel strength and the f_{bd} is the value of the bond strength. The value of l_s has to be greater than $15 \cdot d$ or 300 mm [203].

All the permeability studies and values calculated up to now, only considered the arrays of the single reinforcement bars. For the calculation of the influence of the lap on the

permeability one needs to consider the worst possible situation i.e. the maximum possible length of the lap in reference to the length of the bar itself.
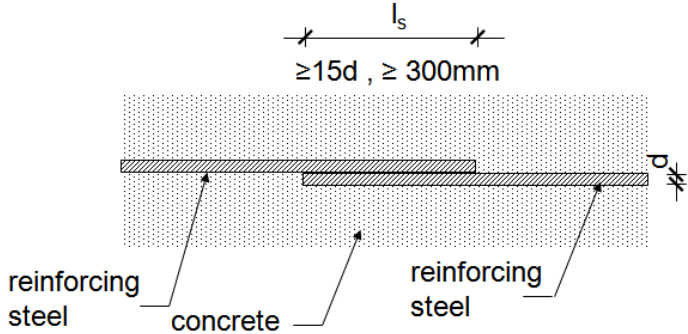
Figure 89: Contact lap splice in reinforced concrete.

It is however rather difficult to calculate the maximum value of the overlapping length and its relation to the length of the bar, since these depend on several factors. If one calculates the l_s taking maximum values of all the parameters in Equation 69, the maximum required lap length is around $54 \cdot d$. The typical maximum length of the reinforcement bar is 6 m, 9 m or 12 m, while the maximum span of the standard concrete constructive elements such as slabs and beams is usually not larger than 6 m. Taking into account that for Ø40 bars the maximum possible required l_s around 2 m, the maximum l_s can be roughly approximated as $0.3 \cdot l$, where l is the whole length of the steel bar. For the case of the maximum overlapping, we will perform numerical studies to calculate the influence of the presence of the overlapping on the permeability.
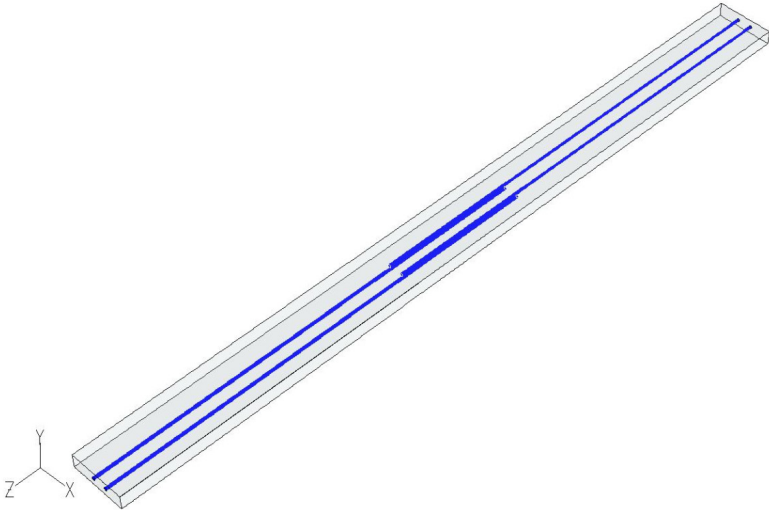
Figure 90: One of the numerical setups used to determine the influence of the lap of the bars on the permeability values.

One of the numerical setups used for this calculation is shown in Figure 90. The bar diameter is d = 14 mm, the distance between the bars is varied as M = 50 mm and

148

M = 100 mm. The length of the overlapping bars is l = 2000 mm and the length of the lap is l_s = 600 mm. Here calculated permeabilities are compared with the 3D cases with no overlapping bars shown in Figure 87.

Table 11: Influence of overlapping of the rebars on the permeability in x, y and z direction.

permeability in [m^2]		k_x	k_y	k_z
d = 14 mm, M = 50 mm	bars	3.18E-04	3.18E-04	6.36E-04
	bars overlapping	3.06E-04	3.11E-04	6.39E-04
	difference	3.7%	2.3%	0.5%
d = 14 mm, M = 100 mm	bars	1.57E-03	1.57E-03	3.14E-03
	bars overlapping	1.63E-03	1.59E-03	3.34E-03
	difference	3.8%	1.5%	6.5%

Table 11 shows the results of the numerical simulations for the permeability in x, y and z direction. If we compare geometries with single bars arrays with the cases where the bars overlap, it can be seen that the relative difference is not greater than 6% in the studied range. Furthermore, we can consider that the simulated cases are worse than the real situations where the members are much longer than 200 mm and it is to be expected that the difference between the situations with and without lap will be even lower than the simulated ones. Therefore, it can be assumed here, that the influence of the bars laps on the permeability can be neglected.

9.2.2.2 Web rebars

In concrete elements, in addition to the main reinforcement designed to resist longitudinal tension, transverse reinforcement bars such as stirrups and web reinforcement are present [202, 203]. These steel bars are designed to resist shear and diagonal tension and are perpendicular to the main rebars, having usually smaller diameter than the main reinforcement. The distance between the transverse reinforcement bars can be calculated according to 5.97 in [203]. For instance, for an extreme case of a concrete beam exposed to a very high shear loading, the distance between two web rebars should be lower than 0.8·beam height or 200 mm.

a)   b)
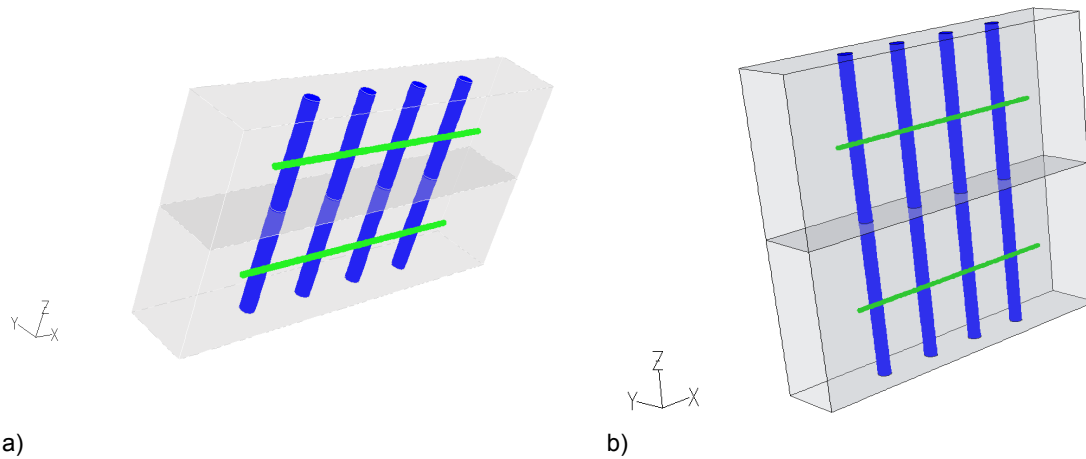
Figure 91: Numerical setups to study the influence of the web rebars on the permeability values. Main vertical rebars and transverse rebars at a) 100 mm distance and b) on the 200 mm distance. Vertical symmetry plane in the middle.

In order to study the influence of the presence of these transversal bars on the permeability of the zone, such an extreme case study is considered here. The numerical setup to study this influence is shown in Figure 91. The bar diameter is d = 14 mm and the distance between the main bars is varied as M = 50 mm and M = 100 mm. The diameter of the web reinforcement bar is d_w = 6 mm and it is placed at the distance M_w = 100 mm, 200 mm or 300 mm. The permeability is calculated from the numerical simulation and compared with the cases where the transverse bars are not present.

Table 12: Influence of the web reinforcement on the permeabilities in x, y and z direction.

permeability [m²]		k_x	k_y	k_z
d = 14 mm, M = 50 mm d_w = 6 mm, M_w = 100 mm	bars	3.3E-04	3.3E-04	6.0E-04
	bars+web reinforcement	2.5E-04	2.1E-04	3.3E-04
	difference	- 26%	- 36%	- 46%
d = 14 mm, M = 50 mm d_w = 6 mm, M_w = 200 mm	bars	3.3E-04	3.3E-04	6.0E-04
	bars+web reinforcement	2.8E-04	2.5E-04	6.4E-04
	difference	- 17%	-22%	-37%
d = 14 mm, M = 100 mm d_w = 6 mm, M_w = 300 mm	bars	1.6E-03	1.6E-03	3.2E-03
	bars+web reinforcement	1.4E-03	1.2E-03	2.0E-03
	difference	-13%	-24%	-35%

The calculated permeabilities in x, y and z direction for the cases with and without the web bars are shown in Table 12. Let us call these permeabilities k_{web} and k respectively. The comparison shows that the permeability of the bar arrays with and without web reinforcement is in the same order of magnitude, but the influence of the web rebars on the permeability is not negligible. As expected, the permeability k_{web} is lower than the one when only bars arrays is considered. The web rebars have the greatest influence on the k_z, and the relative difference is up to 46%. The higher distance between the main bars

the lower the relative difference between k_{web} and k. Figure 92 indicates the trend in relative difference between k_{web} and k as a function of X for the studied cases. From this diagram one can read the dk for certain X in order to calculate k_{web} when k is known. However, this diagram is valid only for the tested scenario and some and some further studies have to be performed in order to study second order parameters such as web effects. These studies will not be topic of this thesis.
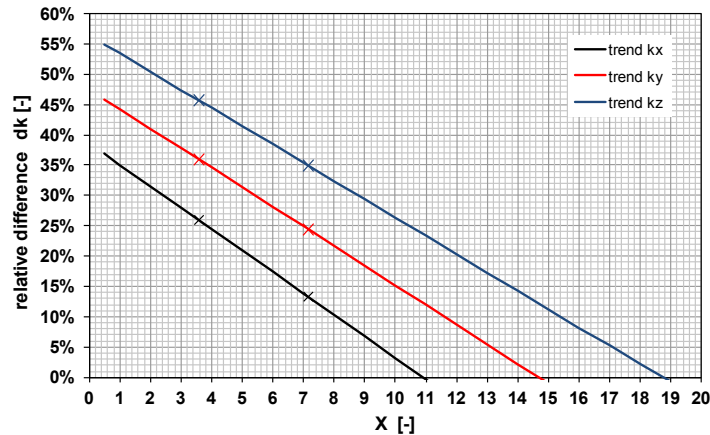
Figure 92: Diagram providing the values of dk as a function of X for calculation of k_{web} for the specific case under investigation.

9.3   Proposed library

Finally, the proposed library at this stage provides the values of porosity permeability in perpendicular and in the parallel direction. The porosity is calculated by using Equation 18 and the permeability is calculated according to Equation 22. The shift factor is assumed to be $\alpha_x = \alpha_y = 1.5$ and $\alpha_z = 3$. The results for the permeability for the arrays of rebars are given in Tables 13 and 14. Table 15 gives the corresponding porosity values.

Table 13: Library for the permeability in the direction perpendicular to the rebar axes. Permeability is given as a function of the bar diameter and the distance between the bars.

perpendicular permeability k_x [m^2]									
distance M [mm]	diameter of the bar [mm]								
	6	8	10	12	14	16	20	25	28
50	4.03E-04	3.66E-04	3.39E-04	3.19E-04	3.02E-04	2.89E-04	2.68E-04	2.48E-04	2.39E-04
55	5.03E-04	4.57E-04	4.24E-04	3.99E-04	3.78E-04	3.61E-04	3.35E-04	3.10E-04	2.99E-04
60	6.15E-04	5.60E-04	5.20E-04	4.89E-04	4.64E-04	4.43E-04	4.10E-04	3.80E-04	3.66E-04
65	7.41E-04	6.75E-04	6.26E-04	5.89E-04	5.59E-04	5.34E-04	4.95E-04	4.59E-04	4.41E-04
70	8.80E-04	8.02E-04	7.45E-04	7.01E-04	6.65E-04	6.35E-04	5.89E-04	5.45E-04	5.25E-04
75	1.03E-03	9.42E-04	8.75E-04	8.23E-04	7.81E-04	7.47E-04	6.92E-04	6.41E-04	6.17E-04
80	1.20E-03	1.09E-03	1.02E-03	9.57E-04	9.09E-04	8.69E-04	8.05E-04	7.46E-04	7.17E-04
85	1.38E-03	1.26E-03	1.17E-03	1.10E-03	1.05E-03	1.00E-03	9.28E-04	8.59E-04	8.27E-04
90	1.57E-03	1.44E-03	1.34E-03	1.26E-03	1.20E-03	1.14E-03	1.06E-03	9.83E-04	9.45E-04
95	1.78E-03	1.63E-03	1.52E-03	1.43E-03	1.36E-03	1.30E-03	1.20E-03	1.12E-03	1.07E-03
100	2.01E-03	1.84E-03	1.71E-03	1.61E-03	1.53E-03	1.46E-03	1.36E-03	1.26E-03	1.21E-03
105	2.25E-03	2.06E-03	1.91E-03	1.80E-03	1.71E-03	1.64E-03	1.52E-03	1.41E-03	1.36E-03
110	2.50E-03	2.29E-03	2.13E-03	2.01E-03	1.91E-03	1.83E-03	1.70E-03	1.57E-03	1.51E-03
115	2.77E-03	2.54E-03	2.36E-03	2.23E-03	2.12E-03	2.03E-03	1.88E-03	1.74E-03	1.68E-03
120	3.05E-03	2.80E-03	2.61E-03	2.46E-03	2.34E-03	2.24E-03	2.08E-03	1.93E-03	1.85E-03
125	3.35E-03	3.08E-03	2.87E-03	2.71E-03	2.57E-03	2.46E-03	2.29E-03	2.12E-03	2.04E-03
130	3.67E-03	3.37E-03	3.14E-03	2.96E-03	2.82E-03	2.70E-03	2.51E-03	2.32E-03	2.24E-03
135	4.00E-03	3.67E-03	3.43E-03	3.24E-03	3.08E-03	2.95E-03	2.74E-03	2.54E-03	2.44E-03
140	4.35E-03	3.99E-03	3.73E-03	3.52E-03	3.35E-03	3.21E-03	2.98E-03	2.76E-03	2.66E-03
145	4.71E-03	4.33E-03	4.04E-03	3.82E-03	3.63E-03	3.48E-03	3.23E-03	3.00E-03	2.89E-03
150	5.09E-03	4.68E-03	4.37E-03	4.13E-03	3.93E-03	3.77E-03	3.50E-03	3.25E-03	3.13E-03
155	5.49E-03	5.05E-03	4.72E-03	4.46E-03	4.24E-03	4.06E-03	3.78E-03	3.51E-03	3.37E-03
160	5.90E-03	5.43E-03	5.07E-03	4.80E-03	4.57E-03	4.38E-03	4.07E-03	3.78E-03	3.63E-03
165	6.33E-03	5.83E-03	5.45E-03	5.15E-03	4.91E-03	4.70E-03	4.37E-03	4.06E-03	3.91E-03
170	6.78E-03	6.24E-03	5.84E-03	5.52E-03	5.26E-03	5.04E-03	4.68E-03	4.35E-03	4.19E-03
175	7.24E-03	6.67E-03	6.24E-03	5.90E-03	5.62E-03	5.39E-03	5.01E-03	4.66E-03	4.48E-03
180	7.72E-03	7.11E-03	6.66E-03	6.30E-03	6.00E-03	5.75E-03	5.35E-03	4.97E-03	4.79E-03
185	8.22E-03	7.57E-03	7.09E-03	6.71E-03	6.39E-03	6.13E-03	5.70E-03	5.30E-03	5.10E-03
190	8.74E-03	8.05E-03	7.54E-03	7.13E-03	6.80E-03	6.52E-03	6.07E-03	5.64E-03	5.43E-03
195	9.27E-03	8.55E-03	8.00E-03	7.57E-03	7.22E-03	6.92E-03	6.45E-03	5.99E-03	5.77E-03
200	9.82E-03	9.05E-03	8.48E-03	8.03E-03	7.66E-03	7.34E-03	6.84E-03	6.36E-03	6.12E-03
205	1.04E-02	9.58E-03	8.98E-03	8.50E-03	8.11E-03	7.78E-03	7.24E-03	6.73E-03	6.48E-03
210	1.10E-02	1.01E-02	9.49E-03	8.98E-03	8.57E-03	8.22E-03	7.66E-03	7.12E-03	6.86E-03
215	1.16E-02	1.07E-02	1.00E-02	9.48E-03	9.05E-03	8.68E-03	8.09E-03	7.52E-03	7.25E-03
220	1.22E-02	1.13E-02	1.06E-02	1.00E-02	9.54E-03	9.16E-03	8.53E-03	7.94E-03	7.64E-03
225	1.28E-02	1.19E-02	1.11E-02	1.05E-02	1.00E-02	9.64E-03	8.99E-03	8.36E-03	8.06E-03
230	1.35E-02	1.25E-02	1.17E-02	1.11E-02	1.06E-02	1.01E-02	9.46E-03	8.80E-03	8.48E-03
235	1.42E-02	1.31E-02	1.23E-02	1.16E-02	1.11E-02	1.07E-02	9.94E-03	9.25E-03	8.91E-03
240	1.49E-02	1.37E-02	1.29E-02	1.22E-02	1.17E-02	1.12E-02	1.04E-02	9.72E-03	9.36E-03
245	1.56E-02	1.44E-02	1.35E-02	1.28E-02	1.22E-02	1.17E-02	1.09E-02	1.02E-02	9.82E-03
250	1.63E-02	1.51E-02	1.41E-02	1.34E-02	1.28E-02	1.23E-02	1.15E-02	1.07E-02	1.03E-02

Table 14: Library for the permeability in the direction parallel to the rebar axes. Permeability is given as a function of the bar diameter and the distance between the bars.

parallel permeability k_z [m^2]									
distance M [mm]	diameter of the bar [mm]								
	6	8	10	12	14	16	20	25	28
50	8.05E-04	7.32E-04	6.79E-04	6.38E-04	6.05E-04	5.78E-04	5.35E-04	4.97E-04	4.78E-04
55	1.01E-03	9.14E-04	8.48E-04	7.97E-04	7.56E-04	7.22E-04	6.69E-04	6.20E-04	5.97E-04
60	1.23E-03	1.12E-03	1.04E-03	9.77E-04	9.27E-04	8.86E-04	8.21E-04	7.60E-04	7.32E-04
65	1.48E-03	1.35E-03	1.25E-03	1.18E-03	1.12E-03	1.07E-03	9.90E-04	9.17E-04	8.82E-04
70	1.76E-03	1.60E-03	1.49E-03	1.40E-03	1.33E-03	1.27E-03	1.18E-03	1.09E-03	1.05E-03
75	2.07E-03	1.88E-03	1.75E-03	1.65E-03	1.56E-03	1.49E-03	1.38E-03	1.28E-03	1.23E-03
80	2.40E-03	2.19E-03	2.03E-03	1.91E-03	1.82E-03	1.74E-03	1.61E-03	1.49E-03	1.43E-03
85	2.76E-03	2.52E-03	2.34E-03	2.21E-03	2.09E-03	2.00E-03	1.86E-03	1.72E-03	1.65E-03
90	3.15E-03	2.88E-03	2.68E-03	2.52E-03	2.39E-03	2.29E-03	2.12E-03	1.97E-03	1.89E-03
95	3.57E-03	3.26E-03	3.03E-03	2.86E-03	2.72E-03	2.60E-03	2.41E-03	2.23E-03	2.15E-03
100	4.01E-03	3.67E-03	3.42E-03	3.22E-03	3.06E-03	2.93E-03	2.71E-03	2.52E-03	2.42E-03
105	4.49E-03	4.11E-03	3.83E-03	3.61E-03	3.43E-03	3.28E-03	3.04E-03	2.82E-03	2.71E-03
110	5.00E-03	4.58E-03	4.27E-03	4.02E-03	3.82E-03	3.66E-03	3.39E-03	3.14E-03	3.02E-03
115	5.54E-03	5.07E-03	4.73E-03	4.46E-03	4.24E-03	4.06E-03	3.76E-03	3.49E-03	3.36E-03
120	6.11E-03	5.60E-03	5.22E-03	4.92E-03	4.68E-03	4.48E-03	4.16E-03	3.85E-03	3.71E-03
125	6.71E-03	6.15E-03	5.74E-03	5.41E-03	5.15E-03	4.93E-03	4.57E-03	4.24E-03	4.08E-03
130	7.34E-03	6.73E-03	6.28E-03	5.93E-03	5.64E-03	5.40E-03	5.01E-03	4.65E-03	4.47E-03
135	8.00E-03	7.34E-03	6.86E-03	6.47E-03	6.16E-03	5.89E-03	5.47E-03	5.08E-03	4.89E-03
140	8.70E-03	7.99E-03	7.46E-03	7.04E-03	6.70E-03	6.42E-03	5.96E-03	5.53E-03	5.32E-03
145	9.43E-03	8.66E-03	8.09E-03	7.64E-03	7.27E-03	6.96E-03	6.47E-03	6.00E-03	5.77E-03
150	1.02E-02	9.36E-03	8.75E-03	8.26E-03	7.86E-03	7.53E-03	7.00E-03	6.50E-03	6.25E-03
155	1.10E-02	1.01E-02	9.43E-03	8.91E-03	8.49E-03	8.13E-03	7.56E-03	7.01E-03	6.75E-03
160	1.18E-02	1.09E-02	1.01E-02	9.59E-03	9.14E-03	8.75E-03	8.14E-03	7.55E-03	7.27E-03
165	1.27E-02	1.17E-02	1.09E-02	1.03E-02	9.81E-03	9.40E-03	8.74E-03	8.12E-03	7.81E-03
170	1.36E-02	1.25E-02	1.17E-02	1.10E-02	1.05E-02	1.01E-02	9.37E-03	8.70E-03	8.38E-03
175	1.45E-02	1.33E-02	1.25E-02	1.18E-02	1.12E-02	1.08E-02	1.00E-02	9.31E-03	8.96E-03
180	1.54E-02	1.42E-02	1.33E-02	1.26E-02	1.20E-02	1.15E-02	1.07E-02	9.94E-03	9.57E-03
185	1.64E-02	1.51E-02	1.42E-02	1.34E-02	1.28E-02	1.23E-02	1.14E-02	1.06E-02	1.02E-02
190	1.75E-02	1.61E-02	1.51E-02	1.43E-02	1.36E-02	1.30E-02	1.21E-02	1.13E-02	1.09E-02
195	1.85E-02	1.71E-02	1.60E-02	1.51E-02	1.44E-02	1.38E-02	1.29E-02	1.20E-02	1.15E-02
200	1.96E-02	1.81E-02	1.70E-02	1.61E-02	1.53E-02	1.47E-02	1.37E-02	1.27E-02	1.22E-02
205	2.08E-02	1.92E-02	1.80E-02	1.70E-02	1.62E-02	1.56E-02	1.45E-02	1.35E-02	1.30E-02
210	2.19E-02	2.02E-02	1.90E-02	1.80E-02	1.71E-02	1.64E-02	1.53E-02	1.42E-02	1.37E-02
215	2.31E-02	2.14E-02	2.00E-02	1.90E-02	1.81E-02	1.74E-02	1.62E-02	1.50E-02	1.45E-02
220	2.44E-02	2.25E-02	2.11E-02	2.00E-02	1.91E-02	1.83E-02	1.71E-02	1.59E-02	1.53E-02
225	2.57E-02	2.37E-02	2.22E-02	2.11E-02	2.01E-02	1.93E-02	1.80E-02	1.67E-02	1.61E-02
230	2.70E-02	2.49E-02	2.34E-02	2.22E-02	2.11E-02	2.03E-02	1.89E-02	1.76E-02	1.70E-02
235	2.83E-02	2.62E-02	2.46E-02	2.33E-02	2.22E-02	2.13E-02	1.99E-02	1.85E-02	1.78E-02
240	2.97E-02	2.75E-02	2.58E-02	2.44E-02	2.33E-02	2.24E-02	2.09E-02	1.94E-02	1.87E-02
245	3.11E-02	2.88E-02	2.70E-02	2.56E-02	2.45E-02	2.35E-02	2.19E-02	2.04E-02	1.96E-02
250	3.26E-02	3.01E-02	2.83E-02	2.68E-02	2.56E-02	2.46E-02	2.29E-02	2.14E-02	2.06E-02

Table 15: The library for the porosity values as a function of the bar diameter and the distance between the bars.

porosity ϕ [-]									
distance M [mm]	**diameter of the bar [mm]**								
	6	**8**	**10**	**12**	**14**	**16**	**20**	**25**	**28**
50	0.9910	0.9851	0.9782	0.9706	0.9624	0.9538	0.9359	0.9127	0.8988
55	0.9924	0.9873	0.9814	0.9748	0.9677	0.9601	0.9441	0.9233	0.9106
60	0.9935	0.9891	0.9840	0.9782	0.9719	0.9652	0.9509	0.9321	0.9205
65	0.9944	0.9906	0.9860	0.9809	0.9753	0.9694	0.9565	0.9394	0.9288
70	0.9951	0.9917	0.9877	0.9832	0.9782	0.9728	0.9612	0.9456	0.9359
75	0.9957	0.9927	0.9891	0.9851	0.9806	0.9757	0.9652	0.9509	0.9420
80	0.9962	0.9935	0.9903	0.9866	0.9826	0.9782	0.9686	0.9555	0.9472
85	0.9966	0.9942	0.9913	0.9880	0.9843	0.9803	0.9715	0.9594	0.9518
90	0.9969	0.9948	0.9921	0.9891	0.9858	0.9821	0.9740	0.9629	0.9558
95	0.9972	0.9953	0.9929	0.9901	0.9870	0.9837	0.9762	0.9659	0.9593
100	0.9975	0.9957	0.9935	0.9910	0.9882	0.9851	0.9782	0.9686	0.9624
105	0.9977	0.9961	0.9941	0.9917	0.9891	0.9863	0.9799	0.9710	0.9652
110	0.9979	0.9964	0.9945	0.9924	0.9900	0.9873	0.9814	0.9731	0.9677
115	0.9981	0.9967	0.9950	0.9930	0.9907	0.9883	0.9828	0.9750	0.9699
120	0.9982	0.9969	0.9954	0.9935	0.9914	0.9891	0.9840	0.9767	0.9719
125	0.9984	0.9972	0.9957	0.9940	0.9920	0.9899	0.9851	0.9782	0.9737
130	0.9985	0.9974	0.9960	0.9944	0.9926	0.9906	0.9860	0.9796	0.9753
135	0.9986	0.9975	0.9963	0.9948	0.9931	0.9912	0.9869	0.9808	0.9768
140	0.9987	0.9977	0.9965	0.9951	0.9935	0.9917	0.9877	0.9820	0.9782
145	0.9988	0.9979	0.9967	0.9954	0.9939	0.9922	0.9885	0.9830	0.9794
150	0.9988	0.9980	0.9969	0.9957	0.9943	0.9927	0.9891	0.9840	0.9806
155	0.9989	0.9981	0.9971	0.9959	0.9946	0.9931	0.9897	0.9848	0.9816
160	0.9990	0.9982	0.9973	0.9962	0.9949	0.9935	0.9903	0.9857	0.9826
165	0.9990	0.9983	0.9974	0.9964	0.9952	0.9939	0.9908	0.9864	0.9835
170	0.9991	0.9984	0.9976	0.9966	0.9955	0.9942	0.9913	0.9871	0.9843
175	0.9991	0.9985	0.9977	0.9968	0.9957	0.9945	0.9917	0.9877	0.9851
180	0.9992	0.9986	0.9978	0.9969	0.9959	0.9948	0.9921	0.9883	0.9858
185	0.9992	0.9987	0.9979	0.9971	0.9961	0.9950	0.9925	0.9889	0.9864
190	0.9993	0.9987	0.9980	0.9972	0.9963	0.9953	0.9929	0.9894	0.9870
195	0.9993	0.9988	0.9981	0.9974	0.9965	0.9955	0.9932	0.9899	0.9876
200	0.9993	0.9988	0.9982	0.9975	0.9966	0.9957	0.9935	0.9903	0.9882
205	0.9994	0.9989	0.9983	0.9976	0.9968	0.9959	0.9938	0.9907	0.9887
210	0.9994	0.9989	0.9984	0.9977	0.9969	0.9961	0.9941	0.9911	0.9891
215	0.9994	0.9990	0.9984	0.9978	0.9971	0.9962	0.9943	0.9915	0.9896
220	0.9994	0.9990	0.9985	0.9979	0.9972	0.9964	0.9945	0.9918	0.9900
225	0.9995	0.9991	0.9986	0.9980	0.9973	0.9965	0.9948	0.9921	0.9904
230	0.9995	0.9991	0.9986	0.9981	0.9974	0.9967	0.9950	0.9925	0.9907
235	0.9995	0.9991	0.9987	0.9981	0.9975	0.9968	0.9952	0.9927	0.9911
240	0.9995	0.9992	0.9987	0.9982	0.9976	0.9969	0.9954	0.9930	0.9914
245	0.9996	0.9992	0.9988	0.9983	0.9977	0.9970	0.9955	0.9933	0.9917
250	0.9996	0.9992	0.9988	0.9984	0.9978	0.9972	0.9957	0.9935	0.9920

s

10 Conclusions and perspectives

10.1 Main findings

The presented thesis dealt with numerical simulations of SCC casting in reinforced elements. Numerical simulation of fresh concrete flow is a promising tool to link rheological properties of concrete and its casting behaviour on site. However, the use of existing numerical tools for casting prediction leads to complicated and time-consuming computations, what prevents numerical simulations of being widely used in concrete industry. In a simulation of a concrete casting, the time needed to take each reinforcing bar into account consumes a considerable part of the simulation time. This time is quite excessive, since SCC is mainly used for highly-reinforced elements with high density and number of bars. By proposing a simplified model of reinforcement zones that avoids modelling of each bar, the objective of this thesis was to develop a practical tool for casting prediction, which would be handier and less time-consuming than the existing numerical tools.

In the presented thesis a computational model for the SCC flow through reinforced formwork zones was developed. The model is based on Computational Fluid Dynamics, where SCC is modelled as a yield-stress fluid and arrays of rebars as porous media. The influence of the bars on the flow i.e. the relation between the viscometric behaviour of concrete and its observed behaviour in the porous matrix, is characterised by defining the apparent properties of the material within the medium namely apparent shear rate and apparent viscosity. The apparent properties were included in the extra source term added to the model standard momentum conservation equations in the PM zone. The apparent properties are dependent on the porous medium parameters namely permeability, porosity and shift factor. This study suggested numerical procedures to calculate the unknown porous medium parameters and justified the obtained values through numerous numerical case studies.

The equations of the mathematical model were presented in Chapter 3. The studies were conducted to convert the proposed mathematical model into a numerical source file, written in C language. The source code was compiled and implemented into the commercial CFD software ANSYS Fluent©, which was previously proved to be suitable for the simulations of the free-surface flows of cementitious materials. It was hereby shown, that the software ANSYS Fluent© enables a relatively uncomplicated compiling and implementation of the source file into the software code using so called User Defined Functions.

The numerical case studies with Newtonian fluids in Chapter 5 showed that the unknown permeability can be determined from the numerical simulations with Newtonian fluids and that, regardless of the geometry, reinforced sections behave as porous media when a Newtonian fluid is propagating. In the numerical studies with the yield-stress fluids shown in Chapter 6 the values of the unknown shift factor appropriate for concrete flows were determined. The value of the shift factor was found to be 1.5 for the perpendicular direction and 3 for the direction parallel to the rebars. These simulations also validated two basic postulates of this thesis: 1) when crossed by a yield stress fluid, a reinforcement network behaves as a porous medium and can be mathematically modelled as such; 2) when using the porous medium analogy, the pre-processing and computational time significantly decrease.

The model was furthermore validated through a comparison of numerical simulations with the experimental results of the experiments performed with a model yield stress fluid. Finally, the model was validated by large-scale (scale 1:1) concrete experiments. The good match between the simulated and experimental results proved that the model is able to simulate the free-surface flow of concrete through reinforcement networks. The results also showed, that the model is capable of predicting the behaviour of different SCC, having various rheological properties. Comparing the PM simulations with the simulations where the exact geometry was used, the significant decrease in the computational time was achieved.

The presented model can be used as an upgrade in an arbitrary CFD numerical simulation of concrete casting to include the influence of the reinforcement on the flow material behaviour and to predict the form filling. The user-friendly tables with porous medium parameters for different reinforcement grades, which enable an uncomplicated employment of the PM model, were provided in Chapter 9. In the following lines, the steps that have to be performed during this simplified meshing and simulation procedure are listed.

As a first step, the boundaries of the porous medium formed by rebars have to be defined as explained in Subchapter 5.3. The size of the porous medium is usually the size of the area formed by the bars enlarged in each direction for one half of the bar clearance in this direction. The simplified geometry, with the porous zones defined in this way (volumes without obstacles), has to be built and meshed.

In the second step, the permeability values in perpendicular and parallel direction and the values of porosity have to be read from Tables 13, 14 and 15, respectively. These tables provide parameter values for certain bar diameter and certain distance between the bars. The values of permeability are valid for both aligned or distorted arrays of bars as well as for the areas where the bars are overlapping.

Finally, material parameters yield stress and plastic viscosity have to be introduced, and the simulation can be conducted. Since the used setup is far simpler than the geometry with obstacles, the geometry and mesh generation is far easier and pre-processing time is significantly shorter. Additionally, as it was shown through this study, since the number of the calculation points is far lower than when modelling each reinforcement bar, the corresponding computation time is far lower for the PM case.

10.2   Limits of the model and future perspectives

The proposed model assumes that concrete is a yield-stress fluid. The study focused on the flow at stoppage and it was supposed that the yield stress is the decisive factor for the final state of the flow, relevant to predict a proper filling of a formwork. Since thixotropic and shear-thickening behaviour do not have a crucial influence on the slow flows at stoppage, the model does not take thixotropy and the shear-thickening behaviour into account. However, the model equations can be easily modified to integrate thixotropic and shear-thickening behaviour and should be considered for the further development of the model.

At the end of a casting process, concrete is in a flow regime in which the contribution of yield stress exceeds and dominates the contribution of plastic viscosity. Therefore, in this study was assumed that the plastic viscosity does not have a crucial influence on the proper form filling. Consequently, the values of plastic viscosity of the used concretes are estimated to be several tens of Pa·s. Although it was fully legitimate to choose these values in the present study, in order to be able to perform a fully reliable numerical simulation of concrete flow, the material parameters plastic viscosity and yield stress have to be determined in absolute values. The difficulty to determine material parameters, in particular plastic viscosity, is a well-known problem in concrete technology. This is also shown to be an issue in this thesis. Up to now, there are no reliable methods to determine absolute values of plastic viscosity of concrete in Pa·s neither from the rheometer measurements nor from the V-funnel experiments. The further research in this field should concentrate on the determination of viscosity from rheometer or V-funnel measurements using numerical tools. The latter would also have to include comprehensive studies on the wall-concrete interaction, since the friction between the wall and the material plays an important role in this experiment and the friction coefficients are a necessary input for the simulation.

The assumption that concrete is a continuum prevents the model from being able to simulate particle migrations and inner structure changes responsible for the phenomena such as segregation, blocking or bleeding. That means that the proposed model is limited only to stable, non-segregating, non-bleeding and non-blocking concretes. However, inability to properly simulate concrete as a suspension, is a general problem in simulations

of concrete flow and a reliable multiphase model of concrete is still not developed. A development of such a multiphase model was not a goal of this study. Nevertheless, further research should concentrate on the development of the suspension model for concrete and multiphase simulations of concrete casting. Due to the wide range of particles in concrete and their high concentrations and due to the numerical limitations, the appropriate approach to model concrete as a suspension might be the so called Euler-Euler approach. This approach is particularly suitable to model suspensions with a high solid content and depicts both liquid and dispersed phases as a continuum.

The tables with characteristic porous medium parameters provided in Chapter 9 are valid for the arrays of rebars in both aligned or distorted configurations. In case when the transverse reinforcement (for instance web rebars) is present, the permeabilities from the Table 13 and Table 14 have to be reduced. However, this topic was studied in this thesis only to a small extent, hence further comprehensive studies concerning this matter are necessary. In addition, this thesis did not deal with reinforcing mats, so further studies on the characteristic parameters of the zones formed by reinforcing mats are also necessary.

In this PhD work, the model was implemented into the commercial software ANSYS Fluent©. The proposed simplified approach should be made accessible for the research community by creating a non-commercial version of the software package. Therefore, in further research steps, the proposed model should be implemented in an open source CFD software.

Bibliography

[1]   EFNARC, Specification and Guidelines for Self-Compacting Concrete Surrey, UK, 2002.

[2]   bibm, CEMBUREAU, EFCA, EFNARC, and ERMCO, The European Guidelines for Self-Compacting Concrete - Specification, Production and Use, 2005.

[3]   K. H. Khayat, C. Hu, and H. Monty, "Stability of SCC, advantages and potential applications", in Proceedings of the First RILEM International Conference on Self-Compacting Concrete, RILEM Publications S.A.R.L, Stockholm, 1999, pp. 143 - 152.

[4]   K. Ozawa, K. Maekawa, M. Kunishima, and H. Okamura, "Development of high performance concrete based on the durability design of concrete structures", in Proceedings of the second East-Asia and Pacific Conference on Structural Engineering and Construction, 1989, pp. 445-450.

[5]   H. Okamura and M. Ouchi, "Self-compacting concrete. Development, present and future", in Proceedings of the 1st International Rilem Symposium on Self-Compacting Concrete, vol. 7, A. Skarendahl and O. Petersson, Eds., RILEM Publications, Bagneux, 1999, pp. 3-14.

[6]   H. Okamura and M. Ouchi, "Self-Compacting Concrete", Journal of Advanced Concrete Technology, vol. 1, 2003, pp. 5-15.

[7]   W. Brameshuber and S. Uebachs, "Self-Compacting Concrete – Application in Germany", in Proceedings of the 6th International Symposium on Utilization of High Strength / High Performance Concrete, vol. 2, G. König, V. Dehn, and T. Faust, Eds., Leipzig, 2002, pp. 1503-1514.

[8]   "Measurement of properties of fresh self-compacting concrete, Final report of the European Union Growth Contract No. G6RD-CT-2001-00580", ACM Centre, University of Paisley, UK, 2005.

[9]   N. Roussel, M. R. Geiker, F. Dufour, L. N. Thrane, and P. Szabo, "Computational modeling of concrete flow: General overview", Cement and Concrete Research, vol. 37, 2007, pp. 1298-1307.

[10]   A. Gram and J. Silfwerbrand, "Numerical simulation of fresh SCC flow: applications", Materials and Structures, vol. 44, 2011, pp. 805-813.

[11]   L. N. Thrane, "Modelling the flow of self-compacting concrete", in Understanding the Rheology of Concrete, N. Roussel, Ed., Woodhead Publ Ltd, Cambridge, 2012, pp. 259-285.

[12]   N. Roussel and A. Gram, Simulation of Fresh Concrete Flow, State-of-the Art Report of the RILEM Technical Committee 222-SCF, RILEM State-of-the-Art Reports, vol. 15, Springer Netherlands, 2014.

[13]   M. Ouchi, S. Nakamura, T. Osterson, S. E. Hallberg, and M. Lwin, "Applications of self-compacting concrete in Japan, Europe and the United States", in Proceedings of ISHPC, Sixth International Symposium on the Utilization of High-Strength/High-Performance Concrete, Florida, 2003, pp. 1-20.

[14]   K. Vasilic, B. Meng, H. C. Kuehne, and N. Roussel, "Flow of fresh concrete through steel bars: A porous medium analogy", Cement and Concrete Research, vol. 41, 2011, pp. 496-503.

[15]   K. Vasilic, N. Roussel, B. Meng, and H. C. Kuehne, "Computational Modeling of SCC Flow through Reinforced Sections", in Design, Production and Placement of Self-Consolidating Concrete, Proceedings of SCC2010, Montreal, Canada, vol. 1, K. H. Khayat and D. Feys, Eds., Springer, 2010, pp. 187-195.

[16]   K. Vasilic, N. Roussel, B. Meng, and H. C. Kuehne, "Computational Modelling of SCC Flow through Reinforced Sections", in Proceedings of the 3rd International

Symposium on Rheology of Cement Suspensions such as Fresh Concrete, vol. 1, RILEM Publications S.A.R.L, Rheykjavik, Iceland, 2009, pp. 148 - 154.

[17] C. I. Goodier, "Development of self-compacting concrete", Proceedings of the Institution of Civil Engineers: Structures and Buildings, vol. 156, 2003, pp. 405-414.

[18] Å. Skarendahl and P. Billberg, Casting of Self Compacting Concrete - Final report of RILEM Technical Committee 188-CSC, RILEM State-of-the-Art Reports, vol. 35, Bagneux - France, RILEM Publications S.A.R.L, 2006.

[19] D. Bonen and S. P. Shah, "Fresh and hardened properties of self-consolidating concrete", Progress in Structural Engineering and Materials, vol. 7, 2005, pp. 14-26.

[20] G. D. Schutter, "Guidelines for testing fresh self-compacting concrete", 2005.

[21] G. Heirman, R. Hendrickx, L. Vandewalle, D. Van Gemert, D. Feys, G. De Schutter, B. Desmet, and J. Vantomme, "Integration approach of the Couette inverse problem of powder type self-compacting concrete in a wide-gap concentric cylinder rheometer Part II. Influence of mineral additions and chemical admixtures on the shear thickening flow behaviour", Cement and Concrete Research, vol. 39, 2009, pp. 171-181.

[22] W. Schmidt, Design Concepts for the Robustness Improvement of Self-Compacting Concrete - Effects of admixtures and mixture components on the rheology and early hydration at varying temperatures, PhD, Eindhoven University of Technology, Eindhoven, the Netherlands, 2014.

[23] K. Ozawa, K. Maekawa, and H. Okamura, "Development of High Performance Concrete ", University of Tokyo, Faculty of Engineering Journal, 1992,

[24] P. Billberg, "Self-compacting concrete for civil engineering structures - the Swedish experience, CBI report", Swedish Cement and Concrete Research Institute, Stockholm, 1999.

[25] P. L. Domone and H. W. Chai, "Design and testing of SCC: Production methods and workability of concrete", in Proceedings of the International RILEM Conference, E. & F. N. Spon, London, 1996.

[26] O. Petersson and P. Billberg, "A model for SCC: Production methods and workability of concrete", in Proceedings of International RILEM Conference, E & F N Spon, London, 1996.

[27] Å. Skarendahl and O. Petersson, Self-Compacting Concrete - State-of-the-Art Report of RILEM TC 174-SCC, RILEM State-of-the-Art Reports, vol. 23, RILEM Publications S.A.R.L, 2000.

[28] ERMCO, "European ready-mixed concrete industry statistics", European Ready Mixed Concrete Organization, 2013.

[29] C. F. Ferraris and N. S. Martys, "Concrete rheometers", in Understanding the Rheology of Concrete, N. Roussel, Ed., Woodhead Publ Ltd, Cambridge, 2012, pp. 63-82.

[30] ASTM, Standard Test Method for Slump of Hydraulic-Cement Concrete, West Conshohocken PA, ASTM International 2010.

[31] D. Kuzmin, "Introduction to Computational Fluid Dynamics", Lecture, Institute of Applied Mathematics, University of Dortmund.

[32] P. Banfill, "Rheology of fresh cement and concrete", Rheology Reviews, 2006, pp. 61 - 130.

[33] L. D. Schwartzentruber, R. Le Roy, and J. Cordin, "Rheological behaviour of fresh cement pastes formulated from a Self Compacting Concrete (SCC)", Cement and Concrete Research, vol. 36, 2006, pp. 1203-1213.

[34] C. W. Macosko, Rheology Principles, Measurements, and Applications, New York, Wiley, VCH, 1994.

[35]   P. Coussot, Rheometry of Pastes, Suspensions, and Granular Materials: Applications in Industry and Environment, Hoboken, New Jersey, John Wiley & Sons, Inc., 2005.

[36]   R. P. Chhabra and J. F. Richardson, Non-Newtonian Flow and Applied Rheology: Engineering Applications, Second Edition, Oxford, UK, Butterworth-Heinemann, 2008.

[37]   M. Schatzmann, Rheometry for large particle fluids and debris flows, PhD, ETH Zürich, Zürich 2005.

[38]   J. C. Gelin and O. Ghouati, "An Inverse Method for Material Parameters Estimation in the Inelastic Range", Computational Mechanics, vol. 16, 1995, pp. 143-150.

[39]   A. Gavrus, E. Massoni, and J. L. Chenot, "An inverse analysis using a finite element model for identification of rheological parameters", Journal of Materials Processing Technology, vol. 60, 1996, pp. 447-454.

[40]   C. Ancey, "Solving the Couette inverse problem using a wavelet-vaguelette decomposition", Journal of Rheology, vol. 49, 2005, pp. 441-460.

[41]   P. Schümmer and R. Worthoff, "An elementary method for the evaluation of a flow curve", Chemical Engineering Science, vol. 33, 1978, pp. 759 - 764.

[42]   Y. L. Yeow, W. C. Ko, and P. P. P. Tang, "Solving the inverse problem of Couette viscometry by Tikhonov regularization", Journal of Rheology, vol. 44, 2000, pp. 1335-1351.

[43]   G. Heirman, L. Vandewalle, D. Van Gemert, and O. Wallevik, "Integration approach of the Couette inverse problem of powder type self-compacting concrete in a wide-gap concentric cylinder rheometer", Journal of Non-Newtonian Fluid Mechanics, vol. 150, 2008, pp. 93-103.

[44]   R. Forestier, E. Massoni, and Y. Chastel, "Estimation of constitutive parameters using an inverse method coupled to a 3D finite element software", Journal of Materials Processing Technology, vol. 125, 2002, pp. 594-601.

[45]   O. H. Nouatin, L. Gavrus, T. Coupez, B. Vergnes, and J.-F. Agassant, "Inverse methods for the identification of the rheology of molten polymers", in Proceedings of the 13th International Congress on Rheology, Cambridge, UK, 2000.

[46]   A. Gavrus, E. Massoni, and J. L. Chenot, "Constitutive Parameter Identification Using a Computer Aided Rheology Approach", in Simulation of Materials Processing - Theory, Methods and Applications: Proceedings of the Fifth International Conference on Numerical Methods in Industrial Forming Processes-Numiform '95 Ithaca/New York/Usa/18-21 June 95, P. Dawson and S.-F. Shen, Eds., Golden Valley Publications 1995, pp. 563-568.

[47]   N. Roussel, "The LCPC BOX: a cheap and simple technique for yield stress measurements of SCC", Materials and Structures, vol. 40, 2007, pp. 889-896.

[48]   N. Roussel and P. Coussot, ""Fifty-cent rheometer" for yield stress measurements: From slump to spreading flow", Journal of Rheology vol. 49, 2005, pp. 705-718.

[49]   E. J. Garboczi, "Three-dimensional mathematical analysis of particle shape using X-ray tomography and spherical harmonics: Application to aggregates used in concrete", Cement and Concrete Research, vol. 32, 2002, pp. 1621-1638.

[50]   C. F. Ferraris, "Measurement of the rheological properties of high performance concrete; State of the art report", Journal of Research of the National Institute of Standards and Technology, vol. 104, 1999, pp. 461-478.

[51]   J. J. Stickel and R. L. Powell, "Fluid mechanics and rheology of dense suspensions", Annual Review of Fluid Mechanics, vol. 37, 2005, pp. 129-149.

[52]   P. Coussot, "Introduction to the rheology of complex fluids", in Understanding the Rheology of Concrete, N. Roussel, Ed., Woodhead Publ Ltd, Cambridge, Philadelphia, 2012, pp. 3-22.

[53]   N. Roussel, "Understanding the rheology of concrete - Introduction", in Understanding the Rheology of Concrete, N. Roussel, Ed., Woodhead Publ Ltd, Cambridge, 2012, pp. xi-xiv.

[54]   P. Coussot and C. Ancey, "Rheophysical classification of concentrated suspensions and granular pastes", Physical Review E, vol. 59, 1999, pp. 4445-4457.

[55]   P. F. G. Banfill and D. R. Kitching, " Use of a controlled stress rheometer to study the yield value of oilwell cement slurries", in The rheology of fresh cement and concrete, P. F. G. Banfill, Ed., Spon, London, 1991, pp. 125-136.

[56]   R. M. Edmeades and P. C. Hewlett, in Lea's chemistry of cement and concrete, P. C. Hewlett, Ed., Arnold, London, 1998, pp. 837-896.

[57]   V. S. E. Ramachandran, Concrete admixtures handbook, New Jersey, USA, Noyes publications, 1996.

[58]   G. Tatersall, Banfill, P., The Rheology of Fresh Concrete, London, Pitman, 1983.

[59]   J. E. Wallewik, Rheology of particle suspensions; Fresh concrete, mortar and cement paste with various types of lignosulfonates, PhD, Department of Structural Engineering, The Norwegian University of Science and Technology, Norway, Trondheim, Norway, 2003.

[60]   N. Roussel, "Steady and transient flow behaviour of fresh cement pastes", Cement and Concrete Research, vol. 35, 2005, pp. 1656-1664.

[61]   D. Feys, R. Verhoeven, and G. De Schutter, "Fresh self compacting concrete, a shear thickening material", Cement and Concrete Research, vol. 38, 2008, pp. 920-929.

[62]   N. Roussel and A. Gram, "Physical Phenomena Involved in Flows of Fresh Cementitious Materials", in Simulation of Fresh Concrete Flow, N. Roussel and A. Gram, Eds., Springer Netherlands, 2014, pp. 1-24.

[63]   D. Lowke, Segregation resistance and robustness of self-compacting concrete (in German), PhD thesis, Centre for building Materials, Technical University of Munich, Munich, 2013.

[64]   D. Bonen, Y. Deshpande, J. Olek, L. Shen, L. Struble, D. Lange, and K. Khayat, "Robustness of self-consolidating concrete", in Proceedings of the fifth International RILEM Symposium on Self-Compacting Concrete - SCC 2007, G. D. Schutter and V. Boel, Eds., RILEM Publications S.A.R.L, 2007, pp. 33 - 42.

[65]   F. de Larrard, C. F. Ferraris, and T. Sedran, "Fresh concrete: A Herschel-Bulkley material", Materials and Structures, vol. 31, 1998, pp. 494-498.

[66]   N. Roussel, "A thixotropy model for fresh fluid concretes: Theory, validation and applications", Cement and Concrete Research, vol. 36, 2006, pp. 1797-1806.

[67]   L. Heymann and N. Aksel, "Transition pathways between solid and liquid state in suspensions", Physical Review E, vol. 75, 2007,

[68]   P. F. G. Banfill, "The Rheology of Fresh Mortar", Magazine of Concrete Research, vol. 43, 1991, pp. 13-21.

[69]   B. H. Min, L. Erwin, and H. M. Jennings, "Rheological Behavior of Fresh Cement Paste as Measured by Squeeze Flow", Journal of Materials Science, vol. 29, 1994, pp. 1374-1381.

[70]   H. A. Barnes and J. O. Carnali, "The Vane-in-cup as a novel rheometer geometry for shear thinning and thixotropic materials", Journal of Rheology, vol. 34, 1990, pp. 841-866.

[71]   R. J. Mannheimer, "Laminar and turbulent-flow of cement slurries in large diameter pipe - a comparison with laboratory viscometers", Journal of Rheology, vol. 35, 1991, pp. 113-133.

[72]   T. L. H. Nguyen, N. Roussel, and P. Coussot, "Correlation between L-box test and rheological parameters of a homogeneous yield stress fluid", Cement and Concrete Research, vol. 36, 2006, pp. 1789-1796.

[73]   C. F. Ferraris and F. de Larrard, "Modified slump test to measure rheological parameters of fresh concrete", Cement Concrete and Aggregates, vol. 20, 1998, pp. 241-247.

[74]   D. Feys, R. Verhoeven, and G. De Schutter, "Why is fresh self-compacting concrete shear thickening?", Cement and Concrete Research, vol. 39, 2009, pp. 510-523.

[75]   D. Feys, R. Verhoeven, and G. D. Schutter, "The mechanisms behind shear thickening behaviour of fresh self-compacting concrete", in Rheology of Cement Suspensions such as Fresh Concrete, Proceedings of the 3rd international RILEM Symposium, O. Wallevik, S. Kubens, and S. Oesterheld, Eds., RILEM Publications S.A.R.L, 2009, pp. 105 - 112.

[76]   N. Roussel, G. Ovarlez, S. Garrault, and C. Brumaud, "The origins of thixotropy of fresh cement pastes", Cement and Concrete Research, vol. 42, 2012, pp. 148-157.

[77]   K. Dullaert, Constitutive Equations for Thixotropic Dispersions PhD, Katholieke Universiteit Leuven, Leuven, 2005.

[78]   P. C. F. Moller, J. Mewis, and D. Bonn, "Yield stress and thixotropy: on the difficulty of measuring yield stresses in practice", Soft Matter, vol. 2, 2006, pp. 274-283.

[79]   D. Lowke, "Segregation Resistance of Self-Compacting Concrete", University of Munich, Center for Building Materials (cbm), Munich, Germany, 2004.

[80]   I. Y. T. Ng, H. H. C. Wong, and A. K. H. Kwan, "Passing ability and segregation stability of self-consolidating concrete with different aggregate proportions", Magazine of Concrete Research, vol. 58, 2006, pp. 447-457.

[81]   O. d. Waele, "Ueber die Geschwindigkeitsfunktion der Viskosität disperser Systeme", Colloid & Polymer Science, vol. 36, 1925, pp. 99-117.

[82]   E. C. Bingham, Fluidity and plasticity, 1st ed., New York, Mcgraw-Hill Book Company, Inc., 1922.

[83]   E. C. Bingham, "Discussion on plasticity", Journal of the American Ceramic Society, vol. 7, 1924, pp. 375 - 379.

[84]   W. H. Herschel and R. Bulkley, "Konsistenzmessungen von Gummi-Benzollösungen", Kolloid Zeitschrift, vol. 39, 1926, pp. 291-300.

[85]   A. Yahia and K. H. Khayat, "Analytical models for estimating yield stress of high-performance pseudoplastic grout", Cement and Concrete Research, vol. 31, 2001, pp. 731-738.

[86]   D. Feys, J. E. Wallevik, A. Yahia, K. H. Khayat, and O. H. Wallevik, "Extension of the Reiner-Riwlin equation to determine modified Bingham parameters measured in coaxial cylinders rheometers", Materials and Structures, vol. 46, 2013, pp. 289-311.

[87]   H. A. Barnes, "Thixotropy - A review", Journal of Non-Newtonian Fluid Mechanics, vol. 70, 1997, pp. 1-33.

[88]   J. Labanda and J. Llorens, "A structural model for thixotropy of colloidal dispersions", Rheologica Acta, vol. 45, 2006, pp. 305-314.

[89]   A. Prosperetti and G. Tryggvason, Computational Methods for Multiphase Flow, Cambridge, UK, Cambridge University Press, 2007.

[90]   D. L. Davidson, "The role of computational fluid dynamics in process industries", Eighth Annual Symposium on Frontiers of Engineering, 2003, pp. 21-28.

[91]   K. Vasilic, M. Geiker, J. Hattel, L. Martinie, N. Martys, N. Roussel, and J. Spangenberg, "Advanced Methods and Future Perspectives", in Simulation of Fresh Concrete Flow, vol. 15, N. Roussel and A. Gram, Eds., Springer Netherlands, 2014, pp. 125-146.

[92]   J. D. Anderson, Jr., "Governing Equations of Fluid Dynamics", in Computational Fluid Dynamics, J. Wendt, Ed., Springer Berlin Heidelberg, 1992, pp. 15-51.

[93]   J. Ferziger and M. Perić, Computational Methods for Fluid Dynamics, Berlin Heidelberg, Springer, 2002.

[94]   J. Wendt, Computational Fluid Dynamics, Springer Berlin Heidelberg, 1992.

[95]   J. D. Anderson, Computational Fluid Dynamics: The basics with applications, Mcgraw Hills, 1995.

[96]   A. Thom, "The Flow Past Circular Cylinders at Low Speeds", Proc. Royal Society, vol. A141, 1933, pp. 651-666.

[97]   M. Kawaguti, "Numerical Solution of the Navier-Stokes Equations for the Flow around a Circular Cylinder at Reynolds Number-40", Journal of the Physical Society of Japan, vol. 8, 1953, pp. 747-757.

[98]   F. H. Harlow, "Fluid dynamics in group T-3 Los Alamos National Laboratory (LA-UR-03-3852)", Journal of Computational Physics, vol. 195, 2004, pp. 414-433.

[99]   W. P. Jones and B. E. Launder, "The prediction of laminarization with a two-equation model of turbulence", International Journal of Heat and Mass Transfer, vol. 15, 1972, pp. 301-314.

[100]   L. Thrane, A. Bras, P. Bakker, W. Brameshuber, B. Cazacliu, L. Ferrara, D. Feys, M. Geiker, A. Gram, S. Grünewald, S. Mokeddem, N. Roquet, N. Roussel, S. Shah, N. Tregger, S. Uebachs, F. Waarde, and J. Wallevik, "Computational Fluid Dynamics", in Simulation of Fresh Concrete Flow, vol. 15, N. Roussel and A. Gram, Eds., Springer Netherlands, 2014, pp. 25-63.

[101]   Y. Tanigawa and H. Mori, "Rheological analysis of slumping behavior of fresh concrete", in Proceedings of the 29th Japan congress on materials research, 1986.

[102]   Y. Tanigawa and H. Mori, "Analytical Study on Deformation of Fresh Concrete", Journal of Engineering Mechanics-Asce, vol. 115, 1989, pp. 493-508.

[103]   G. Christensen, Modelling the flow of fresh concrete: the slump test, PhD, Princeton University, USA, 1991.

[104]   L. N. Thrane, P. Szabo, M. R. Geiker, M. Glavind, and H. Stang, "Simulation of the test method L-box for self-compacting concrete", Annual Transactions of the Nordic Rheology Society, vol. 12, 2004, pp. 47-54.

[105]   L. N. Thrane, P. Szabo, M. R. Geiker, H. Stang, and C. Pade, "Simulation and verification of flow in test methods", in Proceedings of the 2nd North American Conference on the Design and Use of SCC and the 4th International RILEM Symposium on SCC Chicago, USA, 2005, pp. 551 – 556.

[106]   S. Uebachs and W. Brameshuber, "Numerical simulation of the flow behaviour of self-compacting concretes using fluid mechanical methods", in Proceedings of the 2nd North American Conference on the Design and Use of SCC and the 4th International RILEM Symposium on SCC Chicago, USA, 2005, pp. 597 - 605.

[107]   F. Van Waarde, E. A. B. Koenders, L. Nijeholt, and J. C. Walraven, "Theoretical and practical investigations on SCC formwork", in Proceedings of the 5th International RILEM Symposium on Self-Compacting Concrete - SCC 2007, G. D. Schutter and V. Boel, Eds., RILEM Publishing S.A.R.L., Ghent, 2007, pp. 417-423.

[108]   N. Tregger, L. Ferrara, and S. R. Shah, "Identifying Viscosity of Cement Paste from Mini-Slump-Flow Test", Aci Materials Journal, vol. 105, 2008, pp. 558-566.

[109]   A. Gram, Numerical modelling of self-compacting concrete flow, discrete and continuous approach Licentiate thesis, Royal Institute of Technology , Stockholm 2009.

[110]   A. Bras, Grout optimization for masonry consolidation ,, PhD, Universidade Nova de Lisaboa, Portugal, 2010.

[111]   M. Cremonesi, L. Ferrara, A. Frangi, and U. Perego, "Simulation of the flow of fresh cement suspensions by a Lagrangian finite element approach", Journal of Non-Newtonian Fluid Mechanics, vol. 165, 2010, pp. 1555-1563.

[112]   N. Roussel, "Correlation between yield stress and slump: Comparison between numerical simulations and concrete rheometers results", Materials and Structures, vol. 39, 2006, pp. 501-509.

[113] G. Ovarlez and N. Roussel, "A physical model for the prediction of lateral stress exerted by self-compacting concrete on formwork", Materials and Structures, vol. 39, 2006, pp. 269-279.

[114] L. N. Thrane, Form filling with SCC PhD Thesis, Department of Civil Engineering, Technical University of Denmark 2007.

[115] L. N. Thrane, H. Stang, and M. R. Geiker, "Flow induced segregation in full scale castings with SCC", in Proceedings of the 5th International RILEM Symposium on Self-Compacting Concrete - SCC 2007, G. D. Schutter and V. Boel, Eds., RILEM Publishing S.A.R.L., Ghent, 2007, pp. 449 - 454.

[116] B. Patzak and Z. Bittnar, "Modeling of fresh concrete flow", Computers & Structures, vol. 87, 2009, pp. 962-969.

[117] P. A. Cundall, "A Computer Model for Simulating Progressive Large Scale Movements in Blocky Rock Systems", in Proceedings of the Symposium of the International Society of Rock Mechanics, Nancy, France, 1971, pp. 2 - 8.

[118] V. Mechtcherine, A. Gram, K. Krenzer, J. H. Schwabe, S. Shyshko, and N. Roussel, "Simulation of fresh concrete flow using Discrete Element Method (DEM): theory and applications", Materials and Structures, vol. 47, 2014, pp. 615-630.

[119] V. Mechtcherine, A. Gram, K. Krenzer, J.-H. Schwabe, C. Bellmann, and S. Shyshko, "Simulation of Fresh Concrete Flow Using Discrete Element Method (DEM)", in Simulation of Fresh Concrete Flow, N. Roussel and A. Gram, Eds., Springer Netherlands, 2014, pp. 65-98.

[120] H. Chu and A. Machida, "Numerical simulation of fluidity behaviour of fresh concrete by 2D distinct element method", Transactions of the Japan Concrete Institute, vol. 18, 1996 pp. 1-8.

[121] H. Chu, A. Machida, and N. Suzuki, "Experimental investigation and DEM simulation of filling capacity of fresh concrete", Transactions of the Japan Concrete Institute, vol. 16, 1996 pp. 9-14.

[122] M. A. Noor and T. Uomoto, "Three-dimensional discrete element simulation of rheology tests of self-compacting concrete", in Proceedings of the 1st International Rilem Symposium on Self Compacting Concrete, A. Skarendahl and O. Petersson, Eds., 1999, pp. 35-46.

[123] Ö. Petersson and H. Hakami, "Simulation of SCC-laboratory experiments and numerical modeling of slump flow and L-box tests", in Proceedings of 2nd International RILEM Symposium on SCC, Tokyo, 2001, pp. 79-88.

[124] Ö. Petersson, "Simulation of self-compacting concrete – laboratory experiments and numerical modeling of testing methods, J-ring and L-box tests", in Proceedings of the 3rd International RILEM Symposium on SCC, Reykjavik 2003, pp. 202 – 207.

[125] J.-H. Schwabe and H. Kuch, "Development and control of concrete mix processing procedures", in Proceedings of the 18th BIBM International Congress and Exhibition, Amsterdam, the Netherlands, May 11-14, 2005, M. Borghoff, Gottschalg, A., Mehl, R., Ed., Bond van Fabrikanten van Betonproducten in Nederland, Woerden 2005, pp. 108-109.

[126] K. Krenzer and J. H. Schwabe, "Calibration of parameters for particle simulation of building materials, using stochastic optimization procedures", in Proceedings of the 3rd International Symposium on Rheology of Cement Suspensions such as Fresh Concrete, vol. 1, RILEM Publications S.A.R.L, Rheykjavik, Iceland, 2009, pp. 135–142.

[127] J. Wallevik, K. Krenzer, and J.-H. Schwabe, "Numerical Errors in CFD and DEM Modeling", in Simulation of Fresh Concrete Flow, N. Roussel and A. Gram, Eds., Springer Netherlands, 2014, pp. 99-124.

[128] V. Mechtcherine and S. Shyshko, "Modelling the behaviour of fresh and hardened concrete using the distinct element method", in Proceedings of the 2nd International RILEM Symposium on Advances in Concrete through Science and

Engineering, B. B. J. Marchand, R. Gagné, M. Jolin and F. Paradis, Ed., RILEM Publications S.A.R.L, Quebec City, Canada, 2006, pp. 207 - 224.

[129] V. Mechtcherine and S. Shyshko, "Simulating the behaviour of fresh concrete using distinct element method", in Proceedings of the 5th International RILEM Symposium on Self-Compacting Concrete - SCC 2007, G. D. Schutter and V. Boel, Eds., RILEM Publishing S.A.R.L., Ghent, 2007, pp. 449 - 454.

[130] S. Shyshko and V. Mechtcherine, "Developing a Discrete Element Model for simulating fresh concrete: Experimental investigation and modelling of interactions between discrete aggregate particles with fine mortar between them", Construction and Building Materials, vol. 47, 2013, pp. 601-615.

[131] S. Shyshko and V. Mechtcherine, "Simulating the behaviour of fresh concrete with the Distinct Element Method – Deriving model parameters related to the yield stress", Cement and Concrete Composites, vol. 55, 2015, pp. 81-90.

[132] H. Mori and M. Tanigawa, "Simulation methods for fluidity of fresh concrete", Memoirs of the School of Engineering, Nagoya University vol. 44 1992, pp. 71-134.

[133] F. Dufour and G. Pijaudier-Cabot, "Numerical modelling of concrete flow: homogeneous approach", International Journal for Numerical and Analytical Methods in Geomechanics, vol. 29, 2005, pp. 395-416.

[134] M. Modigell, K. Vasilic, W. Brameshuber, and S. Uebachs, "Modelling and simulation of the flow behaviour of Self-compacting Concrete", in Proceedings of the 5th International RILEM Symposium on Self-Compacting Concrete - SCC 2007, vol. 1, G. D. Schutter and V. Boel, Eds., RILEM Publishing S.A.R.L., Ghent, 2007, pp. 387 - 393.

[135] J. Spangenberg, N. Roussel, J. H. Hattel, J. Thorborg, and M. R. Geiker, "Prediction of the impact of fl ow induced inhomogeneities in self compacting concrete (SCC)", in Design, Production and Placement of Self-Consolidating Concrete, Proceedings of SCC2010, Montreal, Canada, vol. 1, K. H. Khayat and D. Feys, Eds., Springer, 2010, pp. 209-215.

[136] N. S. Martys, "Study of a dissipative particle dynamics based approach for modeling suspensions", Journal of Rheology, vol. 49, 2005, pp. 401-424.

[137] N. S. Martys, W. L. George, B. W. Chun, and D. Lootens, "A smoothed particle hydrodynamics-based fluid model with a spatially dependent viscosity: application to flow of a suspension with a non-Newtonian fluid matrix", Rheologica Acta, vol. 49, 2010, pp. 1059-1069.

[138] N. S. Martys, "A classical kinetic theory approach to lattice Boltzmann simulation", International Journal of Modern Physics C, vol. 12, 2001, pp. 1169-1178.

[139] P. J. Hoogerbrugge and J. M. V. A. Koelman, "Simulating Microscopic Hydrodynamic Phenomena with Dissipative Particle Dynamics", Europhysics Letters, vol. 19, 1992, pp. 155-160.

[140] D. R. Foss and J. F. Brady, "Structure, diffusion and rheology of Brownian suspensions by Stokesian Dynamics simulation", Journal of Fluid Mechanics, vol. 407, 2000, pp. 167-200.

[141] N. Roussel, T. L. H. Nguyen, O. Yazoghli, and P. Coussot, "Passing ability of fresh concrete: A probabilistic approach", Cement and Concrete Research, vol. 39, 2009, pp. 227-232.

[142] N. Roussel, T. L. H. Nguyen, and P. Coussot, "General probabilistic approach to the filtration process", Physical Review Letters, vol. 98(11): 114502, 2007,

[143] C. T. Tam, A. M. M. Shein, K. C. G. Ong, and C. Y. Chay, "Modified J-ring approach for assessing passing ability of SCC", in Proceedings of the 1st International Symposium on Design, Performance and Use of Self-Consolidating Concrete, vol. 42, Z. W. Yu, C. Shi, K. H. Khayat, and Y. J. Xie, Eds., RILEM Publications S.A.R.L, Bagneux, 2005, pp. 687-692.

166

[144]   T. L. H. Nguyen, Outils pour la modélisation de la mise en œuvre des bétons (in French) PhD thesis, Laboratoire central des Ponts et chaussées, ENPC, 2007.

[145]   Y. S. Wu and K. Pruess, "Flow of Non-Newtonian Fluids in Porous Media ", in Advances in Porous Media, vol. 3, M. Y. Corapcioglu, Ed., Elsevier, Amsterdam, The Netherlands, 1996, pp. 87-184.

[146]   Y. S. Wu and K. Pruess, "A numerical method for simulating non-Newtonian fluid flow and displacement in porous media", Computational Methods in Water Resources, vol 1: Computational Methods in Subsurface Flow and Transport Problems, 1996, pp. 109-119.

[147]   X. Lopez, P. H. Valvatne, and M. J. Blunt, "Predictive network modeling of single-phase non-Newtonian flow in porous media", Journal of Colloid and Interface Science, vol. 264, 2003, pp. 256-265.

[148]   K. S. Sorbie, P. J. Clifford, and E. R. W. Jones, "The Rheology of Pseudoplastic Fluids in Porous-Media Using Network Modeling", Journal of Colloid and Interface Science, vol. 130, 1989, pp. 508-534.

[149]   R. de Boer, "Theory of Porous Media - Past and Present", ZAMM - Journal of Applied Mathematics and Mechanics / Zeitschrift für Angewandte Mathematik und Mechanik, vol. 78, 1998, pp. 441-466.

[150]   L. Orgeas, C. Geindreaua, J. L. Auriault, and J. F. Bloch, "Upscaling the flow of generalised Newtonian fluids through anisotropic porous media", Journal of Non-Newtonian Fluid Mechanics, vol. 145, 2007, pp. 15-29.

[151]   S. P. Sullivan, L. F. Gladden, and M. L. Johns, "Simulation of power-law fluid flow through porous media using lattice Boltzmann techniques", Journal of Non-Newtonian Fluid Mechanics, vol. 133, 2006, pp. 91-98.

[152]   J. P. Reese, K. Long, C. T. Kelley, C. T. Miller, and W. G. Gray, "Simulating Non-Darcy Flow through Porous Media using Sundance", in Proceedings of the 16th International Conference on Computational Methods in Water Resources (CMWR XVI),, Copenhagen, Denmark, 2006, p. 8.

[153]   M. Modigell, Mehrphasenströmung (in German), Aachen, Germany, RWTH Aachen University, 2006.

[154]   J. G. Savins, "Flow of Non-Newtonian Fluids through Porous Media", Industrial and Engineering Chemistry, vol. 61, 1969, pp. 8-47.

[155]   P. H. Valvatne, M. Piri, X. Lopez, and M. J. Blunt, "Predictive pore-scale modeling of single and multiphase flow", Transport in Porous Media, vol. 58, 2005, pp. 23-41.

[156]   M. J. Blunt, M. D. Jackson, M. Piri, and P. H. Valvatne, "Detailed physics, predictive capabilities and macroscopic consequences for pore-network models of multiphase flow", Advances in Water Resources, vol. 25, 2002, pp. 1069-1089.

[157]   M. Chen, W. Rossen, and Y. C. Yortsos, "The flow and displacement in porous media of fluids with yield stress", Chemical Engineering Science, vol. 60, 2005, pp. 4183-4202.

[158]   J. R. A. Pearson and P. M. J. Tardy, "Models for flow of non-Newtonian and complex fluids through porous media", Journal of Non-Newtonian Fluid Mechanics, vol. 102, 2002, pp. 447-473.

[159]   C. L. Perrin, P. M. J. Tardy, K. S. Sorbie, and J. C. Crawshaw, "Experimental and modeling study of Newtonian and non-Newtonian fluid flow in pore network micromodels", Journal of Colloid and Interface Science, vol. 295, 2006, pp. 542-550.

[160]   C. Zhangxin, H. Guanren, and M. Yuanle, Computational Methods for Multiphase Flows in Porous Media, Computational Science & Engineering, Society for Industrial and Applied Mathematics, 2006.

[161]   M. T. Balhoff and K. E. Thompson, "Modeling the steady flow of yield-stress fluids in packed beds", Aiche Journal, vol. 50, 2004, pp. 3034-3048.

[162] D. A. S. Rees, "The Modelling of Flow and Convection of a Bingham Fluid in a Porous Medium", submitted to Handbook of Porous Media, third edition, K. Vafai, Ed., CRC Press, 2015.

[163] T. Chevalier, C. Chevalier, X. Clain, J. C. Dupla, J. Canou, S. Rodts, and P. Coussot, "Darcy's law for yield stress fluid flowing through a porous medium", Journal of Non-Newtonian Fluid Mechanics, vol. 195, 2013, pp. 57-66.

[164] M. M. Zdravkovich, Flow Around Circular Cylinders, Flow Around Circular Cylinders, vol. 1: Fundamentals, Oxford, UK, Oxford University Press, 1997.

[165] P. D. M. Spelt, A. Y. Yeow, C. J. Lawrence, and T. Selerland, "Creeping flows of Bingham fluids through arrays of aligned cylinders", Journal of Non-Newtonian Fluid Mechanics, vol. 129, 2005, pp. 66-74.

[166] A. O. Nieckele, M. F. Naccache, and P. R. S. Mendes, "Crossflow or viscoplastic materials through tube bundles", Journal of Non-Newtonian Fluid Mechanics, vol. 75, 1998, pp. 43-54.

[167] D. A. Nield and A. Bejan, Convection in Porous Media, Convection in Porous Media, Springer New York, 2006.

[168] J. A. Kolodziej, R. Dziecielak, and Z. Konczak, "Permeability tensor for heterogeneous porous medium of fibre type", Transport in Porous Media, vol. 32, 1998, pp. 1-19.

[169] G. W. Jackson and D. F. James, "The Permeability of Fibrous Porous-Media", Canadian Journal of Chemical Engineering, vol. 64, 1986, pp. 364-374.

[170] M. Poreh and C. Elata, "An Analytical Derivation of Darcys Law", Israel Journal of Technology, vol. 4, 1966, pp. 214-&.

[171] S. P. Neuman, "Theoretical derivation of Darcy's law", Acta Mechanica, vol. 25, 1977, pp. 153-165.

[172] P. A. Rice, D. J. Fontugne, R. G. Latini, and A. J. Barduhn, "Anisotropic Permeability in Porous Media", Industrial and Engineering Chemistry, vol. 62, 1970, pp. 23-31.

[173] G. Neale and W. K. Nader, "Prediction of Transport Processes within Porous-Media - Diffusive Transport Processes within Anisotropic or Isotropic Swarms of Nonspherical Particles", Aiche Journal, vol. 22, 1976, pp. 182-188.

[174] G. Neale, "Degrees of Anisotropy for Fluid-Flow and Diffusion (Electrical-Conduction) through Anisotropic Porous-Media", Aiche Journal, vol. 23, 1977, pp. 56-62.

[175] J. Happel, "Viscous Flow Relative to Arrays of Cylinders", Aiche Journal, vol. 5, 1959, pp. 174-177.

[176] S. Kuwabara, "The Forces Experienced by Randomly Distributed Parellel Circular Cylinders or Spheres in a Viscous Flow at Small Reynolds Numbers", Journal of the Physical Society of Japan, vol. 14, 1959, pp. 527-532.

[177] C. Boutin, "Study of permeability by periodic and self-consistent homogenisation", European Journal of Mechanics-A/Solids, vol. 19, 2000, pp. 603-632.

[178] A. Tamayol and M. Bahrami, "Analytical determination of viscous permeability of fibrous porous media", International Journal of Heat and Mass Transfer, vol. 52, 2009, pp. 2407-2414.

[179] A. Tamayol and M. Bahrami, "Transverse Permeability of Fibrous Porous Media", in Proceedings (CD) of the 3rd International Conference on Porous Media and its Applications in Science and Engineering, ICPM3, June 20-25, 2010, Montecatini, Italy, 2010.

[180] A. Tamayol and M. Bahrami, "Parallel Flow Through Ordered Fibers: An Analytical Approach", Journal of Fluids Engineering-Transactions of the Asme, vol. 132, 2010,

[181] W. J. Canella, C. Huh, and R. S. Seright, "Prediction of Xanthan Rheology in Porous Media", in Proceedings of SPE 63rd Ann. Tech. Conf. and Exhibition of SPE, Houston, TX, USA, 1988.

[182] N. Roussel, A. Lemaitre, R. J. Flatt, and P. Coussot, "Steady state flow of cement suspensions: A micromechanical state of the art", Cement and Concrete Research, vol. 40, 2010, pp. 77-84.

[183] J. Yammine, M. Chaouche, M. Guerinet, M. Moranville, and N. Roussel, "From ordinary rhelogy concrete to self-compacting concrete: A transition between frictional and hydrodynamic interactions", Cement and Concrete Research, vol. 38, 2008, pp. 890-896.

[184] N. Roussel, Understanding the Rheology of Concrete, Cambridge, Woodhead Publishing in Materials, 2012.

[185] C. Hu and F. de Larrard, "The rheology of fresh high-performance concrete", Cement and Concrete Research, vol. 26, 1996, pp. 283-294.

[186] R. J. Flatt, N. Martys, and L. Bergstrom, "The rheology of cementitious materials", MRS Bulletin, vol. 29, 2004, pp. 314-318.

[187] N. Roussel, "Rheology of fresh concrete: from measurements to predictions of casting processes", Materials and Structures, vol. 40, 2007, pp. 1001-1012.

[188] W. R. Schowalter and G. Christensen, "Toward a rationalization of the slump test for fresh concrete: Comparisons of calculations and experiments", Journal of Rheology, vol. 42, 1998, pp. 865-870.

[189] H. Darcy, Les Fontaines Publiques de la Ville de Dijon, Paris, Dalmont, 1856.

[190] ANSYS Inc., "FLUENT 6.3 User's Guide", 2006.

[191] E. Mitsoulis, "Flows of viscoplastic materials: models and computations", Rheology Reviews, 2007, pp. 135 - 178.

[192] R. I. Tanner and J. F. Milthorpe, "Numerical simulation of the flow of fluids with yield stress", in Numerical methods in laminar and turbulent flow: proceedings of the third international conference held in Seattle, 8th-11th August 1983, C. Taylor, J. A. Johnson, and W. R. Smith, Eds., Pineridge Press, Swansea, UK, Swansea, 1983, pp. 680-690.

[193] ANSYS Inc., FLUENT 6.3 UDF Manual", 2006.

[194] ANSYS Inc., www.ansys.com/Products/ANSYS+Fluent.

[195] M. Day, "The no-slip condition of fluid dynamics", Erkenntnis, vol. 33, 1990, pp. 285-296.

[196] ANSYS Inc., "ANSYS FLUENT Theory Guide", 2011.

[197] C. Djelal, Y. Vanhove, and A. Magnin, "Tribological behaviour of self-compacting concrete", Cement and Concrete Research, vol. 34, 2004, pp. 821-828.

[198] S. H. Kwon, T. P. Quoc, H. Y. Park, J. H. Kim, and S. P. Shah, "Effect of wall friction on variation of formwork pressure over time in self-consolidating concrete", Cement and Concrete Research, vol. 41, 2011, pp. 90-101.

[199] S. Mindess, J. Young, and D. Darwin, Concrete, Second ed., Prentice Hall, New Jersey, USA, 2003.

[200] M. Sonebi and P. J. M. Bartos, "Performance of Reinforced Columns Cast with Self-Compacting Concrete", in SP-200: Recent Advances in Concrete Technology-Proceedings, Fifth International Conference, V. M. Malhortra, Ed., Singapore, 2001, pp. 415-431.

[201] K. H. Khayat, "Workability, testing, and performance of self-consolidating concrete", ACI Materials Journal, vol. 96, 1999, pp. 346-353.

[202] Eurocode 2: Design of concrete structures – Part 1-1: General – Common rules for building and civil engineering structures, 2005.

[203] K.-J. Schneider, Bautabellen für Ingenieure: mit Berechnungshinweisen und Beispielen, 12. ed., Düsseldorf, Werner-Verlag, 1996.

[204] S. Balint and A. M. Balint, "Mathematical models for mass and heat transport in porous media, Part I", Lecture at Summer University, Vrnjacka Banja, Serbia, 2007.

[205] H. X. Bai, P. Yu, S. H. Winoto, and H. T. Low, "Boundary conditions at the interface between fluid layer and fibrous medium", International Journal for Numerical Methods in Fluids, vol. 60, 2009, pp. 809-825.

[206] D. F. James and A. M. J. Davis, "Flow at the interface of a model fibrous porous medium", Journal of Fluid Mechanics, vol. 426, 2001, pp. 47-72.

[207] M. Shams Saryazdi, Study of flow at the interface of a porous medium using particle image velocimetry, PhD Thesis, Graduate Department of Mechanical and Industnal Engineering, University of Toronto, 1999.

[208] S. K. Gupte and S. G. Advani, "Flow near the permeable boundary of a porous medium: An experimental investigation using LDA", Experiments in Fluids, vol. 22, 1997, pp. 408-422.

[209] N. Roussel and A. Gram, "Physical Phenomena Involved in Flows of Fresh Cementitious Materials", in Simulation of Fresh Concrete Flow: State-of-the-Art Report of the Rilem Technical Committee 222-SCF, vol. 15, N. Roussel and A. Gram, Eds., Springer, 2014, pp. 1-24.

[210] S. Jarny, N. Roussel, S. Rodts, F. Bertrand, R. Le Roy, and P. Coussot, "Rheological behavior of cement pastes from MRI velocimetry", Cement and Concrete Research, vol. 35, 2005, pp. 1873-1881.

[211] DIN 1045-1, 2008-08, Concrete, reinforced and prestressed concrete structures – Part 1: Design and construction, Berlin, DIN Deutsches Institut für Normung e.V., 2008.

[212] ConTec. ConTec Rheometer-4SCC. Available: http://www.contec.is/page17.htm.

[213] S. Nagataki, T. Kawai, and H. Fujiwara, "State of the Art Report on SCC in Japan", in Design, Production and Placement of Self-Consolidating Concrete, Proceedings of SCC2010, Montreal, Canada, vol. 2, K. H. Khayat and D. Feys, Eds., Springer, 2010, pp. 5-24.